



This work is protected by copyright and other intellectual property rights and duplication or sale of all or part is not permitted, except that material may be duplicated by you for research, private study, criticism/review or educational purposes. Electronic or print copies are for your own personal, non-commercial use and shall not be passed to any other individual. No quotation may be published without proper acknowledgement. For any other use, or to quote extensively from the work, permission must be obtained from the copyright holder/s.

Changes in human endothelial cells and astrocytes of the blood-brain barrier (BBB) in cerebral malaria: using *in vitro* BBB models

Nana Efua Andoh

A thesis submitted for the Degree of Doctor of Philosophy

June 2019

Keele University

Abstract

During cerebral malaria (CM), sequestration of *Plasmodium falciparum* infected red blood cells (PRBC) to the blood-brain barrier (BBB) is associated with BBB disruption and long-term neurological sequelae in CM survivors, possibly linked to the activation of astrocytes. The aim of this study was to investigate the indirect effect of sequestration of PRBC during CM on endothelial cells and astrocytes of the BBB using two *in vitro* BBB models, the human brain endothelial cell (HBEC)-alone and the HBEC-astrocyte BBB models. This is the first time the HBEC-astrocyte BBB has been used to study sequestration in cerebral malaria. The HBEC-astrocyte BBB formed a tighter BBB over 5 days as indicated by the significantly higher transendothelial electrical resistance (TEER) than the HBEC-alone BBB. Inflammatory mediators released in response to coculturing of PRBC with HBEC caused a statistically significant increase in HBEC-alone BBB permeability but had no effect on the HBEC-astrocyte BBB integrity. However, these inflammatory mediators caused activation of astrocytes in the HBEC-astrocyte BBB shown by an increase in the adhesion molecule ICAM-1 and astrocyte marker GFAP in the astrocyte supernatant, and the increased expression of the protease ADAMTS-4 in astrocytes. A novel study was performed to investigate the effect of serum from malaria patients on HBEC-alone BBB integrity *in vitro*. Results showed that serum from uncomplicated malaria, severe malaria and CM patients caused an increase in HBEC-alone BBB permeability, with a more pronounced increase with serum from CM patients. This suggests that inflammatory mediators present in the serum of malaria patients had the ability to disrupt endothelial integrity. Our results suggest that during CM, sequestration of PRBC to the BBB results in the release of inflammatory mediators that cause astrocyte activation. Activated astrocytes released inflammatory cytokines that could cause damage to neurons and this could be responsible for the neurological sequelae observed in some CM survivors.

Table of Contents

Abstract	i
List of figures	vi
List of tables	viii
Abbreviations.....	ix
Acknowledgements.....	xii
Dedication	xiv
Chapter 1: General Introduction.....	1
1.1 Overview	2
1.2 Life Cycle of the malaria parasite.....	3
1.3 Clinical symptoms of malaria	6
1.3.1 Severe malaria	7
1.3.2 Cerebral malaria	7
1.4 The Blood-brain barrier	8
1.4.1 Brain endothelial cells.....	9
1.4.2 Basement membrane.....	12
1.4.3 Astrocytes.....	12
1.5 CM and BBB.....	17
1.5.1 Astrogliosis and cerebral malaria.....	19
1.6 Hypothesis of cerebral malaria	23
1.6.1 Sequestration hypothesis	24
1.6.2 Inflammation hypothesis	31
1.7 Aims of thesis.....	34
Chapter 2 : General Materials and Methods.....	35
2.0 Materials and Methods	36
2.1 Transformed Human Brain Endothelial cells	36
2.2 Astrocytes.....	37
2.3 Thawing of cells.....	37
2.4 Subculturing of cells.....	38
2.4.1 Cell culturing	40
2.5 Freezing of Human Brain Endothelial cells and astrocytes	40
2.6 Cell Counting.....	40
2.7 <i>Plasmodium falciparum</i> parasite culture	41
2.8 Preparation of growth medium for <i>Plasmodium falciparum</i> cultures.....	42

2.9 Washed human red blood cells (WRBC).....	42
2.10 Reconstitution of frozen <i>P. falciparum</i> culture stabilates	43
2.11 Assessment of <i>Plasmodium falciparum</i> parasite culture.....	43
2.12 Freezing of <i>Plasmodium falciparum</i> parasites	44
2.13 Plasmagel Trophozoite enrichment.....	45
2.14 Coculture of transformed Human Brain Endothelial cells with PRBC.....	45
2.15 Conditions for coculture experiment	47
2.16 Harvesting of PRBC-HBEC coculture supernatant and HBEC lysate.....	47
2.17 Making of the SDS PAGE gel.....	47
2.18 Sample preparation	48
2.19 Gel transfer	49
2.20 Ponceau S stain	50
2.21 Antibody incubation.....	51
2.22 Imaging and data analysis	51
2.23 Immunofluorescence analysis.....	52
2.24 Cell based ELISA.....	52
2.25 Development of <i>in vitro</i> HBEC and HBEC-astrocyte BBB models.....	55
2.26 Measurement of transendothelial electrical resistance (TEER).....	55
2.27 FITC dextran permeability assay.....	55
2.28 Sandwich ELISA.....	55
2.28.1 Calculation of amount of sICAM-1, MCP-1 and ADAMTS-4	57
2.29 Biorad protein assay.....	57
2.30 Statistical analysis.....	58
Chapter 3 : Development and characterisation of <i>in vitro</i> blood-brain barrier models	59
3.1 Introduction	60
3.2 Materials and methods.....	65
3.2.1 MTS assay	65
3.2.2 Detection of ICAM-1, Vinculin and Claudin-5 using immunofluorescence analysis ...	68
3.2.3 Detection of Glial fibrillary acidic protein (GFAP) in astrocytes.....	68
3.2.4 Cell-based ELISA for detection of ICAM-1 in HBEC	69
3.2.5 Cell-based ELISA GFAP	69
3.2.6 Western blot analysis for detection of GFAP in astrocytes.....	71
3.2.7 Development of <i>in vitro</i> BBB models.....	71
3.2.8 Measurement of Transendothelial Electrical resistance (TEER).....	75
3.2.9 Statistical Analysis.....	76

3.2.10 Densitometry analysis	76
3.3 Results	77
3.3.1 Characterisation of HBEC	77
3.3.2 Characterisation of astrocytes.....	83
3.3.3 Optimisation of HBEC-astrocyte and HBEC-BBB model	91
3.4 Discussion.....	95
Chapter 4 : Changes occurring at the blood barrier during cerebral malaria ...	101
4.1 Introduction.....	102
4.2 Materials and Methods	104
4.2.1 Sandwich ELISA	104
4.2.2 Western blot analysis for detection of ADAMTS-4.....	104
4.2.3 FITC dextran permeability assay	104
4.2.4 Statistics	108
4.3 Results	110
4.3.1 Detecting MCP-1, sICAM-1 and ADAMTS-4 levels in PRBC-HBEC coculture supernatants	110
4.3.2 Changes in ADAMTS-4 levels in the PRBC-HBEC coculture supernatant	112
4.3.3 Alterations in HBEC-alone BBB permeability following treatment with coculture supernatants	113
4.3.4 Alterations in HBEC-alone BBB following treatment with HBEC lysates	115
4.3.5 Effect of the broad spectrum metalloprotease inhibitor, GM6001 on HBEC-alone BBB permeability induced by PRBC-HBEC coculture supernatant	117
4.3.6 Effect of coculture supernatants on the HBEC-astrocyte BBB model	120
4.3.7 Effect of HBEC lysates on HBEC-astrocyte BBB permeability.....	120
4.4 Discussion.....	123
Chapter 5 : Investigating activation of components of the BBB during cerebral malaria.....	128
5.1 Introduction.....	129
5.2 Materials and methods	133
5.2.1 Cell-based ELISA for detection of GFAP	133
5.2.2 Treatment and harvesting of the HBEC-astrocyte BBB model	133
5.2.3 Western blot analysis for detection of GFAP	133
5.2.4 Western blot analysis on supernatants harvested from the luminal and basolateral side of the HBEC-astrocyte BBB	134
5.2.5 Sandwich ELISA	136
5.2.6 Densitometry analysis	138
5.3 Results	139

5.3.1 Effect of coculture supernatants on GFAP expression in astrocytes	139
5.3.2 Changes in GFAP expression in the HBEC-astrocyte BBB.....	141
5.3.3 Alterations in ADAMTS-4 expression in astrocytes of the HBEC-astrocyte BBB	144
5.3.4 Alterations in ICAM-1 expression in astrocytes of the HBEC-astrocyte BBB	147
5.3.5 GFAP expression in astrocytes following treatment of the HBEC-astrocyte BBB model with HBEC lysates	150
5.3.6 Alterations in ADAMTS-4 expression in astrocytes following treatment of the HBEC-astrocyte BBB model with HBEC lysates	152
5.4 Discussion	156
Chapter 6 : Effect of serum from malaria patients on BBB permeability <i>in vitro</i>	163
6.1 Introduction	164
6.2 Methods	165
6.2.1 Serum from malaria patients.....	165
6.2.2 FITC dextran permeability assay.....	166
6.2.3 Statistical analysis.....	168
6.3 Results.....	169
6.3.1 Effect of serum from malaria patients on HBEC-alone BBB permeability	169
6.4 Discussion	171
Chapter 7 : Final discussion	176
7.1 General discussion	177
7.2 Limitations and Future studies	184
References.....	187
Appendices.....	206
Appendix 1: List of kits	207
Appendix 2: List of reagents and chemicals.....	207
Appendix 3: List of equipment	209
Appendix 4: List of antibodies.....	210
Appendix 5: Table of Buffers	211
Appendix 6: Media and components used in media	213
Appendix 7: Materials Transfer Agreement.....	215

List of figures

Figure 1.1 Map showing the geographical population at risk of malaria.....	2
Figure 1.2 The life cycle of <i>Plasmodium</i> spp	4
Figure 1.3 Scanning electron micrograph of a normal uninfected red blood cell and <i>Plasmodium falciparum</i> infected red blood cell (PRBC).....	5
Figure 1.4 Schematic representation of the blood-brain barrier.....	8
Figure 1.5 Constituents of endothelial cell tight junctions.....	10
Figure 1.6 The two main types of astrocytes, protoplasmic and fibrous astrocytes.....	13
Figure 1.7 Function of astrocytes in the CNS.....	14
Figure 1.8 Hypothesis explaining the pathogenesis of cerebral malaria.....	23
Figure 1.9 <i>Plasmodium falciparum</i> infected red blood cells sequestered to blood vessels in the brain.....	24
Figure 1.10 Receptor-binding domains on PfEMP1.....	27
Figure 2.1 Thawing procedure of HBEC and astrocytes <i>in vitro</i>	38
Figure 2.2 Schematic representation of HBEC and astrocytes subculture <i>in vitro</i>	39
Figure 2.3 Schematic of Haemocytometer.....	41
Figure 2.4 Schematic of Plasmagel Trophozoite Enrichment.....	46
Figure 2.5 Schematic of SDS PAGE gel electrophoresis and western blot procedure	50
Figure 3.1 Different types of <i>in vitro</i> BBB models.....	61
Figure 3.2 Schematic diagram of MTS assay	66
Figure 3.3 Conversion of MTS to a coloured formazan product	67
Figure 3.4 Set up of HBEC-alone BBB model schematic	72
Figure 3.5 The experimental process for growing HBEC and astrocytes in tandem on different sides of the transwell membrane	73
Figure 3.6 Transendothelial electrical resistance (TEER) measurement of transwells.....	75
Figure 3.7 Images of resting HBEC.....	77
Figure 3.8 MTS assay used to determine if HBEC could survive in AM/HBEC, HBEC and Astrocyte media.....	78
Figure 3.9 Determining the effect of AM and HBEC media on ICAM-1 expression in HBEC using cell-based ELISA.....	79
Figure 3.10 Changes in ICAM-1 expression in response to treatment of HBEC with varying concentrations of IL-1 β	80
Figure 3.11 Expression of endothelial and BBB markers by HBEC	82
Figure 3.12 Determining if astrocytes could survive in AM/HBEC, HBEC and Astrocyte media using an MTS assay.....	83
Figure 3.13 Images of primary human astrocytes <i>in vitro</i>	84
Figure 3.14 Optimized anti-GFAP antibody and Goat anti-rabbit (GAR) antibody dilutions for cell-based ELISA	85
Figure 3.15 Determination of GFAP expression in astrocytes treated with AM, AM/HBEC and HBEC media.....	86
Figure 3.16 Cell-associated GFAP expression in astrocytes treated with different concentrations of IL-1 β diluted in AM.....	87
Figure 3.17 Increase in cell-associated GFAP expression in astrocytes treated with different concentrations of IL-1 β diluted in AM/HBEC media.....	88
Figure 3.18 Optimisation of protein loading of astrocytes in the resting state.	89
Figure 3.19 Soluble GFAP observed in the supernatant of astrocytes treated with 15, 30, 60 and 100ng/ml IL-1 β diluted in AM and AM/HBEC media.....	90
Figure 3.20 TEER of astrocyte alone, HBEC-alone BBB, and HBEC-astrocyte BBB using protocol 1	93
Figure 3.21 TEER values of HBEC-alone BBB model and HBEC-astrocyte BBB using protocol 2 ..	94
Figure 4.1 Schematic of FITC dextran permeability assay procedure.....	105

Figure 4.2 Mean MCP-1, sICAM-1 and ADAMTS-4 levels in coculture supernatants.....	111
Figure 4.3 Detection of ADAMTS-4 in coculture supernatants in a pilot study	112
Figure 4.4 Effect of coculture supernatants on HBEC-alone BBB permeability	114
Figure 4.5 Effect of HBEC lysates on HBEC-alone BBB permeability	116
Figure 4.6. Changes in HBEC-alone BBB permeability following treatment with coculture supernatants and addition of DMSO (control diluent of inhibitor) and presence of the inhibitor (GM6001)	118
Figure 4.7 Changes in HBEC-alone BBB permeability following treatment with PRBC-HBEC lysate and addition of DMSO or GM6001	119
Figure 4.8 Effect of coculture supernatants on HBEC-astrocyte BBB permeability	121
Figure 4.9 Effect of HBEC lysates on HBEC-astrocyte BBB permeability.....	122
Figure 5.1 Schematic showing the different spectrum of reactive astrogliosis that changes with insult severity	129
Figure 5.2 Summary of experiments performed to analyse GFAP, ICAM-1 and ADAMTS-4 expression in the luminal and basolateral supernatants of the HBEC-astrocyte BBB that had been treated with different coculture supernatants and lysates.	135
Figure 5.3 GFAP expression in astrocytes directly treated with coculture supernatants.....	140
Figure 5.4 Changes in GFAP expression in the astrocyte supernatant of astrocytes following treatment of the HBEC-astrocyte BBB model with coculture supernatants.....	142
Figure 5.5 Alteration in cell-associated GFAP expression following treatment of the HBEC-astrocyte BBB model with the different coculture supernatants.....	143
Figure 5.6 Alterations in ADAMTS-4 expression in astrocytes supernatants following treatment of the HBEC-astrocyte BBB model with coculture supernatants	145
Figure 5.7 Changes in ADAMTS-4 expression in astrocyte lysates following treatment of the HBEC- astrocyte BBB model with coculture supernatants for 48 hours	146
Figure 5.8. Alterations in ICAM-1 expression in astrocytes following treatment of the HBEC- astrocyte BBB model with coculture supernatants	148
Figure 5.9 Alterations in ICAM-1 expression in astrocytes following treatment of the HBEC-astrocyte BBB model with coculture supernatants for 48 hours	149
Figure 5.10 Soluble GFAP expression in luminal and basolateral supernatants of HBEC-astrocyte BBB that has been treated with HBEC lysates	151
Figure 5.11 ADAMTS-4 expression in luminal supernatant of astrocytes following treatment of the HBEC-astrocyte BBB model with HBEC lysates	153
Figure 5.12 ADAMTS-4 expression in basolateral supernatant of astrocytes following treatment of the HBEC-astrocyte BBB with HBEC lysates	155
Figure 6.1 Schematic showing FITC dextran permeability assay of HBEC-alone BBB treated with serum from malaria patients.	167
Figure 6.2 Effect of serum from malaria patients on HBEC-alone BBB permeability	170
Figure 7.1 The proposed effect of sequestration of PRBC to the BBB during cerebral malaria	183
Figure 7.2 BBB on-chip model.....	185

List of tables

Table 1.1 Symptoms of severe malaria.	6
Table 1.2 Description of the cellular properties of brain endothelial cells.	9
Table 2.1 Primary Antibodies	51
Table 2.2 Secondary Antibodies	51
Table 3.1 Antibody dilutions used for immunofluorescence.	68
Table 3.2 Different anti-GFAP antibody combinations for optimisation of cell-based GFAP ELISA in astrocytes.....	70
Table 4.1 Summary of treatments used in the HBEC and HBEC-astrocyte BBB model	107
Table 4.2 Summary of Inhibitor concentrations used in the permeability assay	108
Table 6.1 Summary of patient serum used in the treatment of the HBEC-alone BBB model.	166

Abbreviations

µg	Microgram
µg/ml	Microgram per ml
µl	microlitre
µM	Micromolar
2D	2 dimensional
3D	3 dimensional
ACE-1	Angiotensin-converting enzyme
ACT	Artemisinin-based combination therapy
AD	Alzheimer's disease
ADAMTS-4	A disintegrin and metalloproteinase with thrombospondin motifs-4
AGT	Angiotensinogen
Aldehyde dehydrogenase	ALDH1A1
AM	Astrocyte medium
ANG 1	Angiotensin 1
ANGPT-1	Angiopoietin 1
ANGPT-2	Angiopoietin 2
ANOVA	Analysis of variance
AP-1	Transcription factor activator protein
ApoE	Apolipoprotein
AQP4	Aquaporin 4
ATI	Type I angiotensin receptors
AXD	Alexander disease
BBB	Blood-Brain Barrier
BBB-EC	BBB derived endothelial cells
BDP	Breakdown products
BEC	Brain endothelial cells
bFGF	Basic fibroblast growth factor
BM	Basement membrane
BSA	Bovine serum albumin
CD36	Cluster of differentiation 36
CIDR	Cysteine rich interdomain region
CL3	Containment level 3
CM	Cerebral malaria
cm ²	Centimetre squared
CNS	Central Nervous System
CO ₂	Carbon dioxide
CSA	Chondroitin sulphate A
CSF	Cerebrospinal fluid
CSPG	Chondroitin sulphate proteoglycans
DAPI	4' 6-diamidino-2-phenylindole
DBL	Duffy Binding Like
DC	Domain cassette
DMSO	Dimethyl sulfoxide
DNA	Deoxyribonucleic acid
EA	Experimental autoimmune encephalomyelitis
ECM	Extracellular matrix
EDTA	Ethylenediaminetetraacetic acid
ELISA	Enzyme-linked immunosorbent assay

EMCM	Experimental murine cerebral malaria
EPCR	Endothelial protein C receptor
FBS	Foetal Bovine Serum
FITC	Fluorescein isothiocyanate
FMCM	Fatal murine cerebral malaria
GAR	Goat anti-rabbit
GDNF	Glial derived neurotrophic factor
GFAP	Glial fibrillary acidic protein
GFAP δ	GFAP delta
Gli1-3	Glioma-associated oncogene homolog 1-3
GPI	Glycosylphosphatidylinositol
H ₂ O	Water
H ₂ SO ₄	Sulphuric acid
HBEC	Human brain endothelial cells
HCT	Haematocrit
HEPES	(4-(2-hydroxyethyl)-1-piperazineethanesulfonic acid)
Hh	Hedgehog
HRP	Horseshoe peroxidase
HRP2	Histidine-rich protein 2
HSE	Health and Safety Executive
HTA	Human Tissue Authority
HUVEC	Human umbilical vein endothelial cells
HZ	Haemozoin
ICAM-1	Intercellular adhesion molecule-1
IFN γ	Interferon gamma
IL-1	Interleukin- 1
JAM	Junction adhesion molecules
kDa	kilodalton
LFA-1	Leukocyte function associated antigen-1
LIF	Leukaemia inhibitor factor
MAGUK	Membrane-associated guanylate
MCP-1	Monocyte chemoattractant protein-1
ml	Millilitre
mM	Millimolar
MMP	Matrix metalloprotease
MS	Multiple sclerosis
MTA	Material transfer agreement
MTS	3-(4,5-dimethylthiazol-2-yl)-5-(3-carboxymethoxyphenyl)-2-(4-sulfophenyl)-2H-tetrazolium
Mw	Molecular weight
NaCl	Sodium chloride
NADH	Nicotinamide adenine dinucleotide
NADPH	Nicotinamide adenine dinucleotide phosphate
NaOH	Sodium hydroxide
NBTS	National Blood Transfusion Service
ng/ml	Nanogram per ml
NGS	New goat serum
nm	nanometre
nM	Nanomolar
NMIMR	Noguchi Memorial Institute for Medical Research

NO	Nitric oxide
NVU	Neurovascular Unit
OAP	Orthogonal array of particles
<i>P. berghei</i> Anka	<i>Plasmodium berghei</i> Anka
<i>P. falciparum</i>	<i>Plasmodium falciparum</i>
<i>P. ovale</i>	<i>Plasmodium ovale</i>
<i>P. vivax</i>	<i>Plasmodium vivax</i>
<i>P.malariae</i>	<i>Plasmodium malariae</i>
P/S	Penicillin Streptomycin
PBS	Phosphate buffered saline
PCV	Packed cell volume
PDGF	Platelet-derived growth factor
PES	Phenazine ethosulfate
PfEMP1	<i>Plasmodium falciparum</i> erythrocyte membrane protein
pg/ml	Picogram per ml
PKC	Protein Kinase C
PRBC	<i>Plasmodium falciparum</i> infected red blood cells
PTCH	Patched
Q1% FBS media	Quiescent 1% FBS
Q5%	Quiescent 5% FBS
RA	Retinoic acid
ROS	Reactive oxygen species
RPMI	Rosewell Park Memorial Institute
SCI	Spinal cord injury
SDS PAGE	sodium dodecyl sulphate polyacrylamide gel electrophoresis
SEM	Standard error of mean
SHH	Sonic hedgehog
sICAM-1	Soluble ICAM-1
SMO	Smoothened
Smo	Smoothened
SSeCKS	Src-suppressed C-kinase
TBI	Traumatic brain injury
TBST	Tris Buffered Saline with Tween®20
TEER	Transendothelial electrical resistance
TEMED	Tetramethylethylenediamine
TGFβ	Transforming growth factor β
TIMP-1	Tissue inhibitors of metalloproteinases-1
TMB	3,3',5,5'-Tetramethylbenzidine
TNFα	Tumour necrosis factor-alpha
URBC	Uninfected red blood cells
v/v	Volume per volume
VCAM-1	Vascular cell adhesion molecule
VE	Vascular endothelial
VEGF	Vascular endothelial growth factor
w/v	Weight per volume
WBC	White blood cells
WHO	World Health Organisation
ZO-1	Zonula occludens
Ω	Ohms

Acknowledgements

First of all, I will like to thank God almighty for giving me the strength, knowledge and patience to complete this PhD.

I would like to express my appreciation and utmost gratitude to my supervisor Dr Srabasti Chakravorty for her continuous support, patience, guidance and motivation throughout this PhD. I appreciate Dr Chakravorty giving me the chance to develop and grow as a research scientist and allowing me to achieve my goal.

A special thanks to my co-supervisor Prof Rosemary Fricker and my advisor Dr Helen price. Thank you for all your support and encouragement.

I will like to thank past and present members of my research team Dr Mohd Hamzah Mohd Nasir and Atieme Ogbolosingha.

I offer my thanks to Prof Ben Gyan from the Noguchi Memorial Institute for Medical Research (NMIMR), Ghana for providing the serum samples from malaria patients used as part of my PhD research. I will also like to thank Prof Michael Wilson, Mr Kwabena Boateng and Prof Gyan for encouraging me to pursue a doctoral degree.

A big thanks to the research colleagues in my office Emma Green, Nancy Dawam, Johnathan Swift, Saja Mohammed, Nwamaka Akpodiete and my Huxley friends, Dr Florian Noulin, Jaksha Chandrathas and Lekia Kumbe. Thanks for all the stimulating discussions and your constant support. My sincere thanks go to all members of the Centre for Applied Entomology and Parasitology and friends and staff in Huxley Building, School of Life Sciences for their friendship and support.

I will like to thank my brothers Jojo and Ato for their encouragement throughout my PhD journey. I really appreciate it. Finally, my sincere gratitude goes out to my Mom and Dad. Thanks for being there for me throughout this PhD. Thanks for your generous support, guidance and providing a listening ear when I needed it. Thank you for believing in me.

Dedication

This thesis is dedicated to my parents who inspired and encouraged me to achieve my goals

Chapter 1: General Introduction

1.1 Overview

Malaria, one of the most deadly diseases worldwide is caused by the protozoan parasite *Plasmodium* spp. (phylum Apicomplexa) and transmitted through the bite of an infected female Anopheles mosquito. Four species of *Plasmodium* i.e. *Plasmodium falciparum* (*P. falciparum*), *Plasmodium vivax* (*P. vivax*), *Plasmodium ovale* (*P. ovale*) and *Plasmodium malariae* (*P. malariae*) are known to cause malaria in humans with *P. falciparum* being responsible for the most severe cases (Kantele and Jokiranta, 2011). Recently, *Plasmodium knowlesi*, the species that causes malaria in monkeys was found to infect humans in South East Asia (White, 2008; William *et al.*, 2014).

In 2016, over half of the world's population were at risk of developing malaria (Figure 1.1). An estimated 216 million cases of malaria and over 445,000 deaths from malaria were reported worldwide, with the most cases and deaths found in Sub-Saharan Africa (WHO, 2018, 2017). Children under 5 years of age are predominantly vulnerable to malaria. Although malaria deaths in children under 5 years of age have reduced from 440,000 in 2010 to 285,000 in 2016, every two minutes a child dies from malaria (WHO, 2018, 2017).

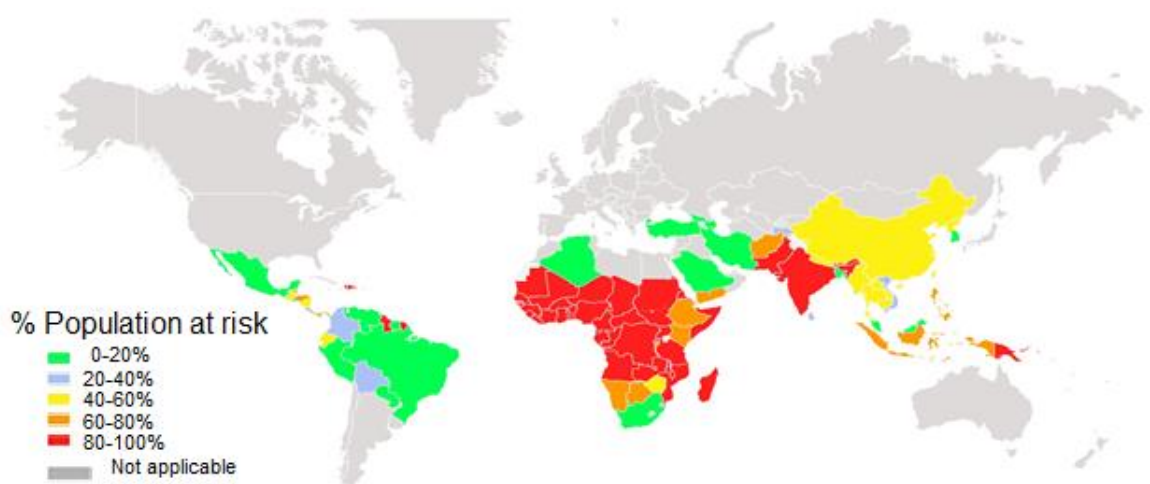


Figure 1.1 Map showing the geographical population at risk of malaria. Adapted from (Malaria Vaccine initiative, 2018).

The vast majority of malaria deaths worldwide is caused by the *Plasmodium falciparum* parasite. There has been significant progress in the eradication of malaria over 50 years. Malaria has been successfully eliminated in Sri-Lanka. Despite the global efforts to eradicate and control malaria, this disease remains a huge public health and socio-economic problem. Resistance to anti-malaria medicine has been reported in South-east Asia. Resistance to artemisinin-based combination therapy (ACTs) the first line treatment for malaria has been found in Cambodia, Lao People's Democratic Republic, Myanmar, Thailand and Vietnam (WHO, 2018). Thus, more research into new therapies to treat malaria need to be developed to help in the control and eventual eradication of this disease.

1.2 Life Cycle of the malaria parasite

Malaria is transmitted when an infected Anopheles mosquito takes a blood meal and injects sporozoites into the blood of the human host (Figure 1.2). The sporozoites then travel through the bloodstream to the hepatic sinusoids, that are made up of endothelial cells and Kupffer cells (specialised macrophages) (Tavares *et al.*, 2013). Sporozoites invade Kupffer cells before invading hepatocytes (Pradel and Frevert, 2001). In the hepatocytes, the sporozoites mature into schizonts within 5 to 16 days (Cowman *et al.*, 2012; Prudêncio *et al.*, 2011). Subsequently, the schizonts rupture and release approximately 10,000 to 30,000 merozoites to invade other red blood cells (White *et al.*, 2014) (Figure 1.2). Certain *Plasmodium* species such as *P. vivax* and *P. ovale* develop into hypnozoites that are dormant in the hepatocytes for weeks or even years after infection (Bartoloni and Zammarchi, 2012). These hypnozoites can be reactivated and undergo asexual division resulting in a malarial relapse.

Merozoites invade red blood cells and develop into immature trophozoites (0-24 hours) referred to as ring forms due to their morphology (Figure 1.2). The parasite then matures into a trophozoite (24-36 hours) within the red blood cells and undergoes mitotic divisions to form

schizonts (40-48 hours). These mature schizonts burst and release 8-32 merozoites, each of which can re-invade uninfected red blood cells and start the cycle again (Billig *et al.*, 2012; Rowe *et al.*, 2009) (Figure 1.2). The erythrocytic cycle lasts approximately 48 hours in *P. falciparum*, *P. vivax*, *P. ovale* and 72 hours in *P. malariae* (Baron, 1996). In *P. malariae*, chronic malaria infection due to the presence of parasites in the blood can persist for life in the human host (Collins and Jeffery, 2007). This is known as recrudescence. Recrudescence can occur if the parasite is resistant to antimalarial drugs (Collins *et al.*, 2007).

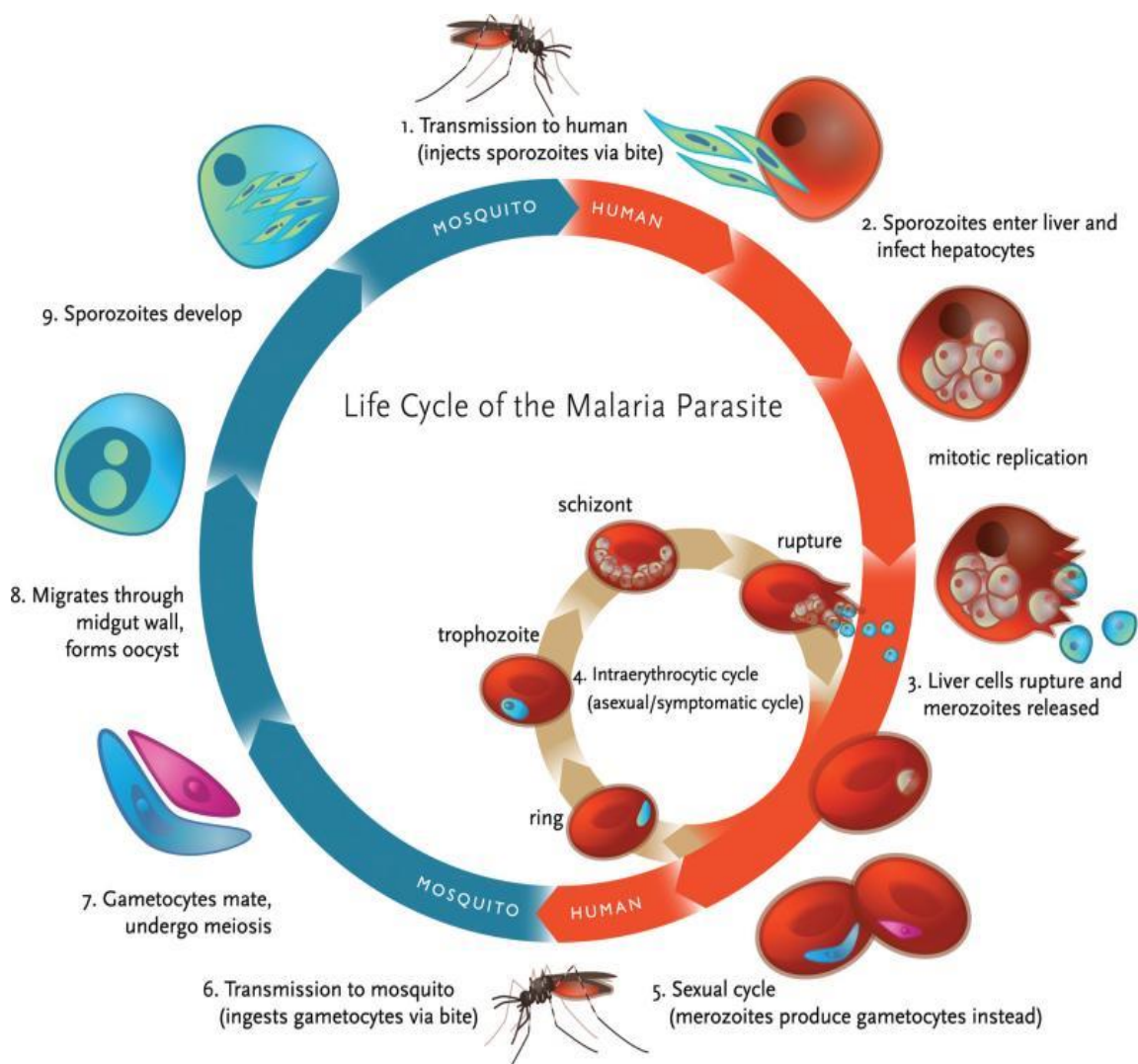


Figure 1.2 The life cycle of *Plasmodium* spp. Image obtained from (Klein, 2013).

During the erythrocytic stage of malaria infection, the *Plasmodium* parasite remodels the cell membrane of the red blood cell via the insertion of parasite derived proteins into the membrane (Moxon *et al.*, 2011). These proteins form protrusions known as knobs during the second part of the asexual life cycle (24-48 hours) (Zhang *et al.*, 2015). These knobs are responsible for the stiffening of the *Plasmodium falciparum* infected red blood cell membrane (Zhang *et al.*, 2015). *Plasmodium falciparum* infected red blood cell (PRBC) are rigid, deformed (Figure 1.3) and bind to the vascular endothelium, uninfected red blood cells (rosetting), to platelets (clumping) to avoid destruction and clearance by the spleen (Zhang *et al.*, 2015).

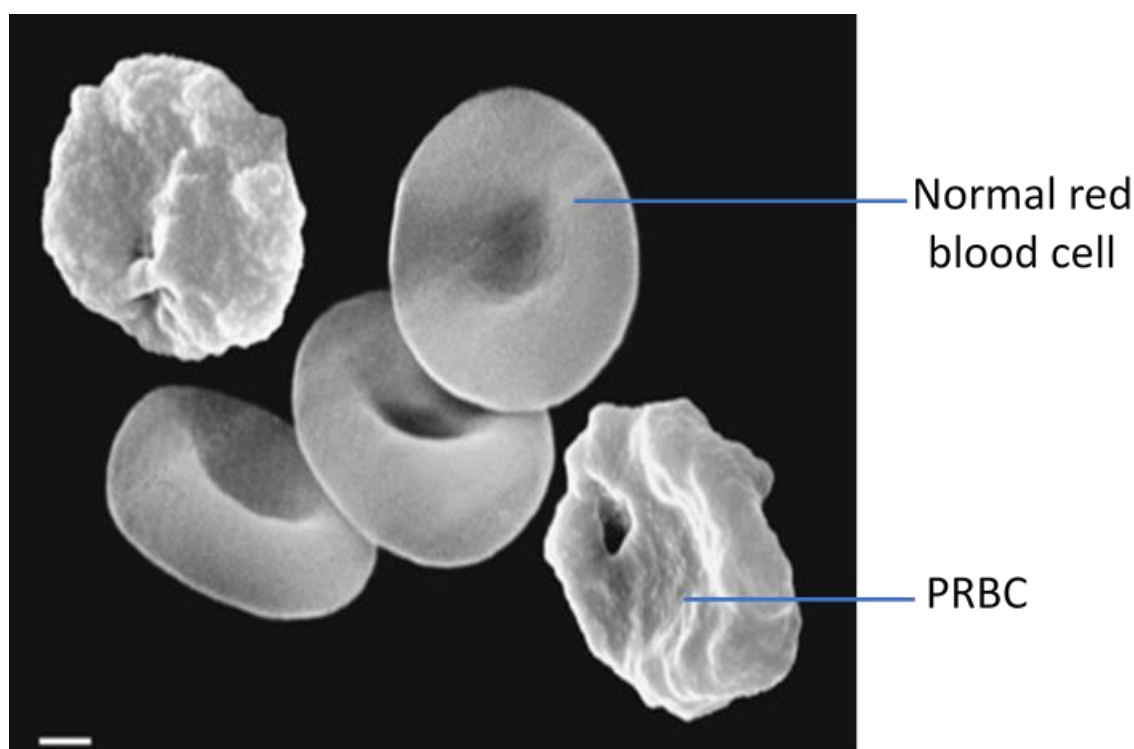


Figure 1.3 Scanning electron micrograph of a normal uninfected red blood cell and *Plasmodium falciparum* infected red blood cell (PRBC). Normal URBC appears biconcave and smooth. PRBC have a rough and irregular surface and are no longer biconcave in shape (Moxon *et al.*, 2011). Scale bar =1 μ m. Image obtained from (Moxon *et al.*, 2011).

Some blood stage merozoites form male and female sexual stages called gametocytes that circulate in the peripheral blood stream. When an Anopheles mosquito takes a blood meal it ingests the gametocytes. In the mosquito gut, the microgamete (male) and macrogamete (female) fuse to form a zygote (Cox, 2010) (Figure 1.2). The zygote develops into a motile ookinete that travels to the midgut epithelium of the mosquito and divides into oocysts (Figure

1.2). The oocyst undergoes asexual multiplication and thousands of sporozoites are formed (Cox, 2010). The oocyst ruptures after 8-15 days and releases sporozoites that migrate to the salivary glands of the mosquito. When the infected mosquito feeds on a human, the malaria life cycle starts again (Cox, 2010) (Figure 1.2).

1.3 Clinical symptoms of malaria

The blood stage parasites (in all malaria species) are responsible for the clinical symptoms of malaria. The early symptoms of malaria are non-specific and include headaches, chills, muscle aches, fatigue, abdominal discomfort usually followed by fever, chills, anorexia, nausea, vomiting and worsening malaise (Bartoloni *et al.*, 2012). Full and rapid recovery occurs if patients are treated at this stage. However, if patients are not treated early this can lead to severe malaria. In this study, we are going to focus on *Plasmodium falciparum* malaria.

Table 1.1 Symptoms of severe malaria. Obtained from (WHO, 2014)

Clinical manifestations	Frequency	
	Children	Adults
Impaired consciousness	Common	Less common
Respiratory distress (acidotic breathing)	Common	Less common
Multiple convulsions	Common	Rare
Prostrations	Common	Common
Shock	Rare	Rare
Pulmonary oedema	Uncommon	Rare
Abnormal bleeding	Uncommon	Rare
Jaundice	Rare	Common
Severe anaemia	Common	Rare
Hypoglycaemia	Common	Less common
Acidosis	Common	Less common
Hyperlactataemia	Common	Less common
Renal impairment	Rare	Common
Hyperparasitaemia	Less common	Rare

1.3.1 Severe malaria

Young children, pregnant women and non-immune individuals are highly susceptible to severe malaria in endemic areas. Symptoms of severe malaria include liver and lung dysfunction, hypoglycaemia, severe anaemia, placental malaria and cerebral malaria (CM) (Table 1.1) (WHO, 2014).

1.3.2 Cerebral malaria

Cerebral malaria is one of the most severe forms of *P. falciparum* infection. Approximately 1% of *P. falciparum* infections develop into CM.

According to WHO cerebral malaria is defined as a diffuse encephalopathy state with a Glasgow Coma Score of 11/15 or less for adults or a Blantyre Coma Scale of 2 out of 5, or less for children, an unarousable coma for at least an hour after a seizure has stopped, detection of asexual forms of *P. falciparum* parasites in peripheral blood smears and the absence of factors that could cause a coma such as hypoglycaemia or meningitis (Idro *et al.*, 2010).

The clinical hallmark of CM is the presence of a coma with convulsions (WHO, 2014). In adults, CM is part of a multi-organ disorder including renal failure, pulmonary oedema and these rarely occur in children. However, in African children, after 1-3 days of fever, coma suddenly develops (Idro *et al.*, 2010). Even though mortality in adults with CM is higher than that of children, the highest number of deaths due to malaria worldwide mostly occurs in children under 5 years of age (Hawkes *et al.*, 2013). 10-20% of children who survive CM are left with long-term neurological sequelae such as speech impairment and learning disabilities (Birbeck *et al.*, 2010; Idro *et al.*, 2010). A Malawian study showed that nearly one-third of survivors of childhood CM had neurological deficits such as epilepsy, gross motor, sensory or language difficulties. Neurological deficits might occur more often in children than in adults because children are more susceptible to neurological injury since their brains are not fully

developed (Birbeck *et al.*, 2010; Hawkes *et al.*, 2013).

1.4 The Blood-brain barrier

Two main barriers exist in the brain, the blood-cerebrospinal fluid (CSF) barrier at the choroid plexuses and the blood-brain barrier found at the endothelial cells in the microvessels of the brain. These barriers serve as interfaces between the periphery and the CNS (Stolp *et al.*, 2013).

In this thesis, we are going to focus on the blood-brain barrier.

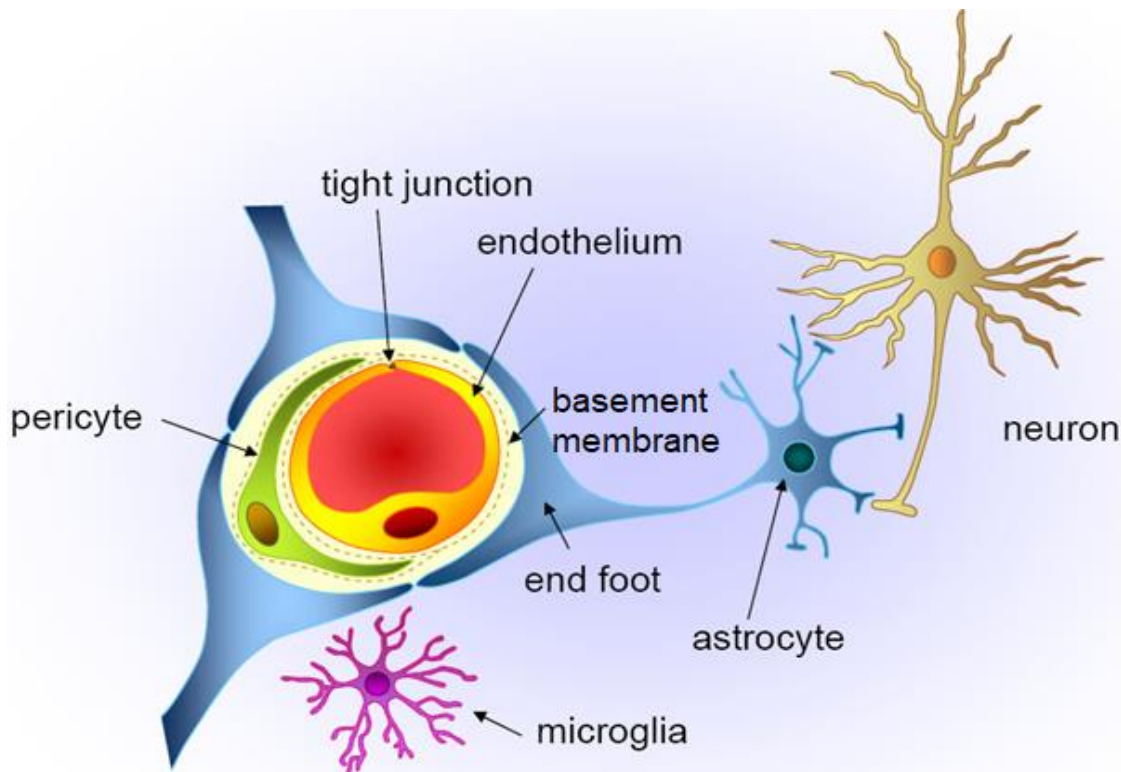


Figure 1.4 Schematic representation of the blood-brain barrier. Image obtained from (Abbott and Yusof, 2010).

The Blood-brain barrier (BBB) is a dynamic barrier between the blood circulation and the central nervous system (CNS) (Hawkins and Davis, 2005). The BBB is composed of a tightly sealed monolayer of brain endothelial cells that line the cerebral capillaries, a basement membrane, pericytes and astrocytes (Hawkins *et al.*, 2005) (Figure 1.4). The BBB is regarded as an integrated neurovascular unit (NVU). Transport of molecules from the blood to the brain is controlled by the BBB. It also prevents molecules, plasma proteins, red blood cells and

leukocytes in the blood from entering into the brain and removes toxic substances from the brain to the blood (Yamazaki and Kanekiyo, 2017).

1.4.1 Brain endothelial cells

Brain endothelial cells (BEC) are specifically designed to prevent movement of molecules across cells (transcellular movement) and between cells (paracellular movements). They vary from endothelial cells in the periphery in that they have: no fenestrae, minimal pinocytic activity, a continuous basement membrane, a negatively charged luminal surface and the existence of tight junctions (Table 1.2) (De Boer and Gaillard, 2006). BEC are joined to adjacent EC by cellular junctions such as adherens and tight junctions (Figure 1.5).

Table 1.2 Description of the cellular properties of brain endothelial cells. Table obtained from (Lawther *et al.* 2011)

Cellular properties	Cerebral capillary endothelium
Enzymatic barrier (BBB specific markers)	Present (metabolizing neuroactive blood-born solutes)
Inductive influence from astrocytes	Mandatory
Fenestrations	Absent
Tight junctions	Present
Transendothelial electrical resistance	>1500 Ω cm ² (low paracellular permeability)
Pinocytic vesicular transport	Minimal
Mitochondrial content	Greater number and volume (increased energy demands of active transports)
Sucrose and K ⁺ permeability	Low
Exposure to flow membrane	Luminal
Established polarity-polarized transporters	Present e.g. Amino acids
Carrier mediated transporters	Glucose, amino acids

1.4.1.1 Tight junctions

Tight junctions between adjacent brain endothelial cells are mainly responsible for the barrier properties of the BBB. Brain capillaries are 50-100 times tighter than peripheral microvessels due to the presence of tight junctions (Abbott, 2002; Abbott *et al.*, 2010). Tight junctions

restrict paracellular movement of small ions and polar solutes between cerebral endothelial cells (van Meer and Simons, 1986; Wong *et al.*, 2013). This results in an *in vivo* electrical resistance of approximately $1500 \Omega \text{ cm}^2$ in rats (Abbott *et al.*, 2010; Butt *et al.*, 1990).

Tight junctions are made up of transmembrane proteins such as occludin, claudin and junction adhesion molecules (JAM) and cytoplasmic scaffolding proteins including zonula occludens (ZO), cingulin, AF-6 and 7H6 (Figure 1.5) (Petty and Lo, 2002; Zlokovic, 2008).

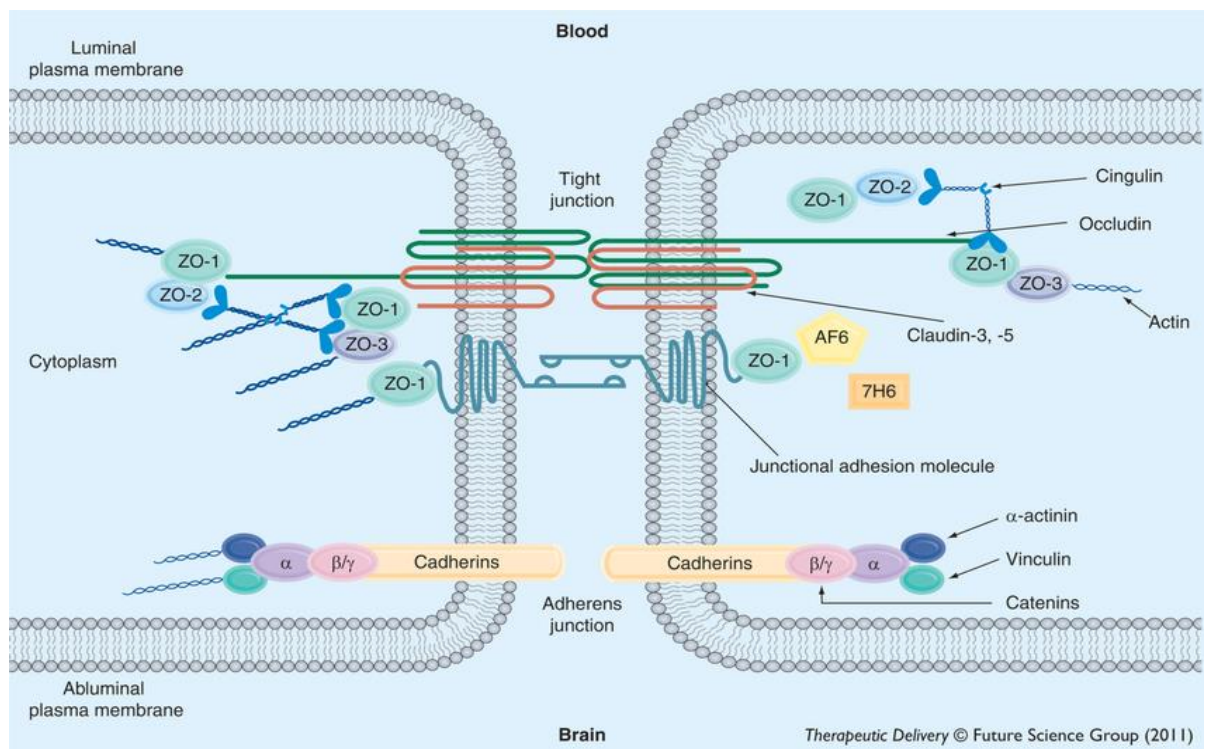


Figure 1.5 Constituents of endothelial cell tight junctions. Obtained from (Ronaldson and Davis, 2011).

Claudin, a 20 – 34 kDa integral membrane protein is a major component of the tight junctions and has been shown to play a vital role in tight junction formation. Of the 27 claudin proteins that exist, claudin 1, 3, 5 and 12 are expressed in brain endothelial cells *in vivo* (Nitta *et al.*, 2003). Claudin-5, specifically is highly expressed in brain endothelial cells (Morita *et al.*, 1999; Yamazaki *et al.*, 2017) and loss of claudin-5 can result in BBB disruption. Deletion of claudin-5 in mice resulted in an increase in BBB permeability and loosening of the BBB (Nitta *et al.*, 2003). Occludin is another important tight junction protein and is mainly linked to zonula

occludens (ZO). Occludin has been reported in the mouse and adult brains of humans but has not been shown in the normal newborn brain (Ballabh *et al.*, 2004). Reduction in barrier integrity was observed *in vitro* following occludin disruption, but this has not been observed in mice lacking occludin (McCarthy *et al.*, 1996; Saitou *et al.*, 2000; Yamazaki *et al.*, 2017). The zonula occludens consisting of ZO-1, ZO-2 and ZO-3 are members of the membrane-associated guanylate (MAGUK) family. They are involved in linking integral membrane proteins to the actin cytoskeleton. ZO-1 acts as a scaffold connecting tight junction proteins to the actin cytoskeleton and loss of this protein from tight junctions is associated with an increase in paracellular permeability of BBB *in vitro* (Mark and Davis, 2002). Besides, tight junctions, adherens junction proteins also regulate the permeability of the BBB. Adherens junctions are found below tight junctions and create a continuous band that holds adjoining cells together (Petty *et al.*, 2002). The adherens junction protein vascular endothelial (VE)-cadherin is a transmembrane protein found in endothelial cells and located at the junctions of endothelial cells (Giampietro, 2016). The cytoplasmic tail of VE-cadherin binds to p120 catenin and β catenin which in turn bind through α catenin and vinculin to the actin cytoskeleton (Cardoso *et al.*, 2010; Rimm *et al.*, 1995). Association of vinculin with adherens junction proteins protects VE-cadherin junctions from being disrupted during force-dependent remodelling (Huvneers *et al.*, 2012).

Disruption of tight junction and adherens junction proteins in the CNS can contribute to neurological diseases such as cerebral malaria and multiple sclerosis where BBB breakdown is thought to occur. A dramatic loss of claudin-5 and VE-cadherin was observed in the small vessels of post-mortem brain tissues of MS patients (Alvarez *et al.*, 2015; Tietz and Engelhardt, 2015). Loss of junction proteins vinculin, ZO-1 and occludin were observed in the blood vessels of post-mortem brain sections of CM patients (Brown *et al.*, 2001).

1.4.2 Basement membrane

The basement membrane (BM) is an important component of the BBB (Figure 1.4). At the BBB, two basement membranes occur, an endothelial BM and a parenchymal basement membrane formed by astrocytes (Baeten and Akassoglou, 2011). Under basal conditions, these BMs are observed as one unit under the light microscope. The extracellular matrix protein constitution in the parenchymal BM varies from that of other BMs, comprised of laminin isoforms 1 and 2 (Baeten *et al.*, 2011). The perivascular spaces are lined by the parenchymal BM (Baeten *et al.*, 2011). The basement membrane anchors endothelial cells and astrocytes, allowing these cells to control barrier function directly (Baeten *et al.*, 2011). Although endothelial cells and astrocytes secrete extracellular matrix (ECM) proteins, once secreted, ECM proteins are believed to communicate with these cells to activate and sustain barrier properties (Baeten *et al.*, 2011).

Disruption of the basement membrane is involved in several neurological disorders. Secretion of ECM protein such as neurocan (a chondroitin sulphate proteoglycan) from activated glia (which include astrocytes) or leakage of plasma protein such as fibrinogen into the brain during CNS disorders like stroke can lead to the deposit of new ECM proteins in the parenchyma while BMs of the BBB are destroyed (Baeten *et al.*, 2011; Baumann *et al.*, 2009; Schachtrup *et al.*, 2010). These alterations such as destruction of BMs may result in BBB break down and contribute to inflammation at the BBB (Baeten *et al.*, 2011).

1.4.3 Astrocytes

Astrocytes are glial cells whose end feet surround >99% of the brain capillaries. They are the most abundant cell type in the brain (Abbott, 2002; Abbott *et al.*, 2006; Cardoso *et al.*, 2010).

Even though astrocytes are heterogeneous, there are two main types of astrocytes that exist, protoplasmic and fibrous astrocytes (Figure 1.6). The protoplasmic astrocytes can be located in the grey matter and they surround neuronal bodies and synapse, whereas fibrous astrocytes can be found in the white matter and they associate with the nodes of Ranvier (Cabezas *et al.*, 2014). Both types of astrocytes have been shown to make extensive contact with blood vessels of the BBB (Sofroniew and Vinters, 2010). Astrocytes cover the whole basolateral side of the microvessels with specialised processes known as astrocyte end feet. These end feet have a high density of orthogonal array of particles (OAPs) containing the water channel aquaporin 4 (AQP4) and the potassium ion channel Kir 4.1 (Abbott *et al.*, 2006; Saadoun *et al.*, 2002) and these are attached to the basement membrane through the dystroglycan complex (Baeten *et al.*, 2011; Hawkins *et al.*, 2013).

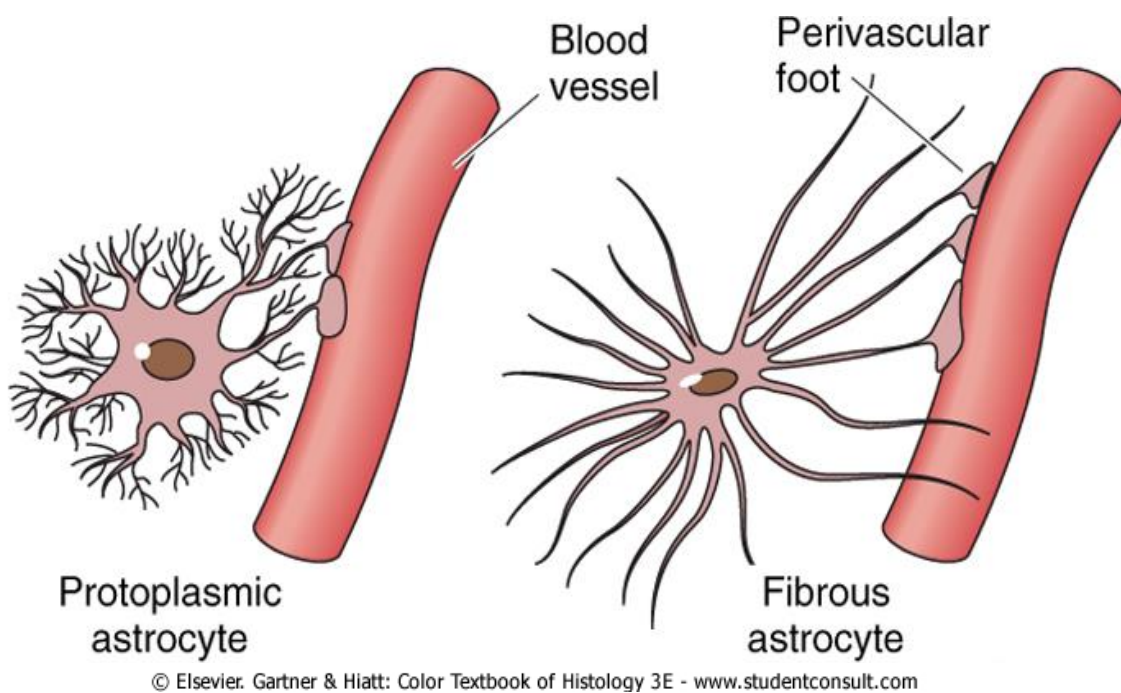


Figure 1.6 The two main types of astrocytes, protoplasmic and fibrous astrocytes. Protoplasmic astrocytes found in the grey matter have a thick process with many branches and fibrous astrocytes found in the white matter have long slender foot processes. Image obtained from (Timothy Jegla, 2015).

Astrocytes have many functions in the brain (Figure 1.7). They act as a connection between neurons and blood vessels. This neurovascular coupling allows astrocytes to send signals that control blood flow in reaction to neuronal activity (Attwell *et al.*, 2010; Daneman and Prat,

2015; Gordon *et al.*, 2011). Astrocytes also regulate synapse formation, provide essential support for neurons, protect neurons from harmful substances in blood and control brain homeostasis. They are essential for the formation of a tight and functional BBB by inducing BBB properties (Cabezas *et al.*, 2014). However, an *in vivo* study has shown that the BBB is present before astrocyte generation, suggesting that astrocytes play a role in the maintenance and not induction of the BBB (Daneman *et al.*, 2010, 2015).

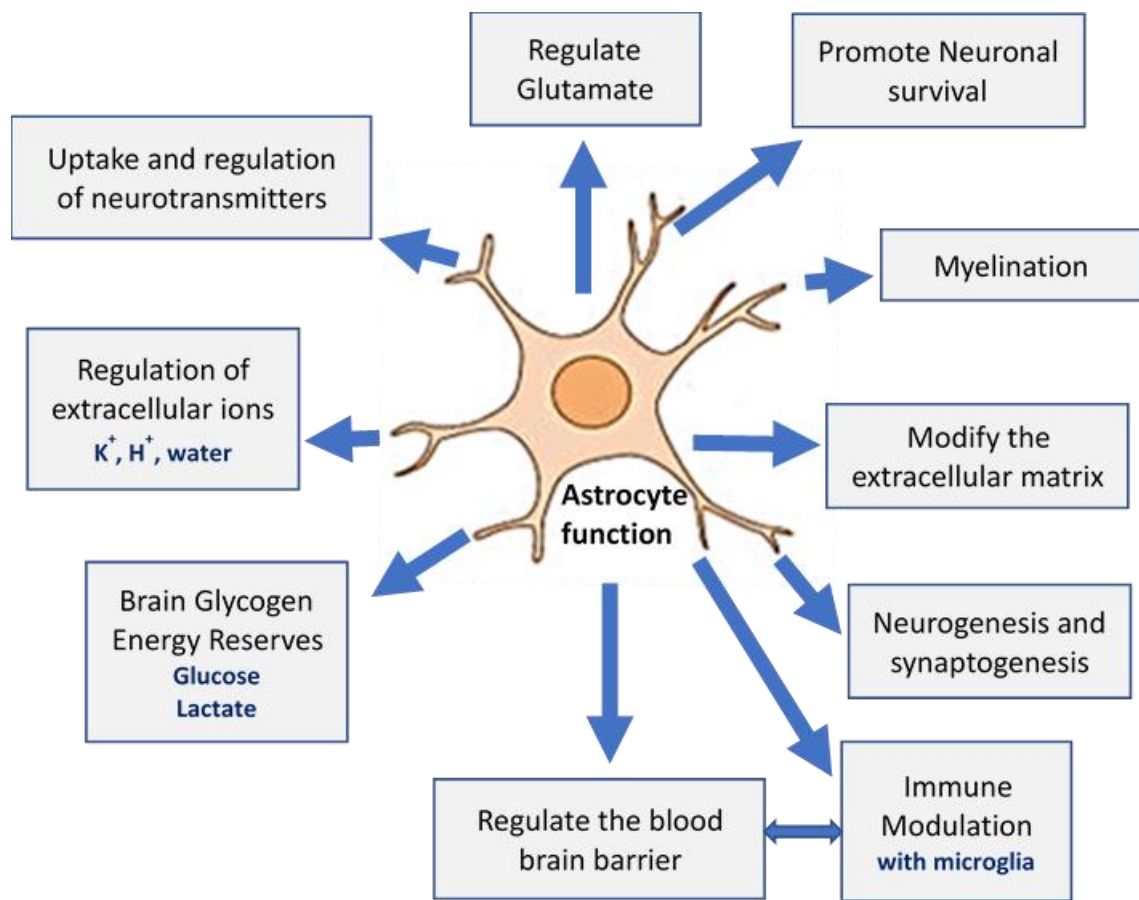


Figure 1.7 Function of astrocytes in the CNS. Image modified from (Magnusson and Frisén, 2016; VandenBerg, 2010).

Astrocytes secrete factors such as the sonic hedgehog (SHH), Src-suppressed C-kinase substrate (SSeCKS), angiotensinogen (AGT) and Apolipoprotein E that modulate the BBB (Alvarez *et al.*, 2013). SHH binds and blocks the receptor Patched (PTCH) on endothelial cells relieving repression of Smoothed (SMO) and results in activation of the glioma-associated oncogene homolog 1-3 (Gli1-3) transcription factors that activate the transcription factor Sox-

18 which has been shown to regulate expression of the tight junction protein claudin-5 and EC-BBB functions. (Alvarez *et al.*, 2013; Daneman *et al.*, 2015; Fontijn *et al.*, 2008; Obermeier *et al.*, 2013)

SHH promotes the quiescence of the human endothelial cell (EC)-BBB by reducing secretion of MCP-1, ICAM-1 and VCAM-1. Also, SHH induces expression of junctional proteins (Alvarez *et al.*, 2013, 2011). *In vitro*, culturing human recombinant SHH with human primary brain endothelial cells induced the expression of the junctional proteins occludin and claudin-5 (Alvarez *et al.*, 2013, 2011). Blocking of the Hh pathway *in vivo* caused an increase in BBB permeability (Alvarez *et al.*, 2013, 2011).

SSeCK activates astrocyte angiopoietin 1 (ANGPT-1) expression by decreasing the activity of the transcription factor activator protein 1 (AP-1). ANGPT-1 can activate the TIE2 receptor resulting in an increased expression of ZO-1 and Claudin-1 and decrease in the EC-BBB permeability *in vitro* (Lee *et al.*, 2003, Alvarez *et al.*, 2013)

Astrocytes produce the angiotensin-converting enzyme-1 (ACE-1) that cleaves angiotensin I (ANG1) to angiotensin II (Alvarez *et al.*, 2013). Angiotensin II binds to type I angiotensin receptors (AT1) present on brain endothelial cells and activation of AT1 restricts BBB permeability (Alvarez *et al.*, 2013). An irregular expression of occludin was observed in AT1 knockout mice and this was associated with a leaky BBB that was permeable to the serum protein plasminogen thus suggesting that AT1 can enhance formation of tight junctions in brain endothelial cells (Alvarez *et al.*, 2013; Wosik *et al.*, 2007).

Apolipoprotein E is secreted by astrocytes and delivers cholesterol and important lipids to neurons (Blanchette and Daneman, 2015). In ApoE knockout mice, BBB disruption that increased with age was observed (Alvarez *et al.*, 2013; Blanchette *et al.*, 2015; Nishitsuji *et al.*, 2011). A triple coculture *in vitro* BBB model consisting of endothelial cells and pericytes from wild type mice and astrocytes from ApoE3- and ApoE4- knock in mice, showed a decrease in

protein kinase C (PKC) activity and phosphorylation of occludin in ApoE4- against ApoE3- knock in the *in vitro* BBB (Alvarez *et al.*, 2013; Blanchette *et al.*, 2015; Nishitsuji *et al.*, 2011). A decrease in TEER was also observed in the in ApoE4-knock in BBB model (Alvarez *et al.*, 2013; Blanchette *et al.*, 2015; Nishitsuji *et al.*, 2011). These results suggested that ApoE4 secreted by astrocytes contributed to the regulation of tight junction proteins in the BBB (Alvarez *et al.*, 2013; Blanchette *et al.*, 2015; Nishitsuji *et al.*, 2011). Overall these studies show that astrocytes secrete essential factors that influence brain endothelial phenotype and that regulate the BBB.

A human genetic disease, Alexander disease, that affects astrocytes and is associated with BBB disruption, may shed light on the role of astrocytes in the BBB.

Alexander disease (AXD) is a neurodegenerative disease caused by a mutation in the glial fibrillary acidic protein (GFAP) gene (Sofroniew *et al.*, 2010). GFAP forms the cytoskeleton of astrocytes. In AXD clustering of intracellular GFAP, astrocytic protein aggregates (Rosenthal fibres) lead to astrocyte death (Sofroniew *et al.*, 2010). Severity of AXD varies according to the phenotype (infantile, juvenile or adult) (Sofroniew *et al.*, 2010). Neurodegeneration in AXD is associated with BBB breakdown increase in pinocytotic vesicles and sporadic damage of the basement membrane of the BBB (Keller, 2013; Mignot *et al.*, 2004).

Astrocyte activation occurs in response to several CNS injuries such as stroke, trauma, neurodegenerative diseases and CM and can result in astrogliosis (Pekny *et al.*, 2014; Pekny and Pekna, 2004). Reactive astrocytes undergo several morphological changes and can exert both beneficial and harmful effects (Pekny *et al.*, 2014, 2004). Protein markers used to identify astrocytes include Glial Fibrillary Acidic Protein (GFAP), Aquaporin 4 (AQP4), S100B and Aldehyde dehydrogenase 1A1 (ALDH1A1).

GFAP is the major intermediate filament (IF) of human astrocytes (Petzold, 2015) and is the main biomarker for detecting astrocytes in the human brain. GFAP is tightly arranged into polymers and it forms a cross-linked cytoskeletal network organised by monomers (49.8kDa), dimers and tetramers. In each of these individual stages, GFAP assembly can be controlled by amino acid replacements produced as a result of post-translational modifications, gene mutations, competing isoforms of GFAP and proteins such as S100 and vimentin (Petzold, 2015) (Tykhomyrov and Nedzvetsky, 2016). GFAP is insoluble in intact astrocytes, however, astrogliosis can result in the production and release of soluble fragments of GFAP. The protease calpain is thought to cause this GFAP degradation resulting in the conversion of GFAP from ~50kDa into soluble fragments of 39-44kDa (Petzold, 2015; Yang and Wang, 2015). GFAP breakdown products were observed in the serum of patients with traumatic brain injury (TBI) within an hour of injury (Papa *et al.*, 2012). Increased GFAP breakdown products (BDP) were linked with TBI severity (Papa *et al.*, 2012). GFAP is rapidly altered following stimuli and injury of astrocytes. These morphological modifications can be observed in the different stages of astrogliosis described in chapter 5 (Petzold, 2015).

1.5 CM and BBB

Evidence from post-mortem studies, *in vitro* and *in vivo* models of CM suggest that the BBB is impaired during cerebral malaria. Examination of post-mortem brain tissues of CM patients showed a reduction in junction proteins vinculin, ZO-1 and occludin in blood vessels where PRBC sequestration was present (Brown *et al.*, 2001, 1999). Also, *in vitro* studies showed a reduction in endothelial electrical resistance of HBEC following coculturing of PRBC with HBEC (Tripathi *et al.*, 2006). A reduction in mRNA levels of occludin, ZO-1 and vinculin were observed when PRBC from patients with CM was cocultured with Human umbilical vein endothelial cells (HUVEC) (Susomboon *et al.*, 2006). However coculturing PRBC from

patients with severe malaria and uncomplicated malaria produced an increase and no change in mRNA levels of occludin, ZO-1 and vinculin respectively (Susomboon *et al.*, 2006). These results suggest that a reduction in junction proteins during cerebral malaria could result in BBB disruption and leakage across the BBB.

In the post-mortem brain tissues of Vietnamese adults who died from CM, fibrinogen (found in the blood) was present in the perivascular space and there was some uptake of fibrinogen by astrocyte end feet (Brown *et al.*, 1999; Polimeni and Prato, 2014). Also, the perivascular macrophages showed an increased expression of macrophage markers, macrophage scavenger receptor and sialoadhesin (Brown *et al.*, 1999; Polimeni *et al.*, 2014). Sialoadhesin and macrophage scavenger receptor are not typically expressed in the brain by the perivascular macrophages (Brown *et al.*, 1999; Polimeni *et al.*, 2014). Hence, upregulation of these markers imply that plasma proteins have moved across the BBB and have been in contact with the perivascular macrophages in the Virchow-Robin space, a compartment surrounding small cerebral blood vessels that penetrate the brain parenchyma (Brown *et al.*, 1999; Polimeni *et al.*, 2014). These results suggested that BBB disruption occurred in CM, resulting in the leakage of proteins from the blood into the brain.

Changes in CSF composition have been used to determine if the BBB integrity is compromised in several CNS diseases. The albumin CSF/serum ratio was used as an indicator of BBB integrity (Polimeni *et al.*, 2014). It is thought that local alterations in the BBB will also be seen at the blood-CSF barrier resulting in alterations in the compositions of proteins found in the CSF (Medana and Turner, 2006). In adults, CSF albumin ratios suggested that subtle BBB breakdown was present in some CM patients (Brown *et al.*, 2000; Polimeni *et al.*, 2014). However, in children with CM, a marginal but significant increase in the albumin CSF/plasma ratio was observed (Brown *et al.*, 2001; Polimeni *et al.*, 2014).

These results suggest that BBB breakdown in CM is more frequent in children than in adults. Indeed, CM occurs at an important stage in brain development in children and thus developmental changes in the neurovascular unit could be responsible for the differences and outcomes in clinical presentations of CM between adults and children (Adams *et al.*, 2002; Hawkes *et al.*, 2013).

Several lines of evidence suggest a possible role of matrix metalloproteases (MMPs) in severe malaria and CM. In human post-mortem brain tissues of CM patients, increase in MMP-1 levels was observed (Deininger *et al.*, 2003). Also, an increase in serum levels of MMP-8 and TIMP1 was observed in serum of patients with severe malaria and uncomplicated malaria as compared to the serum of healthy individuals (Dietmann *et al.*, 2008). Results from a genome-wide analysis showed an increase in MMP-9 mRNA expression in blood cell samples from Kenyan children with severe malaria (Griffiths *et al.*, 2005). *In vitro* studies by D'Alessandro *et al.* (2013) showed that coculturing of human microvascular brain endothelial cells with PRBC resulted in the release of proMMP-9 and active MMP-9 (D'Alessandro *et al.*, 2013). MMPs cleave a huge variety of molecules including ECM proteins and tight junction proteins such as occludin, ZO-1, and claudin-5 (Giebel *et al.*, 2005; Gurney *et al.*, 2006; Nagase and Woessner Jr, 1999; Polimeni *et al.*, 2014; Qiu *et al.*, 2011). Excess production of MMPs, if not controlled by their inhibitors could possibly contribute to BBB impairment observed in CM patients.

1.5.1 Astrogliosis and cerebral malaria

Investigations from human CM models and experimental murine cerebral malaria (EMCM) models implicate a role of astrocytes in cerebral malaria pathogenesis. During CM the breakdown of the BBB allows leakage of normally restricted substances such as plasma

proteins, cytokines and malaria antigens into the brain. This could result in the activation and/or damage of astrocytes in the brain.

In the brain of Vietnamese patients who died from severe malaria, an increase in astrogliosis was observed (Medana *et al.*, 2002). Analysis of CSF markers S-100B (for astrocytes) and microtubule associated protein tau (for degenerated axons tau) in Kenyan children with varying neurological severities of malaria (Medana *et al.*, 2007) showed that the level of tau proteins in CSF was significantly elevated in children with CM (coma) as compared to children with malaria with seizures but normal consciousness (Medana *et al.*, 2007). The levels of S-100B proteins in CSF was higher in patients with CM compared with non-CM patients however this was not statistically significant. Children admitted with raised levels of S-100B had an increased risk of repeated seizures (Medana *et al.*, 2007). These results suggested that astrocytes contributed to seizure activity. The data implied that the occurrence of seizures post admission was possibly an exhibition of neurological damage and not a cause of brain damage (Medana *et al.*, 2007). Significantly higher levels of tau observed in CM patients (coma) suggested that axonal injury was associated with coma that occurs in CM (Medana *et al.*, 2007). Similarly, results from an autopsy study on Malawian children who died from CM showed the presence of axonal and myelin injury and this was linked with ring haemorrhages located in the white matter and brainstem of CM patients (Dorovini-Zis *et al.*, 2011). In this study, astrogliosis was observed in the brain tissues of CM patients but the severity of astrogliosis ranged from mild to moderate (Dorovini-Zis *et al.*, 2011).

Immunohistochemistry studies comparing astrogliosis and perivascular GFAP expression between EMCM and non-EMCM mice showed a higher GFAP expression in the perivascular area of EMCM mice than non-EMCM mice (Ampawong *et al.*, 2014), with an increasing

number of large astrocytes clusters observed in EMCM mice. These results provide evidence that during EMCM, astrogliosis and astrocyte hypertrophy occurs (Ampawong *et al.*, 2014).

In vivo studies using mice infected with *P. berghei* ANKA suggest that astrocytes are activated during EMCM. Medana *et al.* (1996) using retinal whole mount techniques, showed that astrocyte activation occurred prior to the onset of EMCM (Medana *et al.*, 1996). In this study breakdown of the BBB resulted in morphological changes in astrocytes. Loss of astrocyte ensheathment of vessel segment was only observed in the fatal model of EMCM (Combes *et al.*, 2012; Medana *et al.*, 1996). Treatment of fatal EMCM mice with an immunosuppressive and the anti-inflammatory agent dexamethasone stopped astrocyte loss (Medana *et al.*, 2000, 1996). These results suggested that the inflammatory response produced during fatal EMCM could have been responsible for the astrocyte loss observed.

Activated astrocytes are known to also release several pro- and anti-inflammatory cytokines such as interleukins, interferons, tumour necrosis factors and chemokines. It has been suggested that astrocytes can participate in the inflammatory response that occurs in the brain parenchyma during CM (Garwood *et al.* 2011). Immunohistochemistry studies on the brain of fatal murine cerebral malaria (FMCM) mice showed the presence of TNF α mRNA and proteins in astrocytes, microglia and cerebral vascular endothelium of FMCM mice but were absent in the brain of uninfected mice. These results suggest that TNF α is a key facilitator of FMCM pathogenesis and that astrocytes contribute to the inflammatory response observed in FMCM (Medana, Hunt & Chaudhri 1997).

The studies above implicate a role for astrocytes in the pathogenesis of cerebral malaria.

Although mouse models have been used extensively to study the role of the BBB in cerebral malaria, the pathology of EMCM appears to be different than that of human cerebral malaria.

Very little or no sequestration of infected red blood cells is observed in EMCM, whereas sequestration of PRBC has been observed in post-mortem brain tissues of CM patients (Brown *et al.*, 2001, 1999; Polimeni *et al.*, 2014). Also, a strong breakdown of the BBB is observed in EMCM whereas in human CM models moderate BBB disruption occurs (Polimeni *et al.*, 2014). EMCM is characterised by marked inflammation and local vascular endothelial activation (De Souza *et al.*, 2018; Hansen, 2012; Reichmann *et al.*, 1999). Thus, the use of EMCM as a model for human CM is contentious and caution must be taken when interpreting the results obtained from EMCM (Craig *et al.*, 2012).

1.6 Hypothesis of cerebral malaria

Despite the vast amount of research in CM, the pathogenesis resulting in CM is still not fully understood. During CM, PRBC do not enter the brain parenchyma but bind to the endothelial cells of the blood-brain barrier causing devastating neurological damage. This poses the question of how the *P. falciparum* parasite can induce such detrimental neurological effects in CM without crossing the BBB. There are two theories that exist to explain the pathogenesis of CM, the sequestration hypothesis and inflammation hypothesis. Summary of these theories can be seen in Figure 1.8.

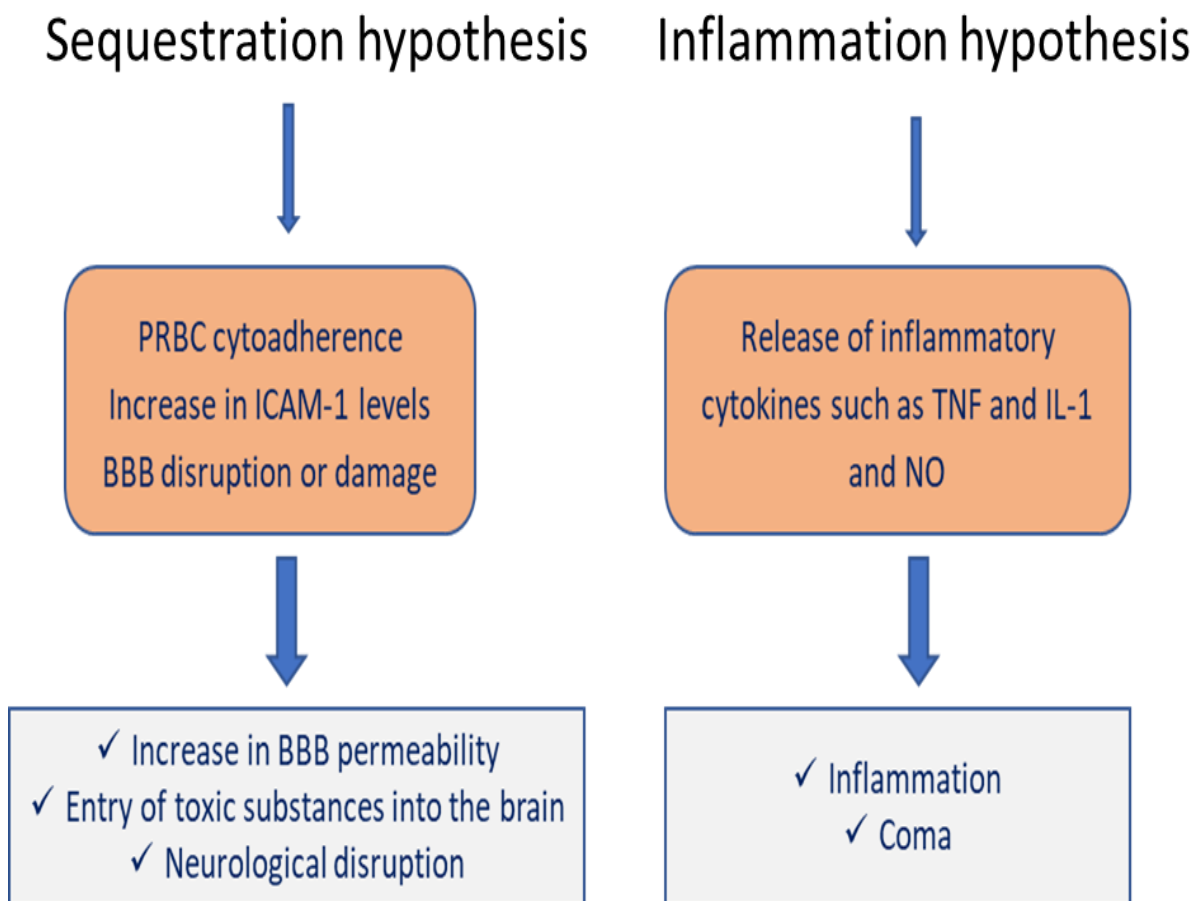


Figure 1.8 Hypothesis explaining the pathogenesis of cerebral malaria.

1.6.1 Sequestration hypothesis

PRBC in the late stages of the intraerythrocytic cycle (late trophozoite and schizont stage) disappear from the peripheral blood and cytoadhere to the microvascular endothelium of vital organs including the brain (Figure 1.9), heart, kidney and liver in a process termed sequestration (Mebius and Kraal, 2005). Cytoadherence is beneficial to the *P. falciparum* parasite, as binding of the parasite to the vascular endothelium prevents the parasite from being cleared by the spleen which recognises the loss of deformability of the PRBC (Mebius *et al.*, 2005).

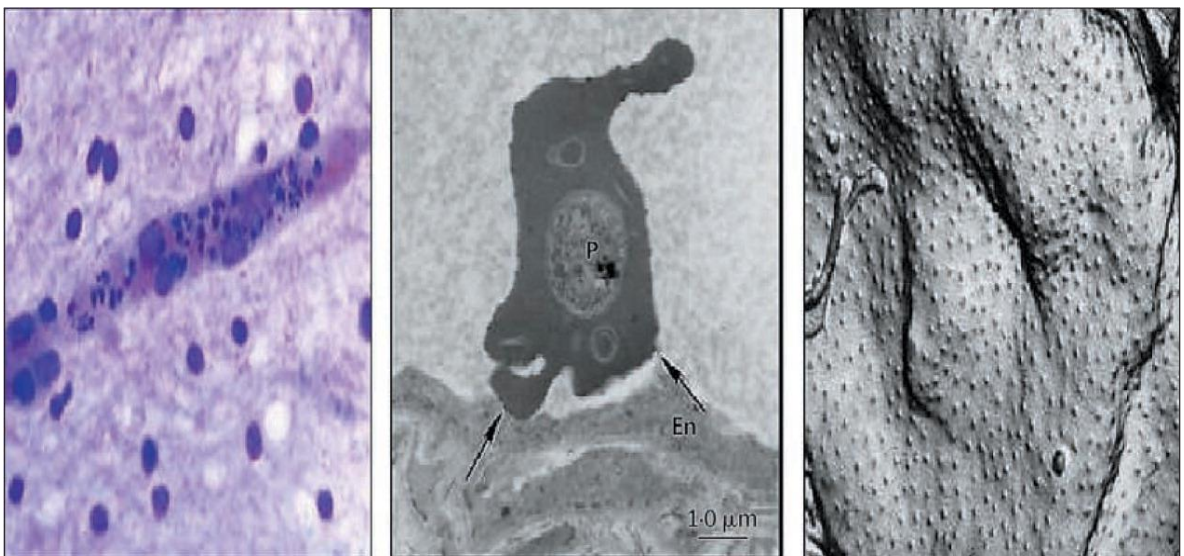


Figure 1.9 *Plasmodium falciparum* infected red blood cells sequestered to blood vessels in the brain.

Obtained from (Idro *et al.*, 2005). Left: Sequestration of PRBC to post-mortem cerebral vessel of a Vietnamese adult with fatal malaria X400. Middle: Electron microscopy image showing the ultrastructural details of a PRBC bound to an endothelial cell *in vitro*. P= parasite, En=endothelial cells. Right: freeze-fracture electron micrograph of PRBC surface showing an even distribution of knob proteins on the surface. Image and Legend obtained from (Idro *et al.*, 2005).

Also, cytoadherence allows the parasite to sequester into deeper tissues where it can develop and mature in a microaerophilic venous environment that is more suitable for the parasite.

Sequestration of PRBC in the brain microvascular endothelium is the hallmark of CM.

Even though sequestration can be found in the brain of non-CM patients, levels of sequestered PRBC are particularly higher in the brains of CM patients (MacPherson *et al.*, 1985; Milner Jr *et al.*, 2014). Evidence from several post-mortem studies suggest a correlation between

sequestration and CM. Post-mortem studies of Thai patients who had died from malaria showed a high accumulation of PRBC in the cerebral vasculature as compared to other organs such as the lung and kidney (MacPherson *et al.*, 1985; Turner *et al.*, 1994). These results were consistent with post-mortem microscopy studies of Vietnamese adults who died from CM, where a significantly higher number of PRBC were found in the cerebral microvasculature of CM patients than non-CM patients (Ponsford *et al.*, 2012). Also, in this study, microvascular obstruction by PRBC and uninfected red blood cells was observed in the brains of patients with CM.

Indeed, in CM, increased stiffness of PRBC and sequestration can cause vascular occlusion (Dunst *et al.*, 2017; Ponsford *et al.*, 2012). Similarly, rosetting, the binding of uninfected red blood cells by PRBC and aggregation of PRBC and platelets (clumping) can also exacerbate microvascular obstruction in CM (Dunst *et al.*, 2017; Rowe *et al.*, 2009). Malaria severity is associated with rosetting in several African studies. In clinical isolates of 209 Malian children with severe malaria, rosetting was considerably increased in parasite isolates from patients with severe malaria as compared to patients with uncomplicated malaria (Dumbo *et al.*, 2009). Also, *in vitro* studies on parasite isolates of Kenyan children with CM showed that, in the presence of platelets, PRBC formed clumps that were made up of 3 or more PRBC clustered together (Dunst *et al.*, 2017; Pain *et al.*, 2001).

Microvascular congestion could result in a decrease in blood flow, ischaemia and reduced oxygen supply (hypoxia) (Dunst *et al.*, 2017) and this could contribute to the CM pathology.

1.6.1.1 Parasite sequestration and specific receptor mediated adhesion

During the intraerythrocytic stage of *P. falciparum* life cycle, the parasite remodels the host cells through the transport of parasite-derived proteins such as the *Plasmodium falciparum*

erythrocyte membrane protein (PfEMP1) to the erythrocyte membrane (Baruch *et al.*, 2002; Grau and Craig, 2012; Gruenberg *et al.*, 1983; Leech *et al.*, 1984).

PfEMP1 is a high molecular weight protein of 240kDa, encoded by a family of approximately 60 var genes (Guizetti and Scherf, 2013). At any given time, a single var gene is expressed on the surface of the PRBC; each mature parasite expresses only one PfEMP1 variant (Baruch *et al.*, 1995; Smith *et al.*, 2013, 1995; Su *et al.*, 1995). *P. falciparum* evades the host immune system by switching a small population of parasite clones to a different PfEMP1 variant (Scherf *et al.*, 1998). The different binding phenotypes of PfEMP1 allow the parasite to cytoadhere within the microvasculature of different organs in the host (Pasternak and Dzikowski, 2009; Scherf *et al.*, 2008).

1.6.1.2 Structure of PfEMP1

PfEMP1 is made up of seven Duffy Binding Like (DBL) domains and cysteine rich interdomain region (CIDR) domain. PfEMP1 can be subdivided into three main groups A-C (Figure 1.10) (Bengtsson *et al.*, 2013). Based on sequence, the PfEMP1 domains can be further divided into domain cassettes that play a vital role in malaria. Domain cassettes DC8 and DC13 have been shown to be associated with severe malaria (Figure 1.10). PfEMP1 has variable binding extracellular domains that can adhere to multiple host receptors including intercellular adhesion molecule 1 (ICAM-1), vascular cell adhesion molecule-1 (VCAM1), chondroitin sulphate A (CSA), CD36, endothelial protein C receptor (EPCR) and P-selectin (Beeson *et al.*, 2000; Chakravorty and Craig, 2005; Esser *et al.*, 2014; Ho *et al.*, 2000; Smith and Craig, 2005; Viebig *et al.*, 2007). PfEMP-1 mediates binding of PRBC to the microvasculature of organs such as the brain, lung, heart, liver, kidney and placenta (El-Assaad *et al.*, 2013).

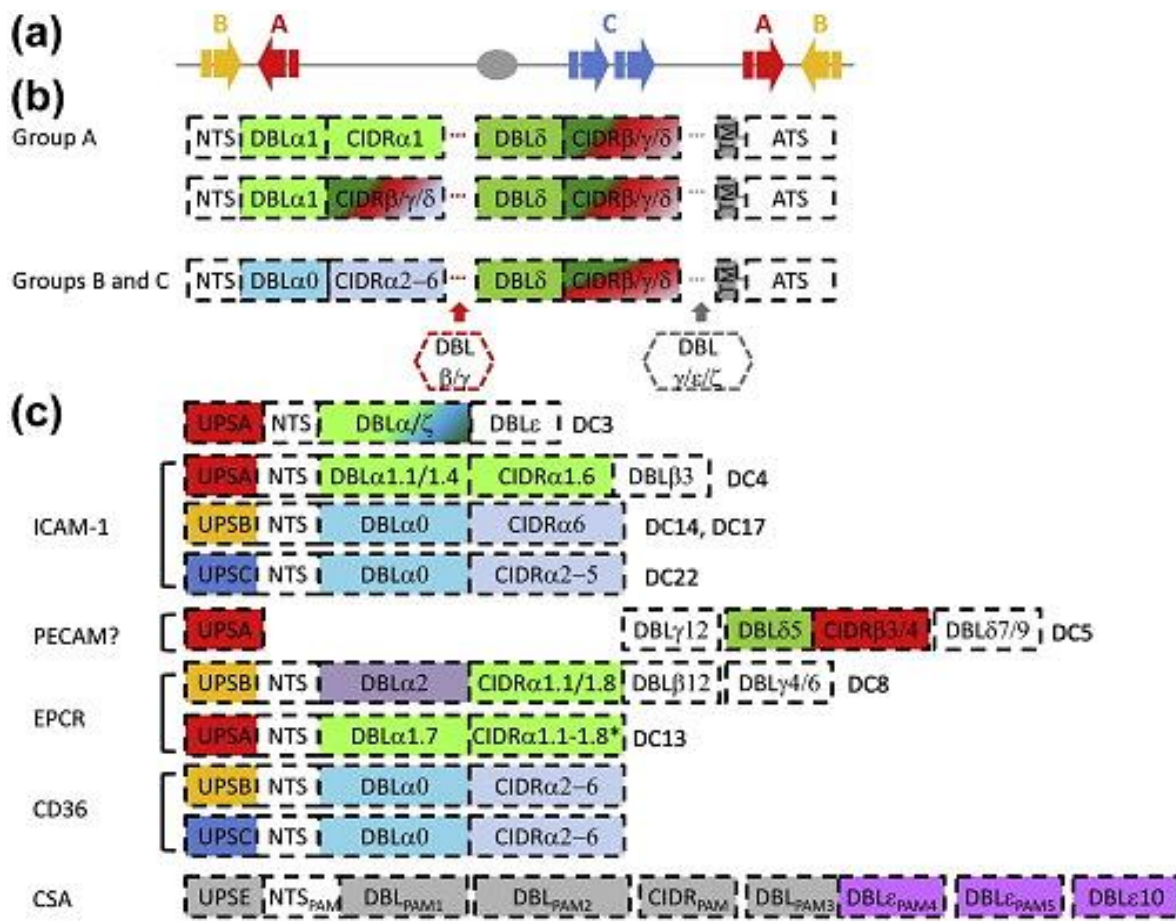


Figure 1.10 Receptor-binding domains on PfEMP1. Image obtained from (Hviid and Jensen, 2015).

1.6.1.3 CD36

The receptor CD36 can be found in several tissues. Binding of PfEMP1 to CD36 mediates sequestration of PRBC to varying sites in the vascular endothelium such as adipose tissue and skeletal muscles but not the brain. Binding of PfEMP1 to CD36 is linked to uncomplicated malaria but not severe malaria.

PRBC isolates from CM Benin patients were shown to cytoadhere better to CD36 as compared to that of uncomplicated malaria isolates (Almelli *et al.*, 2014). Although CD36 is not expressed by brain endothelial cells, *in vitro* studies showed that platelets could act as bridges between CD36 deficient brain endothelial cells and PRBC (that only bind CD36 expressing cells) and can thus contribute to sequestration of PRBC to brain endothelial cells during CM (Wassmer *et al.*, 2004). However, studies by Ochola *et al.* (2011) show that adhesion of

PfEMP-1 to CD36 is raised in parasites from uncomplicated malaria patients whereas binding of ICAM-1 is higher in parasite isolates from CM patients (Ochola *et al.*, 2011). These results suggest that ICAM-1 is the main receptor PRBC bind to on the endothelial cells of the BBB during CM.

1.6.1.4 ICAM-1

ICAM-1 is a 90-115kDa cell surface glycoprotein, composed of five immunoglobulin (Ig)-like domains. It is expressed on several cell types including endothelial cells, astrocytes and leukocytes. ICAM-1 has been shown to play a role in malaria. The DBL β 2-C2 region of PfEMP-1 was previously thought to be the binding domain of ICAM-1 because constructs that contained only one domain of PfEMP-1 i.e. only the DBL β 2 or the C2 domain, did not bind ICAM-1 (Chakravorty *et al.*, 2005; Smith *et al.*, 2000a, 2000b).

Recent studies have shown that DC4 domain cassette of PfEMP-1 binds specifically to ICAM-1 particularly to the DBL- β 3-D4 domain (Figure 1.10) (Bengtsson *et al.*, 2013). CIDR α 1.6 present in DC4 was observed in *P. falciparum* isolates from CM patients (Figure 1.10) (Bengtsson *et al.*, 2013). Also, PRBC that expressed DC4 containing PfEMP-1 proteins did not cytoadhere to CD36 (Bengtsson *et al.*, 2013). Since CD36 is not found on endothelial cells in the brain this suggests that during CM, DC4 domain cassette of PfEMP-1 binds specifically to ICAM-1 on brain endothelial cells (Bengtsson *et al.*, 2013).

Panning studies revealed that ICAM-1 did not bind to DC8 and DC13, domains shown to be associated with severe malaria. Nonetheless, several post-mortem studies have implicated the role of ICAM-1 in cerebral malaria. Post-mortem examinations of Thai patients who died from cerebral malaria showed an increased endothelial expression of ICAM-1 in the brain microvasculature in association with sequestration (Turner *et al.*, 1994). Parasite isolates from children with severe malaria showed higher binding to ICAM-1 compared to that of

uncomplicated malaria. Soluble ICAM-1 (sICAM-1) can be detected in the blood after proteolytic cleavage from the endothelial cell surface and has also been shown to be increased in CM patients. Analysis of plasma levels of sICAM-1 in 69 children with malaria, (37 with cerebral malaria and 32 with uncomplicated malaria), showed significantly elevated levels of soluble ICAM-1 in patients with CM as compared to those with uncomplicated malaria (Adukpo *et al.*, 2013). *In vitro* studies also support a role of ICAM-1 in sequestration and severe malaria. Tripathi *et al.* (2006) showed that exposure of HBEC to PRBC resulted in an upregulation of ICAM-1 on HBEC (Tripathi *et al.*, 2006).

ICAM-1 expression in endothelial cells can be stimulated by inflammatory cytokines such as IL-1 β and TNF α . Studies by Chakravorty *et al.* (2007) showed that exposure of HUVEC to PRBC and low levels of TNF α (5pg/ml) was vital for the upregulation of ICAM-1 in endothelial cells *in vitro* (Chakravorty *et al.*, 2007). The authors also showed that trypsin digestion of PfEMP-1 from PRBC did not affect upregulation of ICAM-1 expression that was caused by PRBC binding to endothelial cells (Chakravorty *et al.*, 2007). However, when PRBC were no longer in contact with endothelial cells, upregulation of ICAM-1 did not occur (Chakravorty *et al.*, 2007). This study suggested that close apposition of PRBC and endothelial cells play a key role in the activation of endothelial cells during CM (Chakravorty *et al.*, 2007).

It has been suggested that ICAM-1 is not the main receptor for adherence of PfEMP-1 to endothelial cells during cerebral malaria. Recent studies have implicated a role for the endothelial protein c receptor (EPCR) in cerebral malaria.

1.6.1.5 Endothelial Protein C receptor (EPCR)

EPCR promotes activation of Protein C and thus contributes to the anticoagulant pathway. Dysfunction of the Protein C anticoagulant system can result in interruption of the endothelial barrier function and promote inflammation. *In vitro* studies show that binding of PRBC to

EPCR prevents EPCR facilitated induction of Protein C (Mosnier and Lavstsen, 2016; Storm and Craig, 2014). This could be responsible for BBB disruption and inflammation observed in CM. Recent studies implicate a role of EPCR in CM. Post-mortem brain samples from CM patients showed that loss of EPCR in the cerebral microvessels was associated with sequestration of PRBC (Moxon *et al.*, 2013). These authors also showed reduced levels of EPCR and its coagulation partner thrombomodulin in CM patients compared to healthy controls (Moxon *et al.*, 2013). Domain cassettes (DC) of PfEMP-1 DC8 and DC13 have been shown to bind EPCR (Figure 1.10) (Turner *et al.*, 2013). Increased levels of EPCR binding to PfEMP-1 were higher in patients with severe malaria compared to patients with asymptomatic malaria (asymptomatic *Plasmodium falciparum*) (Shabani *et al.*, 2017).

Interestingly, certain PRBC lines have also been found to bind to both ICAM-1 and EPCR (Ndam *et al.*, 2017). Ndam *et al.* (2017) showed that binding to ICAM-1 and EPCR was more frequent in PRBC isolates from CM patients than uncomplicated malaria (Ndam *et al.*, 2017). Dual EPCR and ICAM-1 binding activities were observed in PRBC expression group A DC-13 containing PfEMP-1 variants (Ndam *et al.*, 2017). The ability of some PfEMP-1 variants to bind both ICAM-1 and EPCR in CM could suggest that both receptors play a vital role in CM.

In the sequestration hypothesis, cytoadherence of PRBC to the brain microvasculature causes obstruction of blood flow, a reduction in tissue perfusion and a decrease in the removal of waste metabolites (lactic acid) (Idro *et al.*, 2010). Impaired perfusion can cause hypoxia and this could result in comas (Idro *et al.*, 2010, 2005; van der Heyde *et al.*, 2006). Also, lactic acid produced in response to microvascular obstruction is linked to disease severity of CM (van der Heyde *et al.*, 2006).

The sequestration hypothesis on its own does not fully explain the CM pathogenesis. Clinical data show a small correlation between mortality and parasitaemia. Indeed, symptomatic patients sometimes show low parasitaemia whereas asymptomatic patients show high parasitaemia (van der Heyde *et al.*, 2006). This hypothesis also suggests obstruction of blood vessels in CM occurs like in stroke. However, in cerebral malaria, 10% of CM patients are left with neurological deficits whereas in stroke 81% of survivors show motor and neurological deficits (van der Heyde *et al.*, 2006). Also, recovery occurs quickly in CM possibly ruling out a role for ischemic damage and necrosis in CM (van der Heyde *et al.*, 2006). In addition, PRBC sequester to endothelial cells in organs such as the small intestine and the heart without producing significant detrimental effects (Martins and Daniel-Ribeiro, 2013). Moreover, sequestration is not present in all brain post-mortem tissues of patients who died from CM (van der Heyde *et al.*, 2006). Sequestration was absent in a fraction of post-mortem brain tissues from Malawian children who died from CM (Rénia *et al.*, 2012). Nonetheless, it is possible that post-mortem studies were done on CM brain tissues where the previously sequestered PRBC had been cleared probably by antimalarial drugs, but these treatments failed to stop the sequence of events resulting in CM (Rénia *et al.*, 2012). This might mean that other factors may contribute to CM.

1.6.2 Inflammation hypothesis

The inflammation hypothesis proposes that PRBC derived toxins and host intracellular molecules in the circulation activate a systemic inflammatory response that results in multi-organ failure and death (Martins *et al.*, 2013; van der Heyde *et al.*, 2006).

During the erythrocytic life cycle of *P. falciparum* malaria, rupture of schizonts releases parasite products such as glycosylphosphatidylinositol (GPI) and haemozoin (HZ) from the parasite digestive vacuole (Clark *et al.*, 1981; Olivier *et al.*, 2014).

These parasite products bind to pattern recognition receptors found in cells of the innate immune system and activate dendritic cells monocytes and neutrophils on the endothelial cells to secrete proinflammatory cytokines such as interleukin (IL)-1, IL-6, TNF (Martins *et al.*, 2013; van der Heyde *et al.*, 2006). This can lead to CD4⁺ and CD8⁺ recruitment and further production of proinflammatory cytokines (Martins *et al.*, 2013). In the initial stages of inflammation, the inflammation response can remove parasite products and host molecules that are toxic in large quantities (Martins *et al.*, 2013). However, when unregulated, it can have detrimental effects on the host. Increasing parasitaemia results in a higher amount of Hz being engulfed by dendritic cells. This can impair the functions of dendritic cells leading to detrimental effects on the T cell response and promoting immune suppression in acute *Plasmodium* infection (Millington *et al.*, 2006; Urban and Todryk, 2006).

TNF is the major cytokine involved in CM and linked with severity of malaria. TNF α can also activate and increase the production of nitric oxide (NO) through the NO synthase (iNOS) and this has been suggested to be responsible for the coma observed in CM patients (Clark *et al.*, 1992; Jain *et al.*, 2013). NO is thought to play both a negative and positive role during cerebral malaria based on the amount of NO being generated (Idro *et al.*, 2005; Jain *et al.*, 2013).

Increased levels of proinflammatory cytokines are associated with malaria. High levels of TNF α , IFN- γ , IL-2, IL-8 were observed in the serum of malaria patients (Mandala *et al.*, 2017). The inflammatory hypothesis on its own does not depict the malaria pathogenesis for the following reasons mentioned below.

Serum levels of TNF α in patients with *P. vivax* were higher than patients with CM (Hunt *et al.*, 2014; Karunaweera *et al.*, 1992). Also, administration of an anti-TNF monoclonal antibody (B7) to 610 Gambia children with CM did not improve survival of cerebral malaria in these patients and rather a marked increase in neurological sequelae was found in these patients (Hunt *et al.*, 2014; van Hensbroek *et al.*, 1996).

A review of these hypotheses suggests that the pathogenesis of cerebral malaria is a multifactorial process and one hypothesis cannot explain the complex events that occur in cerebral malaria.

Although the presence of astrocyte activation has been reported in CM post-mortem studies, these investigations fail to explain the cause and consequence of astrogliosis in cerebral malaria. Also, *in vivo* mouse models show astrogliosis in the mouse brain, but as mentioned previously EMCM is not the same as human cerebral malaria and this makes it difficult to make an inference from the results obtained in these types of experiments. *In vitro* studies exist to study cerebral malaria, but most of these studies focus on what happens when the PRBC bind to endothelial cells of the BBB and the other components that make up the BBB such as astrocytes are not taken into consideration. Thus, there is a need to develop *in vitro* CM models where components of the NVU are considered.

A population of patients who survive CM even after treatment are left with long-term neurological sequelae and the exact cause of these disabilities is not understood. Astrocytes are in close proximity to endothelial cells of the BBB and contribute to normal functions of neurons in the CNS. Thus, we hypothesise that astrocyte activation or damage contributes to the neurological sequelae observed in some CM survivors.

1.7 Aims of thesis

The aim of my thesis is to:

1. Develop a novel *in vitro* HBEC-astrocyte BBB model that mimics the BBB more closely in order to understand the pathogenesis of CM
2. Investigate the effect of endothelial cell-derived factors produced in response to sequestration of PRBC on endothelial cells and astrocytes of the BBB during CM using the HBEC-astrocyte BBB model
3. Investigate the effect of endothelial cell-derived factors produced in response to sequestration of PRBC on the integrity of the HBEC-astrocyte BBB model
4. Investigate the effect of serum obtained from malaria patients on the integrity of the BBB

Chapter 2 : General Materials and Methods

2.0 Materials and Methods

This chapter describes the materials and methods common to most of the experiments performed in this thesis. The specific methods for each experiment can be seen in the chapter to which they are unique. Unless specified otherwise, materials, media, reagents, antibodies and equipment used in this thesis are detailed in the Appendix. Storage and disposal of human cells and blood was done in agreement with the Human Tissue Authority (HTA) license held by Keele University.

2.1 Transformed Human Brain Endothelial cells

The transformed human brain endothelial cells (a kind gift from Dr. Monique F Stins, John Hopkins University, Baltimore, USA) were used in this study. Human brain endothelial cells were isolated from human brains and immortalised by transfection with the simian virus 40 large T antigen (Stins *et al.*, 1997). The cells were characterised and positive for VIII-Rag and uptake of Dil Ac LDL (Stins *et al.*, 1997).

Transformed Human Brain endothelial cells (HBEC) were cultured in an aseptic environment using a Class II biological safety cabinet with filtered laminar air flow. HBEC were grown in a vented 25 cm² cell culture flask pre-coated with 1% gelatin (Sigma). HBEC were grown in Roswell Park Memorial Institute (RPMI)-1640 Medium containing 2mM L-Glutamine (Sigma), 100 units/ml penicillin and 100µg/ml of streptomycin per ml (Sigma), 5% new born calf serum (Sigma), 10% Fetal Bovine Serum (FBS) (Sigma) at 37°C in 5% CO₂ humidified atmosphere. Culture media of HBEC were changed every 48 hours with HBEC medium. In all studies, HBEC from passage 22 to 29 were used.

2.2 Astrocytes

Primary human astrocytes were cultured in an aseptic environment using a Class II biological safety cabinet with filtered laminar air flow. Primary cultures of human astrocytes were obtained from ScienCell Research Laboratories. Astrocytes were isolated from the cerebral cortex of the human brain (Sciencell). Astrocytes were grown in a vented 25 cm² cell culture flask pre-coated with 1% gelatin (Sigma). Astrocytes were grown in astrocyte media (Sciencell) supplemented with 1% of 10,000 unit/ml of penicillin and 10,000µg/ml streptomycin (Sciencell), 20% FBS (Sciencell), 1% of 100X astrocyte growth supplement (Sciencell) at 37°C and 5% CO₂ atmosphere. Culture media of astrocytes were changed every 48 hours with astrocyte medium (AM). In all studies, astrocytes from passage 3 to 6 were used.

2.3 Thawing of cells

Cryopreserved vials of astrocytes or HBEC were removed from -80°C. Cells were thawed quickly by placing the lower half of the vial in a 37°C water bath. The vial was removed from the water when a small amount of ice was left in the vials. The vial exterior was sprayed with 70% alcohol and placed in a sterile biological safety cabinet. For HBEC, 1ml of thawed HBEC suspension was added to 8ml of pre-warmed HBEC medium in a centrifuge tube (Figure 2.1). For astrocytes, 1ml of thawed astrocytes was added to 2ml of pre-warmed astrocyte medium (AM) (Figure 2.1). 3 ml of HBEC suspension or astrocyte suspension was transferred into a 25cm² cell culture flask precoated with 1% gelatin (Figure 2.1). The HBEC or astrocyte culture was viewed under an inverted microscope and placed in 37°C, 5% CO₂ incubator. Media of HBEC was changed 2 hours after seeding in order to remove any cells that have not adhered. Media of astrocytes were changed the next day after seeding. HBEC and astrocytes were maintained as described in Chapter 2, section 2.1 and 2.2. For astrocytes, astrocyte media was

changed the next day after seeding. The HBEC or astrocyte cultures were placed in a 37°C, 5% CO₂ humidified incubator. Media was changed every other day until cells were confluent.

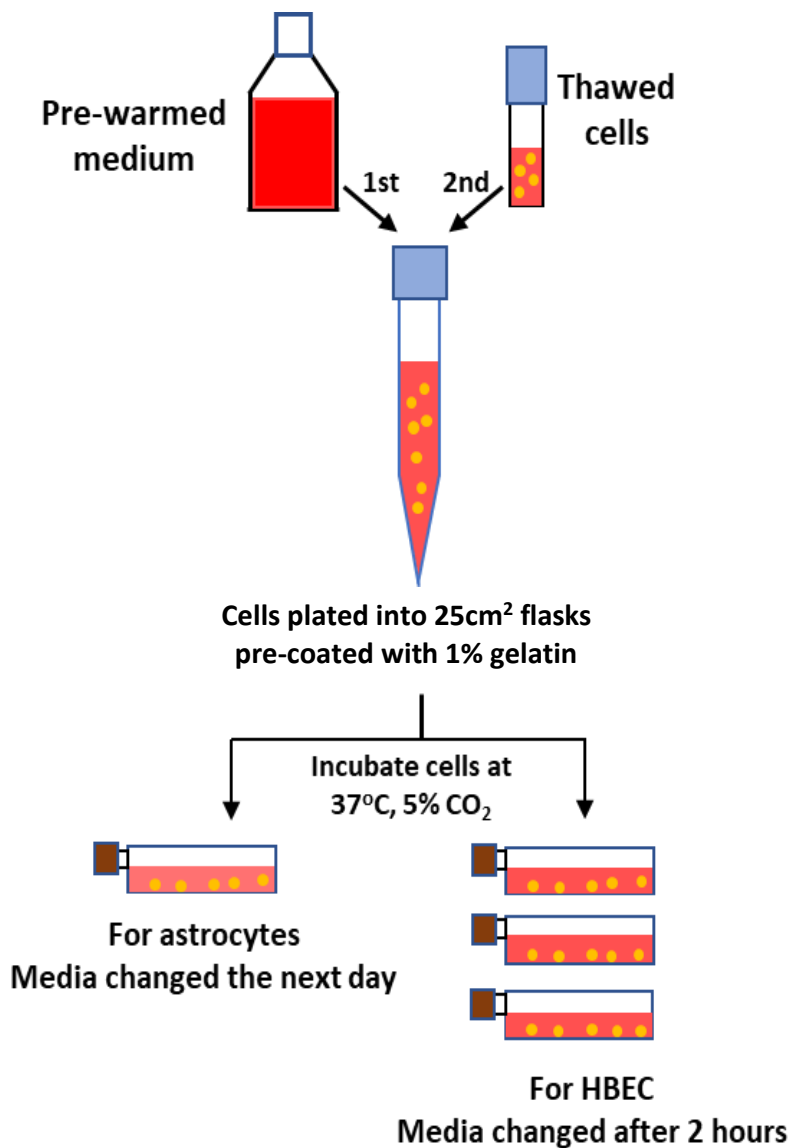


Figure 2.1 Thawing procedure of HBEC and astrocytes *in vitro*.

2.4 Subculturing of cells

Complete growth media was pre-warmed in a water bath at 37°C. Trypsin/EDTA (Sigma) was pre-warmed to room temperature. The culture media was aspirated from the cell culture flask without disturbing the cell monolayer. 1.5ml of phosphate buffered saline (PBS) (Sigma) was used to wash the HBEC or astrocytes. PBS was aspirated from the cell culture flask. 1.5ml of

pre-warmed trypsin/EDTA was added to HBEC or astrocyte monolayer (Figure 2.2). Flasks were rocked gently to ensure the solution covered all the cells. Cells were observed under the inverted microscope to confirm they were dissociated from each other and were rounding up.

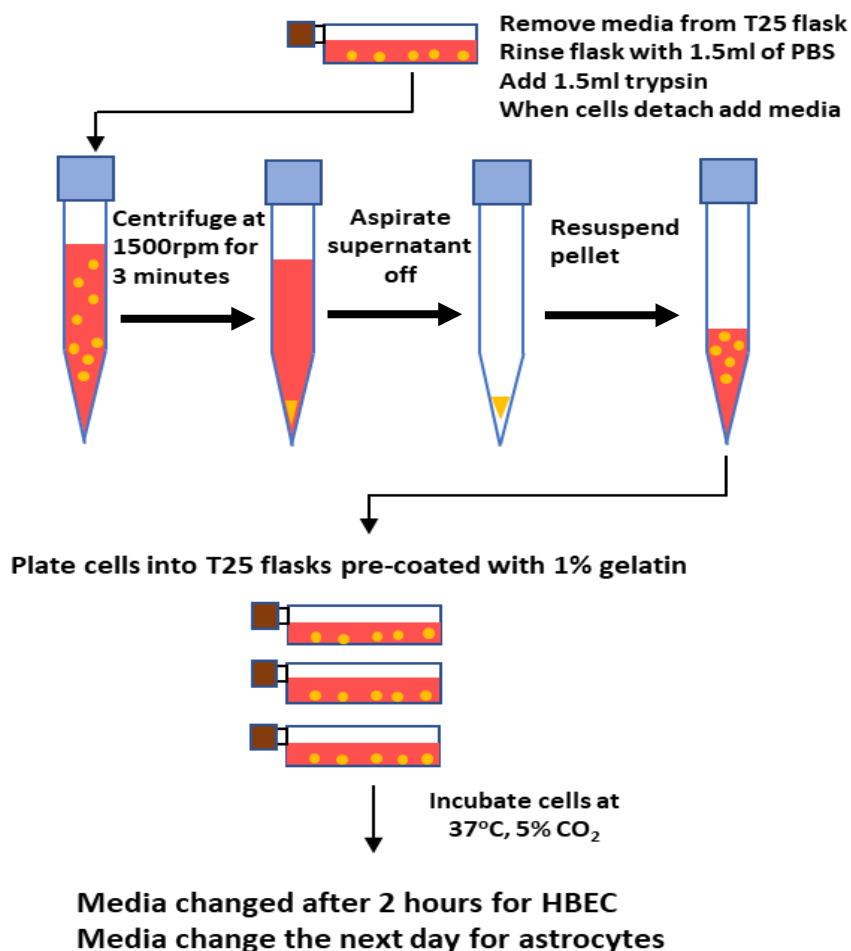


Figure 2.2 Schematic representation of HBEC and astrocytes subculture *in vitro*.

When majority of the cells were detached, an equal volume of complete medium was added to the 25cm² flask to neutralise the trypsin/EDTA. The culture suspension was transferred into a sterile 15 ml centrifuge tube. The cell suspension was centrifuged at 480g for 3 minutes to pellet the cells. The supernatant was aspirated from the tube without disturbing the cells (Figure 2.2). The cell pellet was re-suspended in 0.5 ml pre-warmed fresh complete media by gently pipetting the cells to break up the clumps (using a pipette with a tip attached to it). Cells were seeded in new 25cm² cell culture flasks at an appropriate cell density (Figure 2.2). The newly

seeded 25 cm² cell culture flasks were viewed under an inverted microscope and placed in a 37°C, 5% CO₂ humidified incubator. Media for HBEC and astrocytes in 25cm² flasks were changed as described in Chapter 2, section 2.1-2.3.

2.4.1 Cell culturing

Before seeding of cells in all experiments, 25cm² flasks, coverslips or 96 well plates were coated with 1% gelatin for 20 minutes at 37°C in a humidified incubator to facilitate adherence of cells. For 96 well plates, 2x10⁴ cells were seeded in each well and for glass coverslips 1x10⁵ cells were seeded on each coverslip.

2.5 Freezing of Human Brain Endothelial cells and astrocytes

Human brain endothelial cells and astrocytes were at least 90% confluent before freezing. Cells were gently detached from the cell culture flask into a centrifuge tube following the subculturing protocol as described in Chapter 2, section 2.4. The cell suspensions were centrifuged at 480g for 3 minutes. The supernatant was aspirated without disturbing the pellet. The cell pellet was resuspended in 0.5 ml of cryopreservation medium, Cryo-SFM (PromoCell). For HBEC, 2.5 ml of Cryo-SFM was added to the 0.5ml cell suspension. For astrocytes 0.5ml of Cryo-SFM was added to the 0.5ml cell suspension. 1ml of the cell suspension was pipetted into cryovials. Cells were wrapped in tissue for insulation and frozen at -20°C for at least 2 hours. Cryovials containing HBEC and astrocytes were then transferred to -80°C freezer for long-term storage.

2.6 Cell Counting

Before a cell count was performed, a glass coverslip was placed on the centre chamber of the haemocytometer until Newton rings were observed (Figure 2.3). Cells were trypsinised as in

Chapter 2, section 2.4. After centrifugation, the pellet was resuspended in 0.5ml of pre-warmed complete medium. For HBEC, 10 μ l of cell suspension was placed into a microcentrifuge tube containing 90 μ l of pre-warmed complete media (1 in 10 dilution) and mixed thoroughly. For astrocytes, 10 μ l of cell suspension was placed into a microcentrifuge tube containing 40 μ l of pre-warmed AM (1 in 5 dilution) and mixed thoroughly. With a coverslip in place, 10 μ l of the mixture was placed in the chambers of the haemocytometer and the cells were counted in the middle chamber. All the cells in the two middle chambers shown in Figure 2.3 were counted and the average was calculated. The number of cells were calculated by multiplying the mean by 10⁴ (conversion factor) and then multiplied by the dilution factor as seen in the formula below.

Cell count formula: Mean cell count in middle chamber x 10⁴ x dilution factor = cells/ml.

Dilution factor = 10 for HBEC. Dilution factor = 5 for astrocytes.

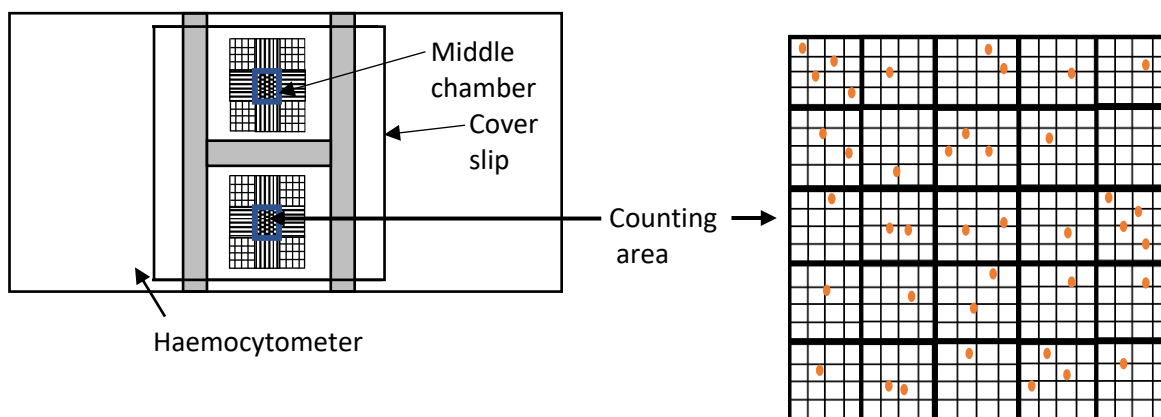


Figure 2.3 Schematic of Haemocytometer. Cells in the middle square of the two counting chambers were counted, averaged, multiplied by the conversion factor 10⁴ and multiplied by the dilution factor.

2.7 *Plasmodium falciparum* parasite culture

The *Plasmodium falciparum* ITG strain was used in this study. The ITG strain was derived from the Brazilian line IT4/25/5 (Ockenhouse *et al.*, 1992). This strain has been well characterised for its ability to bind to ICAM-1 expressed on the surface of endothelial cells (Chakravorty *et al.*, 2007; Gray *et al.*, 2003; Ockenhouse *et al.*, 1992). ITG stabilates were

thawed and maintained in culture for a maximum of 3 weeks to reduce the effect of antigenic switching in culture (Tse *et al.*, 2004). The *P. falciparum* ITG strains of the parasite were cultured using the techniques described by (Trager and Jensen, 1976).

Cultures were grown in complete growth medium supplemented with freshly isolated 50 % v/v haematocrit (HCT) of washed red blood cells (WRBC). Cultures were maintained in 1% O₂, 3% CO₂ and 96% N₂ at 37°C.

The *Plasmodium falciparum* culture was performed in a containment level 3 (CL3) facility which is approved by the Health and Safety Executive (HSE) for the use of *Plasmodium falciparum* according to the rules in the CL3 suite code of practice. Leukocyte-depleted human blood was supplied by the National Blood Transfusion Service (NBTS) UK and stored in 50ml aliquots at 4°C. Storage and disposal of blood were done in accordance with the Human Tissue Authority (HTA) license held by Keele University.

2.8 Preparation of growth medium for *Plasmodium falciparum* cultures

Serum free medium was prepared by supplementing RPMI-1640 with 37.5mM *N*-2-hydroxyethylpiperazine-*N'*-2-ethanesulfonic acid (HEPES), 7mM Glucose (filter sterilised), 6mM NaOH (filter sterilised), 2mM L-glutamine and 25 µg/ml gentamicin sulphate solution. To prepare complete growth medium, serum free medium was supplement with 10% (v/v) pooled human serum. Use of pooled human serum for use in *Plasmodium falciparum* cultures was ethically approved.

2.9 Washed human red blood cells (WRBC)

To make a 50 % v/v washed red blood cells, 5ml of red blood cells (Type O) was mixed with an equal volume of serum free medium in a sterile 50ml tube. The mixture was layered onto 5ml of histopaque (Sigma) to remove all white blood cells (WBC). The tube was then

centrifuged at 2000g for 15 minutes at room temperature. The supernatant containing WBC was carefully aspirated, leaving the red blood cells pellet. The pellet was resuspended in 25 ml of serum free media and centrifuged for 10 minutes at 2500g. The packed red blood cells were resuspended in an equal volume of serum free medium and stored at 4°C for 7-10 days.

2.10 Reconstitution of frozen *P. falciparum* culture stabilates

Ring state ITG parasites were stored in the -80°C freezer. Thawing solutions, serum free RPMI and growth medium were prewarmed to 37°C. The thawed culture was transferred to a 50 ml sterile tube and 12% (w/v) NaCl in PBS (0.2ml/ml of stabilate) was added dropwise very slowly, constantly swirling the tube and incubated at room temperature for 5 minutes. 1.8% (w/v) NaCl in PBS (5ml/ml of stabilate) was added slowly and incubated at room temperature for 5 minutes. Then 0.9% (w/v) NaCl with 0.2% (w/v) glucose in PBS (5ml/stabilate) was added slowly and incubated at room temperature for 5 minutes. The ITG parasite suspension was then centrifuged at 1200g for 5 minutes and the supernatant was gently aspirated. Cells were resuspended in serum free medium and centrifuged at 1200g for 5 minutes. The supernatant was aspirated and the pelleted was resuspended in 5 ml of serum free medium and transferred into a 25 cm² tissue culture flask, gassed, sealed and placed in the 37°C incubator. 24 hours after thawing of PRBC, 50µl of WRBC were added to the culture to enable PRBC invade uninfected red blood cells. All cultures were maintained at a haematocrit of 1-2% and assessed every 48 hours to mimic the intra-erythrocytic cycle of *Plasmodium falciparum*.

2.11 Assessment of *Plasmodium falciparum* parasite culture

Plasmodium falciparum cultures were assessed every 48 hours. Thin blood smears were prepared on a glass slide, fixed with 100% methanol and stained with 10% v/v Giemsa solution (Acros Organics). Microscope slides were viewed on a light microscope with the 100X oil

immersion objective lens. The parasitaemia was calculated by counting the number of *Plasmodium falciparum* infected red blood cells (PRBC) in a total of at least 200 red blood cells over randomly selected fields on the slide.

The percentage parasitaemia was calculated using the formula below.

$$\% \text{ Parasitaemia} = \frac{\text{Number of PRBC}}{\text{Total number of red blood cells counted}} \times 100$$

Plasmodium falciparum culture medium was changed every 48 hours. The culture was transferred to a 50ml falcon tube and centrifuged at 1200g for 5 minutes. The supernatant was aspirated, the pellet was resuspended in an appropriate volume of prewarmed complete growth medium and placed in a sterile non-vented 25cm² flask. An appropriate volume of 50% (v/v) WRBC was then added to the flask to adjust the parasitaemia. The culture was gassed with 1% O₂, 3% CO₂ and 96% N₂ and placed in a 37°C humidified incubator.

2.12 Freezing of *Plasmodium falciparum* parasites

Plasmodium falciparum parasites at the ring-stage of the growth cycle were frozen for long term storage. The culture was transferred to a clean, sterile Falcon tube and cells were pelleted by centrifugation in a bench-top centrifuge at 1200g for 5 minutes at room temperature. The supernatant was aspirated, and pellet was gently resuspended. Glycerolyte was added in a ratio of 5 volumes of glycerolyte to 3 volumes of cell pellet. The first volume of glycerolyte was added slowly using a pipette and allowed to stand for 5 minutes at room temperature. The remaining 4 volumes of glycerolyte were slowly added using a pipette. The cell/glycerolyte mixture was transferred to sterile freezing vials and wrapped in tissue for insulation and frozen at -20°C for at least 2 hours. Cryovials containing the *Plasmodium falciparum* parasites were stored at -80°C for long-term storage.

2.13 Plasmagel Trophozoite enrichment

For PRBC/HBEC coculture experiments, plasmagel flotation was used to harvest the mature trophozoite stage of *Plasmodium falciparum*. Plasmagel solution and serum free medium were warmed at 37°C in a water bath. The culture was transferred to a sterile 50ml tube and cells were centrifuged at 1430g for 5 minutes. The supernatant was aspirated and resuspended in 15ml of pre-warmed serum free medium in a 15 ml centrifuge tube. The mixture was centrifuged at 1430g for 5 minutes and the packed cell volume (PCV) was estimated. The pellet was thoroughly resuspended in a ratio of 2 volumes pellet to 3 volumes serum free medium and 5 volumes Plasmion (Laboratoire Fresenius Kabi, France) and incubated upright at 37°C for 1 hour. A clear separation of the top and bottom layer was observed after 1 hour (Figure 2.4). The top layer containing trophozoites was removed carefully and transferred to a new sterile tube and centrifuged at 1430g for 5 minutes. The pellet was washed twice in serum free medium and the parasitaemia was assessed using a Giemsa stained smear. The desired parasitaemia for the coculture experiments was around 50%.

2.14 Coculture of transformed Human Brain Endothelial cells with PRBC

Coculture experiments were done in Human Brain Endothelial Cells (HBEC) quiescent medium (Q 1% FBS medium) (Appendix 6). This was made up of RPMI-1640 supplemented with 2mM L-glutamine, 100 units/ml penicillin and 100µg/ml of streptomycin per ml (Blank media) and 1% FBS. HBEC was cultured in a 25cm² flask for 48 hours or until confluent. 4 hours before the coculture, medium of HBEC culture was replaced with Q1% FBS medium. Trophozoites were enriched to a parasitaemia of at least 50% and were adjusted to 1% haematocrit using Q1% FBS medium. 3ml of 1% PRBC haematocrit was added to HBEC in the flask. Coculture experiments were performed for 20 hours at 37°C, CO₂ in a humidified incubator.

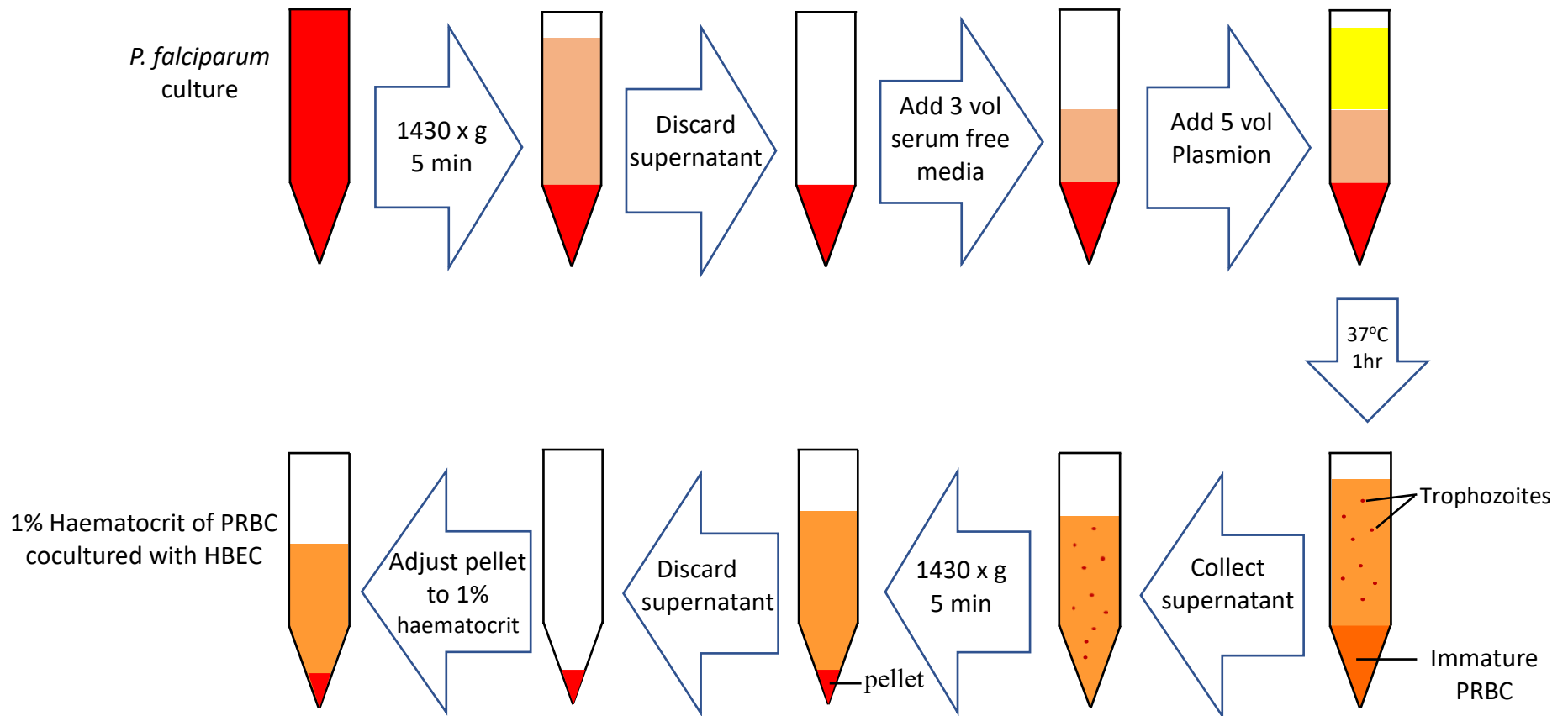


Figure 2.4 Schematic of Plasmagel Trophozoite Enrichment. Image adapted from (Ranford-Cartwright *et al.*, 2010).

2.15 Conditions for coculture experiment

PRBC was cocultured with the resting HBEC (PRBC/HBEC) for 20 hours at 37°C and 5% CO₂. For negative controls, HBEC was cultured in Q1% FBS medium to monitor cells in a resting state and uninfected red blood cells at 1% haematocrit were cocultured with HBEC (URBC/HBEC). HBEC were treated with 1ng/ml IL-1 β diluted in Q1% FBS medium to serve as a positive control for HBEC activation. The cocultures were placed in the humidified incubator at 37°C and 5% CO₂ for 20 hours.

2.16 Harvesting of PRBC-HBEC coculture supernatant and HBEC lysate

After 20 hours, PRBC-HBEC coculture supernatants and control coculture supernatant were harvested. Supernatants from each flask were transferred into sterile 15ml tubes on ice. Subsequently, flasks were washed three times with ice cold blank media and media was aspirated. 100 μ l of ice cold RIPA was pipetted into each flask and incubated in the fridge at 4°C for 3 minutes. A cell scraper was used to scrape cells in the flask and HBEC lysate was transferred into a microcentrifuge tube. The microcentrifuge tube was centrifuged at 14000g for 5 minutes to pellet cell debris. Cell debris was removed, and lysate was stored at -20°C. Coculture supernatants on ice were centrifuged at 478g for 3 minutes to remove cell debris or residual URBC or PRBC. The supernatant was then transferred to a sterile microcentrifuge tube and stored at -20°C for future use.

2.17 Making of the SDS PAGE gel

SDS page gel was prepared according to Appendix 5. The short plate was layered over the long plate with spacers in between them. The casting frame was used to lock both plates together. The unit was then placed onto the casting stand to make a tight seal. Water was pipetted between plates to make sure there was no leakage. The resolving gel solution was prepared as

shown in Appendix 5. An appropriate amount of resolving gel solution was pipetted between glass plates carefully to avoid the formation of air bubbles. Water was layered on top of the gel solution to give a flat gel surface and to prevent exposure of gel to oxygen. After the gel was polymerized, excess water was blotted off using a filter paper. The stacking gel was prepared using the components in Appendix 5. The stacking gel mixture was pipetted between the plates up to the edge of the short plate. The comb was gently inserted between the two glass plates making sure there was no air trapped under the teeth. After the gel had polymerized the comb was slowly removed. The glass plates were then taken out of the casting frame and placed into the electrode assembly making sure the short plate faced inwards. The glass plates in the electrode assembly were then placed in the buffer tank. The electrode assembly (inner chamber) was filled with running buffer. The outer chamber was filled with running buffer (Appendix 5) to the indicator mark for 2 or 4 gels depending on the number of gels being run.

2.18 Sample preparation

All samples were mixed with the 2X sample buffer (1:1) (Appendix 5) and heated on a heating block at 100°C for 5 minutes to aid denaturation. The samples were centrifuged briefly. The appropriate amount of protein lysates or supernatants were loaded into corresponding wells alongside a lane containing a Precision Plus Protein™ Kaleidoscope prestained protein standards (Sigma) (Figure 2.5). The tank was covered with the cell lid and the electrodes on the cell lid were connected to the power supply (Figure 2.5). The gel was run at 35mA for 1 hour or dependent on the size of protein being investigated. The power supply was turned off and leads were disconnected after gel electrophoresis was complete.

2.19 Gel transfer

Prior to gel transfer, a nitrocellulose membrane (GE Healthcare), blotting pads and filter papers were soaked in transfer buffer (appendix 5). The gel was removed from its cassette and the stack gel wells were trimmed away. A presoaked pad was placed on the white side of the cassette. Presoaked filter papers were placed on top of the pad. The presoaked nitrocellulose membrane was placed on the filter paper. The gel was then placed on the membrane. Presoaked filter papers were placed on top of the gel and a roller was used to remove trapped air bubbles. A presoaked pad was then placed on the filter paper and the cassette was closed (Figure 2.5). The gel cassette was placed in the electrode assembly, with the gel side of the cassette holder facing the cathode (-) and the membrane side facing the anode (+). The gel tank was then filled with transfer buffer to the indicator mark for 4 gels (Figure 2.5). The tank lid was placed on top of the tank and the transfer was run at 300mA for 1 hour.

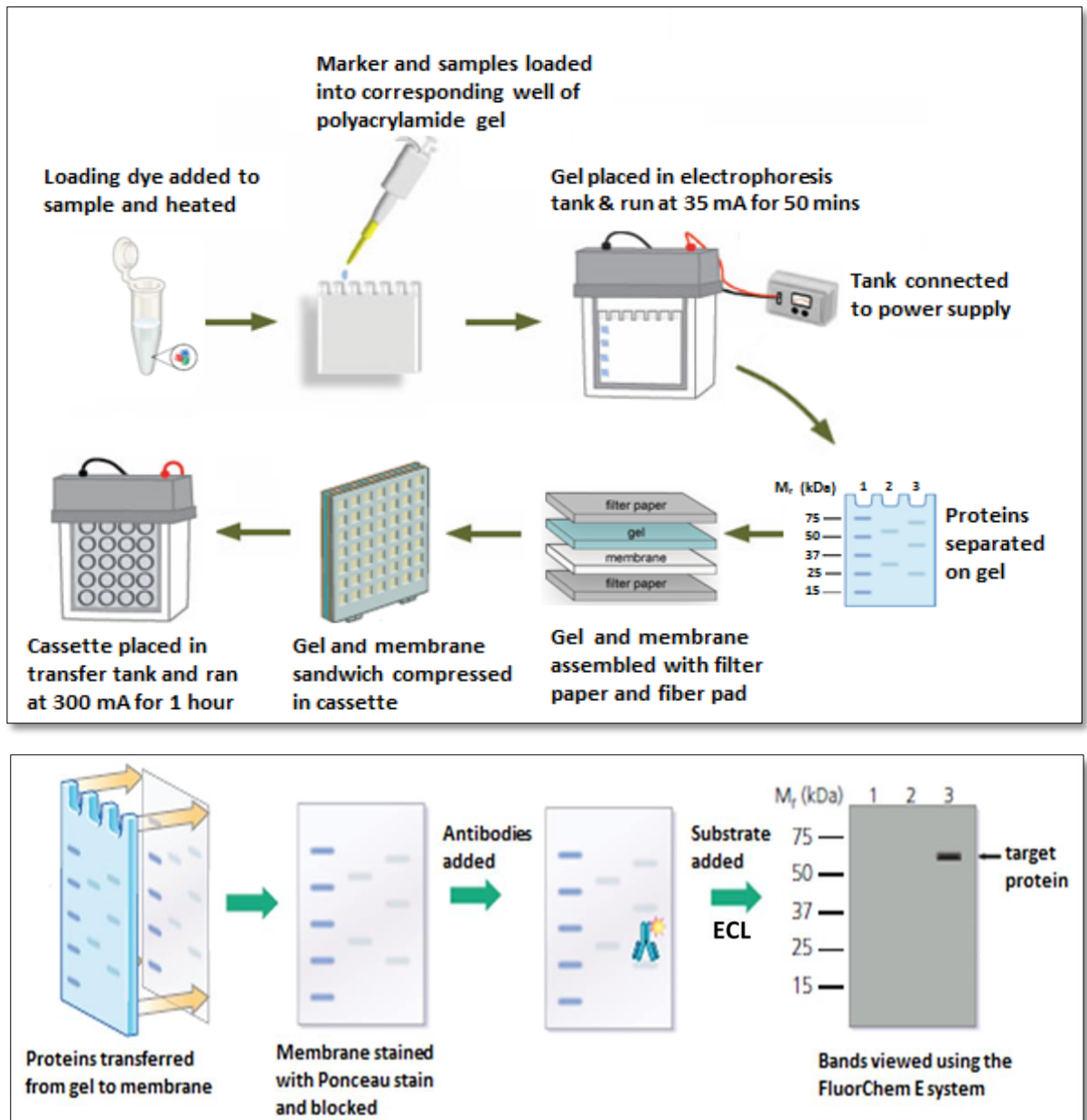


Figure 2.5 Schematic of SDS PAGE gel electrophoresis and western blot procedure. Images obtained from (Advansta, 2018; Bio-Rad, 2018).

2.20 Ponceau S stain

The transfer stack was disassembled using forceps. The membrane was stained with Ponceau S solution (Sigma) to verify successful transfer of proteins from the gel to the membrane and equal loading in each well. Transferred bands were visible on the membrane and were photographed using the FluorChem E system. The Ponceau S stain was washed off and 10ml

blocking buffer (Sigma) diluted in H₂O was added to the membrane for 1 hour on a rocking platform.

2.21 Antibody incubation

After blocking, the membrane was incubated with the appropriate primary antibodies (Table 2.1) (diluted in TBST) (appendix 5) overnight on a rocking platform. The membrane was washed in TBST three times for 15 minutes with 10ml of 1XTBST to remove excess primary antibodies (Figure 2.5). The membrane was then incubated with the recommended dilution of HRP conjugated secondary antibody (diluted in TBST) (Table 2.2) for 2 hours at room temperature (Figure 2.5). The membrane was washed in TBST twice for 5 minutes.

Table 2.1 Primary Antibodies

Name	Primary antibody	Dilution	Supplier
ADAMTS-4	Anti-Human ADAMTS-4 goat polyclonal IgG antibody	1:250	Santa Cruz
GFAP	Polyclonal Rabbit anti-GFAP antibody	1:500 1:1000	Dako

Table 2.2 Secondary Antibodies

Name	Secondary Antibody	Dilution	Supplier
ADAMTS-4	Donkey anti-goat IgG HRP antibody	1:1000	Santa Cruz
GFAP	Goat anti-rabbit IgG HRP conjugated antibody	1:1000	Biorad

2.22 Imaging and data analysis

The chemiluminescent substrate (Fisher Scientific) at room temperature was applied to the membrane. 750µl of the detection peroxidase and 750µl of luminol enhancing solution were mixed in a tube. 750µl of the mixture was added to the membrane for 1 minute. The excess

reagents were removed, and the membrane was wrapped in cling film and viewed in the FluorChem E system.

2.23 Immunofluorescence analysis

Glass coverslips were coated with 500µl of 1% gelatin and incubated for 20 minutes in a 37°C humidified incubator at 5% CO₂ to facilitate binding of HBEC and astrocytes. 1X10⁵ cells were grown on gelatin coated coverslips for 5 days. Cells were then washed with ice cold blank media. Cells were then fixed with 500µl of 4% paraformaldehyde in PBS for 20 minutes at 4°C. Cells were then washed three times with PBS for 3 minutes each. Cells were blocked with blocking buffer as described in Chapter 3, section 3.2.2 and 3.2.3 to prevent non-specific binding of antibodies. Cells were then incubated with the primary antibody overnight or for 1 hour (details in Chapter 3, section 3.2.2 and 3.2.3). Cells were then washed as described before to remove unbound antibodies. The secondary antibody was added to cells for up to 2 hours. Cells were then washed as before. Coverslips were mounted on slides using vectashield with DAPI (4' 6-diamidino-2-phenylindole). DAPI was used to visualize nuclear DNA in cells. All antibody incubations were done at room temperature.

2.24 Cell based ELISA

Cell based ELISA was used to determine GFAP and ICAM-1 expression in astrocytes and HBEC respectively. 2x10⁴ cells were seeded into 96 well plates pre-coated with gelatin. 2 hours after seeding HBEC media was changed and cells were cultured for 24 hours. Media of astrocytes were changed the next day after seeding. Astrocytes were grown in culture for a total of 48 hours.

For **cell based GFAP ELISA**, astrocytes were treated for 48 hours. Cells were then washed with 100µl of cold PBS. Cells were then fixed with cold 4% paraformaldehyde for 20 minutes at room temperature. Astrocytes were then washed 3 times with 150µl PBS at room temperature to remove 4% paraformaldehyde. 50µl of blocking buffer (5% donkey serum and 0.3% Triton in H₂O) was added to each well and incubated for 30 minutes at room temperature to remove background caused by non-specific binding of antibodies. 50µl of the diluted polyclonal rabbit anti-GFAP antibody (1:500) was added to corresponding wells. The plate was covered with parafilm and left overnight at 4°C. Astrocytes were then washed as before. 50µl of blocking buffer was added to each well for 30 minutes at room temperature. 50µl of the diluted goat anti-rabbit IgG HRP conjugated antibody (1:1000) was added to corresponding wells and incubated for 2 hours at room temperature. Cells were then washed as before. 100µl of TMB solution was added to each well and incubated at room temperature in the dark for 30 minutes or till colour changed from clear to blue. 100µl of stop solution (H₂SO₄) was added to each well to stop the reaction, changing the colour from blue to yellow. The absorbance was read at 450nm immediately using a microplate reader (GLOMAX™ Multi+detection system, Promega). The concentration of GFAP was directly proportional to the intensity of the yellow colour.

After measuring the absorbance of the plate at 450nm, the plate was washed twice with 200µl of PBS for 5 minutes each. The plate was air dried for 5 minutes at room temperature. Crystal violet binds to nuclei and gives absorbance reading proportional to cell density at 600nm. 50µl of crystal violet solution was added to each well and incubated for 30 minutes at room temperature on the rocking platform. Subsequently, contents in plates were tipped out to remove crystal violet solution and rinsed with tap water. The plate was washed as before. 100µl of 1% SDS was added to each well and incubated on a rocking platform at room temperature

for 1 hour. The absorbance of the plate was read at 600nm with a microplate reader. Results were analysed by normalizing the absorbance at 450nm (GFAP) to absorbance at 600nm (which represented the cell amounts) :

$$\textit{Absorbance reading at 450nm} \div \textit{Absorbance reading at 600nm}$$

For **Cell based ICAM-1 ELISA**, 24 hours after cells were grown in culture, media was changed to Q5% FBS medium. This was done to bring HBEC into a resting state and thereby decreasing the noise value produced by replicating cells. After 24 hours, different treatments were added to HBEC in the 96 well plates. 48 hours after treatment, supernatants were aspirated off each well and HBEC were washed with 150µl of cold 0.1%BSA/PBS. Cells were then fixed with 150µl of methanol for 5 minutes at room temperature. Cells were then washed with 150µl of 0.1% BSA/PBS at room temperature. 50µl of 0.05% Triton/PBS was then added to each well for 1 minute. Cells were washed three times with 150µl of PBS. To minimize background due to non-specific binding of the primary antibody, cells were blocked with 50µl of 1% BSA/PBS for 1 hour at room temperature. Blocking solution was then removed from plate by flicking and 50µl of the 1:200 dilution of anti-ICAM-1 mouse monoclonal IgG antibody in 0.1% BSA was added to corresponding wells for 2 hours at room temperature. HBEC were then washed as before. 50µl of the 1:2000 goat anti-mouse IgG-HRP conjugated antibody was added to corresponding wells. The plate was incubated for 2 hours at room temperature in the dark. HBEC were then washed as before. 100µl of TMB solution was added to each well and incubated at room temperature in the dark for 30 minutes or till colour change from clear to blue. 100µl of stop solution (H₂SO₄) was added to each well to stop the reaction, changing the colour from blue to yellow. The absorbance was read at 450nm immediately using a microplate reader (GLOMAX™ Multi+detection system, Promega). The concentration of ICAM-1 was directly proportional to the intensity of the yellow colour.

2.25 Development of *in vitro* HBEC and HBEC-astrocyte BBB models

HBEC-alone BBB and HBEC-astrocyte BBB tandem BBB models were developed as described in Chapter 3, section 3.2.7.

2.26 Measurement of transendothelial electrical resistance (TEER)

Transendothelial electrical resistance (TEER) was used to measure the BBB integrity of the HBEC-alone BBB and the HBEC-astrocyte BBB. The TEER of the *in vitro* BBB models were measured using Endohm chamber connected to an EVOM resistance meter as described in Chapter 3, section 3.2.8.

2.27 FITC dextran permeability assay

FITC dextran permeability assay was performed on HBEC-alone BBB and HBEC-astrocyte BBB models as described in Chapter 4, section 4.2.3

2.28 Sandwich ELISA

Sandwich ELISA for GFAP was performed according to the manufacturer's kit instructions and as described in Chapter 5, section 5.2.5. Details of GFAP, sICAM-1, MCP-1 and ADAMTS-4 ELISA kits can be seen in Appendix 1.

sICAM-1 ELISA was done according to the manufacturer's guidelines (Human CD54 ELISA kit Diaclone). 100µl of the diluted capture antibody was used to coat the 96 well plate overnight at 4°C. Each well was washed with 150µl of washing solution 3 times and blocked with 250µl of blocking buffer per well for 2 hours at room temperature. Serial dilutions of the standards were prepared to provide the concentration range from 0.25 to 8 ng/ml. 50µl of coculture supernatants and standards were added to the appropriate wells in duplicates. 50µl of the

biotinylated antibody was then added to each well and incubated at room temperature for 1 hour. 100µl of streptavidin HRP solution was added to each well for 30 minutes at room temperature. Contents of wells were emptied by flipping of plate and each well was washed with 150µl of washing solution. Plate was washed to remove unbound HRP. For colour development 100µl of TMB was added to each well as the substrate for HRP and plate was incubated for 10 minutes in the dark. 100µl of H₂SO₄ was added to each well to stop the catalytic conversion of TMB substrate by HRP. The colour change and absorbance of the plate was read at 450nm on a plate reader.

MCP-1 sandwich ELISA was performed according to the manufacturer's guidelines (Human MCP ELISA Diaclone). 96 well plates provided by the manufacturer were pre-coated with a capture antibody highly specific to MCP-1. Serial dilutions of the standards were prepared to provide the concentration range from 31.25 to 1000 pg/ml were prepared in duplicates. 100µl of each standard, coculture supernatants and controls were plated in corresponding wells in duplicates and incubated for 1 hour at room temperature. 50µl of diluted biotinylated anti-MCP-1 was added to each well and plate was incubated at room temperature for 30 minutes. Contents of the wells were discarded and the plate was washed with 150µl of washing solution 3 times. 100µl of streptavidin-HRP solution was added to each well and plate was incubated for 30 minutes. 100µl of TMB was added to each well for 10 minutes. 100µl of H₂SO₄ was added to each well and absorbance of the plate was read at 450nm on a plate reader.

Human ADAMTS-4 sandwich ELISA (R&D systems) were performed according to the manufacturer's specifications. 96 well plates were coated with 100µl of the diluted capture antibody (1µg/ml) at room temperature overnight. Each well was washed with 150µl washing solution 3 times and blocked with 150µl of reagent diluent (1% BSA in PBS) per well for 1

hour at room temperature. 100µl of coculture supernatants or standards (concentration ranging from 15.6-1000pg/ml) in reagent diluent (1% BSA in PBS) were added in duplicates to corresponding wells and incubated for 2 hours at room temperature. The plate was washed as mentioned earlier. 100µl of detection antibody (0.05µg/ml) diluted in reagent diluent was added to each well and plate was incubated for 2 hours at room temperature. The plate was washed as described earlier. 100µl of Streptavidin-HRP (1:40 dilution) was added to each well and plate was incubated for 20 minutes at room temperature in the dark. 100µl of substrate solution was added to each well and plate was incubated for 20 minutes at room temperature. 50µl of stop solution was added to each well. The colour change and absorbance of the plate was read at 450nm on a plate reader.

2.28.1 Calculation of amount of sICAM-1, MCP-1 and ADAMTS-4

The average absorbance of each duplicate set of standards and samples were calculated. A linear standard curve was produced by plotting the average absorbance of each standard on the vertical axis against the corresponding ICAM-1/MCP-1/ADAMTS-4 standard concentrations on the x-axis. The concentration of ICAM-1, MCP-1 and ADAMTS-4 was determined by extrapolating the optical density values against the standard concentrations using the standard curve. The concentration was then multiplied by the volume of the flask to get the total amount of the protein of interest.

2.29 Biorad protein assay

The protein concentration of samples was determined using the Bio-Rad protein assay for microtiter plates. This assay measured the total protein concentration in the sample.

Dye reagent was prepared by diluting 1-part Dye reagent concentrate with 4 parts double distilled water. The diluted dye reagent was filtered through a Whatman #1 filter to remove

particulates. BSA standards from 1.48mg/ml-0.313mg/ml were prepared. 5 dilutions of the protein standards were prepared, and these were representative of the protein solution being tested. 10µl of each standard and samples were pipetted into separate microtiter plate wells. 200µl of dye reagent was added to each well using a multi-channel pipette. Plate with samples and standards were incubated at room temperature for 1 hour and absorbance read at 600nm. A standard curve was constructed and used to determine protein concentration according to the absorbance values read at 600nm multiplied by the dilution factor.

2.30 Statistical analysis

Statistical analysis was performed using GraphPad Prism, version 7 (GraphPad Software Inc.) and data was expressed as mean \pm standard error of the mean (SEM). Two groups were compared using unpaired two-tailed t-test. One-way analysis of variance (ANOVA), and a post hoc analysis using Tukey's multiple comparison test was used to compare 3 groups or more. Two-way ANOVA was used to test the mean differences between groups that had been split on two factors. Post hoc analysis for Two-way ANOVA was carried out using Tukey's multiple comparison test.

Chapter 3 : Development and characterisation of *in vitro* blood-brain barrier models

3.1 Introduction

The blood-brain barrier (BBB) is made up of brain endothelial cells, a basement membrane, astrocytes and pericytes. Several neurological disorders exist where the BBB is compromised, and thus many *in vitro* BBB models have been developed to understand these disorders. These models can be 2 dimensional or 3 dimensional. 2 dimensional BBB models are based on monocultures of endothelial cells, coculture of endothelial cells and astrocytes or pericytes and triple cultures of endothelial cells, astrocytes and pericytes (Helms *et al.*, 2016)..

Monoculture models made of only endothelial cells do not fully depict the BBB *in vivo* since signals produced from other components of the neurovascular unit (NVU) such as astrocytes and pericytes are absent (Figure 3.1) (Helms *et al.*, 2016). These monocultures also have relatively low transendothelial electrical resistance (TEER). Coculturing HBEC with components of the neurovascular unit (NVU) has been shown to improve BBB integrity and increase TEER (He *et al.*, 2014).

Thus, coculture models where endothelial cells and astrocytes are grown together have been developed. These cocultures can either be contact or non-contact cocultures. In the non-contact coculture models, endothelial cells are grown on the upper part of the transwell membrane and the astrocytes are grown on the bottom of the culture well (Figure 3.1) (Helms *et al.*, 2016). This set up is done to enable the factors released from astrocytes at the bottom of the well to induce BBB properties in the endothelial cells. This model does not fully depict the BBB *in vivo* where astrocytes and endothelial cells are in close proximity to each other. In the contact coculture, astrocytes are grown on the bottom of the transwell whereas as endothelial cells are grown on the upper part of the transwell (Figure 3.1) (Helms *et al.*, 2016). In this model astrocyte released factors are closer to endothelial cells and have a bigger effect on endothelial cells since they are less dilute (Kulczar *et al.*, 2017). Astrocytes are known to release growth factors essential for the formation of a functional BBB. Human brain endothelial cells (HBEC)-

astrocyte cocultures have been reported to have TEER values of greater than $300\Omega\text{cm}^2$ compared to HBEC monolayer TEER values of $50\Omega\text{cm}^2$ (He *et al.*, 2014; Weksler *et al.*, 2013).

Recently triple culture models have been developed where endothelial cells are seeded on the upper part of the transwell, pericytes are seeded on the lower part of the transwell with astrocytes seeded on the bottom of the culture wells (Figure 3.1) (Helms *et al.*, 2016). This set up closely depicts the neurovascular unit and in this model all the three cell types can communicate and produce a slight increase in TEER compared to cocultures (Helms *et al.*, 2016).

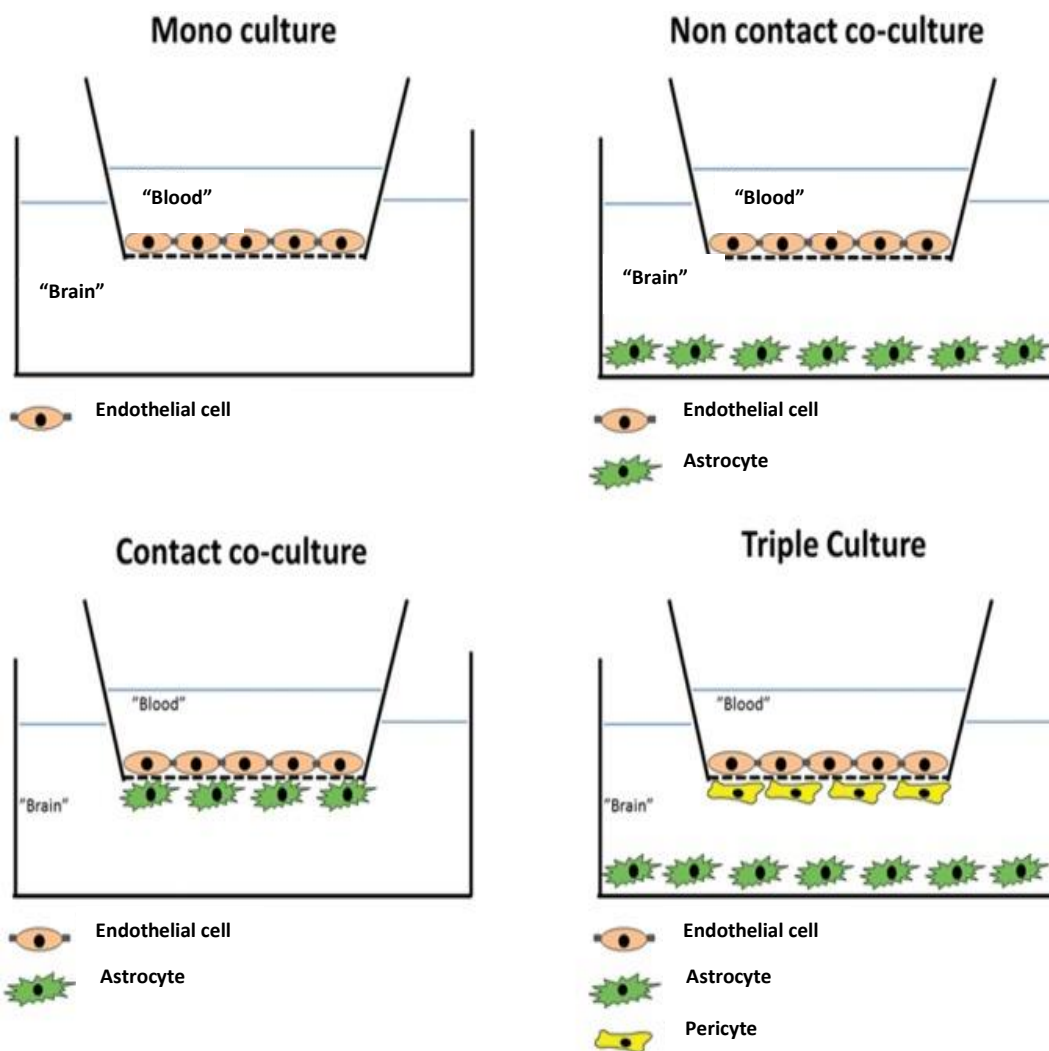


Figure 3.1 Different types of *in vitro* BBB models. Image obtained from (Helms *et al.*, 2016).

There is an increasing use of 3 dimensional BBB models that are composed of astrocytes embedded in collagen hydrogels and overlaid with brain endothelial cells (Sreekanthreddy *et al.*, 2015). These BBB models are a closer resemblance to the anatomical architecture of the neurovascular unit than that of the 2-dimensional (2D) BBB models (Gromnicova *et al.*, 2013; Sreekanthreddy *et al.*, 2015). The 3-dimensional (3D) BBB models have a higher TEER and express more tight junction proteins than that of the 2D BBB models. However, construction of some of these 3D models can be complicated, the inclusion of the third dimension makes these cultures more heterogeneous and this can influence the replication of these studies (Kaisar *et al.*, 2017).

Cell cultures made up of primary cells and transformed cells are widely used in developing *in vitro* BBB models. Brain cells from humans are mostly preferred to that of animals when developing *in vitro* BBB models because they mimic the *in vivo* BBB phenotype better than brain cells derived from animals (Helms *et al.*, 2016). However, primary brain cells are not easy to obtain on a regular basis and as a result other brain cells from different animal origins such as rat, bovine, porcine are often used in *in vitro* BBB models (Helms *et al.*, 2016). Although primary cells from animal origins produce high TEER, obtaining these cells can be laborious and there is a problem of reproducibility between laboratories. As a result of this, transformed immortalised brain cells are used to develop *in vitro* BBB models. Immortalised cell lines have several advantages. These cells lines are easy to use and can produce a large number of cells. Using immortalised cells can provide consistent and reproducible results. However, immortalised cell lines can only maintain endothelial cell properties for a number of passages after which they lose some of the distinctive properties of the BBB *in vivo* (Helms *et al.*, 2016). They have also been shown to express lower levels of BBB specific transporters and enzymes than *in vivo* (Helms *et al.*, 2016). Immortalised human brain endothelial cells are

more ideal for use in *in vitro* BBB than that of animals due to differences in species. Results obtained from animal based *in vitro* BBB models cannot always be extrapolated to certain human diseases such as cerebral malaria.

In vitro BBB models can serve as useful tools for studying the interactions and pathways that occur at the BBB during cerebral malaria. Most *in vitro* CM BBB models are mainly based on coculturing immortalised human brain endothelial cells on the upper part of a transwell with *Plasmodium falciparum* parasites (Tripathi *et al.*, 2007; Wassmer *et al.*, 2006). This model allows solutes or soluble factors released from endothelial cells or PRBC to move from the luminal to the basolateral side of the transwell and gives a closer depiction of what occurs during cerebral malaria *in vivo*. However, this model is limited as it only shows the interactions and responses between *Plasmodium falciparum* infected red blood cells (PRBC) and endothelial cells of the blood-brain barrier but does not address the important components of the NVU such as astrocytes and pericytes (He *et al.*, 2014).

Thus, an ideal *in vitro* BBB model of CM should be composed of human brain endothelial cells and other components of the neurovascular unit such as pericytes, astrocytes and basement membranes. These coculture models should produce high TEER values and would ideally be more representative of the human BBB *in vivo*. We used the HBEC-alone BBB which has previously been characterised in our lab to verify the phenotype and properties of endothelial cells used in this study. Immortalised human brain endothelial cells and primary human astrocytes were used to form an *in vitro* BBB model of HBEC and astrocytes grown in tandem. The transformed human brain endothelial cell line (HBEC) used in this study has previously been shown to have high TEER, uptake of Dil acLDL and upregulation of ICAM-1 (Stins *et*

al., 1997). This BBB model has been used in several *in vitro* cerebral malaria studies (Tripathi *et al.*, 2006).

The aim of this study was to develop a more advanced *in vitro* model of the BBB to use in the study of human cerebral malaria.

The overall objectives of this chapter were to:

1. Characterise HBEC by evaluating:
 - i. ICAM-1 expression on HBEC
 - ii. The effect of the inflammatory cytokine IL-1 β on ICAM-1 expression in HBEC.
Evaluation of ICAM-1 expression constitutively and in the presence of IL-1 β served as quality control for HBEC.
 - iii. Tight and adherens junction protein expression in HBEC.
2. Characterise primary human astrocytes by evaluating:
 - i. GFAP expression in astrocytes
 - ii. Determining the optimal conditions for culturing astrocytes
3. Develop an advanced BBB model where HBEC and astrocytes were grown in tandem on a transwell

3.2 Materials and methods

The overall aim of this experiment was to coculture transformed human brain endothelial cells and primary human astrocytes together. Before this could be done, we determined if HBEC and astrocytes could survive in HBEC media using an MTS assay and also determined if growing HBEC and astrocytes in HBEC media affected basal phenotype of the cell by monitoring ICAM1 and GFAP expression respectively.

3.2.1 MTS assay

An MTS assay was performed to determine if astrocytes would survive in different culture media. HBEC and astrocytes were seeded in 96 well plates as described in Chapter 2, section 2.4.1 for 24 hours. Cells were then treated with **astrocyte media (AM)**, **HBEC media**, **HBEC quiescent medium (Q1%FBS media)** containing RPMI with P/S, L-glutamine and 1% FBS, and **AM/HBEC media** containing 99% of astrocyte media and 1% of Q1%FBS media for 48 hours. The effect of these media on HBEC viability was then tested using the CellTiter 96 aqueous one solution.

The CellTiter 96 Aqueous one solution reagent (Promega) was thawed at room temperature for approximately 90 minutes. 20 μ l of CellTiter 96 Aqueous one solution reagent was pipetted into each well of the 96 well assay plate containing HBEC or astrocytes in 100 μ l of culture medium (Figure 3.2) and placed in a humidified incubator at 37°C, 5% CO₂ for 4 hours (Figure 3.2). The quantity of formazan product measured by absorbance at 450nm is directly proportional to the number of living cells in the culture. Maximum absorbance reading was observed at 4 hours.

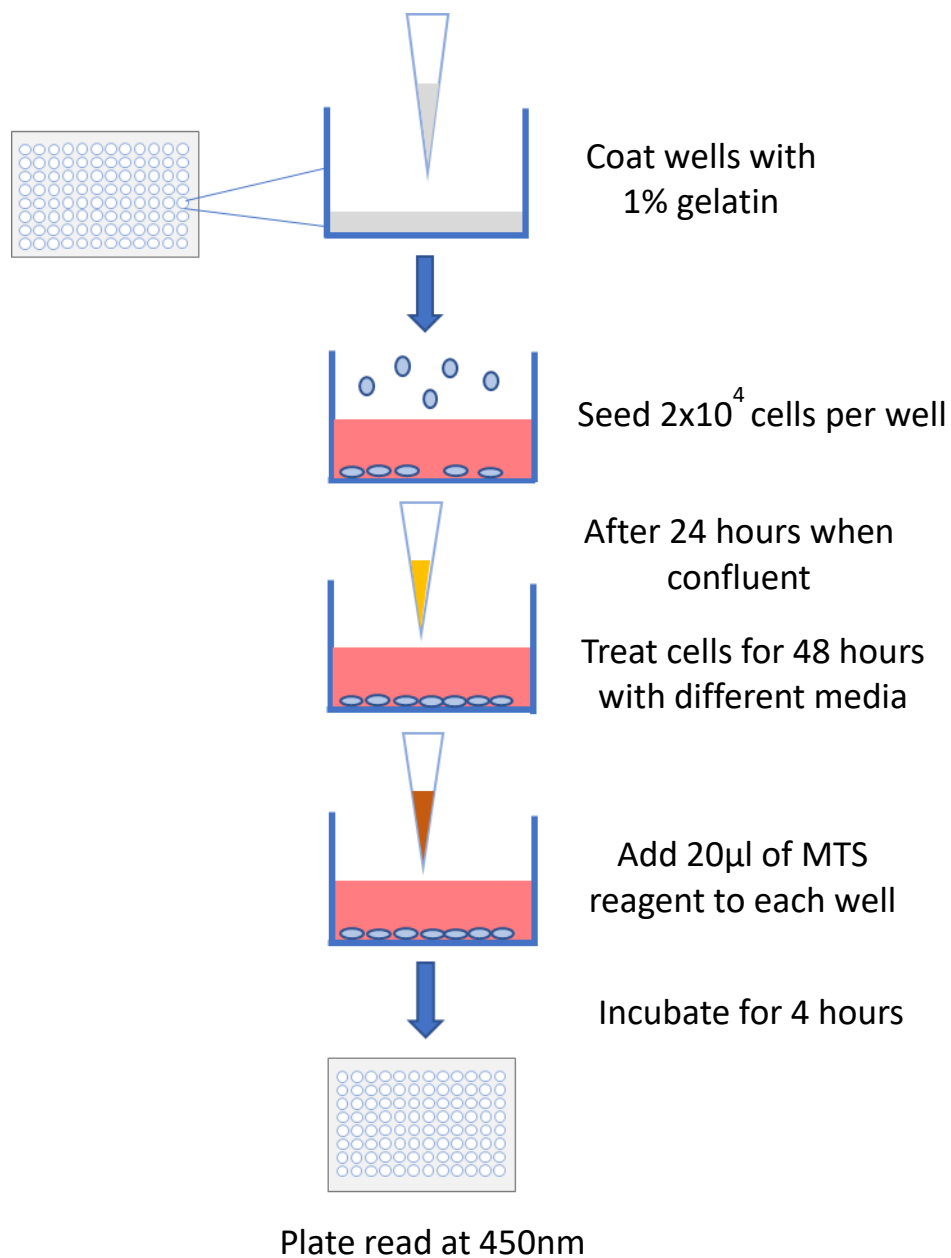


Figure 3.2 Schematic diagram of MTS assay. 96 well plates were seeded with cells. Cells were treated for 48 hours. The reagent was added to each well and incubated at 37°C , 5% CO_2 for 4 hours. The maximum absorbance at 450nm was read after 4 hours.

The CellTiter 96 Aqueous One Solution Cell Proliferation Reagent was used to quantify viable HBEC and astrocyte cells *in vitro*. This reagent is made up of MTS (tetrazolium compound [3-(4,5-dimethylthiazol-2-yl)-5-(3-carboxymethoxyphenyl)-2-(4-sulphophenyl)-2H-tetrazolium]) and phenazine ethosulfate (PES) an electron coupling reagent. This assay is based on the reduction of MTS tetrazolium compound by viable cells to produce a coloured formazan that is soluble in cell culture media (Figure 3.3). NADPH or NADH dehydrogenase enzymes produced in metabolically active cells is thought to be responsible for this reaction.

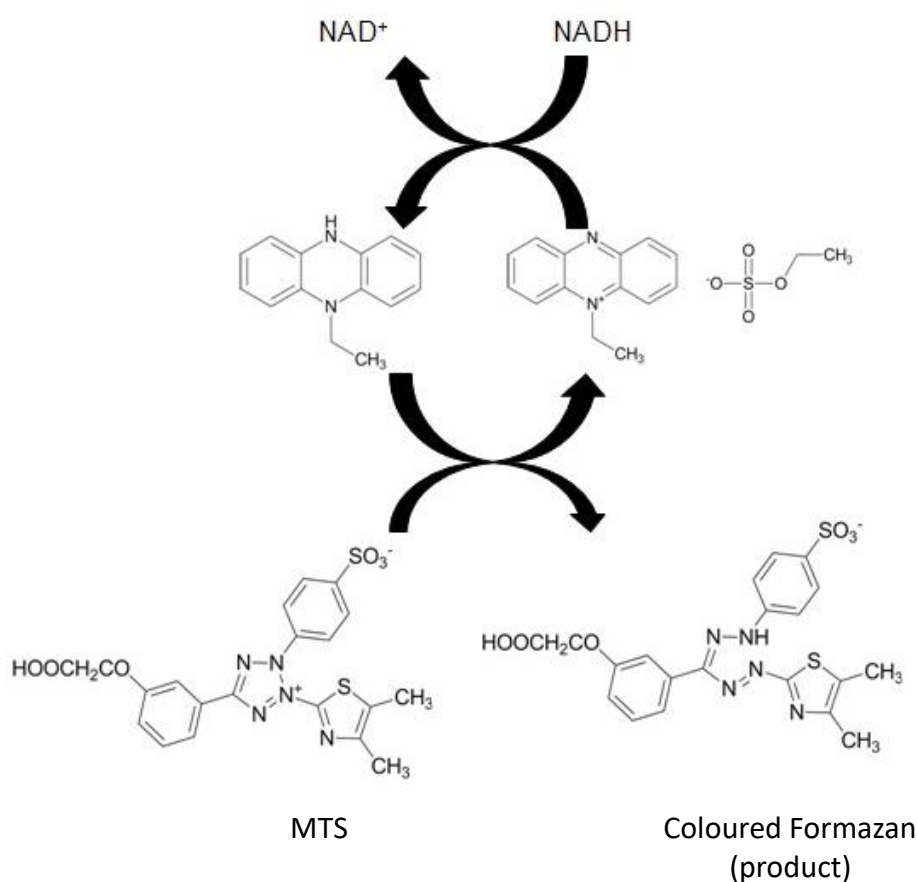


Figure 3.3 Conversion of MTS to a coloured formazan product. Phenazine ethyl sulphate (PES) transfers an electron from NADH in the cytoplasm into the culture media and this reduces MTS to formazan. Image obtained from (Riss *et al.*, 2016).

3.2.2 Detection of ICAM-1, Vinculin and Claudin-5 using immunofluorescence analysis

Immunofluorescence analysis was performed to determine if HBEC expressed tight and adherens junction proteins vinculin and claudin-5 and the adhesion molecule ICAM-1 as described in Chapter 2, section 2.23. HBEC were permeabilized in 0.2% Triton in PBS for 15 minutes at room temperature. HBEC were washed once in PBS and blocked in 3% BSA in PBS for 1.5 hours. 250µl of primary antibody diluted in 1% BSA in PBS was added (all antibody dilutions are listed in Table 3.1) to each coverslip for 1 hour at room temperature. HBEC were then washed three times with PBS for 10 minutes each.

The secondary antibody (dilutions in Table 3.1) was then added to cells for 1 hour and washed as described before. After 1 hour, coverslips were mounted on slides as described in Chapter 2, section 2.23. All antibody incubations were done at room temperature.

Table 3.1 Antibody dilutions used for immunofluorescence.

Primary antibody	Dilution	Secondary antibody	Dilution
Anti-ICAM-1 Mouse monoclonal IgG	1:200	Goat Anti-Mouse IgG-FITC	1:100
Monoclonal Anti-vinculin antibody produced in mouse	1:150	Anti-Mouse IgG-R-Phycoerythrin antibody	1:100
Anti-Claudin-5 Rabbit polyclonal IgG	1:300	Sheep Anti-Rabbit IgG-FITC	1:200
Anti-Claudin-5 Rabbit polyclonal IgG	1:50	CyTM-conjugated AffiniPure Donkey Anti-Rabbit IgG	1:1000
Polyclonal rabbit anti-GFAP	1:500	Goat anti-rabbit Alexa Fluor 488	1:300

3.2.3 Detection of Glial fibrillary acidic protein (GFAP) in astrocytes

Qualitative analysis using immunofluorescence for detection of the astrocyte marker GFAP in astrocytes was performed as described in Chapter 2, section 2.23. Astrocytes were grown on glass coverslips in AM as described in Chapter 2, section 2.23. Astrocytes were blocked with 5% new goat serum (NGS) in 1xTBST (Tris Buffered Saline with Tween®20) for 1 hour at

4°C. Astrocytes were incubated with 250µl of primary antibody (rabbit anti-GFAP) diluted in 1% NGS in 1xTBST (Table 3.1) at 4°C overnight. The next day astrocytes were washed three times with PBS for 3 minutes each. The secondary antibody (goat anti-rabbit) diluted in 1% NGS in TBST (Table 3.1) was then added to cells for 2 hours at room temperature in the dark. Cells were then washed as described before. After 2 hours, coverslips were mounted on slides as described in Chapter 2, section 2.23 and viewed under the Nikon Eclipse 80i fluorescent microscope.

3.2.4 Cell-based ELISA for detection of ICAM-1 in HBEC

Cell-based ELISA for quantitative detection of ICAM-1 in HBEC was performed as described in Chapter 2, section 2.24. ICAM-1 is basally expressed on endothelial cells and upregulated when stimulated with cytokines such as IL-1 β (O'Carroll *et al.*, 2015; Wertheimer *et al.*, 1992). Cell-based ELISA was performed to determine ICAM-1 expression in HBEC in response to treatment with HBEC media, astrocyte media (AM), 1ng/ml and 15ng/ml concentration of IL-1 β for 24 hours as described in Chapter 2, section 2.24. A 1:200 mouse anti-human ICAM-1 antibody dilution and 1:2000 goat anti-mouse secondary antibody dilution was used in the cell-based ELISA.

3.2.5 Cell-based ELISA GFAP

Cell-based ELISA for quantitative detection of GFAP in astrocytes was performed as described in Chapter 2, section 2.24.

3.2.5.1 Optimisation of antibody concentrations

The optimal rabbit anti-GFAP primary antibody and goat anti-rabbit secondary antibody dilutions for detecting GFAP in astrocytes in a cell-based ELISA, was investigated. The different antibody dilutions examined can be observed in (Table 3.2).

3.2.5.2 Detection of GFAP in basal and cytokine treated astrocytes

The effect of different media on GFAP expression was determined by cell-based ELISA as described in Chapter 2, section 2.24 using the optimised rabbit anti-GFAP primary antibody dilution of 1:2000 and goat anti-rabbit secondary antibody dilution of 1:3000. IL-1 β has been shown to upregulate GFAP expression in astrocytes (Brahmachari *et al.*, 2006). In this study we explored IL-1 β as a positive control GFAP upregulation in astrocytes. To determine the optimal concentration of IL-1 β that could upregulate cell-associated GFAP expression in astrocytes, astrocytes were treated with 15, 30, 60 and 100ng/ml of IL-1 β diluted in astrocyte media (AM) or AM/HBEC media and a cell-based GFAP ELISA was performed as described in Chapter 2, section 2.24.

Table 3.2 Different anti-GFAP antibody combinations for optimisation of cell-based GFAP ELISA in astrocytes.

Antibody combination	Rabbit Anti-GFAP antibody dilution	Goat anti-rabbit antibody HRP-conjugate
Combination 1	1:500	1:1000
Combination 2	1:500	1:3000
Combination 3	1:1000	1:3000
Combination 4	1:2000	1:3000
Combination 5	1:2500	1:3000
Combination 6	1:3000	1:3000

3.2.6 Western blot analysis for detection of GFAP in astrocytes

Western blot analysis was performed for qualitative detection of cell-associated GFAP expression in astrocytes *in vitro* as described in Chapter 2, section 2.17-2.22. Varying amounts of protein lysates 7 μ g, 15 μ g, 22 μ g and 44 μ g were run on the SDS PAGE gel to determine the optimal amount of astrocyte lysate needed to be loaded for GFAP detection.

Western blot analysis was used for quantitative detection of soluble GFAP in the supernatant of astrocytes treated with 15, 30, 60 and 100ng/ml IL-1 β concentrations diluted in AM and AM/HBEC media. The supernatants of astrocytes were collected after 48 hours of treatment and western blot analysis was performed as described in Chapter 2, section 2.17-2.22. The rabbit anti-GFAP antibody dilution of 1:500 and goat anti-rabbit antibody dilution of 1:1000 were used.

3.2.7 Development of *in vitro* BBB models

An *in vitro* BBB model was developed that mimicked the BBB *in vivo*. The BBB model was made up of an upper compartment and a lower compartment separated by a polyester membrane (Figure 3.5A) with a pore size of 0.4 μ m. Cells were grown on the top and bottom part of the polyester membrane which had a growth membrane area of 0.33cm² (Corning Incorporated, 2018). The polyester membrane allowed cell visibility under an inverted microscopy and was used to monitor the growth of monolayer of cells.

The upper compartment represented the luminal (blood side) and the lower compartment represented the basolateral (brain side) of the BBB (Figure 3.5A).

3.2.7.1 Set up of HBEC-alone BBB model

On day 1, transwells were coated with 1% gelatin for 20 minutes to facilitate adhesion of HBEC. 2×10^4 cells were seeded on the luminal side of each transwell in 200 μ l of HBEC complete media (Figure 3.4). 1300 μ l of HBEC medium was added to the bottom chamber (Figure 3.4). HBEC were grown in a 37°C, 5% CO₂ humidified incubator for 2 hours after which the medium was changed. The medium was changed on day 3. The culture was maintained for 5 days overall to allow the formation of a confluent HBEC monolayer.

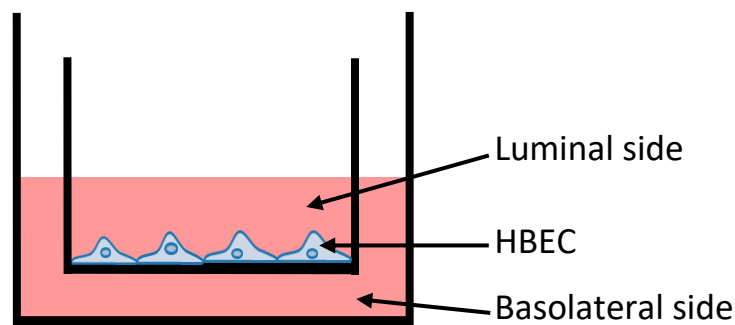


Figure 3.4 Set up of HBEC-alone BBB model schematic.

3.2.7.2 Set up of HBEC-astrocyte tandem BBB model: Protocol 1

To set up the HBEC and astrocyte BBB model, HBEC were grown on the luminal side of the transwell as described above, 2 hours after astrocytes were grown on the basolateral sides of the transwell (Figure 3.5A).

To facilitate adhesion of astrocytes to the membrane, transwell inserts were inverted and the basolateral side coated with 100 μ l of 1% gelatin for 20 minutes in a 37°C, 5% CO₂ humidified incubator (Figure 3.5 B). Gelatin was aspirated off the basolateral side of the transwells. Subsequently, 2×10^4 cells were seeded on the basolateral side of each transwell in 100 μ l of AM and allowed to adhere for 2 hours in a 37°C, 5% CO₂ humidified incubator (Figure 3.5 C). After 2 hours once the astrocytes had adhered to the membrane, the transwell was inverted back, placed in 24 well plates and HBEC was then seeded on the luminal side of the transwell as

described above (Figure 3.5 D). This was counted as Day 1 of growing both HBEC and astrocytes in tandem. The medium from both luminal and basolateral sides of the transwell was changed on day 3. HBEC and astrocytes were cocultured in tandem in HBEC media for 5 days in total in a 37°C, 5% CO₂ humidified incubator. However, due to the fact that astrocytes were observed at the bottom of the 24 well plate after seeding of the HBEC on the luminal side, protocol 1 was optimised and **protocol 2** was adopted for all further studies.

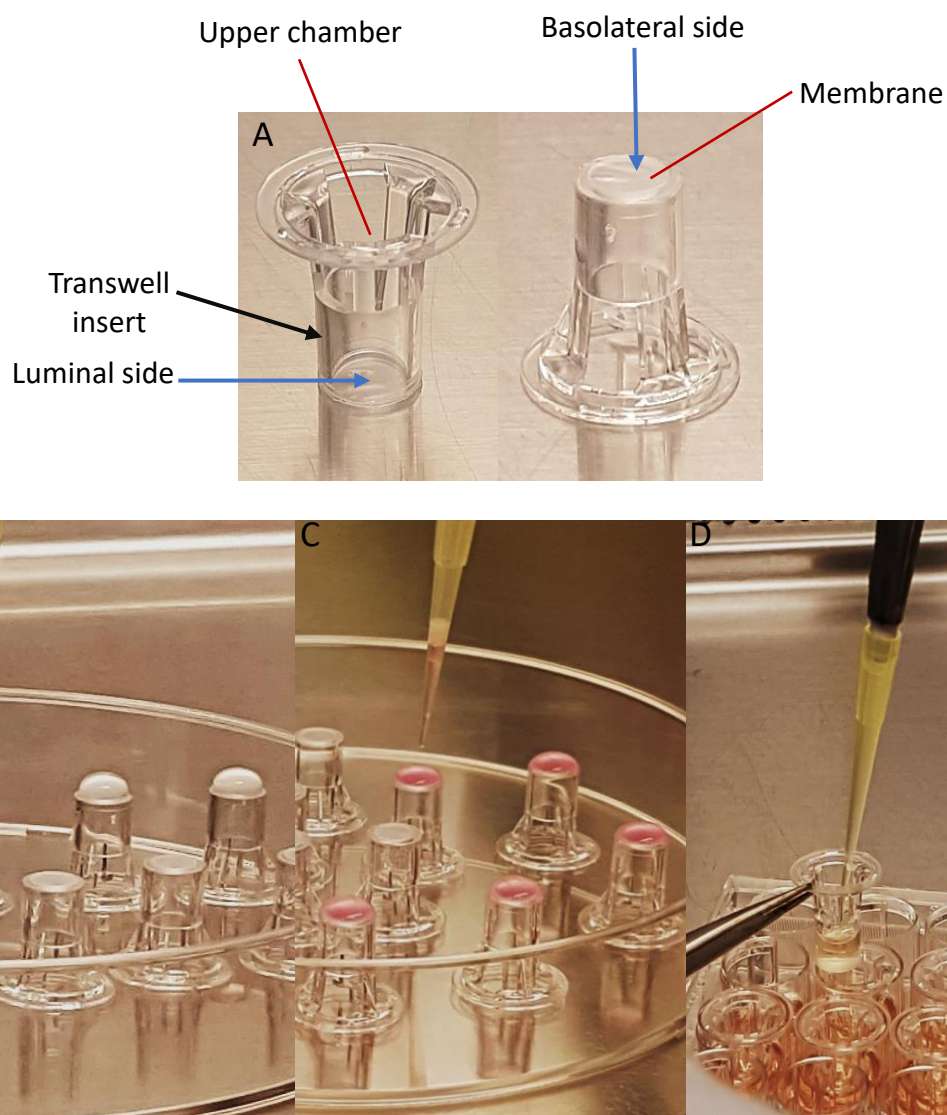


Figure 3.5 The experimental process for growing HBEC and astrocytes in tandem on different sides of the transwell membrane. (A) Corning transwells two-compartment system. (B) The basolateral side of transwell was coated with 1% gelatin. (C) 2×10^4 astrocytes were seeded on the basolateral side of each transwell and allowed to adhere for 2 hours. The transwell was then flipped back and grown in AM for 2 days in a 37°C humidified incubator at 5% CO₂. (D) After 2 hours (protocol 1) or 2 days (protocol 2), 2×10^4 HBEC were seeded on the luminal side of the transwell membrane and cocultured with astrocytes for 5 days in HBEC media in a 37°C incubator, at 5% CO₂.

3.2.7.3 Set up of HBEC-astrocyte tandem BBB model: Protocol 2

To set up the HBEC and astrocyte BBB model using protocol 2, transwell inserts were inverted and the basolateral side coated with 100 μ l of 1% gelatin as described in 3.2.7.2 (Figure 3.5 B). Subsequently, 2×10^4 astrocytes were seeded on the basolateral side of each transwell in 100 μ l of AM and allowed to adhere for 2 hours in a 37°C, 5% CO₂ humidified incubator (Figure 3.5 C). After 2 hours once the astrocytes had adhered to the membrane, the transwell was inverted back, placed in 24 well plates and cultured in 1300 μ l of AM for 2 days. **After 2 days**, HBEC was then seeded on the luminal side of the transwell as described above (Figure 3.5 D). This was counted as Day 1 of growing both HBEC and astrocytes in tandem. The medium from both luminal and basolateral sides of the transwell was changed on day 3. HBEC and astrocytes were cocultured in tandem in HBEC media for 5 days in total in a 37°C, 5% CO₂ humidified incubator. **Protocol 2** was adopted for all further studies.

3.2.8 Measurement of Transendothelial Electrical resistance (TEER)

The structural BBB integrity of HBEC-alone and HBEC-astrocyte BBB model was evaluated by measuring TEER using an Endohm chamber connected to an EVOM resistance meter (World Precision Instruments) (Figure 3.6). An Endohm chamber containing a silver/silver chloride electrode was filled with 1.5ml of pre-warmed (37°C) HBEC media. The transwells were removed with sterile forceps from 24 well plates and placed in the Endohm chamber one at a time. An electrode cap containing concentric electrodes was then placed on top of the cells and TEER measurements were recorded using the EVOM voltohmmeter in duplicate readings (Figure 3.6). The positioning of electrodes on both sides of the membrane in the Endohm chamber produces a constant current density across the membrane (Srinivasan *et al.*, 2015).

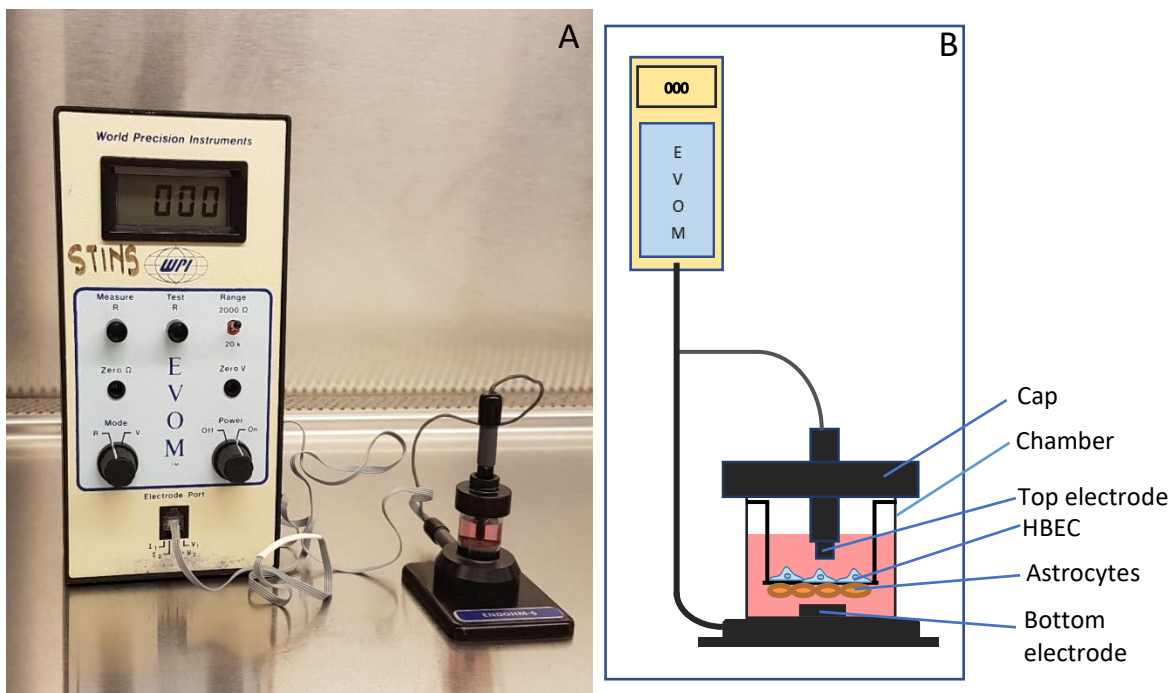


Figure 3.6 Transendothelial electrical resistance (TEER) measurement of transwells. (A). EVOM (left) and Endohm 6 (right) used to measure TEER. (B) Schematic drawing of the Endohm chamber with culture insert. To measure TEER, transwells with HBEC-alone or HBEC-astrocyte were placed in the Endohm chamber and covered with the cap connected to the EVOM. The TEER was then measured.

TEER was measured daily for over 5 days, from day 1 to day 5. Transwells without cells were measured as blank controls. To calculate TEER of each transwell, TEER measurement from

blank controls was subtracted from the TEER reading of each well, the value obtained was then multiplied by the surface area of the filter membrane 0.33 cm^2 . The unit for TEER was $\Omega \text{ cm}^2$.

3.2.9 Statistical Analysis

Data from densitometry analysis, cell based ELISA, MTS assay and TEER measurements were analysed for statistical significance by one-way ANOVA and 2 sample t-tests with $p < 0.05$ considered as statistically significant.

3.2.10 Densitometry analysis

The intensity of bands in western blot analysis was measured using Image J (NIH). The image was initially captured using the FluorChem machine. Lanes were selected on Image J and band densities of each lane were graphed using the Analyze Gel Plugin in Image J. The area under the curve was calculated using the “magic wand” button. These steps were repeated for each antigen of interest and for each lane on the ponceau image. The optical density of each antigen band of interest was divided by the optical density of its corresponding protein band (loading control) to produce an antigen to ponceau band ratio.

3.3 Results

3.3.1 Characterisation of HBEC

3.3.1.1 ICAM-1 expression in resting HBEC

A cobblestone morphology of HBEC was observed using an inverted microscope under basal conditions (Figure 3.7A). Qualitative analysis using immunofluorescence was used to detect ICAM-1 expression in HBEC, to verify HBEC phenotype and properties. ICAM-1 is expressed in HBEC under basal conditions (Wertheimer *et al.*, 1992). Immunofluorescence analysis showed the presence of ICAM-1 on the surface and cell membranes of HBEC (Figure 3.7 B-D).

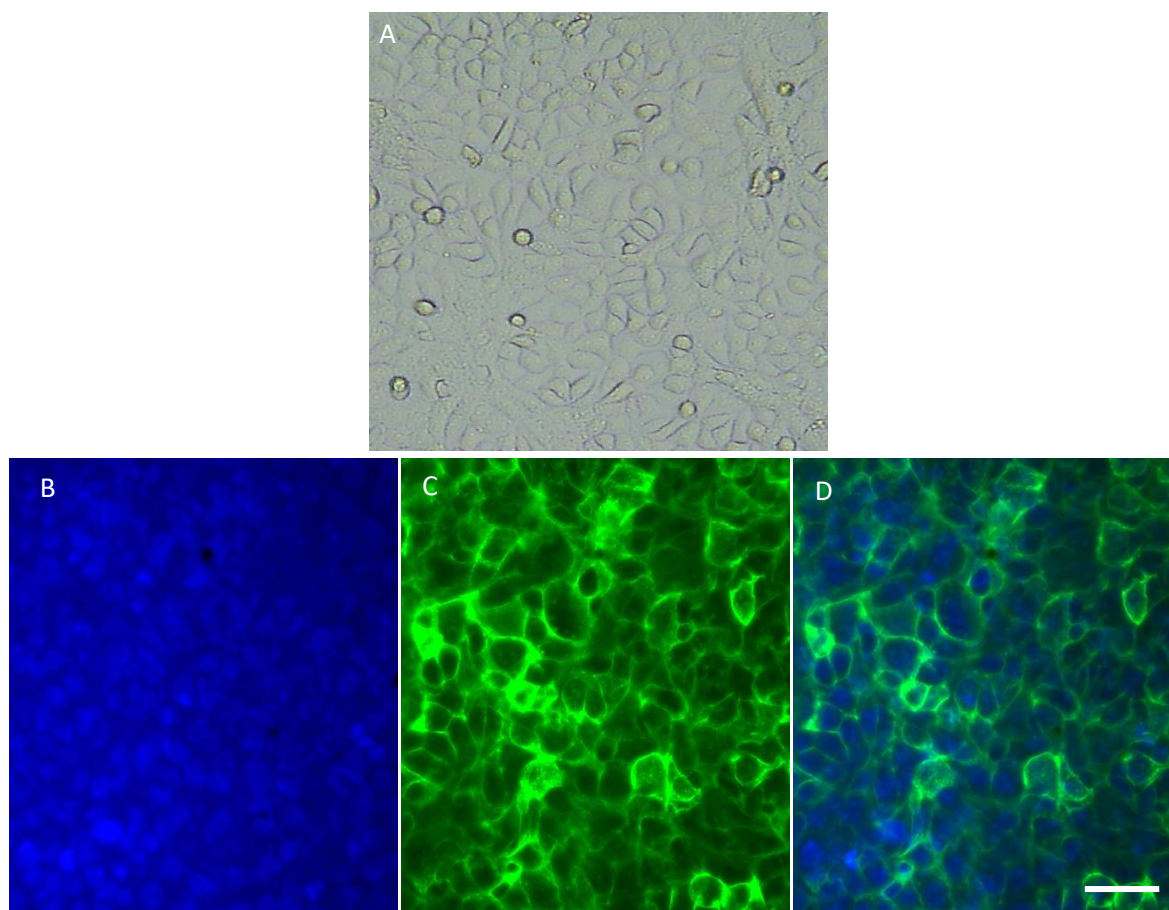


Figure 3.7 Images of resting HBEC. (A) HBEC viewed under an inverted microscope at 10X magnification. HBEC show ‘cobble stone’ morphology. B-C: Immunofluorescence analysis of the endothelial cell marker ICAM-1 in human brain endothelial cells. (B) Nuclei (blue) were stained with vectashield with DAPI (C) ICAM-1 expressed on the surface and membrane of HBEC were stained with FITC (green) (D) Merged image of nuclei and ICAM-1 on the cell surface and membrane of HBEC. The fluorescent image was captured at 20X magnification. Scale bar = 50µm.

3.3.1.2 HBEC viability in different media

An MTS assay was performed to determine the best media for maintaining the HBEC-astrocyte BBB and to determine if HBEC could survive in media other than its usual growth media. Results from four separate biological replicates showed that there was no significant difference in cell viability between HBEC grown in HBEC media and that of HBEC grown in AM and AM/HBEC media (Figure 3.8). These results suggest that HBEC could survive in both AM and AM/HBEC media.

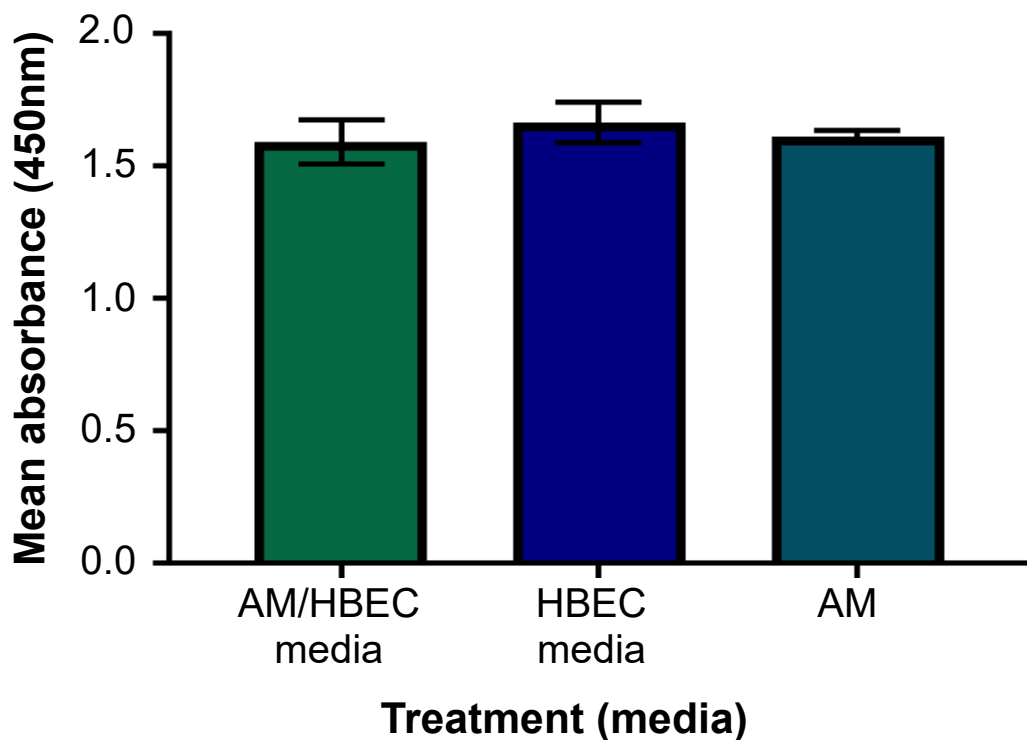


Figure 3.8 MTS assay used to determine if HBEC could survive in AM/HBEC, HBEC and Astrocyte media. Error bars represent the standard error mean (SEM), n=4.

3.3.1.3 Detection of ICAM-1 expression in HBEC grown in AM and HBEC media

The effect of HBEC media and AM on ICAM-1 expression in HBEC was tested using cell-based ELISA. Results from 3 biological replicates showed that there was no significant difference in ICAM-1 expression between HBEC grown in AM or HBEC media (Figure 3.9).

Absorbance at 450nm was a reflection of ICAM-1 expression.

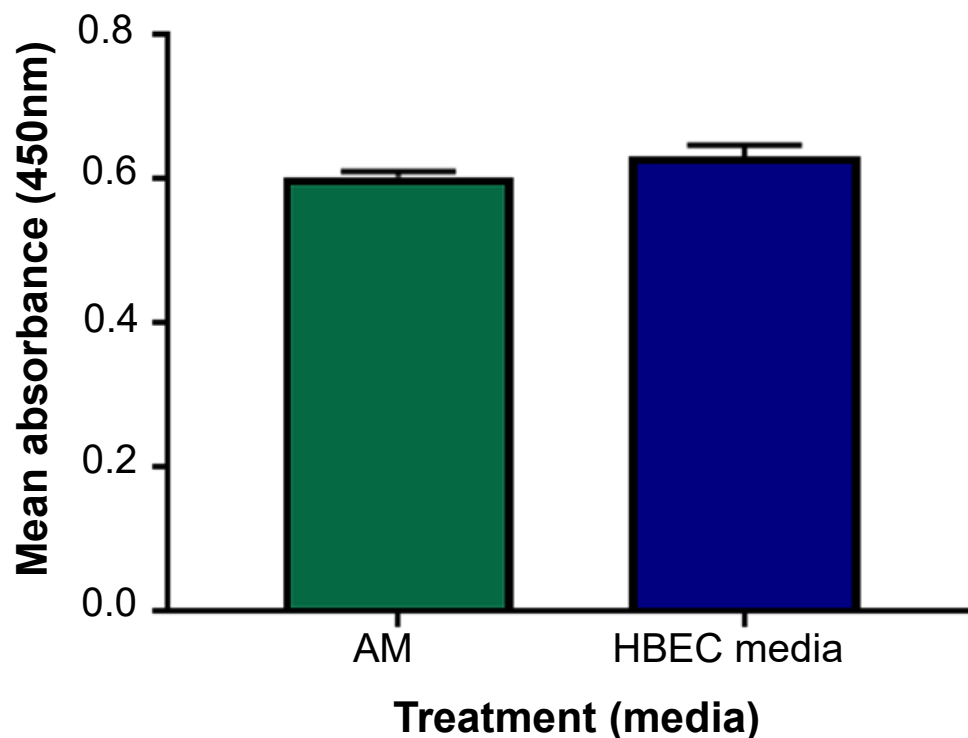


Figure 3.9 Determining the effect of AM and HBEC media on ICAM-1 expression in HBEC using cell-based ELISA. Error bars represent SEM, n=3.

3.3.1.4 Changes in ICAM-1 in HBEC treated with 1ng/ml of IL-1 β

The effect of the cytokine IL-1 β on ICAM-1 expression in HBEC was examined. ICAM-1 was constitutively expressed in resting HBEC (Figure 3.10). Results from 3 separate biological replicates showed that ICAM-1 expression was significantly enhanced in HBEC stimulated with 1ng/ml and 15ng/ml of IL-1 β diluted in Q1%FBS media compared to the control (Figure 3.10).

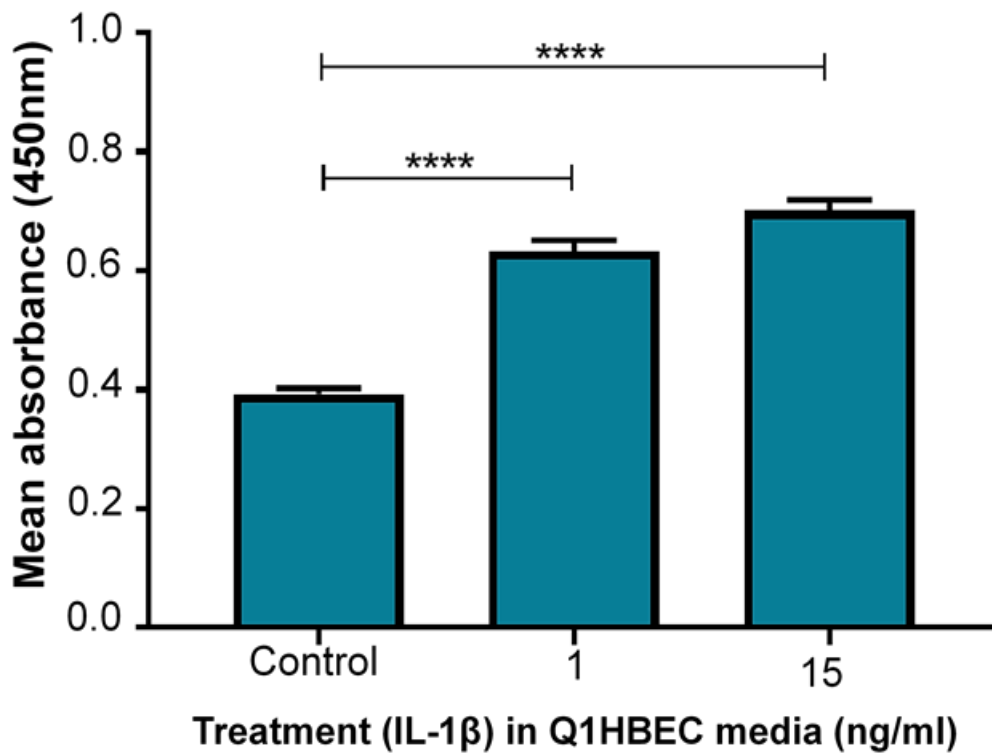


Figure 3.10 Changes in ICAM-1 expression in response to treatment of HBEC with varying concentrations of IL-1 β . Error bars represent standard error of the mean. **** denotes significance at $p < 0.0001$, $n=3$.

3.3.1.5 Vinculin and Claudin-5 expressed by HBEC

The expression of tight junction and adherens junction proteins claudin-5 and vinculin in HBEC, were characterised using qualitative immunofluorescence analysis. Vinculin (red) and Claudin-5 (red) were observed at cell to cell junctions in HBEC (Figure 3.11B-C).

Claudin-5 (green) staining was observed in the cytoplasm of HBEC when a 1:300 dilution of rabbit anti-Claudin-5 antibody (Table 3.1) was used (Figure 3.11A). This was unexpected as previous studies have shown a continuous expression of Claudin-5 at cell to cell contacts in HBEC (Luissint *et al.*, 2012). Further optimisation using a 1:50 dilution of Rabbit anti-Claudin-5 antibody (Table 3.1) showed expression of claudin-5 (red) at cell to cell contacts of HBEC (Figure 3.11B).

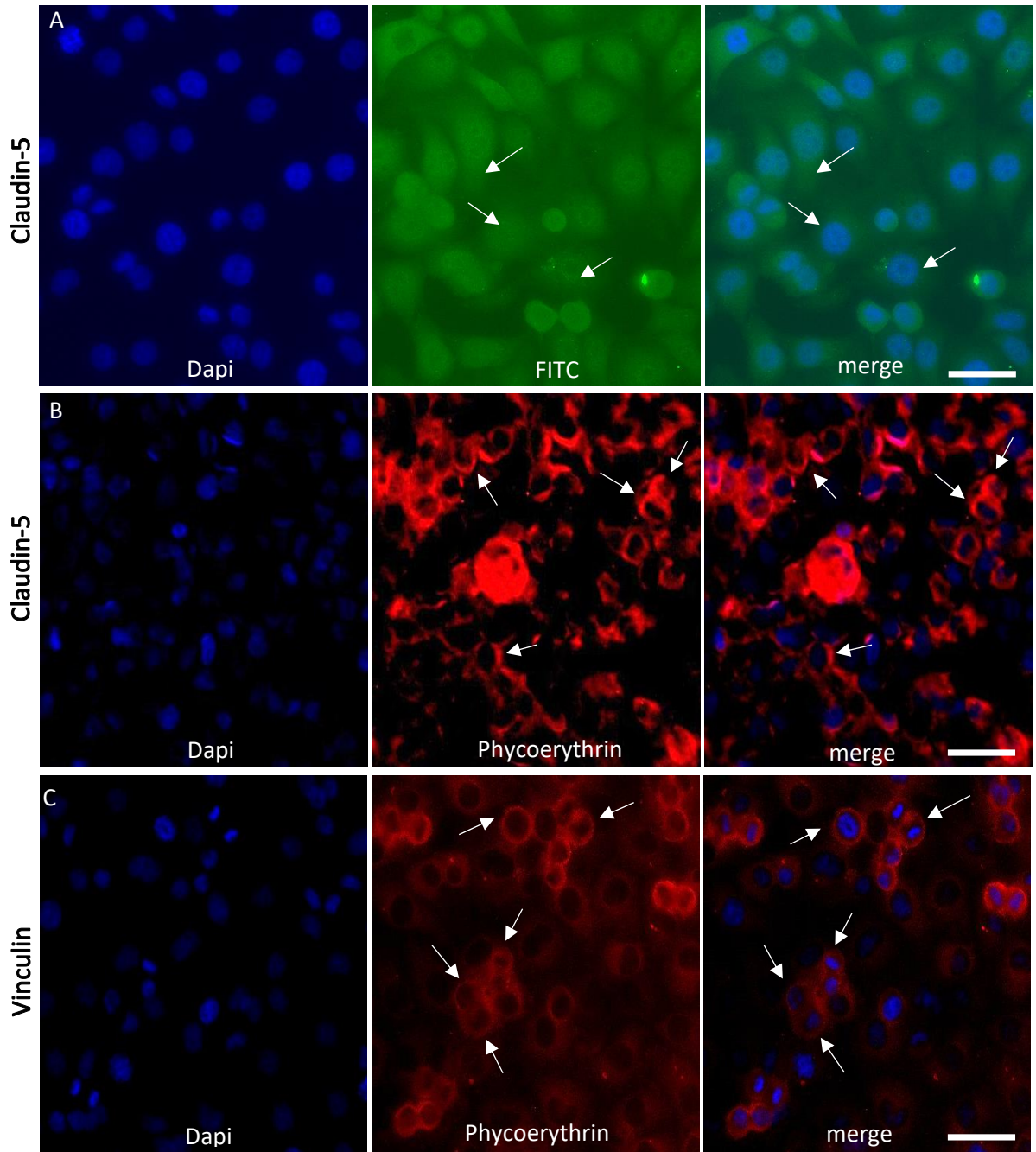


Figure 3.11 Expression of endothelial and BBB markers by HBEC. Immunofluorescence image of tight junction proteins Claudin-5. (A) FITC stain (green) of Claudin-5 (1:300 antibody dilution) observed in the cytoplasm of HBEC. (B) Phycoerythrin stain (red) of Claudin-5 (1:50 antibody dilution) localised at cell to cell junctions of HBEC (shown by the white arrow). (C) Immunofluorescence image of adherens junction protein Vinculin (red) observed at cell to cell junctions (shown by the white arrow). Nuclei (A-C) counterstained with DAPI. Scale bar 15 μ m.

3.3.2 Characterisation of astrocytes

3.3.2.1 Astrocyte viability in different media

An MTS assay was performed to determine the best media for maintaining the HBEC-astrocyte BBB model and for growing astrocytes. Results from 4 separate biological replicates showed that there was no significant difference in cell viability between astrocytes grown in AM and that of astrocytes grown in HBEC and AM/HBEC media (Figure 3.12). These results indicated that astrocytes could grow in the different media mentioned above (Figure 3.12).

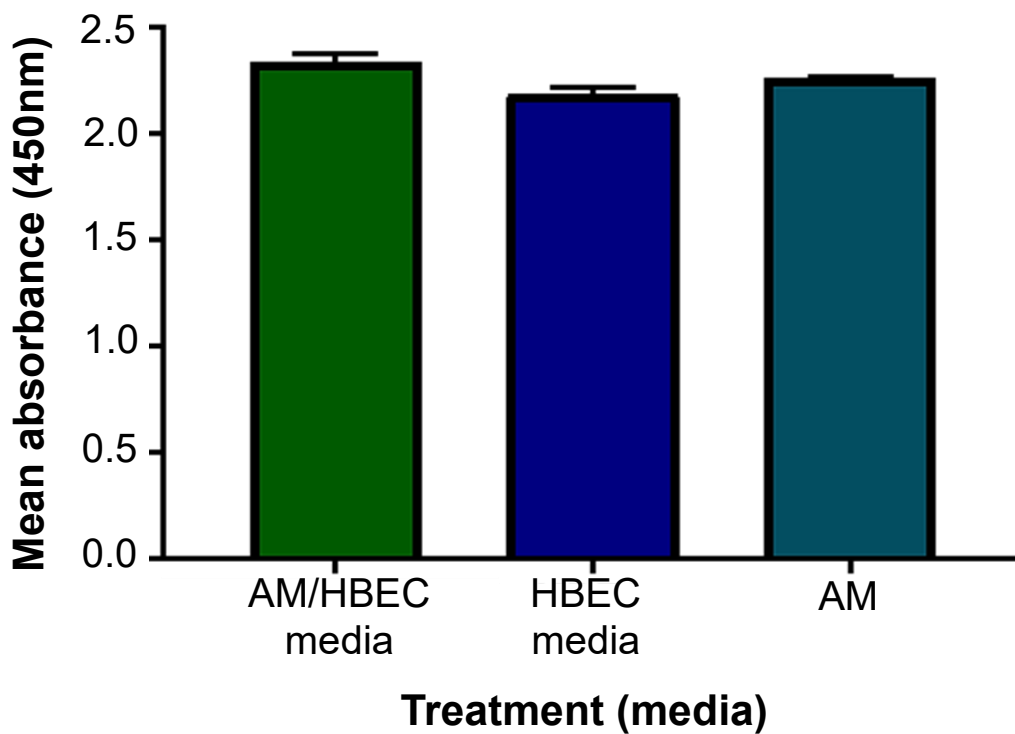


Figure 3.12 Determining if astrocytes could survive in AM/HBEC, HBEC and Astrocyte media using an MTS assay. Error bars represent standard error of the mean, n=4.

3.3.2.2 GFAP expression in primary human astrocytes

Astrocytes *in vitro* showed, a polygonal, fusiform and flat morphology with several branching processes under basal conditions (Figure 3.13A), as shown by phase-contrast microscopy. Astrocytes divided and achieved maximum surface coverage ie growth after 4-5 days (data not shown). Subsequently, the main marker for astrocytes GFAP was characterised using immunofluorescence and western blot analyses. Immunofluorescence analysis showed an intense cytoplasmic staining of GFAP in astrocytes (Figure 3.13C-D). The GFAP staining showed a meshwork of processes throughout the cytoplasm (Figure 3.13C-D).

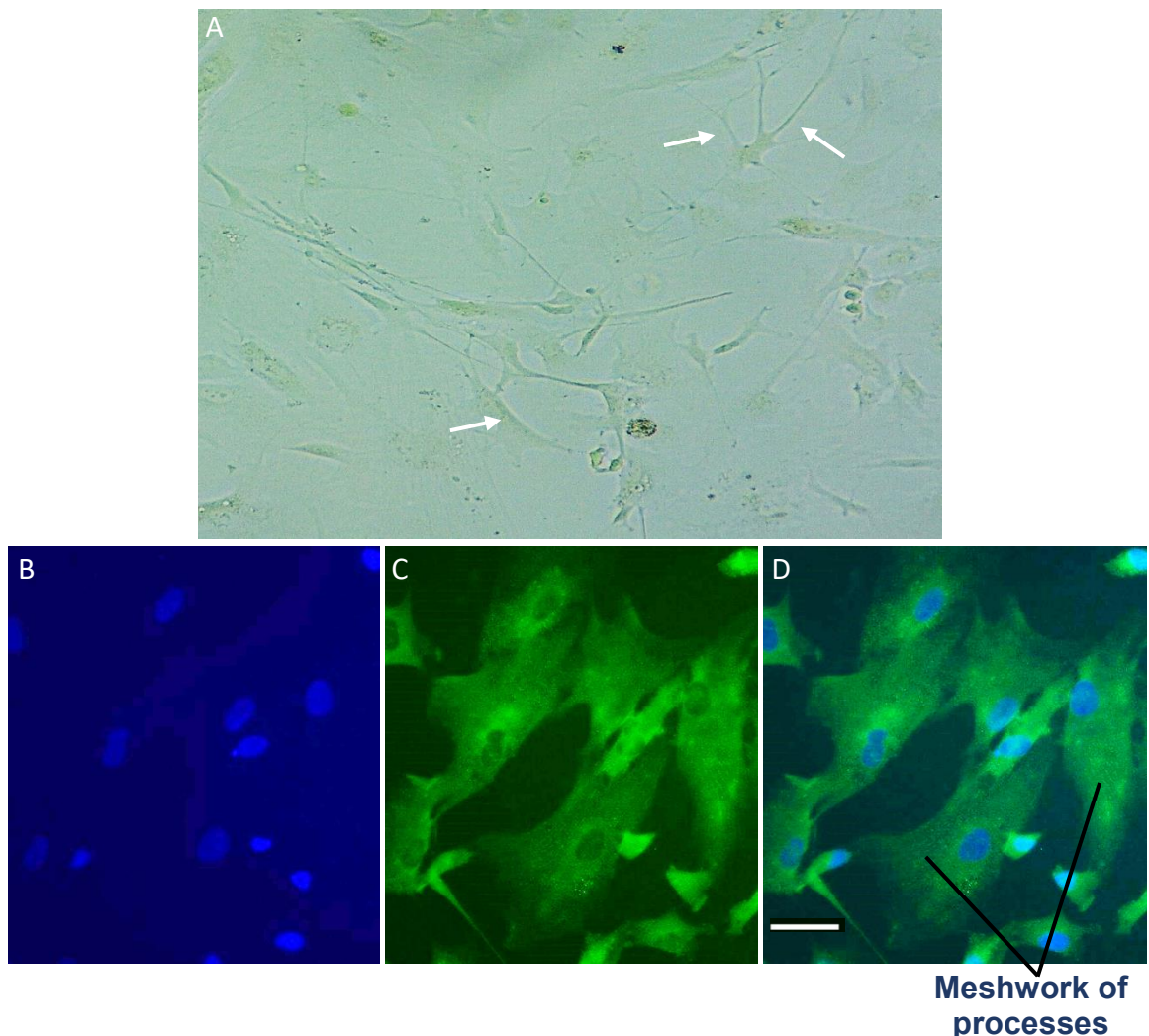


Figure 3.13 Images of primary human astrocytes *in vitro*. (A) Under normal conditions, primary human adult astrocytes presented a polygonal, fusiform and flat morphology (arrows) as shown by phase contrast microscopy. Immunofluorescence analysis of GFAP expression in astrocytes. (B) Nuclei (blue) of astrocytes were stained with vectashield with Dapi (C) Astrocytes tested positive for GFAP (green) under basal conditions (20X magnification). (D) Merged image of (B and C) indicate GFAP expression in the cytoplasm of astrocytes. Scale bar 50µm.

3.3.2.3 Optimisation of cell-based ELISA for detection of GFAP

In this study different combinations of (primary rabbit anti human GFAP antibody) and (secondary goat anti rabbit antibody) concentrations were examined in order to determine the optimal antibody dilutions to be used in subsequent GFAP cell based ELISAs. In the first instance, a 1:500 dilution of Rabbit anti-GFAP antibody and a 1:1000 dilution of goat anti-rabbit (GAR) HRP conjugate antibody were used in cell-based ELISA to detect GFAP expression in astrocytes. Results showed that upon addition of TMB, wells of ELISA plate turned uniformly blue quickly and the reaction colour was too intense. This resulted in high absorbance values (Figure 3.14). Further dilution of the primary and secondary antibodies showed that the combination of the 1:2000 dilution of rabbit anti-GFAP and 1:3000 dilution of Goat anti-rabbit HRP conjugate antibody produced the highest signal and lowest background noise (Figure 3.14).

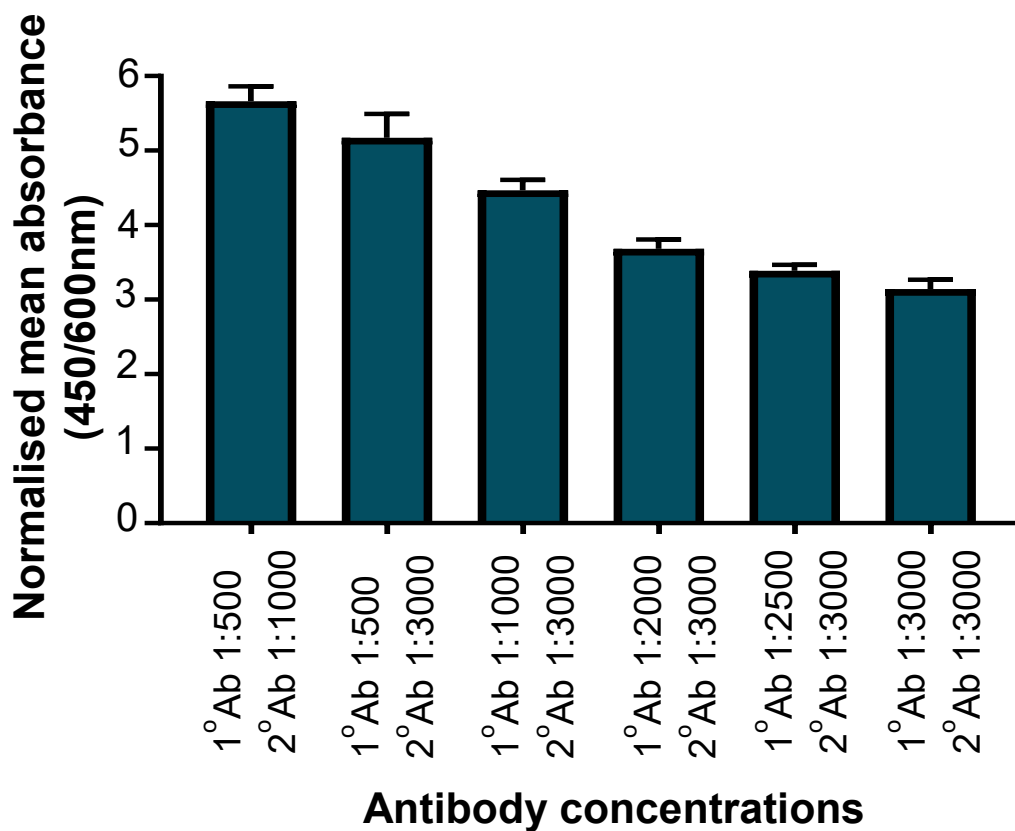


Figure 3.14 Optimized anti-GFAP antibody and Goat anti-rabbit (GAR) antibody dilutions for cell-based ELISA. Based on the data shown above, the anti-GFAP antibody and GAR dilution of 1:2000 and 1:3000 respectively were the optimal dilutions for cell-based ELISA for detection of GFAP in astrocytes. Error bars represent standard error of the mean, n=3.

3.3.2.4 GFAP expression of astrocytes grown in different media

The effect of different media on GFAP expression was tested using cell-based ELISA. Results showed there was no significant difference in GFAP expression in astrocytes grown in HBEC media, AM/HBEC media compared to that of astrocytes grown in AM (Figure 3.15). These results showed that the GFAP expression of astrocytes grown in the different media was not affected by using media other than the usual growth medium (Figure 3.15). Results indicate that astrocytes could grow in any of the media mentioned above.

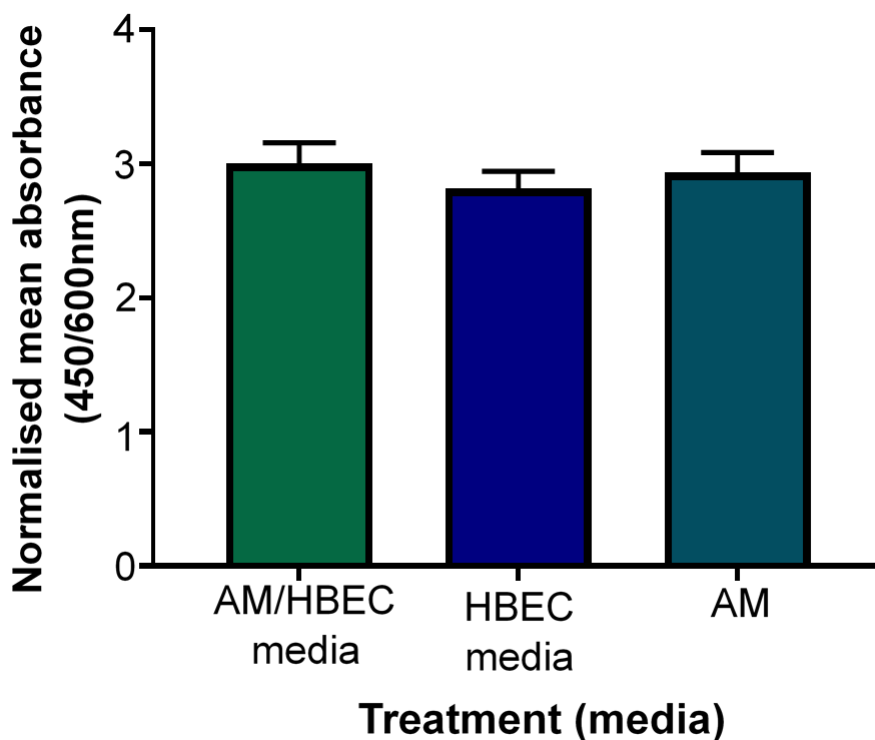


Figure 3.15 Determination of GFAP expression in astrocytes treated with AM, AM/HBEC and HBEC media. Error bars represent standard error of the mean, n=11.

3.3.2.5 Cell-associated GFAP expression in astrocytes treated with different IL-1 β concentrations diluted in AM and AM/HBEC media

The optimal concentration of IL-1 β that could upregulate cell-associated GFAP expression in astrocytes, was determined using a quantitative cell-based GFAP ELISA. The optimum GFAP primary and secondary antibody dilutions from previous experiments, a 1:2000 dilution of rabbit anti-GFAP and a 1:3000 dilution of goat anti-rabbit antibody (Figure 3.14) was used in this experiment. No significant change in GFAP absorbance was observed in astrocytes treated with 15, 30, 60 and 100ng/ml of IL-1 β diluted in AM, as compared to astrocytes grown in AM (Figure 3.16). A trend towards a small increase in GFAP absorbance was observed in astrocytes treated with 100ng/ml IL-1 β diluted in AM, however, this was not statistically significant (Figure 3.16).

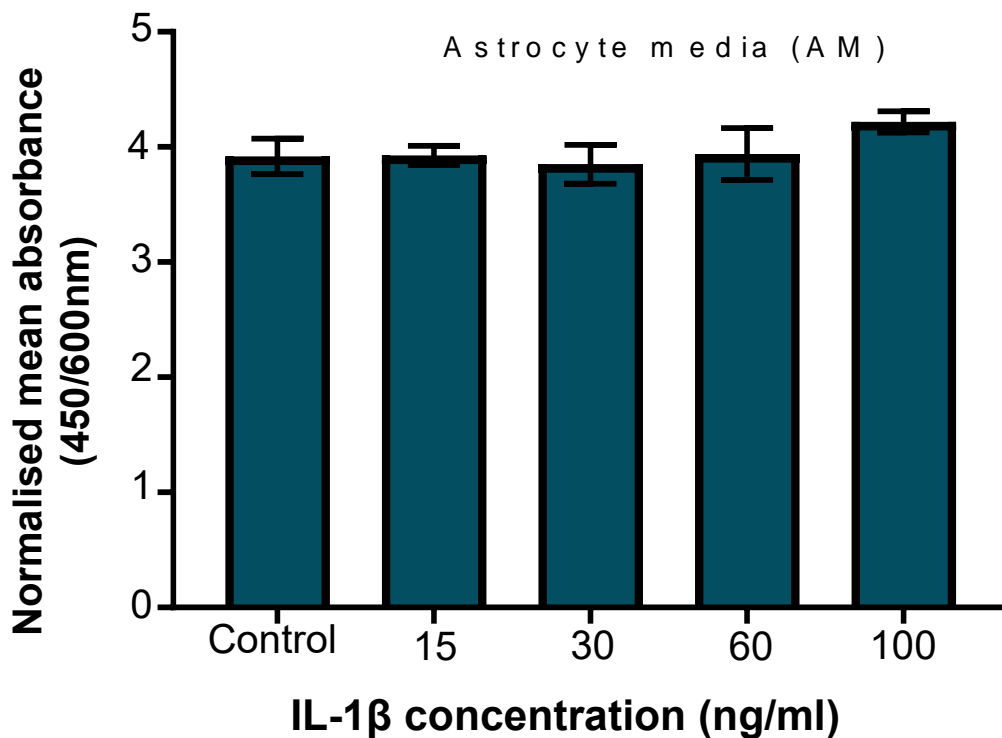


Figure 3.16 Cell-associated GFAP expression in astrocytes treated with different concentrations of IL-1 β diluted in AM. Error bars represent standard error of the mean, n=3.

A significantly higher GFAP absorbance was observed in astrocytes treated with 60 and 100 ng/ml of IL-1 β diluted in AM/HBEC media ($p < 0.05$) compared to astrocytes grown in AM/HBEC media (Figure 3.17). However, treatment of astrocytes with 15 and 30ng/ml IL-1 β diluted in AM/HBEC media caused no significant change in GFAP absorbance (Figure 3.17).

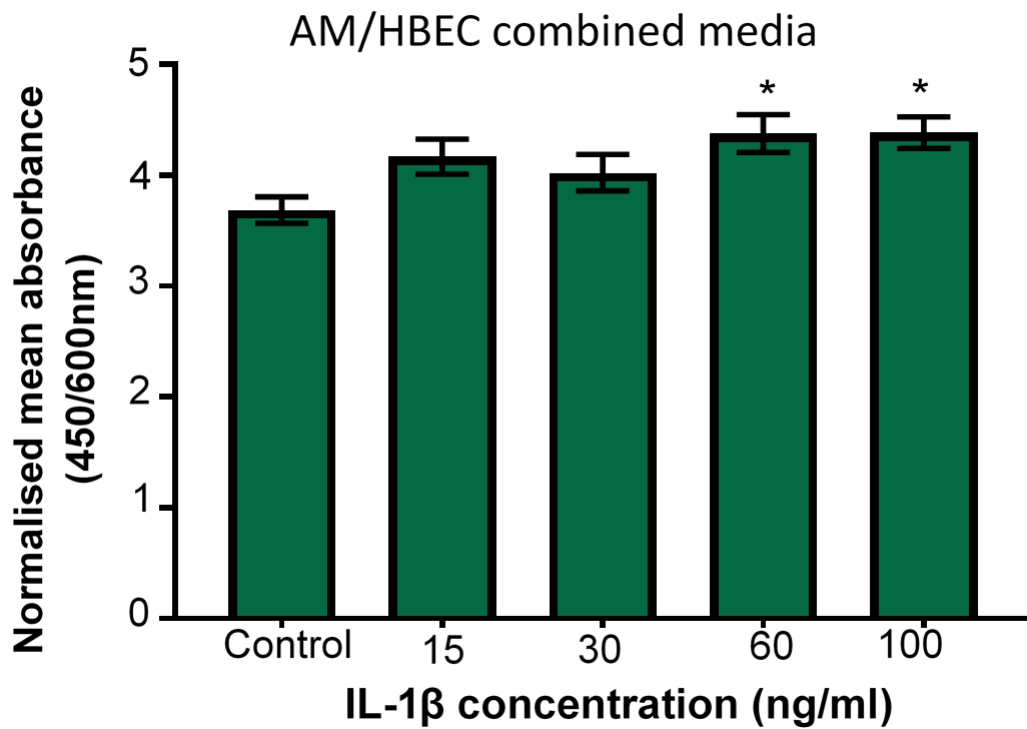


Figure 3.17 Increase in cell-associated GFAP expression in astrocytes treated with different concentrations of IL-1 β diluted in AM/HBEC media. Error bar represents standard error of the mean, $n=3$.

3.3.2.6 GFAP expression in the supernatant of astrocytes treated with IL-1 β diluted in AM and AM/HBEC media

Western blot analysis was used to examine cell-associated GFAP in resting cells and release of GFAP into the supernatant of astrocytes that had been treated with 15, 30, 60 and 100ng/ml IL-1 β diluted in AM and AM/HBEC media. Results showed the presence of bands between 48-60 kDa in resting astrocytes (Figure 3.18) and astrocytes treated with IL-1 β (Figure 3.19).

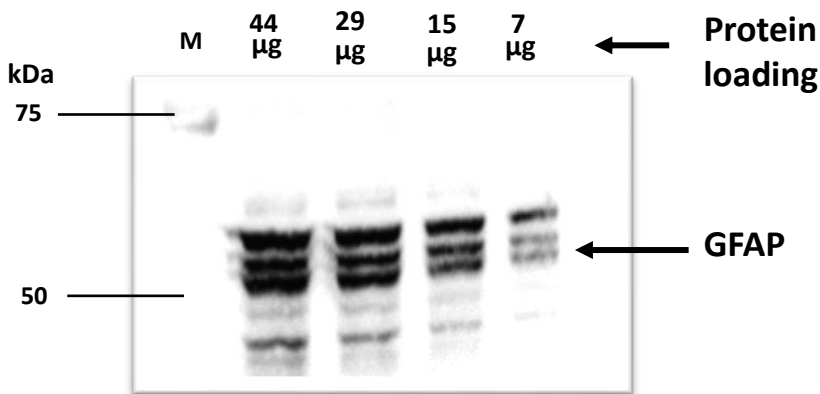


Figure 3.18 Optimisation of protein loading of astrocytes in the resting state.

In the supernatant of astrocytes treated with IL-1 β diluted in AM, a trend towards a gradual increase in soluble GFAP was observed as the concentration of IL-1 β increased from 15-100ng/ml (Figure 3.19). These results were quantified by densitometric analysis on the GFAP bands at 48-60kDA (Figure 3.19). In the supernatant of astrocytes treated with IL-1 β diluted in AM/HBEC media, a trend towards a gradual decrease in soluble GFAP was observed as the concentration of IL-1 β increased from 15-100ng/ml (Figure 3.19).

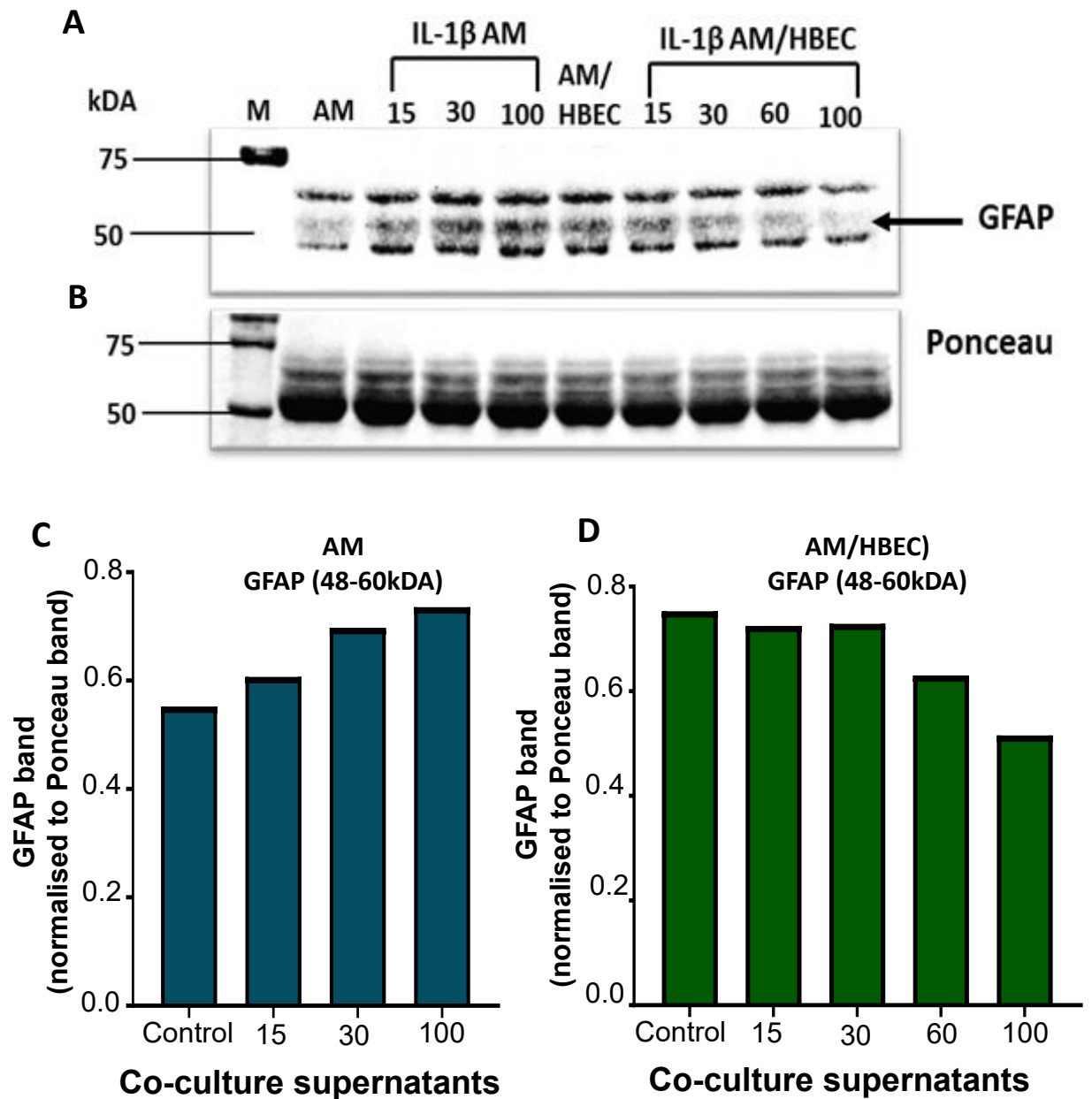


Figure 3.19 Soluble GFAP observed in the supernatant of astrocytes treated with 15, 30, 60 and 100ng/ml IL-1 β diluted in AM and AM/HBEC media. Lane 1 Molecular weight marker, Samples were treated with, Lane 2 AM, Lane 3 IL-1 β AM15ng/ml, Lane 4 IL-1 β AM30ng/ml, Lane 5 IL-1 β AM100ng/ml, Lane 6 AM/HBEC media, Lane 7 IL-1 β AM/HBEC15ng/ml, Lane 8 IL-1 β AM/HBEC30ng/ml, Lane 9 IL-1 β AM/HBEC60ng/ml, Lane 10 IL-1 β AM/HBEC100ng/ml. B. Ponceau stain. (C and D). Densitometry analysis on bands of GFAP between 48-60kDA.

3.3.3 Optimisation of HBEC-astrocyte and HBEC-BBB model

Preliminary experiments were performed to determine the most appropriate conditions for growing HBEC and astrocytes in tandem using protocol 1 (section 3.2.7.2). Astrocytes were grown for 2 hours on the basolateral side of the transwell, after 2 hours HBEC were grown on the luminal side of the transwell and TEER of the cells *in vitro* was measured to determine the number of days needed to achieve an optimal BBB reflected by achievement of maximum TEER. TEER values of the HBEC-alone, astrocyte alone and HBEC-astrocyte BBB were recorded over 10 days. The TEER value of the astrocyte monolayer was significantly lower than that of the HBEC-alone BBB and the HBEC-astrocyte BBB, with TEER values ranging from $0.995\Omega\text{cm}^2$ on day 2 to $8.79\Omega\text{cm}^2$ on day 10 (Figure 3.20). TEER values of HBEC-astrocyte BBB were only $11.78\Omega\text{cm}^2$ on day 2 but by day 10 had reached $33.51\Omega\text{cm}^2$ (Figure 3.20). TEER values of the HBEC-alone BBB increased from $11.78\Omega\text{cm}^2$ on day 2 to $30.94\Omega\text{cm}^2$ on day 7 ($p<0.05$) (Figure 3.20) and plateaued from day 7 (Figure 3.20). Although the TEER values of the HBEC-astrocyte BBB model were significantly higher than that of the HBEC-alone BBB on day 2 ($p<0.005$) and day 3 ($p<0.01$), astrocytes were observed in the bottom chamber of the 24 well plate. This suggested that adding HBEC to the luminal side of the transwell immediately after growing astrocytes for 2 hours did not allow astrocytes to attach properly on the basolateral side of the transwell. Thus, this resulted in astrocytes falling off the basolateral side of the transwell into the bottom of the well. Hence, the conditions for growing HBEC and astrocytes in tandem were optimised and improved using protocol 2.

Using protocol 2 (section 3.2.7.3), astrocytes were grown on the basolateral side of a transwell for 2 days after which HBEC were grown on the luminal side for 5 days (Figure 3.5).

TEER of HBEC and HBEC-astrocyte BBB model were measured over 5 days after seeding HBEC. TEER of HBEC-astrocyte BBB model was significantly higher than the HBEC-alone

BBB model up to day 4 ($p < 0.0001$) (Figure 3.21). On day 5, the TEER of both the HBEC-astrocyte BBB and the HBEC-alone BBB model plateaued with no significant difference in TEER between them. TEER of HBEC-alone BBB increased from $1.43\Omega\text{cm}^2$ on day 1 to $18.25\Omega\text{cm}^2$ on day 5 ($n=73$) (Figure 3.21). TEER of HBEC-astrocyte BBB model increased from $3.97\Omega\text{cm}^2$ on day 1 to $19.62\Omega\text{cm}^2$ on day 5 ($n=73$) (Figure 3.21). The data showed that both *in vitro* BBB models formed a tight BBB over time with the HBEC-astrocyte BBB model forming a tighter BBB than that of the HBEC-alone BBB.

Optimisation TEER of *in vitro* BBB models using Protocol 1

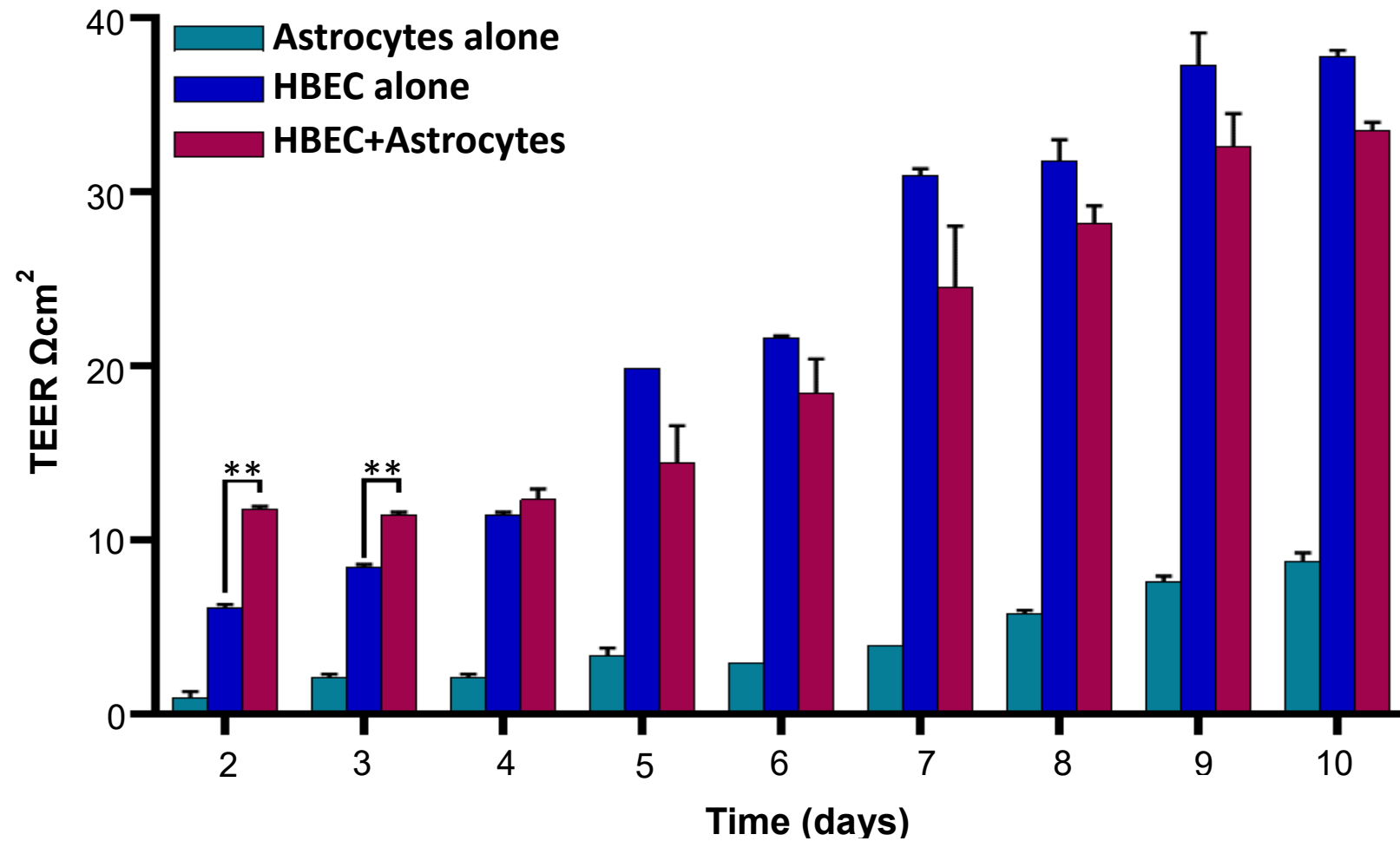


Figure 3.20 TEER of astrocyte alone, HBEC-alone BBB, and HBEC-astrocyte BBB using protocol 1. TEER values of the HBEC-astrocyte BBB model were significantly higher than that of the HBEC-alone BBB on day 2 ($p < 0.005$) and day 3 ($p < 0.01$). Results are described as mean \pm SEM, $n = 10$.

TEER of HBEC-alone and HBEC-astrocyte BBB models using Protocol 2

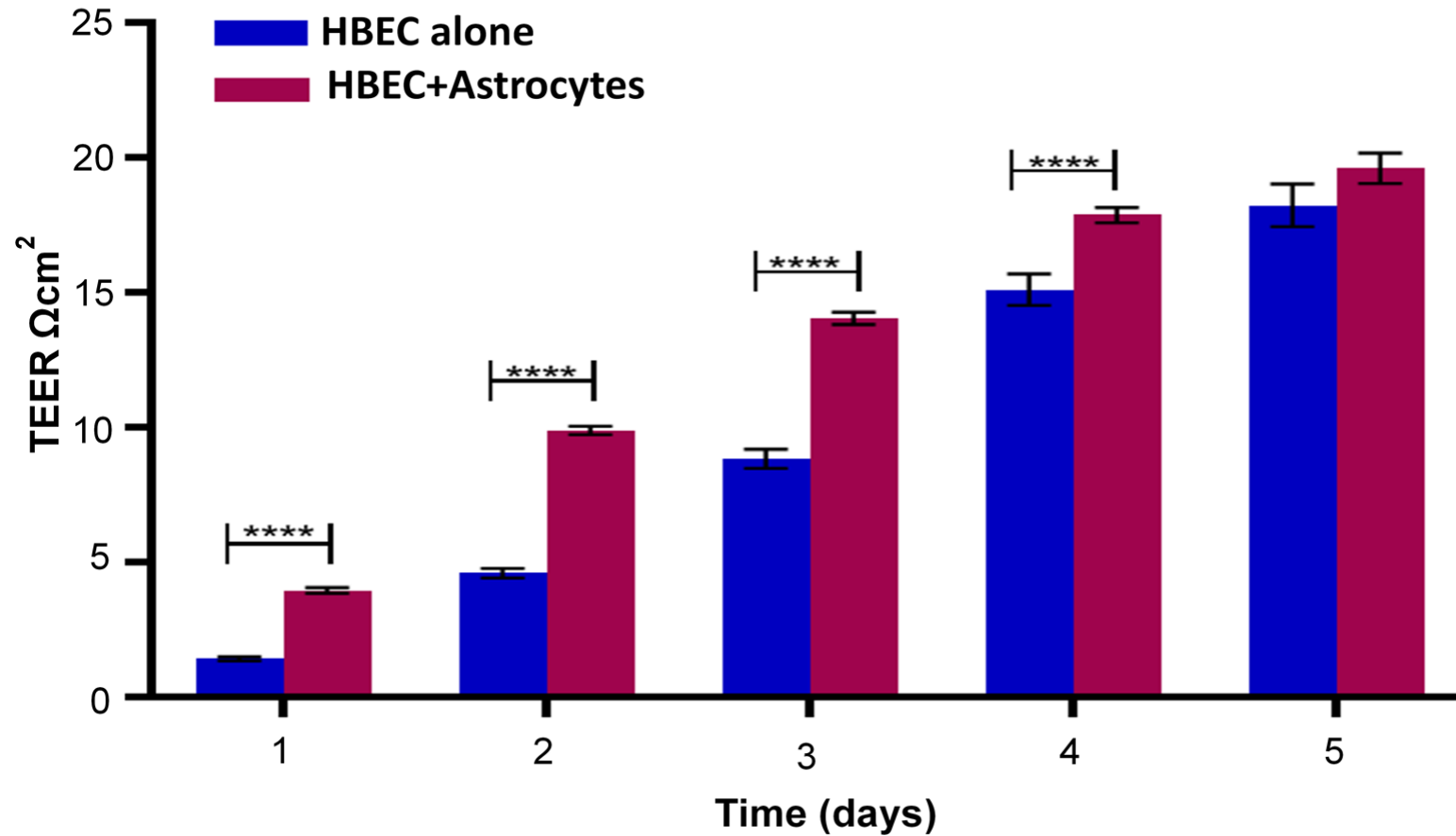


Figure 3.21 TEER values of HBEC-alone BBB model and HBEC-astrocyte BBB using protocol 2. TEER values of both models increased with time over 5 days. TEER of HBEC-astrocyte BBB model was significantly higher than that of HBEC-alone BBB models from day 1 to day 4. The values are presented as mean \pm SE (n=73). ****P<0.0001.

3.4 Discussion

In this study, we set out to develop an advanced human BBB model *in vitro* consisting of primary human astrocytes and immortalised human brain endothelial cells grown in tandem on a transwell.

Prior to developing our advanced *in vitro* BBB model, the best conditions for growing HBEC and astrocytes together were optimised and characterised. HBEC used in this study exhibited a cobblestone like morphology when confluent, expressed junction proteins claudin-5 and vinculin and the adhesion molecule ICAM-1 (Figure.7). These characteristics were similar to other endothelial cells being grown *in vitro* and confirmed the endothelial lineage of the HBEC used in this study (Wallez and Huber, 2008)

Primary human astrocytes were subsequently characterised, and results showed primary astrocytes possessed characteristic features of mature astrocytes. GFAP, a primary intermediate filament of mature astrocytes was observed in the cytoplasm of astrocytes under basal conditions (Figure 3.13C-D). GFAP expression in astrocytes is upregulated in response to stress or injury and thus it is one of the most widely used markers to detect astrocyte activation. (Sofroniew & Vinters, 2010). IL-1 β a proinflammatory cytokine was previously shown to upregulate GFAP expression in astrocytes and thus we explored the possibility of using IL-1 β as a positive control for upregulation of GFAP expression in astrocytes (Brahmachari *et al.*, 2006).

Cell based ELISA results showed that IL-1 β diluted in AM or AM/HBEC media could upregulate GFAP expression and thus could serve as a positive control for GFAP activation in astrocytes (Figure 3.16, Figure 3.17). Cell-based ELISA is not the best assay for detection of cell-associated GFAP since astrocytes do not form a compact monolayer when confluent and

thus results obtained may not be reliable. Western blot analysis enabled the detection of the different GFAP forms produced in astrocytes under basal conditions and in response to stimuli.

The presence of multiple GFAP bands in the supernatants of astrocytes treated with IL-1 β could suggest that IL-1 β was causing damage to astrocytes resulting in the release of GFAP which was then broken down into GFAP products (Figure 3.19). *In vitro*, calpain was shown to proteolytically cleave GFAP into breakdown products between 38-44kDA (Yang *et al.*, 2015). Treatment of astrocytes with higher concentrations of IL-1 β diluted in AM appeared to cause more damage to astrocytes, resulting in the increased release of GFAP (Figure 3.19). GFAP breakdown products were observed in the serum of traumatic brain injury (TBI) patients and this increased with severity of injury (Papa *et al.*, 2012). It was suggested that within hours of astrocyte damage from TBI, GFAP-breakdown products were released.

Interestingly treatment of astrocytes with higher concentrations of IL-1 β diluted in AM/HBEC did not seem to damage astrocytes (Figure 3.19).

These results indicated that astrocytes behaved differently depending on culture conditions such as media. It is possible that components in the AM/HBEC media such as RPMI 1640 that were absent in the AM were making astrocytes less susceptible to damage by IL-1 β .

Preliminary experiments were performed to determine the best media for growing HBEC and astrocytes in tandem. Cell viability assays showed that HBEC and astrocytes could grow in HBEC media, AM and AM/HBEC media suggested by their comparable viabilities (Figure 3.8, Figure 3.12). There was no significant difference in basal ICAM-1 expression in HBEC grown in HBEC media or AM (Figure 3.9). Similarly, there was no significant difference in basal GFAP expression in astrocytes grown in HBEC media, AM or AM/HBEC media (Figure 3.15). HBEC media was chosen as the best option to coculture HBEC and astrocytes because it had

no detrimental effect on the cell viability of astrocytes and it did not affect GFAP expression in astrocytes.

TEER values of our optimised HBEC-astrocyte BBB model were significantly higher than that of the HBEC-alone BBB model from day 1 to day 4 ($p < 0.0001$) (Figure 3.21). In both BBB models the increase in TEER values over 5 days reflect maturation of tight junctions with time (Bauer *et al.*, 2014). Higher TEER values observed in HBEC-astrocyte BBB model could be due to the increase in expression of tight junction proteins produced as a result of cell-cell contact between endothelial cells and astrocytes (Bauer *et al.*, 2014). Cross talk between endothelial cells and astrocytes is essential for the formation of a functional BBB. Direct contact between endothelial cells and astrocytes in the BBB allow astrocytes to directly control and release signals to the endothelial cells. (Nakagawa *et al.*, 2007). Astrocytes secrete soluble factors such as the Sonic Hedgehog (SHH) that promote BBB homeostasis. SHH binds to the Hedgehog (Hh) receptor Patched-1 on brain endothelial cells, resulting in the activation of the signal transducer Smoothed (Smo). This causes activation of Gli transcription family that in turn activates the transcription factor Sox-18 which has been shown to regulate expression of the tight junction protein claudin-5 and EC-BBB functions. (Alvarez *et al.*, 2013; Daneman *et al.*, 2015; Fontijn *et al.*, 2008; Obermeier *et al.*, 2013). Activation of the SHH pathway in human primary brain endothelial cells induced the expression of the junctional protein claudin-5. Blocking of the Hh pathway *in vivo* caused an increase in BBB permeability (Alvarez *et al.*, 2013, 2011). These studies suggest that SHH could contribute to BBB formation.

Also, astrocytes can release growth factors such as vascular endothelial growth factor (VEGF), glial cell line derived neurotrophic factors, basic fibroblast growth factor (bFGF) and angiopoietin (ANGPT)-1 that are believed to be important in the development of tight junctions

(Cabezas *et al.*, 2013, Alvarez *et al.*, 2013). Astrocytes produce the angiotensin-converting enzyme-1 (ACE-1) that cleaves angiotensin I (ANG1) to angiotensin II. Angiotensin II binds to type I angiotensin receptors (ATI) present on brain endothelial cells and activation of ATI restricts BBB permeability (Alvarez *et al.*, 2013). The endothelial cells may also secrete factors essential for the development of astrocytes. The EC-derived leukaemia inhibitory factor (LIF), platelet-derived growth factor (PDGF) and basic fibroblast growth factor (bFGF) enhanced differentiation of astrocytes (Alvarez *et al.*, 2013; Cheslow and Alvarez, 2016).

The Src suppressed C kinase substrate (SSeCKS) produced by astrocytes was shown to control maturation of the BBB by reducing VEGF expression and activating ANGPT-1 expression in astrocytes (Alvarez *et al.*, 2013; Lee *et al.*, 2003). This led to an increase in ZO-1 and claudin-1 expression and reduction in permeability of brain endothelial cells *in vitro* (Alvarez *et al.*, 2013; Lee *et al.*, 2003).

All the factors mentioned above could be responsible for the higher TEER observed in the HBEC-astrocyte BBB compared to the HBEC-alone BBB.

TEER values of approximately $20\Omega\text{cm}^2$ were observed after 5 days of growing HBEC-astrocyte in tandem (Figure 3.21). Although the TEER values obtained were similar to that of Li *et al.*, (2010), they appeared to be lower than some of the TEER values shown in the literature: TEER ranging from $30\Omega\text{cm}^2$ - $80\Omega\text{cm}^2$ (Li *et al.*, 2010). One likely explanation is that varying TEER systems were used to measure TEER. Indeed, some of these studies recorded TEER by using the chopstick method which can overestimate TEER values and produce fluctuating measurements (Srinivasan *et al.*, 2015). Using the Endohm chamber to measure TEER offers a more accurate alternative as transwells can be placed in the Endohm chamber and a more uniform current density is generated across the transwell membrane by concentric electrodes found in the cap and chamber (Srinivasan *et al.*, 2015). Also, in using the Endohm chamber

only small variations of TEER within $1-2\Omega\text{cm}^2$ in a particular sample occurred in comparison to $10-30\Omega\text{cm}^2$ variation observed using chopstick electrodes (Srinivasan *et al.*, 2015). In this study, the Endohm chamber was used to measure TEER. Another factor for the low TEER recorded in our *in vitro* BBB model could have been the difference in cell densities used in our model compared to other *in vitro* BBB models. Also, the length of time endothelial cell and astrocytes were cocultured together *in vitro* could also influence the TEER. Some coculture models grow endothelial cells and astrocytes *in vitro* for longer than 5 days.

In our study we found out that growing of HBEC-astrocyte *in vitro* for more than 5 days caused endothelial cell overgrowth producing a dense mesh (instead of the classical monolayer) suggesting that they change phenotype when cultured for a prolonged period of time. Dynamic coculture BBB models where endothelial cells and astrocytes are grown on the luminal side and basolateral side of porous hollow fibres respectively, and media is pumped in to mimic shear stress produced by blood flow *in vivo*, have been shown to produce higher TEER compared to static cocultures (Li *et al.*, 2010, He *et al.*, 2014). Although 3D BBB models resemble the NVU more closely than 2D BBB models they are not the best *in vitro* models to study the effect of sequestration on components of the BBB during CM. This is because it can be quite challenging to investigate the response of astrocytes to sequestration of PRBC to the BBB *in vitro* since astrocytes are embedded in the hydrogels and are not easily accessible.

The variations in TEER values compared to the literature could also be due to different components in media, temperature and transwells used in the BBB models. There is no standard *in vitro* BBB model used to study disease and differences between labs make it difficult to compare TEER. Thus, in our study it was important before our experiment that the HBEC-alone BBB model and HBEC-astrocyte BBB model were characterised.

In vitro cerebral malaria BBB models have just focussed on the effect of PRBC on brain endothelial cells and not considered the other components that make up the BBB. Thus, in this study we developed a novel HBEC-astrocyte BBB model to examine the impact of the inflammation response mediated by sequestration of PRBC, on endothelial cells and astrocytes in the BBB during cerebral malaria.

Chapter 4 : Changes occurring at the blood barrier during cerebral malaria

4.1 Introduction

The *Plasmodium falciparum* parasite does not cross the BBB during CM but remains in the lumen of the blood vessels of the brain causing BBB impairment and significant neurological disruption.

Evidence from post-mortem and *in vitro* studies suggests that BBB disruption may contribute to the pathogenesis of cerebral malaria. Post-mortem studies showed a reduction in junction proteins vinculin, ZO-1 and occludin in the brain tissues of cerebral malaria patients compared to that of the controls (Brown *et al.*, 1999). *In vitro*, adherence of PRBC to BBB derived endothelial cells (BBB-EC) caused a reduction in BBB-EC integrity (Tripathi *et al.*, 2007).

Sequestration of PRBC to the BBB during cerebral malaria causes activation of the endothelial cells of the BBB (Armah *et al.*, 2007; O'Carroll *et al.*, 2015; Storm *et al.*, 2014). This can result in an increased expression of adhesion molecules and chemokines such as ICAM-1 and MCP-1 respectively and an increased production of pro-inflammatory cytokines such as TNF α and IL-1 β (Armah *et al.*, 2007; O'Carroll *et al.*, 2015; Storm *et al.*, 2014). *In vitro* CM studies showed that ICAM-1 expression was increased following coculturing of PRBC with BBB-EC. Also an increased secretion of MCP-1 was observed in HUVEC that had been cocultured with PRBC (Viebig *et al.*, 2005). Moreover, elevated levels of sICAM-1 were correlated with cerebral malaria (Adukpo *et al.*, 2013). The cause of BBB damage during cerebral malaria is still not known. Several factors such as proinflammatory cytokines, chemokines, metalloproteases have been suggested to contribute to BBB disruption during cerebral malaria.

Previous studies in our laboratory by Mohd Nasir (2015) showed that treatment of the HBEC-alone BBB with soluble factors released in response to sequestration of PRBC caused activation of HBEC and an upregulation of inflammatory mediators such as MCP-1, IL-8 and metalloproteases such as ADAMTS-4, MMP- 2 and MMP-9. Treatment of the HBEC-alone

BBB with these inflammatory mediators caused a significant increase in BBB permeability (Mohd Nasir, 2015).

In this study we set out to investigate the effect of endothelial cell derived factors produced in response to sequestration of PRBC on the integrity of the HBEC-alone BBB and HBEC-astrocyte BBB using a FITC dextran permeability assay. We first of all determined the impact of inflammatory mediators present in the coculture supernatant on the HBEC-alone BBB integrity. Subsequently, we determined the effect of inflammatory mediators on the HBEC-astrocyte BBB.

4.2 Materials and Methods

4.2.1 Sandwich ELISA

Sandwich ELISA was used to determine inflammatory mediators and metalloproteases released in response to sequestration of PRBC to HBEC *in vitro*.

Sandwich ELISA of ICAM-1, MCP-1 and ADAMTS-4 were performed according to the manufacturer's instructions and as described in Chapter 2, section 2.28. Details on the sandwich ELISA kits used can be seen in Appendix 1.

4.2.2 Western blot analysis for detection of ADAMTS-4

Western blot analysis was used to detect change in ADAMTS-4 levels in the coculture supernatants that could not be detected by sandwich ELISA. ADAMTS-4 was released in response to sequestration of PRBC to HBEC *in vitro*. This analysis was performed as in Chapter 2, section 2.17-2.22. A 1:250 dilution of donkey anti-ADAMTS-4 and a 1:1000 dilution of donkey-anti-goat in TBST were used in the western blot analysis.

4.2.3 FITC dextran permeability assay

4.2.3.1 Seeding of HBEC for permeability assay

The HBEC-alone BBB was set up as in Chapter 3, section 3.2.7. On day 4 the media was changed to Quiescent 5% (Q5%) FBS media to equilibrate cells before the experiment. On day 5 the FITC dextran permeability assay was performed (Figure 4.1).

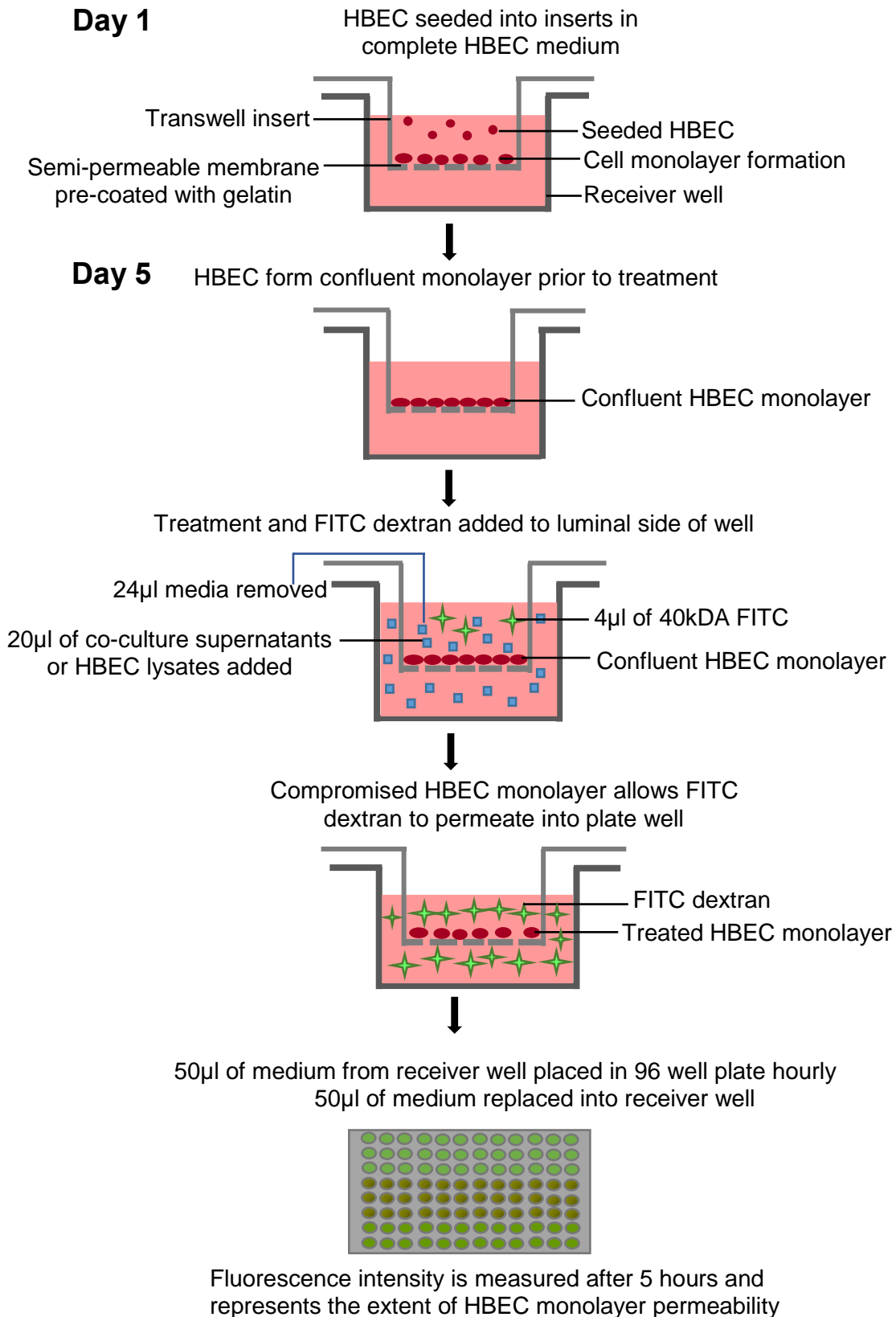


Figure 4.1 Schematic of FITC dextran permeability assay procedure.

4.2.3.2 Seeding the HBEC-astrocyte BBB for FITC experiments

The HBEC-astrocyte BBB model was set up as in Chapter 3, section 3.2.7. After the 4th day of coculturing HBEC and astrocytes together, media of the transwells were aspirated and 200µl of Q5 % FBS media was added to each transwell. On day 5 the FITC dextran assay was performed.

4.2.3.3 Permeability assay

FITC dextran permeability assays were performed to investigate the effect of endothelial cell derived factors on HBEC-alone BBB and HBEC-astrocyte BBB models. The following treatments: PRBC-HBEC coculture supernatant, URBC-HBEC coculture supernatant, control HBEC coculture supernatant or PRBC-HBEC lysate, URBC-HBEC lysate and control HBEC lysate were used in this assay.

2 hours before the FITC dextran permeability assay, media of transwells were changed to 200µl of Q5% FBS media to allow cells to equilibrate to the new media before the start of the experiments. Media of cells was changed carefully to avoid drying or disturbance of the cells. 24µl of media was removed from the luminal side of the transwell and replaced by 20µl of the respective coculture supernatants or HBEC lysates or Q5% FBS media (Table 4.1) to achieve a 1 in 10 dilution for each treatment and to minimise disturbance of the cell monolayer since shear stress can stimulate activation of endothelial cells (DeStefano *et al.*, 2017). 4µl of 40 kDa FITC dextran (stock concentration 20mg/ml) was added to the luminal side of each transwell to make a final concentration of 0.4mg/ml (Figure 4.1). 10 seconds after the 40kDa FITC dextran was added, this was time point 0, the transwells were moved to adjacent empty wells and medium in the receiver well (Figure 4.1) was thoroughly mixed and 50µl was pipetted from each receiver well to corresponding wells in a black 96 well plate for fluorescence measurement (Figure 4.1). 50µl of pre-warmed Q5% FBS media was placed back into each receiver well to compensate for the loss of media from the receiver well. Transwells were carefully placed back

into receiver wells and set up was returned into the humidified incubator at 37°C and 5% CO₂. Sampling was repeated every hour for 5 hours. Permeability was quantified by taking fluorescence measurement of all the samples collected over 5 hours at the same time using a fluorescent plate reader at the end of the experiment.

Table 4.1 Summary of treatments used in the HBEC and HBEC-astrocyte BBB model

Treatment
PRBC-HBEC coculture supernatant
URBC-HBEC coculture supernatant
Control HBEC coculture supernatant
PRBC-HBEC lysate
URBC-HBEC lysate
HBEC lysate
Experiment control Q5% FBS medium

4.2.3.4 Inhibitor assays

Inhibitor assays were performed to determine if proteases could cause disruption of the HBEC-alone BBB model *in vitro*. GM6001 is an inhibitor of metalloproteases and ADAMTS-4.

In this assay, media was changed 2 hours before the FITC dextran permeability assay as described before. 44µl of media was removed from the luminal side of each transwell and replaced by the different treatments to minimise disturbance of the cell monolayer and stimulation of endothelial cells by shear stress. 20µl of coculture supernatants or 20µl of HBEC lysates or 20µl of Q5% FBS media was added to the luminal side of each corresponding transwell. 20µl of GM6001 inhibitor was then added to each transwell (Table 4.2) to achieve a final concentration of 25nM GM6001. 10% of DMSO, the diluent of GM6001 was added to

control wells where no GM6001 inhibitor was added. 4 μ l of 40kDA FITC dextran was added to each well and the permeability assay was performed as in 4.2.1.3.

Table 4.2 Summary of Inhibitor concentrations used in the permeability assay

Inhibitor	Final concentration in each well
GM6001 (10mM)	25nM
DMSO (control)	10% dilution

4.2.3.5 Analysing the fluorescent intensity of samples

Prior to measuring the fluorescent signal of samples, the excitation wavelength of the fluorescent plate reader was measured using a filter at 490nm while the emission wavelength was measured using a filter of range between 510nm and 570nm. To analyse the data, the raw data of each treatment was normalised to the zero time point of its corresponding treatment. This new data was then normalised to the fluorescence value of its corresponding control. This data was then plotted using a scatter plot with the normalised fluorescence on the y-axis and the time on the x-axis. A 2-way ANOVA was used to determine if treatment of the *in vitro* BBB models with the coculture supernatants caused a statistically significant change with time.

4.2.4 Statistics

One-way ANOVA was used to determine if MCP-1, ADAMTS-4 and ICAM-1 levels were significantly higher in the PRBC-HBEC coculture supernatants compared with the URBC-HBEC coculture supernatants and the control HBEC supernatant. 2-way ANOVA was used to determine if the PRBC-HBEC coculture supernatant/PRBC-HBEC lysate caused a significantly higher increase in HBEC-alone BBB permeability compared with the URBC-HBEC coculture supernatant/lysate and the control HBEC supernatant/lysate. 2-way ANOVA was also used to

determine if the addition of the inhibitor GM6001 could cause a significant decrease in BBB permeability in HBEC treated with the coculture supernatants and PRBC-HBEC lysate.

Densitometric analysis of western blot bands was calculated using Image J as described in Chapter 3, section 3.2.10.

4.3 Results

4.3.1 Detecting MCP-1, sICAM-1 and ADAMTS-4 levels in PRBC-HBEC coculture supernatants

To verify coculture experiments were in line with previous studies in our laboratory, the presence of inflammatory mediators MCP-1, ADAMTS-4 and sICAM-1 in the coculture experiments were examined.

A 2-fold statistically significant increase in MCP-1 levels was observed in the PRBC-HBEC coculture supernatants as compared to the control-HBEC and URBC-HBEC coculture supernatants ($p < 0.0001$) (Figure 4.2A). MCP-1 levels in the URBC-HBEC coculture supernatants were comparable to that of the control HBEC supernatant (Figure 4.2A).

A 4-fold statistically significant increase in sICAM-1 levels was observed in the PRBC-HBEC coculture supernatants compared to the control HBEC and URBC-HBEC coculture supernatants ($p < 0.0001$) (Figure 4.2B). sICAM-1 levels in the URBC-HBEC coculture supernatants were comparable to that of the control HBEC supernatant (Figure 4.2B).

ADAMTS-4 levels in PRBC-HBEC coculture supernatants was the same as that of URBC-HBEC coculture supernatants and control (Figure 4.2C). This is the first time ADAMTS-4 expression in the coculture supernatants was quantified using a sandwich ELISA. Previous studies by Mohd Nasir (2015) quantified ADAMTS-4 in the coculture supernatants using western blot analysis (Mohd Nasir, 2015).

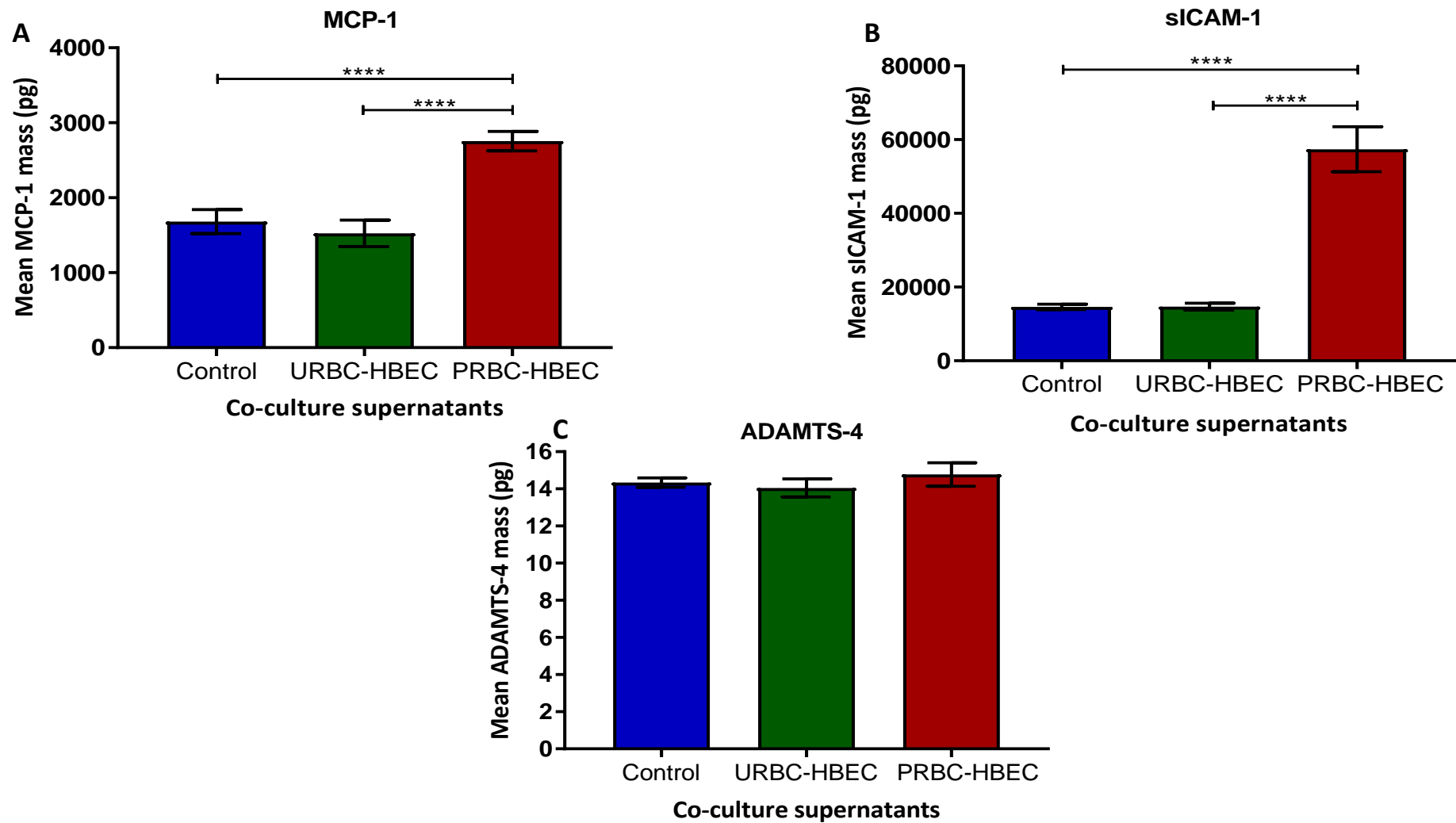


Figure 4.2 Mean MCP-1, sICAM-1 and ADAMTS-4 levels in coculture supernatants. Sandwich ELISA analysis was used to determine the amount of (A) MCP-1, (B) sICAM-1 and (C) ADAMTS-4 in coculture supernatants. Error bars represent standard error of the mean (n=8, **** denotes significance at $p < 0.0001$).

4.3.2 Changes in ADAMTS-4 levels in the PRBC-HBEC coculture supernatant

In a pilot study western blot analysis was used to detect ADAMTS-4 levels in the coculture supernatants. Western blot analysis on one sample showed ADAMTS-4 bands of approximately 100kDa and 47kDa were present in all the coculture supernatants. Densitometric analysis of the 47kDa ADAMTS-4 band showed that ADAMTS-4 was slightly upregulated in the PRBC-HBEC coculture supernatants compared to the controls (Figure 4.3).

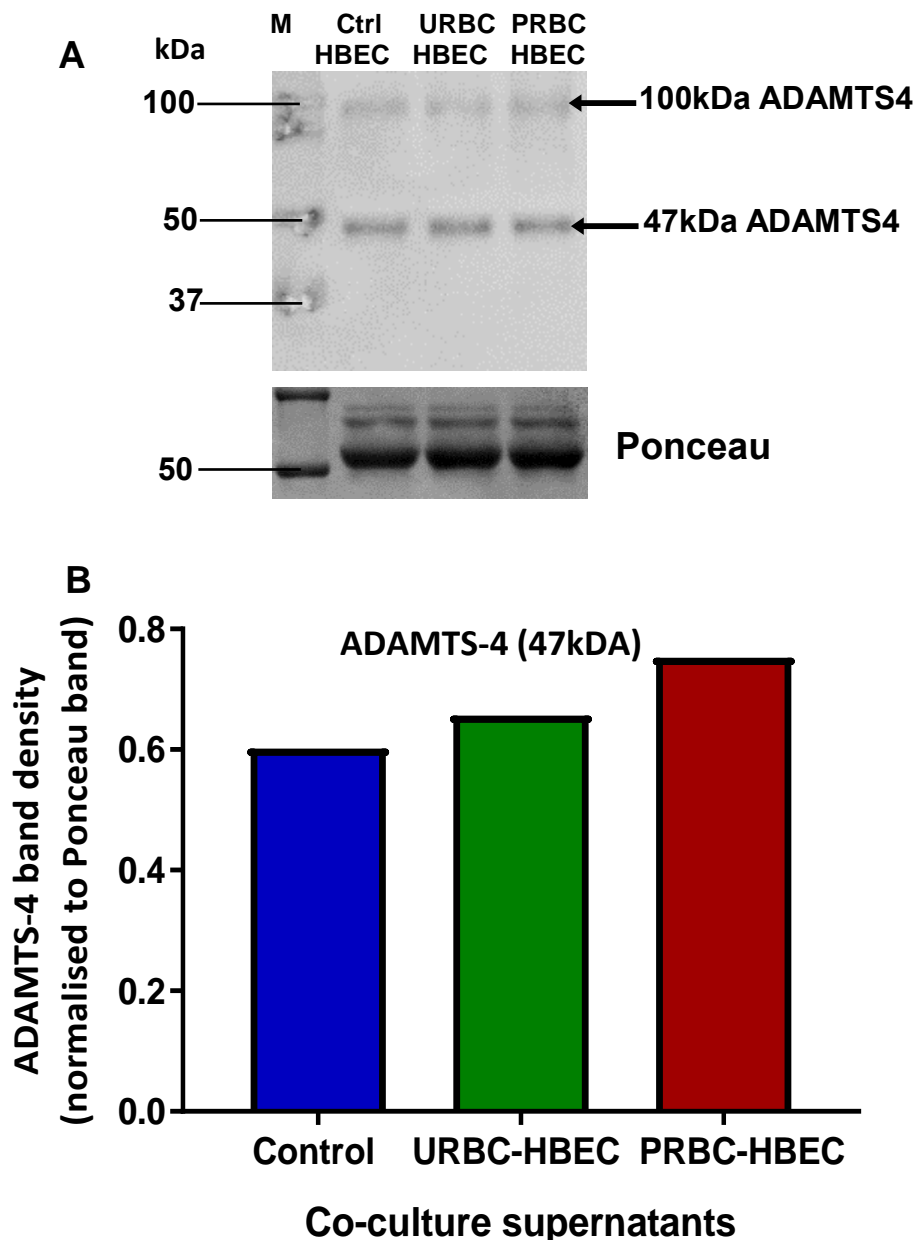


Figure 4.3 Detection of ADAMTS-4 in coculture supernatants in a pilot study. (A) Representative western blot image for ADAMTS-4. From left protein marker (M), control HBEC media, URBC-HBEC coculture supernatant, PRBC-HBEC coculture supernatants. (B) Densitometric data of 47kDa ADAMTS-4 band (n=1).

4.3.3 Alterations in HBEC-alone BBB permeability following treatment with coculture supernatants

Coculture supernatants from 18 separate experiments i.e. biological replicates were examined. A statistically significant increase in HBEC-alone BBB permeability was observed at 2-5 hours following treatment of HBEC monolayer with the PRBC-HBEC coculture supernatant as compared to the control coculture supernatants ($p < 0.01$) (Figure 4.4).

The increase in HBEC-alone BBB permeability caused by the PRBC-HBEC coculture supernatant increased from 1-3 hours, from 3-5 hours this increase plateaued (Figure 4.4). The URBC-HBEC coculture supernatant caused no increase in HBEC-alone BBB permeability as compared to the HBEC control supernatant (Figure 4.4).

HBEC-alone BBB

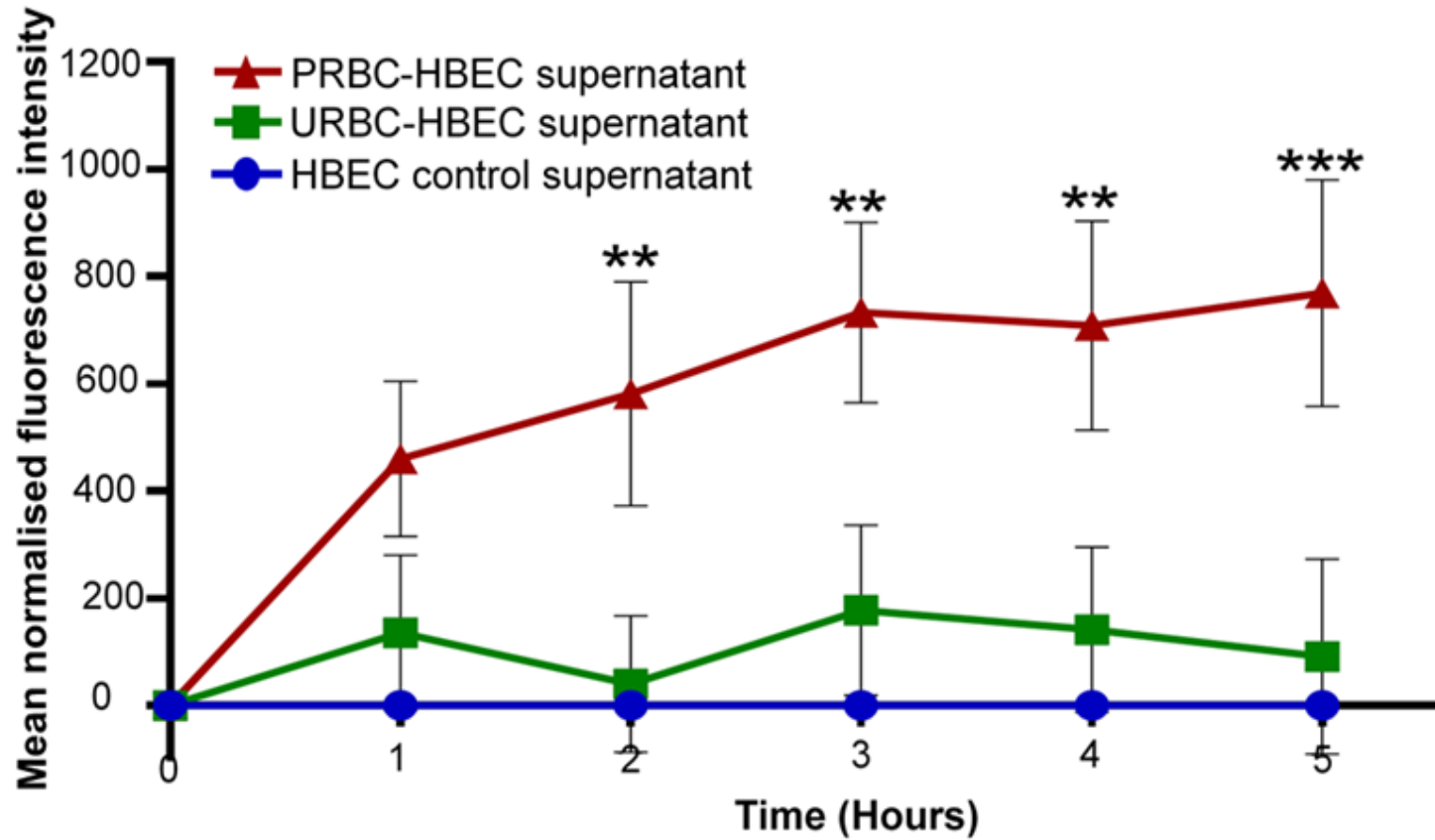


Figure 4.4 Effect of coculture supernatants on HBEC-alone BBB permeability. Alterations in BBB permeability were observed in the HBEC-alone BBB following treatment with PRBC-HBEC coculture supernatants (red), URBC-HBEC coculture supernatants (green) and HBEC control supernatants for over 5 hours (blue). Statistical significance between treatments was tested using a 2-way ANOVA test and Tukey's test (n=18, Error bars \pm SEM, ***p<0.001, **p<0.01).

4.3.4 Alterations in HBEC-alone BBB following treatment with HBEC lysates

After coculture experiments, HBEC lysates were harvested. This was done to investigate the effect of endothelial cell derived factors produced in the HBEC lysate in response to sequestration of PRBC on the HBEC alone BBB. HBEC lysates from 6 separate biological replicates were tested. In the HBEC-alone BBB treated with the PRBC-HBEC lysates, a trend towards an increase in HBEC alone BBB permeability from 0-5hours was observed. However, this was not statistically significantly different from that of the controls used to treat the HBEC-alone BBB permeability (Figure 4.5).

HBEC-alone BBB

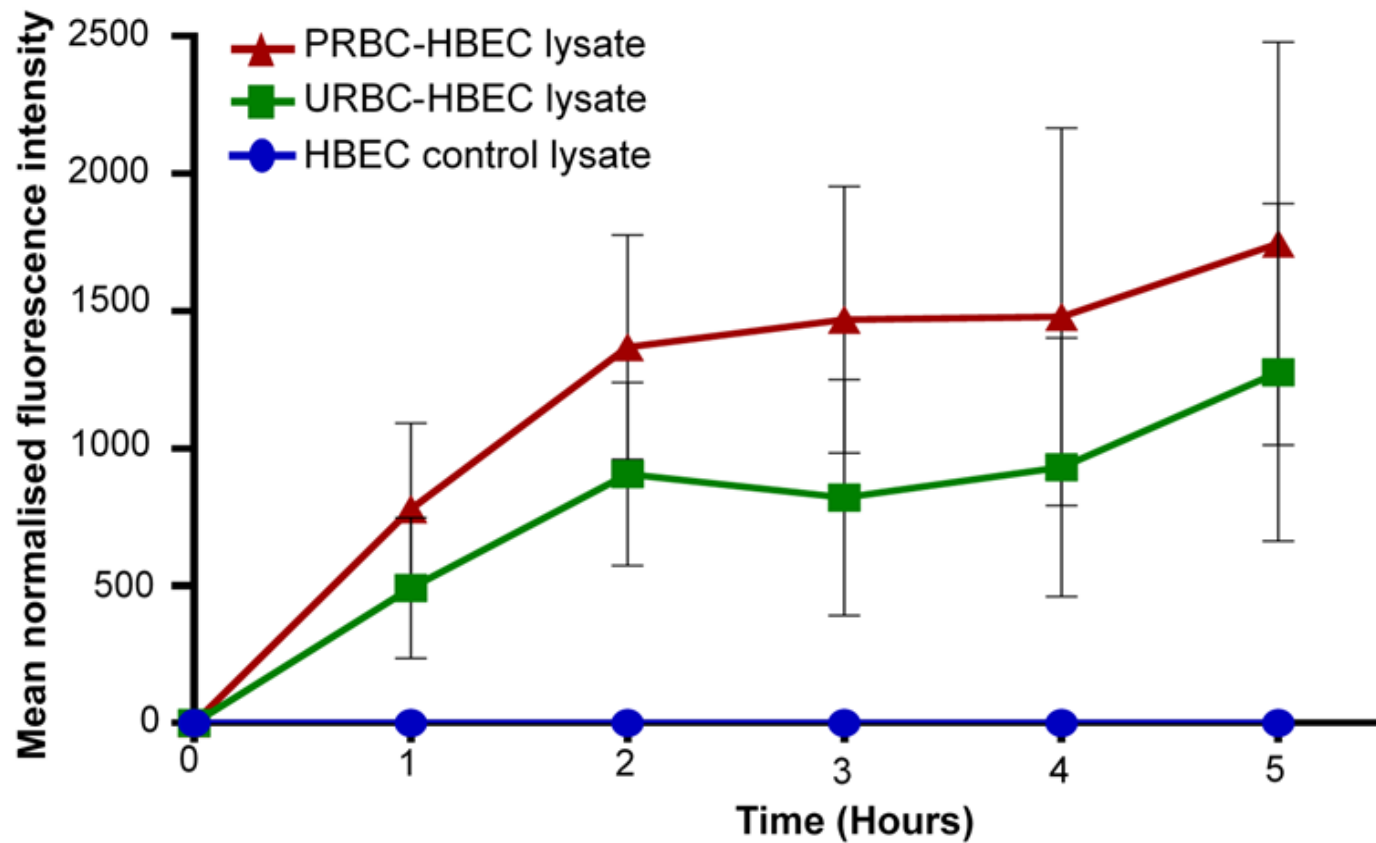


Figure 4.5 Effect of HBEC lysates on HBEC-alone BBB permeability. Alterations in BBB permeability were observed in the HBEC-alone BBB following treatment with PRBC-HBEC lysates (red), URBC-HBEC lysates (green) and HBEC control lysates (blue) for over 5 hours. Error bars represent SEM (n=6).

4.3.5 Effect of the broad spectrum metalloprotease inhibitor, GM6001 on HBEC-alone BBB permeability induced by PRBC-HBEC coculture supernatant

The increase in HBEC-alone BBB permeability caused by the PRBC-HBEC coculture supernatants was reduced over 5 hours when the inhibitor GM6001 was present, compared to the DMSO control (Figure 4.6). The URBC-HBEC coculture supernatant in the presence of GM6001 caused a marginal reduction in the HBEC monolayer permeability (Figure 4.6). Coculture supernatants from 5 separate biological replicates were analysed in this study.

Addition of GM6001 to the HBEC monolayer treated with PRBC-HBEC lysate caused a reduction in BBB permeability over 5 hours compared to the DMSO supernatant of the same lysate (Figure 4.7).

HBEC-alone BBB

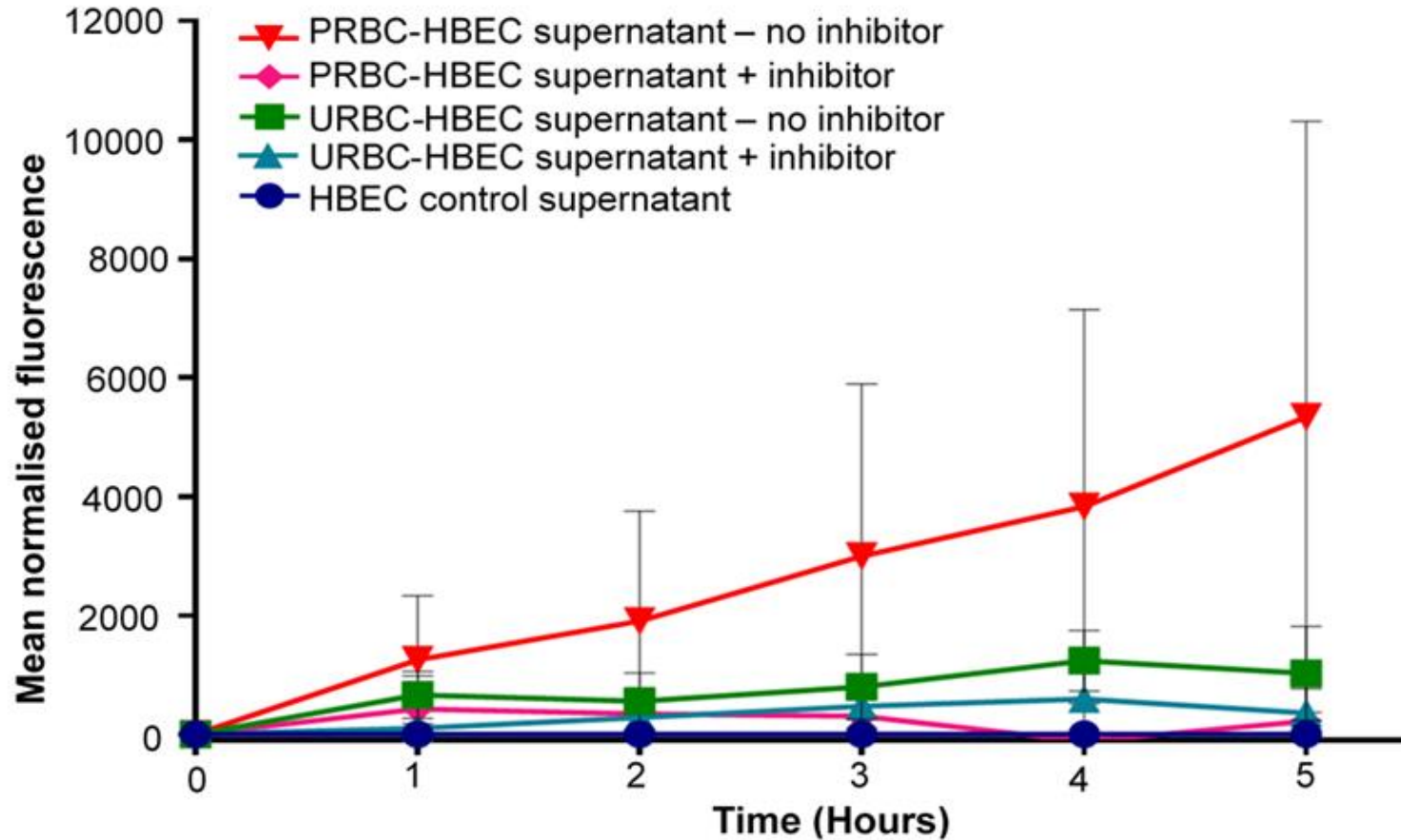


Figure 4.6. Changes in HBEC-alone BBB permeability following treatment with coculture supernatants and addition of DMSO (control diluent of inhibitor) and presence of the inhibitor (GM6001). The graph was the mean normalised fluorescence intensity from 5 separate experiments, using supernatants from 5 separate coculture experiments. Error bars represent SEM (n=5).

HBEC-alone BBB

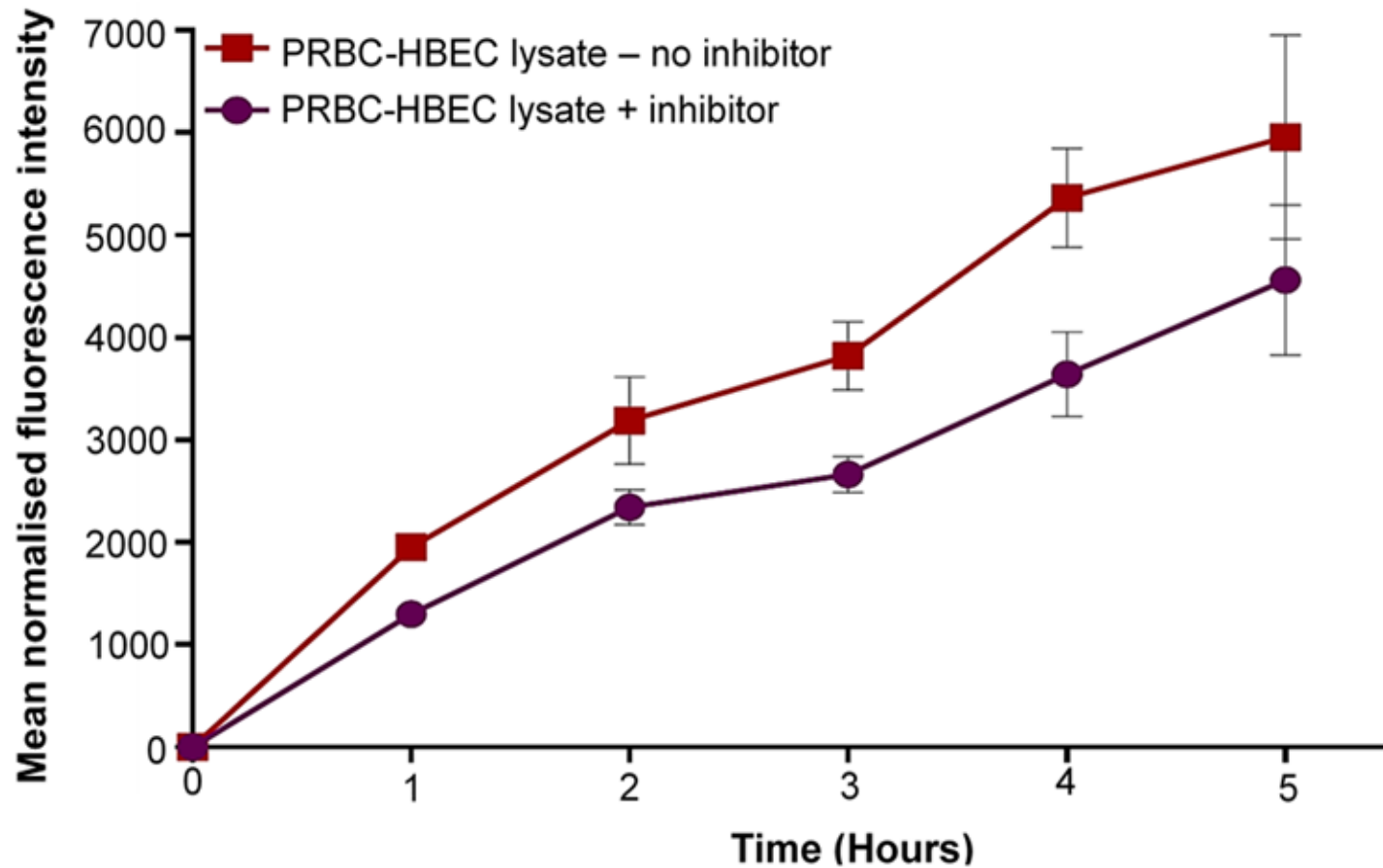


Figure 4.7 Changes in HBEC-alone BBB permeability following treatment with PRBC-HBEC lysate and addition of DMSO or GM6001. The graph was the mean normalised fluorescence intensity from 3 separate experiments, using lysates from 3 separate coculture experiments. Error bars represent SEM (n=3).

4.3.6 Effect of coculture supernatants on the HBEC-astrocyte BBB model

Coculture supernatant from 6 different biological replicates were examined. No significant increase in permeability was observed following treatment of the HBEC-astrocyte BBB model with any of the coculture supernatants over 5 hours (Figure 4.8).

4.3.7 Effect of HBEC lysates on HBEC-astrocyte BBB permeability

HBEC lysates from 5 different biological replicates were examined. Treatment of the HBEC-astrocyte BBB with the HBEC-derived lysates caused no significant change in BBB permeability over 5 hours (Figure 4.9).

HBEC-astrocyte BBB

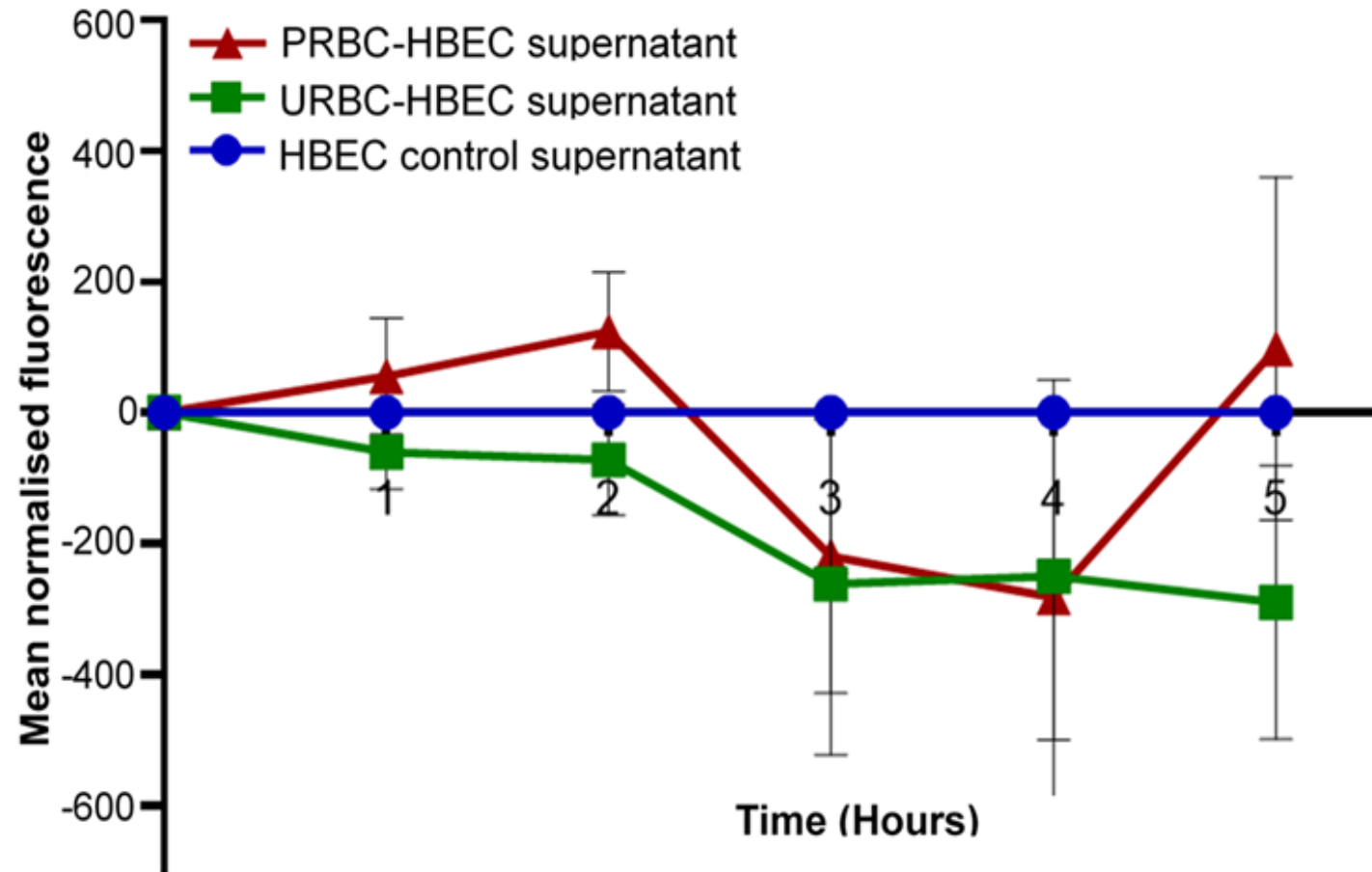


Figure 4.8 Effect of coculture supernatants on HBEC-astrocyte BBB permeability. No changes in BBB permeability were observed in the HBEC-astrocyte BBB following treatment with PRBC-HBEC coculture supernatants (red), URBC-HBEC coculture supernatants (green) and HBEC control supernatants for over 5 hours (blue). Error bars represent SEM (n=8).

HBEC-astrocyte BBB

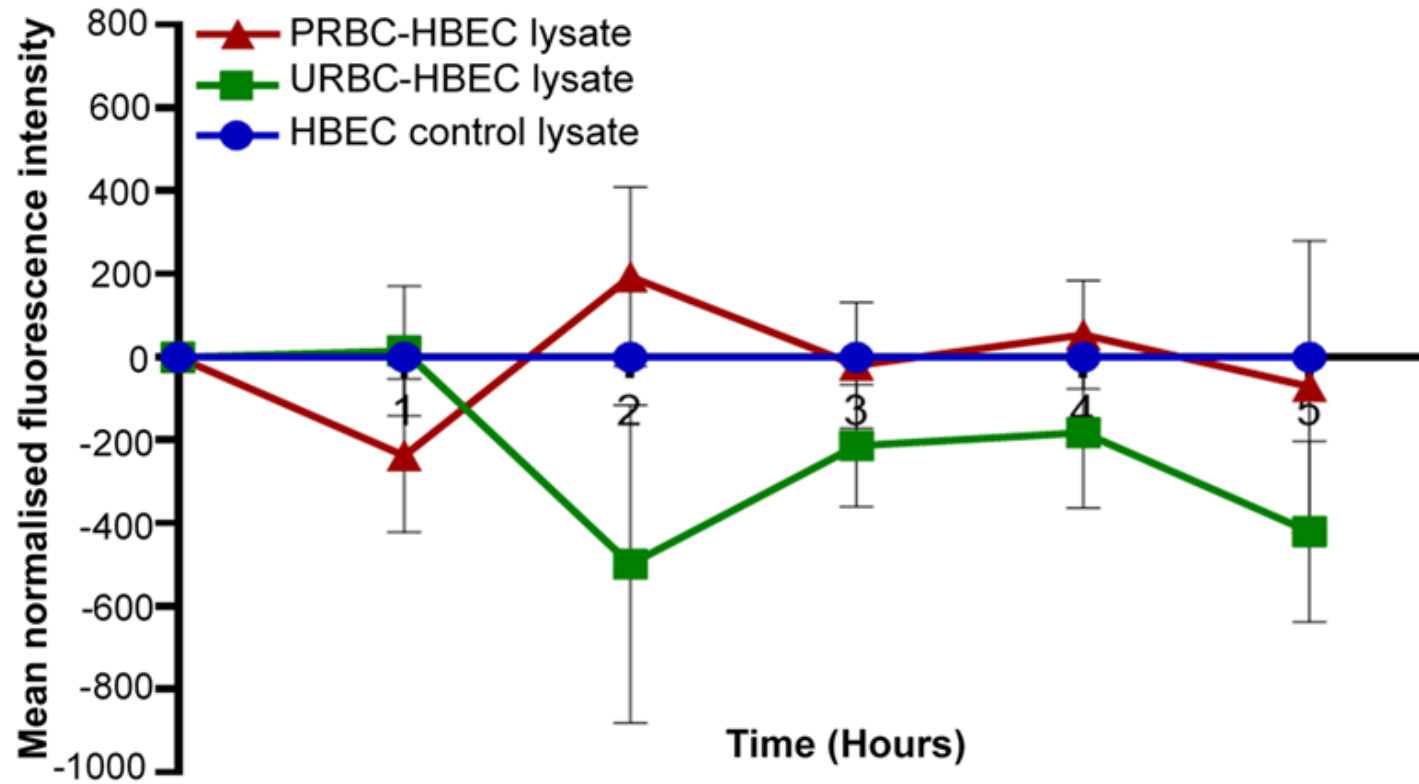


Figure 4.9 Effect of HBEC lysates on HBEC-astrocyte BBB permeability. No changes in BBB permeability were observed in the HBEC-astrocyte BBB following treatment with PRBC-HBEC lysates (red), URBC-HBEC lysates (green) and HBEC control lysates for over 5 hours (blue). Error bars represent SEM (n=5).

4.4 Discussion

Sequestration of PRBC to endothelial cells of the BBB is thought to play an important role in the pathogenesis of cerebral malaria. However, the mechanisms that occur at the BBB following sequestration of PRBC during CM are still unclear. Thus, in this study, we examined the effect of PRBC on the BBB endothelium using *in vitro* BBB models.

Consistent with previous results by Mohd Nasir (2015), accumulation of PRBC to HBEC *in vitro* caused activation of the HBEC-alone BBB resulting in a significant increase in sICAM-1 and MCP-1 released into the PRBC-HBEC coculture supernatants (Figure 4.2A and 4.2B).

Coculturing PRBC with HUVEC caused an upregulation of ICAM-1 (Viebig *et al.*, 2005). Higher sICAM-1 levels were observed in the plasma of patients with cerebral malaria compared to that of uncomplicated malaria patients (Adukpo *et al.*, 2013). Earlier reports by Rollins (1990) showed that activation of HUVEC with IL-1 β caused an increased secretion of MCP-1 *in vitro* (Rollins *et al.*, 1990). MCP-1 levels in the post-mortem serum of CM patients were higher than that of patients with severe malaria and non-malaria patients (Armah *et al.*, 2007). Our results and previous studies showed that PRBC caused activation of the HBEC.

Quantitative sandwich ELISA showed that there was no increase in ADAMTS-4 levels in the PRBC-HBEC coculture supernatants compared to the controls (Figure 4.2C). ELISA quantified the total amount of ADAMTS-4 in the coculture supernatant and thus we used western blot analysis in a pilot study to identify the different forms of ADAMTS-4 in the coculture supernatants. ADAMTS-4 bands at 100kDa and 47kDa were observed in all the coculture supernatants (Figure 4.3). The 100kDa proform of ADAMTS-4 is converted to the inactive form of 75kDa which is associated with the extracellular matrix (ECM) in cells. Further processing converts the 75kDa form to active forms at 60kDa and 50kDa that are released from the extracellular matrix (ECM) (Gao, 2002).

The observance of the faint proform of ADAMTS-4 at 100kDA and more distinct bands of the active ADAMTS-4 at 47kDA in the pilot study suggests that more of the active form of ADAMTS-4 was present in the coculture supernatants (Figure 4.3). The density of the 47kDA ADAMTS-4 band in the PRBC-HBEC coculture supernatant was slightly higher than the controls. Results from the pilot study were not consistent with studies by Mohd Nasir (2015) who observed ADAMTS-4 bands at 60kDA in all the coculture supernatants and significantly higher levels of the 30kDA ADAMTS-4 band in the PRBC-HBEC coculture supernatants (Mohd Nasir, 2015). The difference in data could be due to the fact that different samples were analysed in this study. ADAMTS-4 has different cleavage sites and it is possible that in coculture experiments by Mohd Nasir (2015), further cleavage of the 60kDA ADAMTS-4 by furin proteases expressed by endothelial cells could have resulted in the 30kDA ADAMTS-4 form (Mohd Nasir, 2015).

The significant increase in HBEC-alone BBB permeability we observed following treatment of the HBEC-alone BBB with PRBC-HBEC coculture supernatants was consistent with results by Mohd Nasir (2015) (Figure 4.4). These results suggested that inflammatory mediators released by endothelial cells in response to sequestration of PRBC to BBB caused an increase in HBEC-alone BBB permeability. Previous studies have shown that chemokines such as MCP-1 and metalloproteases could cause an increase in BBB permeability (Stamatovic *et al.*, 2005; Yao and Tsirka, 2011). Indeed, MCP-1 has been shown to alter BBB permeability *in vitro*. Treatment of mouse brain endothelial cells *in vitro* with MCP-1 caused a reduction of TEER with an increase in BBB permeability (Stamatovic *et al.*, 2005; Yao *et al.*, 2011). Tripathi *et al.* (2007) showed that PRBC could cause a reduction in electrical resistance and disruption of the endothelial cell BBB *in vitro* (Tripathi *et al.*, 2007). This could mean MCP-1 or

metalloproteases present in our PRBC-HBEC coculture supernatants were contributing to the increase in HBEC-alone BBB permeability we observed.

The HBEC lysates consisted of proteases or inflammatory mediators such as MCP-1, ICAM-1 that were upregulated or expressed in the HBEC in response to PRBC in the coculture system. The increase in BBB permeability following treatment of the HBEC-alone BBB with PRBC-HBEC lysates confirmed that inflammatory mediators expressed in the HBEC in response to PRBC sequestration could contribute to the disruption of the BBB integrity during CM (Figure 4.5).

We further explored if proteases could be responsible for the increase in BBB permeability observed following treatment of HBEC monolayer with PRBC-HBEC coculture supernatants. Addition of the inhibitor GM6001 caused a reduction in HBEC-alone BBB permeability produced by the PRBC-HBEC coculture supernatant (Figure 4.6).

GM6001 is a metalloprotease inhibitor shown to inhibit MMP-9 in mouse brain endothelial cells and ADAMTS-4 in bovine cartilage explants (Chen *et al.*, 2009; Hawkins *et al.*, 2005; He *et al.*, 2015). Previous studies have shown an upregulation of MMP-2 and MMP-9 in the PRBC-HBEC coculture supernatant (Mohd Nasir, 2015). MMP-2 and MMP-9 can degrade specific components of the extracellular matrix such as collagen, brevican and aggrecan and tight junctions proteins occludin and claudin-5 (Lu *et al.*, 2011). ADAMTS-4 also cleaves versican, brevican and aggrecan (Lemarchant *et al.*, 2013; Porter *et al.*, 2005).

This could mean that during CM, PRBC sequester to BBB resulting in the activation of endothelial cells and the release of metalloproteases such as ADAMTS-4, MMP-2 and MMP-9 that degrade the extracellular matrix and tight junction proteins causing the BBB to be leaky. As CM is a complex disease, it is possible that other mechanisms may contribute to the BBB disruption observed in CM.

The use of HBEC monolayer as an *in vitro* BBB model does not take into consideration the other components that make up the BBB such as astrocytes. Hence, we decided to investigate the effect of endothelial cell derived factors on the permeability of the HBEC-astrocyte BBB model. Our results showed no change in BBB permeability following treatment of the HBEC-astrocyte BBB model with EC derived factors (Figure 4.8, Figure 4.9). The fact that the HBEC-astrocyte BBB used in this study had a significantly higher TEER than the HBEC-alone BBB from day 1 to day 4 could suggest that the HBEC-astrocyte was more resilient and less susceptible to inflammatory mediators in the PRBC-HBEC coculture supernatants and PRBC-HBEC lysates after 5 hours of treatment. Astrocytes have been shown to secrete factors that can protect the BBB during injury. In response to injury soluble factors such as SHH, retinoic acid (RA) and ANGPT-1 are upregulated by activated astrocytes (known as reactive astrocytes) (Cheslow *et al.*, 2016). SHH was shown to reduce the secretion of MCP-1, ICAM-1 and VCAM-1 expression, enhancing quiescence of human EC-BBB (Alvarez *et al.*, 2011). Inhibition of the Hedgehog (Hh) pathway in experimental autoimmune encephalomyelitis (EA) mice (animal model of MS) caused an increase in BBB permeability and an increased inflammatory response (Alvarez *et al.*, 2013).

Reactive astrocytes produce higher levels of retinoic acid (RA). RA was shown to promote the development of EC-BBB by increasing VE-cadherin, ZO-1 and TEER in hCMED/3 (transformed brain EC line used in BBB models) *in vitro* and reducing VEGF expression (Alvarez *et al.*, 2013; Mizee *et al.*, 2013). Increased levels of ANGPT-1 in humans is associated with an improved recovery from subarachnoid haemorrhage (Cheslow *et al.*, 2016). TGF- β is secreted by endothelial cells and astrocytes and is thought to be neuroprotective in the CNS. *In vitro*, exposure of mouse brain endothelial cells to TGF- β caused a reduction in EC-BBB permeability (Dohgu *et al.*, 2004). This suggests that when the BBB is disrupted, astrocytes can release factors that help the BBB to recover and that also act as an adaptive protective

mechanism in response to insults to the BBB. In our study it is possible that astrocytes in the HBEC-astrocyte BBB released soluble factors such as SHH, RA, ANGPT-1, TGF- β to protect the BBB from damage produced by the PRBC-HBEC coculture supernatants.

Further studies will be to treat the HBEC-astrocyte BBB model with a higher concentration of endothelial cell derived factors and to increase exposure of the HBEC-astrocyte BBB to endothelial cell derived factors for over 5 hours to see if this will cause an increase in HBEC-astrocyte BBB permeability.

In conclusion, our results showed an increase in HBEC-alone BBB permeability after a 5 hour exposure of the BBB to inflammatory mediators released in response to sequestration of PRBC. This increase was not observed in the more resilient HBEC-astrocyte BBB suggesting that factors released by astrocytes were protecting this BBB from damage that could have been caused by inflammatory mediators present in the PRBC-HBEC coculture supernatants.

Chapter 5 : Investigating activation of components of the BBB during cerebral malaria

5.1 Introduction

Disruption of the BBB in CNS disorders such as multiple sclerosis (MS), Alzheimer's disease (AD) can result in activation of astrocytes that can lead to astrogliosis.

Astrogliosis consists of a spectrum of changes that occur in astrocytes depending on the severity of the insult (Dossi *et al.*, 2018; Sofroniew, 2015, 2009). Astrocytes can undergo mild to moderate astrogliosis to severe astrogliosis with compact scar formation. In mild to moderate astrogliosis, alterations in gene expression, increase in GFAP expression and a small amount of astrocyte proliferation occurs (Figure 5.1). Cells mostly return to their normal healthy state (Figure 5.1) (Sofroniew, 2015, 2009).

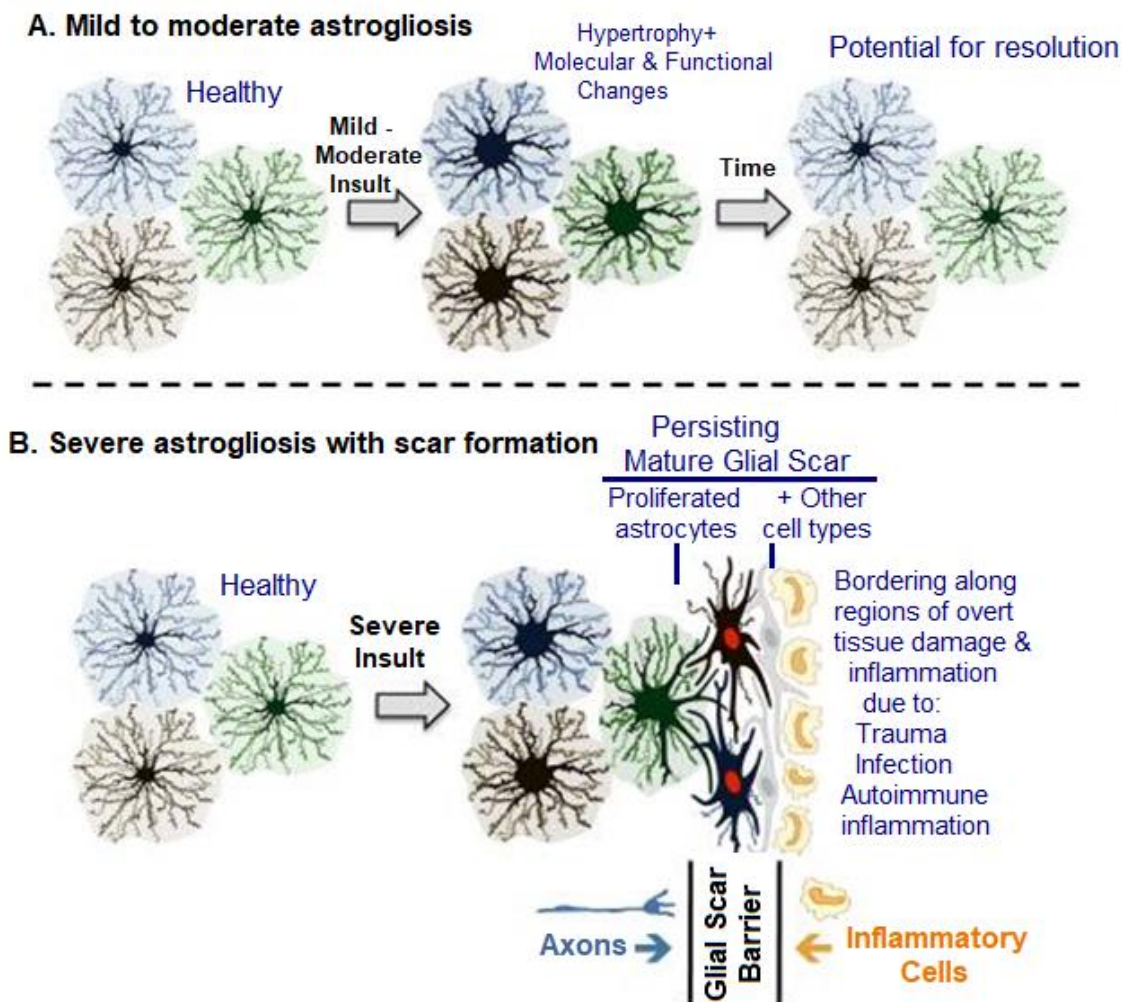


Figure 5.1 Schematic showing the different spectrum of reactive astrogliosis that changes with insult severity. Image obtained from (Sofroniew, 2009).

Conversely, in severe astrogliosis, increased astrocyte proliferation occurs, and this can in some cases result in scar formation. Structural changes that occur in astrocyte scar formation are in effect irreversible and still continue after resolution of the causative insult (Dossi *et al.*, 2018; Sofroniew, 2015, 2009).

Astrogliosis can be both beneficial and detrimental. Reactive astrocytes can protect the CNS through the uptake of excitotoxic glutamate in mice and also by promoting blood-brain barrier repair in mice (Sofroniew *et al.*, 2010; Sofroniew, 2009). Conversely, after CNS injury reactive astrocytes can stop the regeneration of axons in mice (Sofroniew, 2009). Children who survive cerebral malaria after treatment are sometimes left with long term neurological damage such as speech impairment and learning disabilities. The exact cause of this neurological damage is still unknown. Astrocytes protect and support neurons and thus if they are severely damaged during CM can result in neuronal damage and this might be responsible for the neurological sequelae observed in some CM survivors.

Increased levels of GFAP, ADAMTS-4 and ICAM-1 have been observed in activated astrocytes in several CNS disorders such as Alzheimer's disease (AD) and multiple sclerosis (MS) (Dossi *et al.*, 2018; Haddock *et al.*, 2006; Sue Griffin *et al.*, 1989; Tauchi *et al.*, 2012).

In the CNS tissues of human MS patients, ICAM-1 expression was observed in some astrocytes within active MS plaques (Sobel *et al.*, 1990). Reactive astrocytes were observed at the periphery of neuritic plaques in the brains of AD patients (Akiyama *et al.*, 1993). Within these senile plaques, the leukocyte function-associated antigen-1 (LFA-1) were observed in microglia aggregates implying that ICAM-1 on astrocyte surface could possibly associate with LFA-1 on microglia in AD. Lee *et al.* (2000) examined the inflammatory response produced following incubation of anti ICAM-1 antibody with primary rat astrocytes *in vitro* (Lee *et al.*, 2000). Results showed increased expression of cytokines such as IL-1 α , IL-1 β , IL-6 and TNF α when

ICAM-1 was ligated to rat astrocytes *in vitro* (Lee *et al.*, 2000). These results suggested that increased expression of ICAM-1 on astrocytes during CNS disorders such as AD, MS possibly promoted the inflammatory process in these diseases (Lee *et al.*, 2000).

In post-mortem brain tissue of AD patients, increased GFAP levels were identified around amyloid plaques (Dossi *et al.*, 2018; Sue Griffin *et al.*, 1989). GFAP breakdown (GFAP-BDP) products were observed in the serum of traumatic brain injury patients within an hour of injury and this was linked with disease severity (Papa *et al.*, 2012). Higher GFAP expression and large astrocyte clusters were observed in the perivascular area of the brain of EMCM mice than that of wild-type mice (Ampawong *et al.*, 2014). The precise processes leading to increase in GFAP expression and GFAP-BDP in astrocytes are not fully known and could be as a result of astrocyte activation or damage (Okonkwo *et al.*, 2013).

ADAMTS-4 is secreted as a 100kDa proform which can be processed into 75kDa and further processed into active forms at 60 and 50kDa. (Flannery *et al.*, 2002; Gao *et al.*, 2002; Porter *et al.*, 2005). *In vitro*, ADAMTS-4 is expressed basally in astrocytes and increased in response to stimuli such as TNF α and IL-1 β (Cross *et al.*, 2006; Gottschall and Howell, 2015; Hamel *et al.*, 2005). In the spinal cord lysate of rats after injury, elevated levels of ADAMTS-4 and a significant increase in aggrecan degradation by ADAMTS4 was observed. Also in this study, the ADAMTS-4 protein was found in primary rat astrocytes *in vitro*, suggesting that astrocytes were the cellular source of ADAMTS-4 in spinal cord injury (SCI) (Gurses *et al.*, 2016; Tauchi *et al.*, 2012). ADAMTS-4 expression was markedly higher in MS lesions compared to normal brain white matter tissue. In these cases, elevated ADAMTS-4 expression was associated with cells that had been characterised as GFAP positive astrocytes within MS lesions (Haddock *et*

al., 2006). These studies suggest that ADAMTS-4 expression in astrocytes is upregulated following CNS disorders or injury.

Astrogliosis was observed in post-mortem brain tissues from CM patients. In the post-mortem brain tissues of CM patients, astrogliosis was observed in the white matter, cerebellum, basal ganglia, thalamus and brain stem (Dorovini-Zis *et al.*, 2011). Astrogliosis observed in CM patients was not associated with sequestration or myelin/axonal damage (Dorovini-Zis *et al.*, 2011; Medana *et al.*, 2002). Also, high levels of the astrocyte marker S100B in Kenyan children were linked with an increased risk of repeated seizures during cerebral malaria. It was suggested that increased risk of seizure could be due to damaged astrocytes (Medana *et al.*, 2007).

The fact that an increase in GFAP, ICAM-1 and ADAMTS-4 expression have been observed in astrocytes in neurological disorders where BBB disruption has occurred make them good candidate proteins to investigate astrocyte activation during CM.

This study set out to investigate astrocyte activation in cerebral malaria using the HBEC-astrocyte BBB model. We investigated the effect of brain endothelial cell derived factors produced in response to sequestration on astrocytes when grown in tandem with endothelial cells.

5.2 Materials and methods

5.2.1 Cell-based ELISA for detection of GFAP

Primary human astrocytes were directly treated with a 1 in 10 dilution of supernatants from 2 separate coculture experiments for 48 hours, to determine the direct effect of inflammatory mediators produced in response to sequestration on astrocytes *in vitro*. A cell-based ELISA was performed to detect GFAP expression in astrocytes as described in chapter 2, section 2.24. The optimised rabbit anti-GFAP primary antibody dilution of 1:2000 and goat anti-rabbit secondary antibody dilution of 1:3000 were used.

5.2.2 Treatment and harvesting of the HBEC-astrocyte BBB model

HBEC-astrocyte BBB model was set up as described in chapter 3, section 3.2.7. The HBEC-astrocyte BBB was grown *in vitro* for 5 days as described in chapter 3. The HBEC-astrocyte BBB was treated with a 1 in 10 dilution of coculture supernatants and HBEC lysates for 48 hours described in chapter 4, section 4.2.3.3. After 48 hours, the supernatant from the luminal and basolateral side of the HBEC-astrocyte BBB model were harvested and stored at -20°C. The lysates from luminal and basolateral sides of the transwell were independently scraped, lysed and stored at -20°C for further analyses.

5.2.3 Western blot analysis for detection of GFAP

Astrocytes were directly treated with supernatants from 3 different coculture experiments for 48 hours. The astrocytes supernatants were harvested, and western blot analysis was performed on these supernatants to detect GFAP expression as described in chapter 2, section 2.17-2.22. The rabbit anti-GFAP primary antibody dilution of 1:500 and goat anti-rabbit secondary antibody dilution of 1:1000 were used.

5.2.4 Western blot analysis on supernatants harvested from the luminal and basolateral side of the HBEC-astrocyte BBB

The HBEC-astrocyte BBB were treated with 3 different HBEC lysates as described in Chapter 4, section 4.2.3.3 (Table 4.1) for 5 hours. After 5 hours, these supernatants were harvested from luminal and basolateral sides of the HBEC-astrocyte BBB and analysed for the presence of soluble GFAP and ADAMTS-4 using western blot analysis as described in chapter 2, section 2.17-2.22.

For GFAP detection, the Rabbit anti-GFAP primary antibody dilution of 1:500 and goat anti-rabbit secondary antibody dilution of 1:1000 were used (Appendix 4).

For ADAMTS-4 detection, ADAMTS-4 goat polyclonal IgG antibody dilution of 1:250 and donkey anti-goat IgG secondary antibody dilution of 1:1000 were used (Appendix 4).

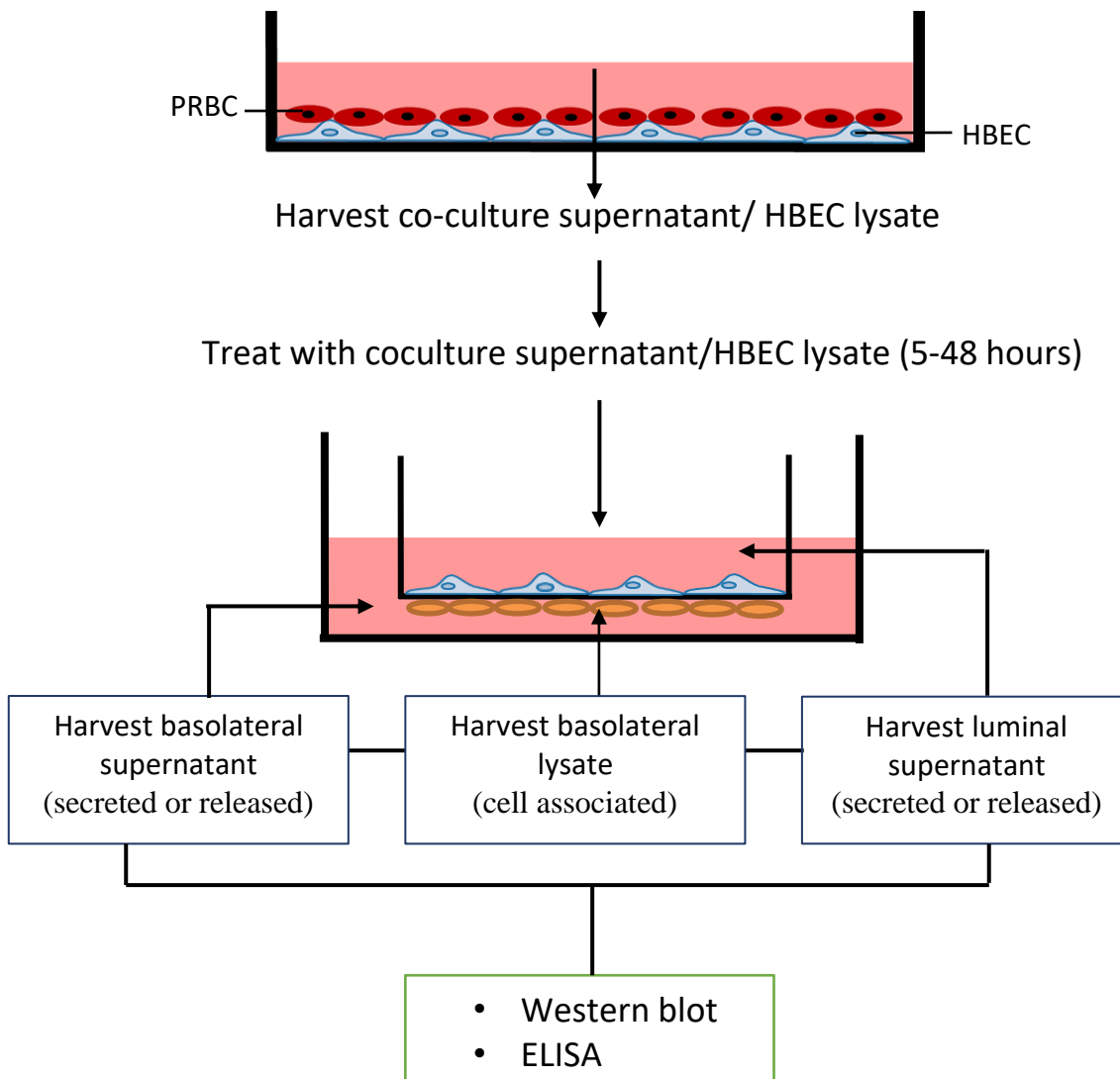


Figure 5.2 Summary of experiments performed to analyse GFAP, ICAM-1 and ADAMTS-4 expression in the luminal and basolateral supernatants of the HBEC-astrocyte BBB that had been treated with different coculture supernatants and lysates.

5.2.5 Sandwich ELISA

HBEC-astrocyte BBB was treated with coculture supernatants for 5 and 48 hours and HBEC-lysates for 48 hours, and luminal and basolateral supernatants and lysates were harvested. Sandwich ELISA to determine GFAP, ADAMTS-4 and ICAM-1 expression in the luminal and basolateral supernatants and lysates of the HBEC-astrocyte BBB was performed as described in Chapter 2, section 2.28.

Human GFAP sandwich ELISA (R&D systems) was performed according to the manufacturer's guidelines. 100µl of capture antibody (5µg/ml) diluted in PBS was used to coat the 96 well plate overnight at 4°C. Each well was washed with 150µl washing solution 3 times and blocked with 250µl of reagent diluent (1% BSA in PBS) per well for 1 hour at room temperature. Serial dilutions of the standards were prepared to provide the concentration range from 39 to 20000pg/ml.

50µl of basolateral supernatants and 50µl of basolateral astrocyte lysates harvested from HBEC-astrocyte BBB after treatment with coculture supernatants and HBEC lysates were added to the appropriate wells in duplicates. 100µl of detection antibody (0.05µg/ml) diluted in reagent diluent was then added to each well and incubated at room temperature for 4 hours. 100µl of streptavidin HRP solution (1:40 dilution) was added to each well for 30 minutes at room temperature. Contents of wells were emptied by flipping of plate and each well was washed with 150µl of washing solution. Plate was washed to remove unbound HRP. After this the colour development was performed as described in Chapter 4, section 4.2.1.

Human ADAMTS-4 sandwich ELISA (R&D systems) were performed as described in Chapter 2, section 2.28. In this study detection antibody concentrations used were different from the concentrations used in Chapter 4, section 4.2.1. 100µl of capture antibody (1µg/ml) diluted in PBS was used to coat 96 well plates. 50µl of basolateral supernatants and 50µl of luminal

lysate and basolateral lysates harvested from the HBEC-astrocyte BBB were added to plate and incubated for 2 hours. 100µl of detection antibody (0.06µg/ml) diluted in reagent diluent (1% BSA in PBS) was added to each well and plate was incubated for 4 hours at room temperature instead of 2 hours reported earlier in Chapter 2, section 2.28. This was to increase assay sensitivity for detection of ADAMTS-4. Also, 100µl of Streptavidin-HRP (1:40 dilution) was added to each well and plate was incubated for 30 minutes at room temperature in the dark instead of 20 minutes as reported in Chapter 2, section 2.28 to increase assay sensitivity.

Sandwich ELISA of ICAM-1 was performed as described in Chapter 2, section 2.28.

Basolateral supernatants and a 1 in 10 dilution of the basolateral lysates harvested from the HBEC-astrocyte BBB were used in this sandwich ELISA as described in Chapter 2, section 2.28.

5.2.5.1 Calculation of results

Calculation of protein of interest after sandwich ELISA experiments

The mean of duplicate readings of each well was calculated. A linear standard curve was calculated by plotting the average optical density of each standard on the vertical axis against the corresponding GFAP or ICAM-1 or ADAMTS-4 concentration on the horizontal axis. The concentration of GFAP, ICAM-1 or ADAMTS-4 in each sample was determined by extrapolating the optical density values against the standard concentrations. The amount of the protein of interest was obtained by multiplying the concentration of the protein by the volume of the basolateral supernatant.

To calculate the ratio of protein of interest to the total protein in the astrocyte lysate, the concentration of the protein of interest was multiplied by the dilution factor to obtain the actual concentration of the protein of interest. The actual concentration was then divided by the total concentration of protein in the given sample.

Calculation of ratio = $\frac{\text{Actual concentration of desired protein}}{\text{Total concentration of protein in sample}}$

5.2.6 Densitometry analysis

Densitometric analysis of western blot was calculated using Image J as described in Chapter 3, section 3.2.10.

5.3 Results

5.3.1 Effect of coculture supernatants on GFAP expression in astrocytes

Cell-based ELISA was used to detect GFAP expression in astrocytes that had been treated with coculture supernatants. GFAP expression was unchanged in astrocytes directly treated with the control media, URBC-HBEC coculture supernatant and PRBC-HBEC coculture supernatants at 48 hours (Figure 5.3A).

Visually, 3 GFAP bands between 45-60 kDa were observed in all the supernatants of astrocytes directly treated with the different coculture supernatants (Figure 5.3B). A more prominent band intensity of GFAP was observed in the supernatant of astrocytes that had been directly treated with the PRBC-HBEC coculture supernatant. Semi-quantitative analysis by densitometry on the 45-60kDa GFAP bands was done. The 45-60kDa GFAP bands were marginally higher in the supernatant of astrocytes that had been treated with the PRBC-HBEC coculture supernatants compared to the controls, however this was not statistically significant (Figure 5.3C).

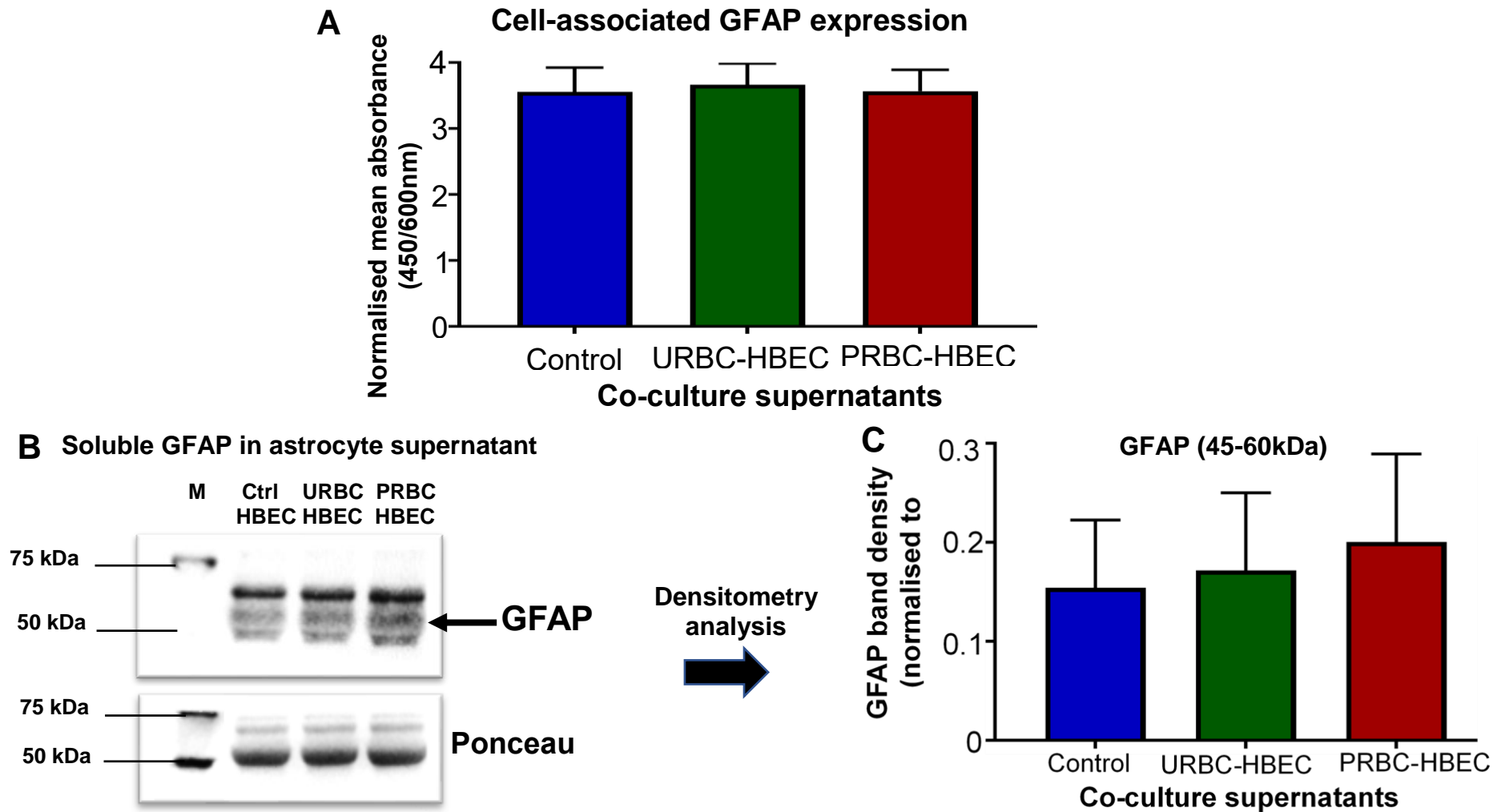


Figure 5.3 GFAP expression in astrocytes directly treated with coculture supernatants. (A) Cell-associated GFAP expression in astrocytes treated with coculture supernatants (n=4). Soluble GFAP expression in supernatant of astrocytes directly treated with coculture supernatants. (B) Western blot for detection of GFAP (C) Densitometry analysis of western blot n=3. Error bars represent standard error mean (SEM).

5.3.2 Changes in GFAP expression in the HBEC-astrocyte BBB

Sandwich ELISA was used to detect GFAP expression in the astrocyte supernatant and astrocyte lysate of the HBEC-astrocyte BBB treated with coculture supernatants. A trend towards a decrease in GFAP expression was observed in the astrocyte supernatants of the HBEC-astrocyte BBB that had been treated with the PRBC-HBEC coculture supernatant for 5 hours, however, this was not statistically significant (Figure 5.4A).

Interestingly, a trend towards an increase in GFAP expression was observed in the astrocyte supernatant in response to treatment of the HBEC-astrocyte BBB model with PRBC-HBEC coculture supernatants and URBC-HBEC coculture supernatants for 48 hours compared to the controls, however this was not statistically significant (Figure 5.4B).

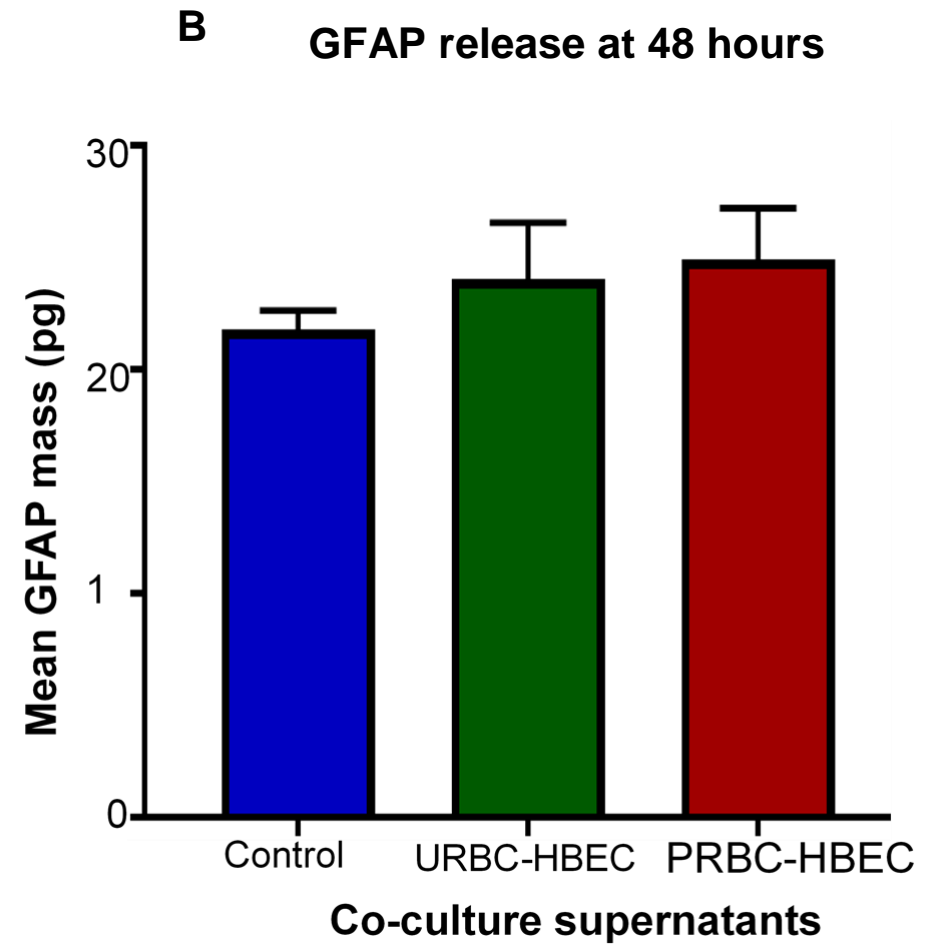
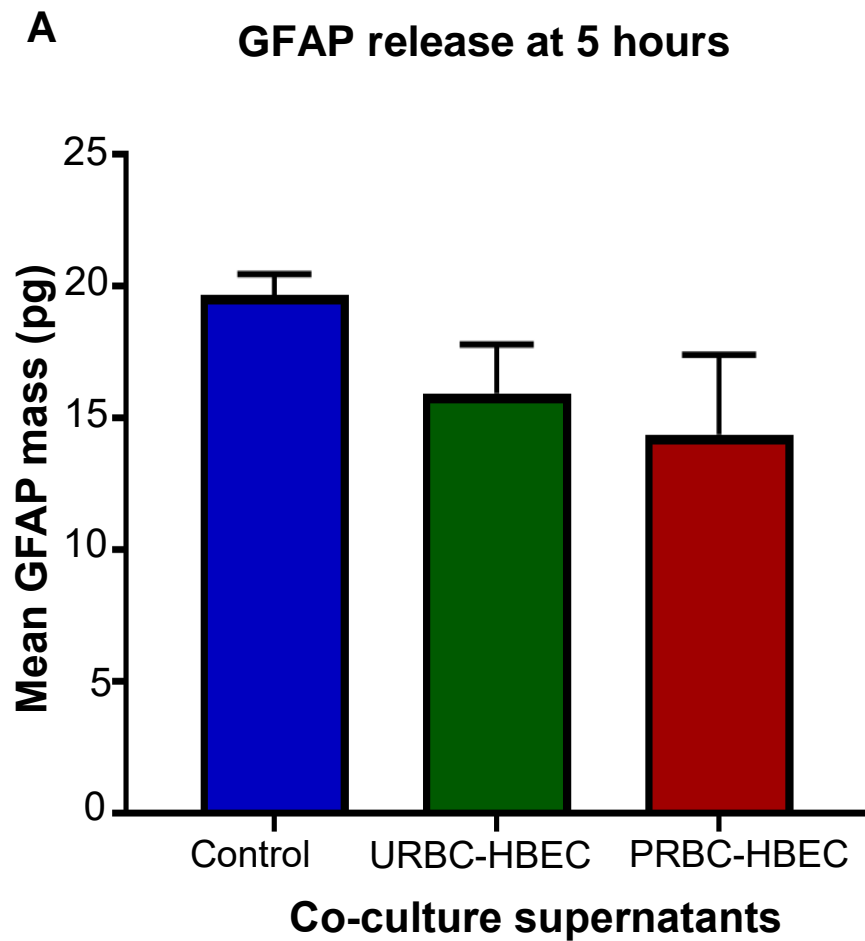


Figure 5.4 Changes in GFAP expression in the astrocyte supernatant of astrocytes following treatment of the HBEC-astrocyte BBB model with coculture supernatants for (A) 5 hours (n=3) and (B) 48 hours (n=10). Error bars represent SEM.

A trend towards a decrease in cell associated GFAP expression in astrocyte lysates was observed following treatment of the HBEC-astrocyte BBB model with PRBC-HBEC and URBC-HBEC coculture supernatants for 48 hours compared to the control (Figure 5.5).

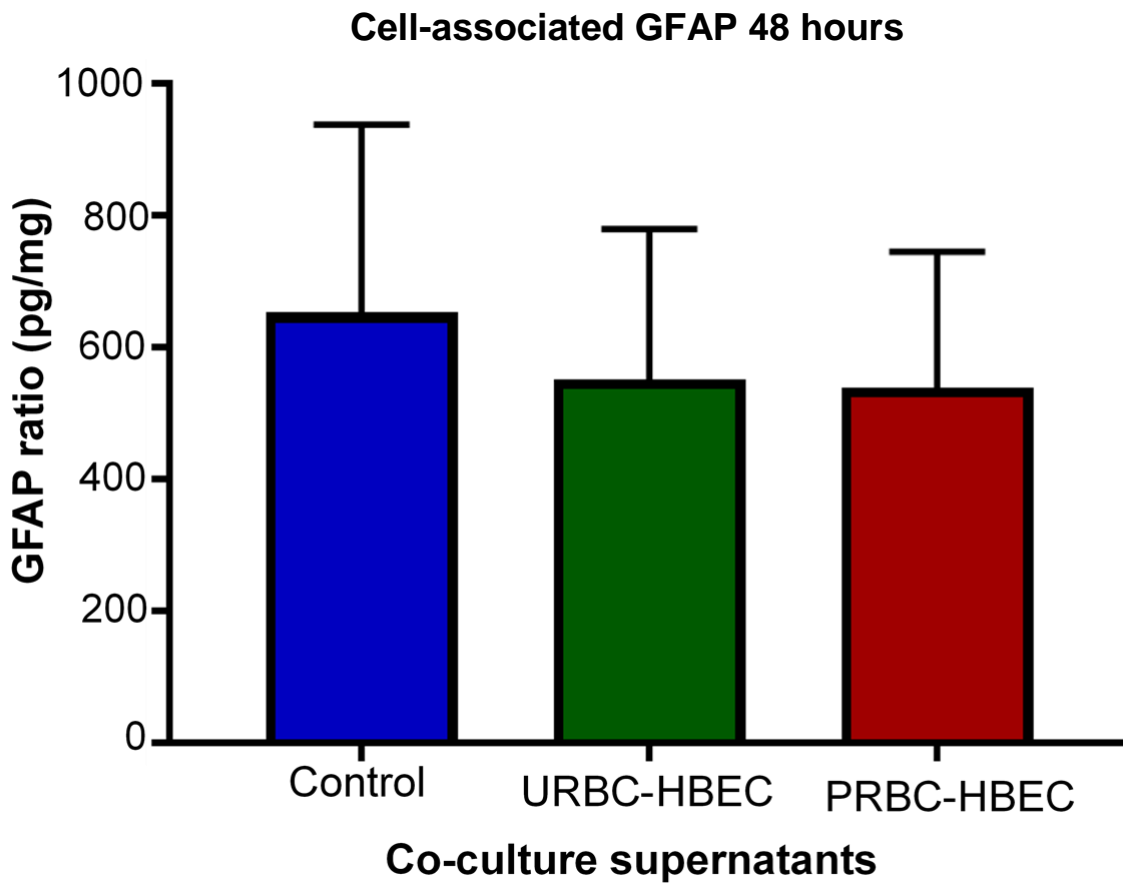


Figure 5.5 Alteration in cell-associated GFAP expression following treatment of the HBEC-astrocyte BBB model with the different coculture supernatants. Error bar represents SEM (n=8).

5.3.3 Alterations in ADAMTS-4 expression in astrocytes of the HBEC-astrocyte BBB

Sandwich ELISA was used to detect ADAMTS-4 expression in astrocyte supernatants and lysates of the HBEC-astrocyte BBB treated with coculture supernatants.

A trend towards an increase in ADAMTS-4 expression was observed in the astrocyte supernatants following treatment of the HBEC-astrocyte BBB model with PRBC-HBEC and URBC-HBEC coculture supernatants for 5 hours compared to the control HBEC supernatants, however this was not statistically significant (Figure 5.6A).

ADAMTS-4 expression was the same in the supernatant of astrocytes from the HBEC-astrocyte BBB treated with PRBC-HBEC, URBC-HBEC and HBEC coculture supernatants for 48 hours (Figure 5.6B).

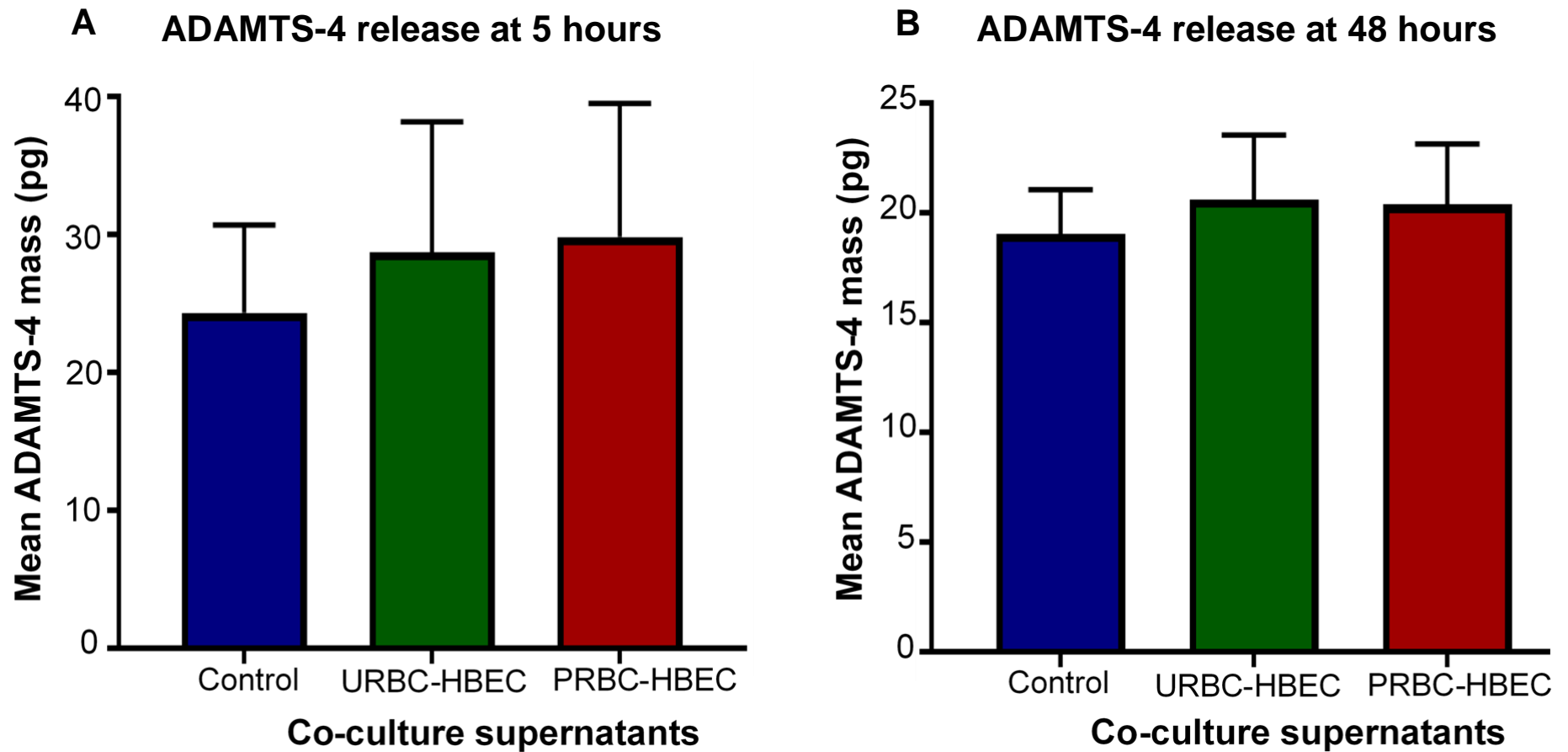


Figure 5.6 Alterations in ADAMTS-4 expression in astrocytes supernatants following treatment of the HBEC-astrocyte BBB model with coculture supernatants for (A) 5 hours (n=6) (B) 48 hours (n=10). Error bars represent SEM.

A trend towards an increase in ADAMTS-4 expression was observed in the astrocyte lysate from the HBEC-astrocyte BBB model treated with the PRBC-HBEC coculture supernatants for 48 hours compared to the controls, however this was not statistically significant (Figure 5.7).

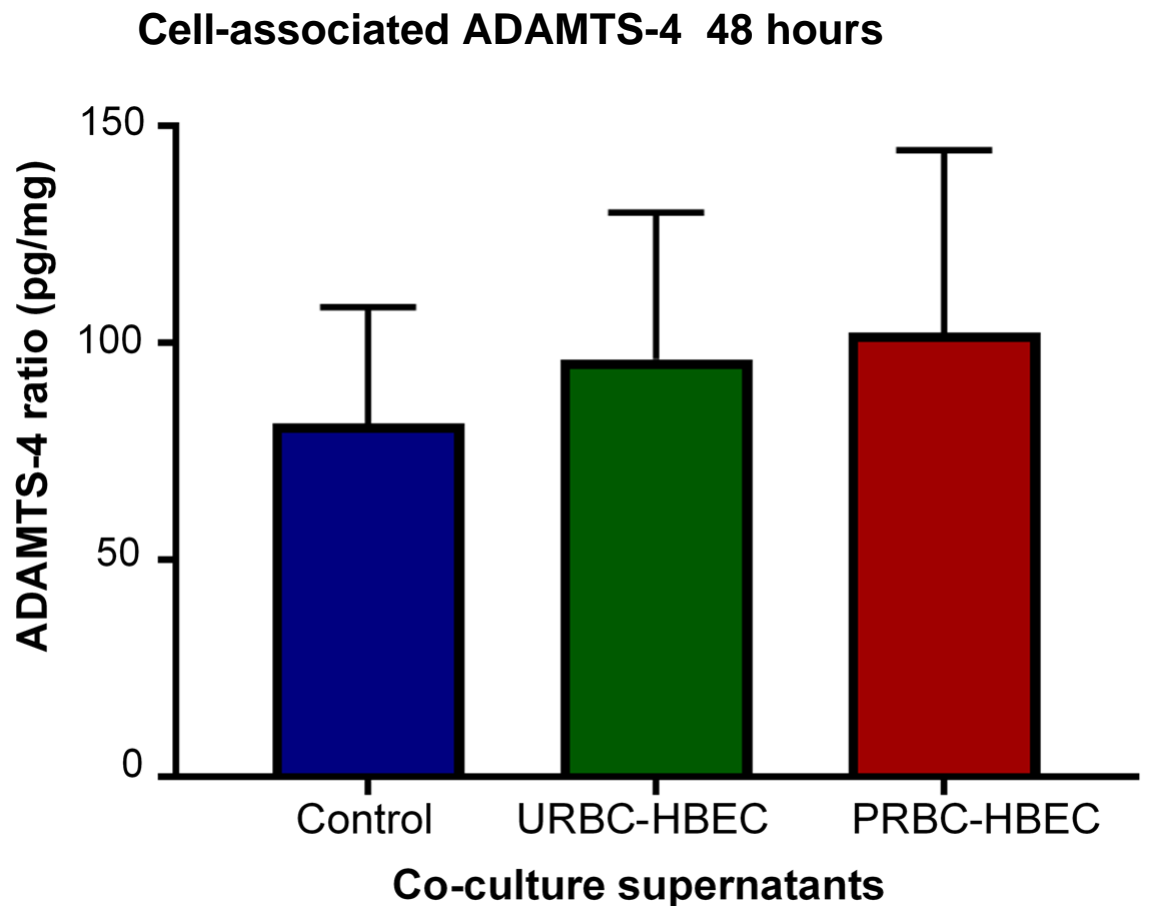


Figure 5.7 Changes in ADAMTS-4 expression in astrocyte lysates following treatment of the HBEC-astrocyte BBB model with coculture supernatants for 48 hours. Error bars represent the standard error of the mean, n=8.

5.3.4 Alterations in ICAM-1 expression in astrocytes of the HBEC-astrocyte BBB

Sandwich ELISA was used to detect ICAM-1 expression in astrocyte supernatants and astrocyte lysates of the HBEC-astrocyte BBB treated with coculture supernatants.

A statistically significant increase in ICAM-1 expression was observed in astrocyte supernatants from the HBEC-astrocyte BBB that had been treated with PRBC-HBEC coculture supernatants for 48 hours compared to the URBC-HBEC coculture supernatants ($p < 0.1$) and control supernatants ($p < 0.05$) (Figure 5.8B).

A trend towards an increase in ICAM-1 expression was observed in astrocyte supernatants, following treatment of the HBEC-astrocyte BBB with PRBC-HBEC coculture supernatants for 5 hours, compared to the controls, however, this was not statistically significant (Figure 5.8A). Interestingly, sICAM-1 levels in the astrocyte supernatant (basolateral) was significantly higher after the HBEC-astrocyte BBB had been treated with PRBC-HBEC coculture supernatants for 48 hours (Figure 5.8B), compared to 5 hours treatment (Figure 5.8A).

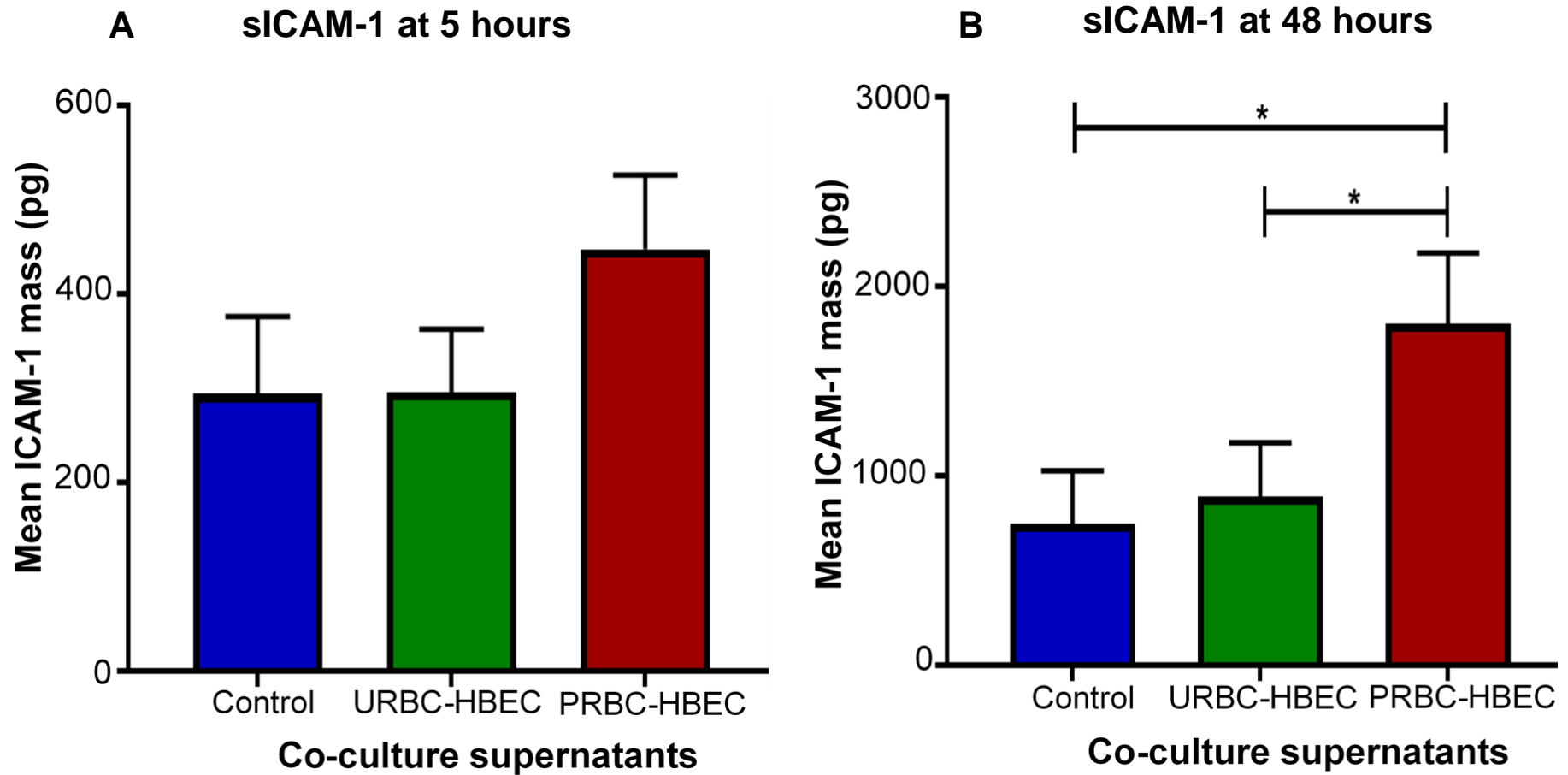


Figure 5.8. Alterations in ICAM-1 expression in astrocytes following treatment of the HBEC-astrocyte BBB model with coculture supernatants for 5 hours (n=9) and 48 hours (n=8) * p<0.1. Error bars represent the SEM.

A trend towards a decrease in ICAM-1 expression was observed in astrocyte lysates from the HBEC-astrocyte BBB treated with PRBC-HBEC coculture supernatants for 48 hours, however, this was not statistically significant (Figure 5.9).

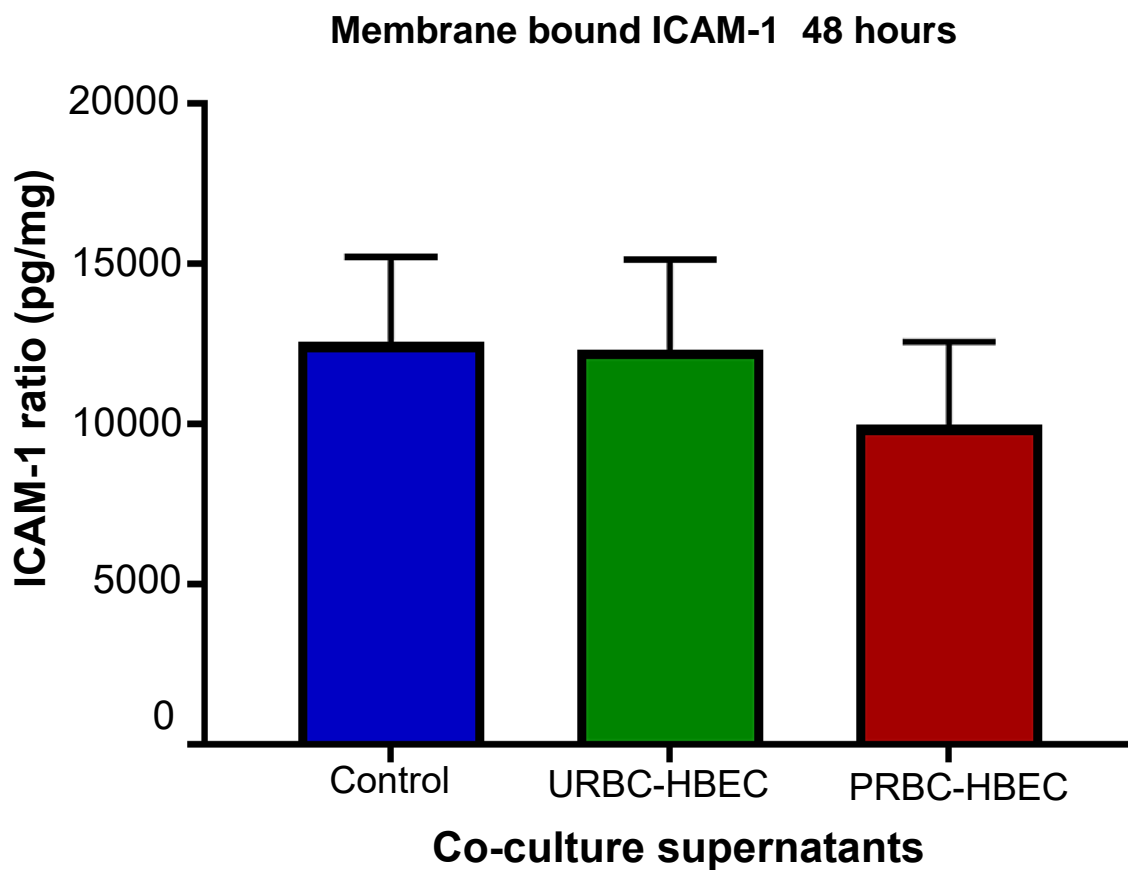


Figure 5.9 Alterations in ICAM-1 expression in astrocytes following treatment of the HBEC-astrocyte BBB model with coculture supernatants for 48 hours. Error bar represents the standard error of the mean, n=10.

5.3.5 GFAP expression in astrocytes following treatment of the HBEC-astrocyte BBB model with HBEC lysates

Double bands of GFAP between 38-50kDa were detected in the luminal supernatants from the HBEC-astrocyte BBB, that had been treated with the different HBEC lysates (Figure 5.10A). A more intense GFAP band was observed in the luminal supernatants, following treatment with PRBC-HBEC lysate (Figure 5.10A). Densitometric analysis showed that the 38-50kDa band density of GFAP were higher in the **luminal** supernatants from the HBEC-astrocyte BBB that had been treated with PRBC-HBEC lysates as compared to the controls (Figure 5.10B).

A single GFAP band of approximately 45kDa was observed in the **basolateral** supernatants from the HBEC-astrocyte BBB that had been treated with the HBEC lysates (Figure 5.10A). Densitometric analysis on the 45kDa band showed GFAP band density was higher in the basolateral supernatants of the HBEC-astrocyte BBB that had been treated with PRBC-HBEC lysates compared to the controls, although this was not statistically significant (Figure 5.10C).

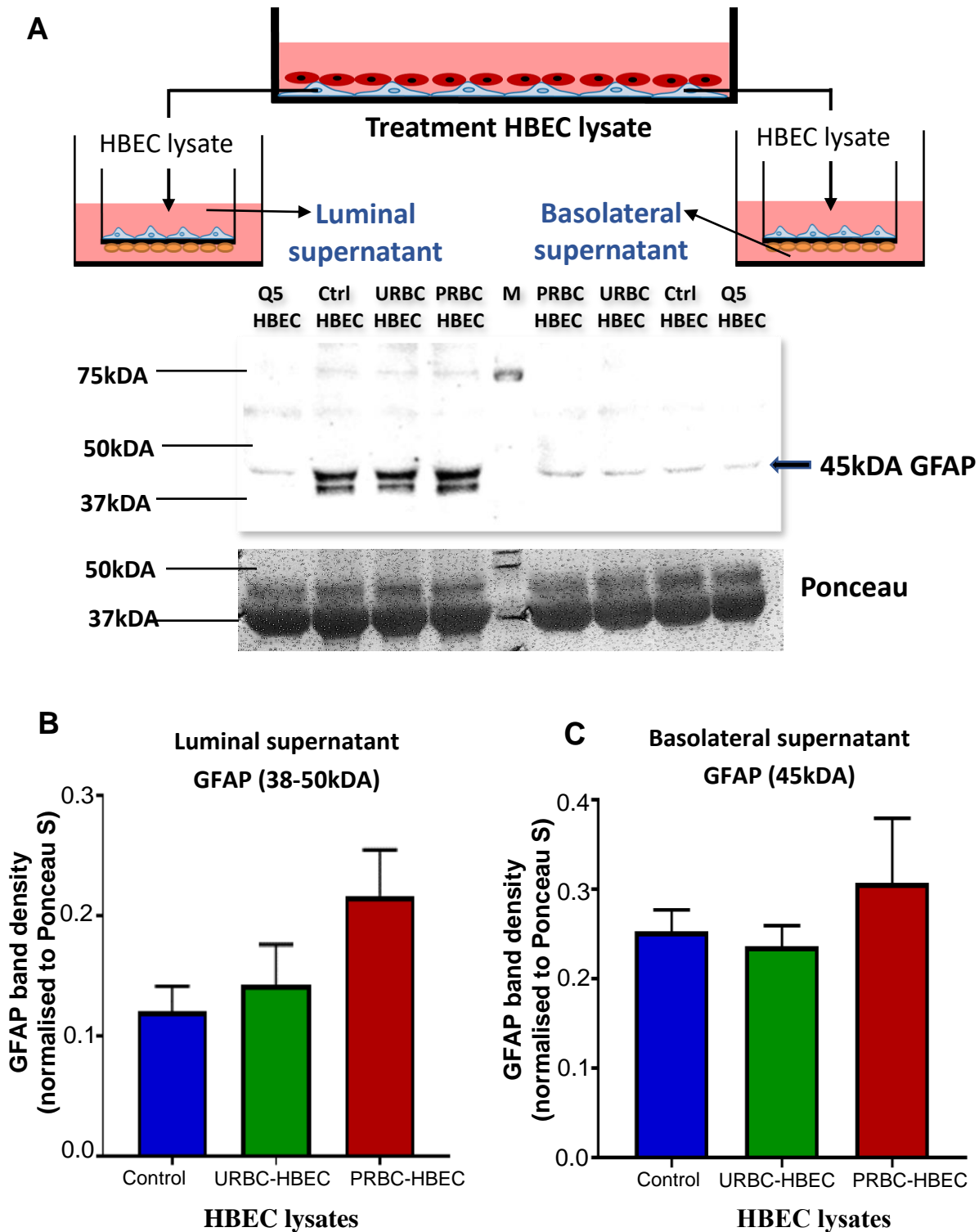


Figure 5.10 Soluble GFAP expression in luminal and basolateral supernatants of HBEC-astrocyte BBB that has been treated with HBEC lysates. (A) Western blot analysis showed 2 GFAP bands between 38-50kDA in the supernatants from the luminal side. Single GFAP bands were observed at approximately 45kDA in the basolateral supernatants. Following treatment of the HBEC-astrocyte BBB with PRBC-HBEC lysate (B) Densitometry analysis showed an increase in GFAP expression in luminal supernatants (n=3). (C) Densitometry analysis showed an increase in GFAP expression in the basolateral supernatant (n=3).

5.3.6 Alterations in ADAMTS-4 expression in astrocytes following treatment of the HBEC-astrocyte BBB model with HBEC lysates

Two distinct bands of ADAMTS-4 at 100kDA and 47kDA approximately were observed in the luminal and basolateral side of the HBEC-astrocyte BBB that had been treated with the HBEC lysates (Figure 5.11, Figure 5.12). Visually, a more intense ADAMTS-4 band at 100kDA was observed in samples from the **luminal** side of the HBEC-astrocyte BBB, that had been treated with the PRBC-HBEC lysates compared to the controls (Figure 5.11A). Semiquantitative densitometric analysis showed that the 100kDA ADAMTS-4 band density was higher in the **luminal** supernatant from the HBEC-astrocyte BBB that had been treated with PRBC-HBEC lysates (Figure 5.11B) compared to the controls. The 47kDA ADAMTS-4 band density was marginally higher in the luminal supernatant from the HBEC-astrocyte BBB that had been treated with PRBC-HBEC lysates. (Figure 5.11C).

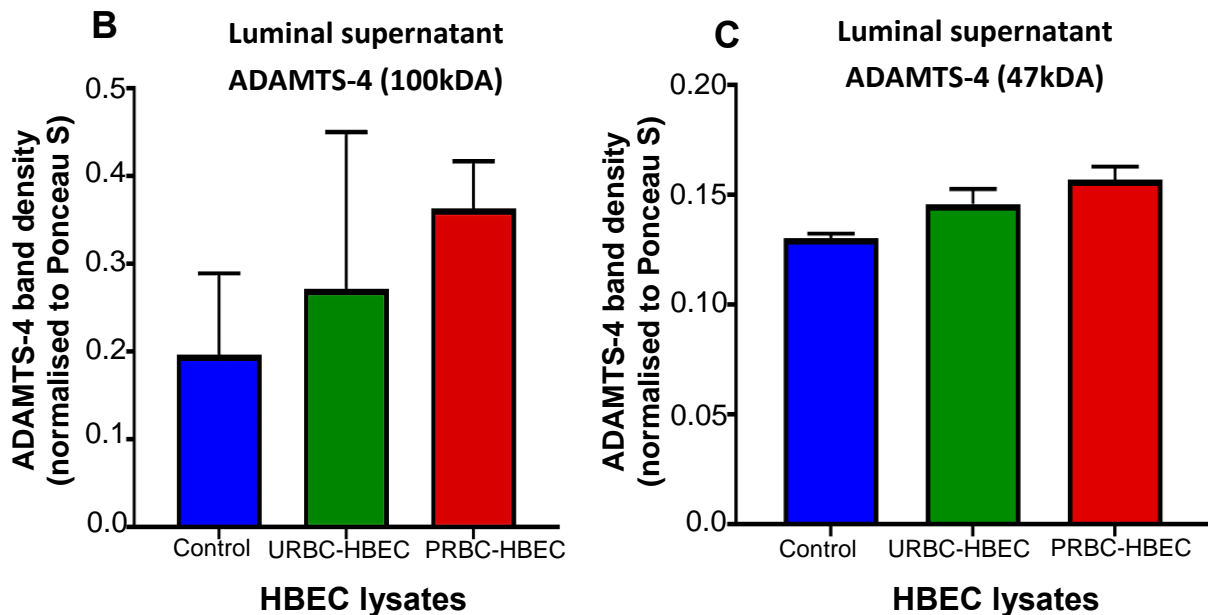
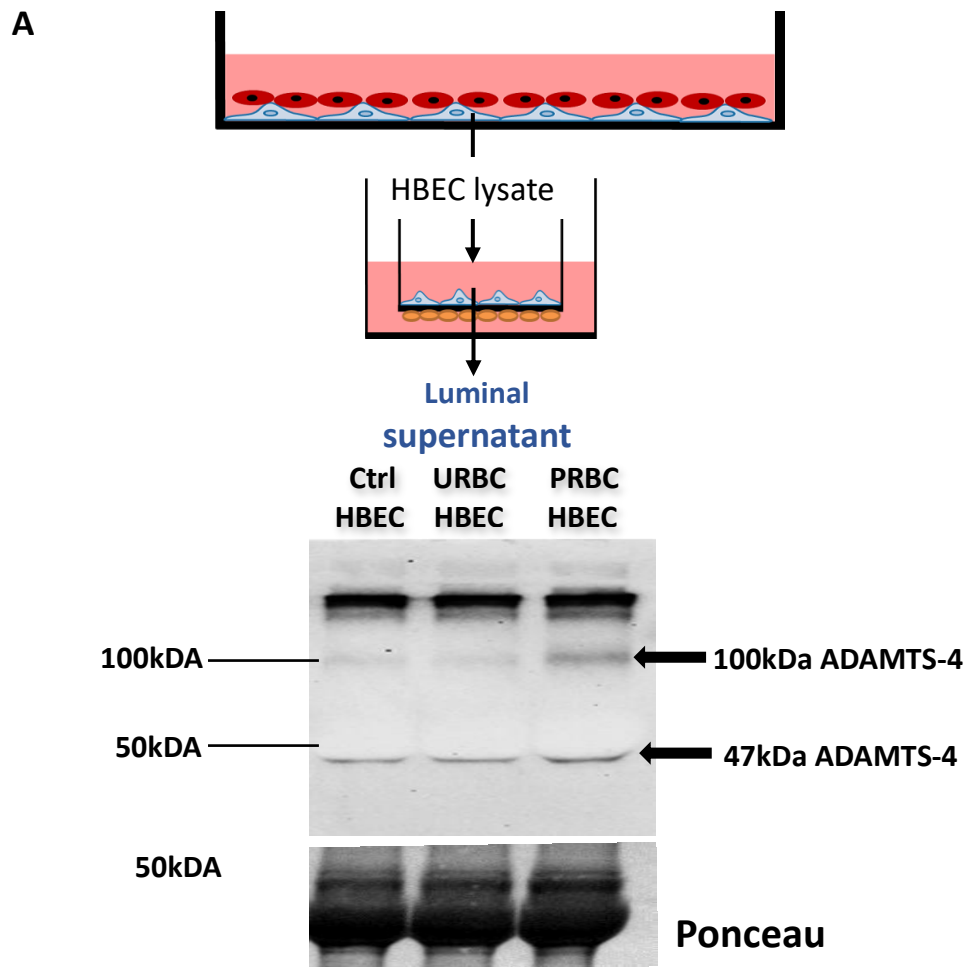


Figure 5.11 ADAMTS-4 expression in luminal supernatant of astrocytes following treatment of the HBEC-astrocyte BBB model with HBEC lysates. (A) In the luminal side, ADAMTS-4 bands at 100kDa and 47kDa present. Densitometry analysis on the 100kDa band (B) and 47kDa band (C) showed a higher band density in luminal supernatants following treatment with PRBC-HBEC lysate (n=2).

Visually, ADAMTS-4 band intensities at 100kDA and 47kDA were the same in all the **basolateral** supernatants from the HBEC-astrocyte model that had been treated with the different HBEC lysate conditions. (Figure 5.12A). However, semiquantitative densitometric analysis showed that the 100kDA and 47kDA ADAMTS-4 band density was higher in the basolateral supernatant from the HBEC-astrocyte BBB that had been treated with the PRBC-HBEC lysates compared to the controls (Figure 5.12B, Figure 5.12C). 100kDA and 47kDA ADAMTS-4 bands were also observed in all the coculture supernatants (Figure 4.3).

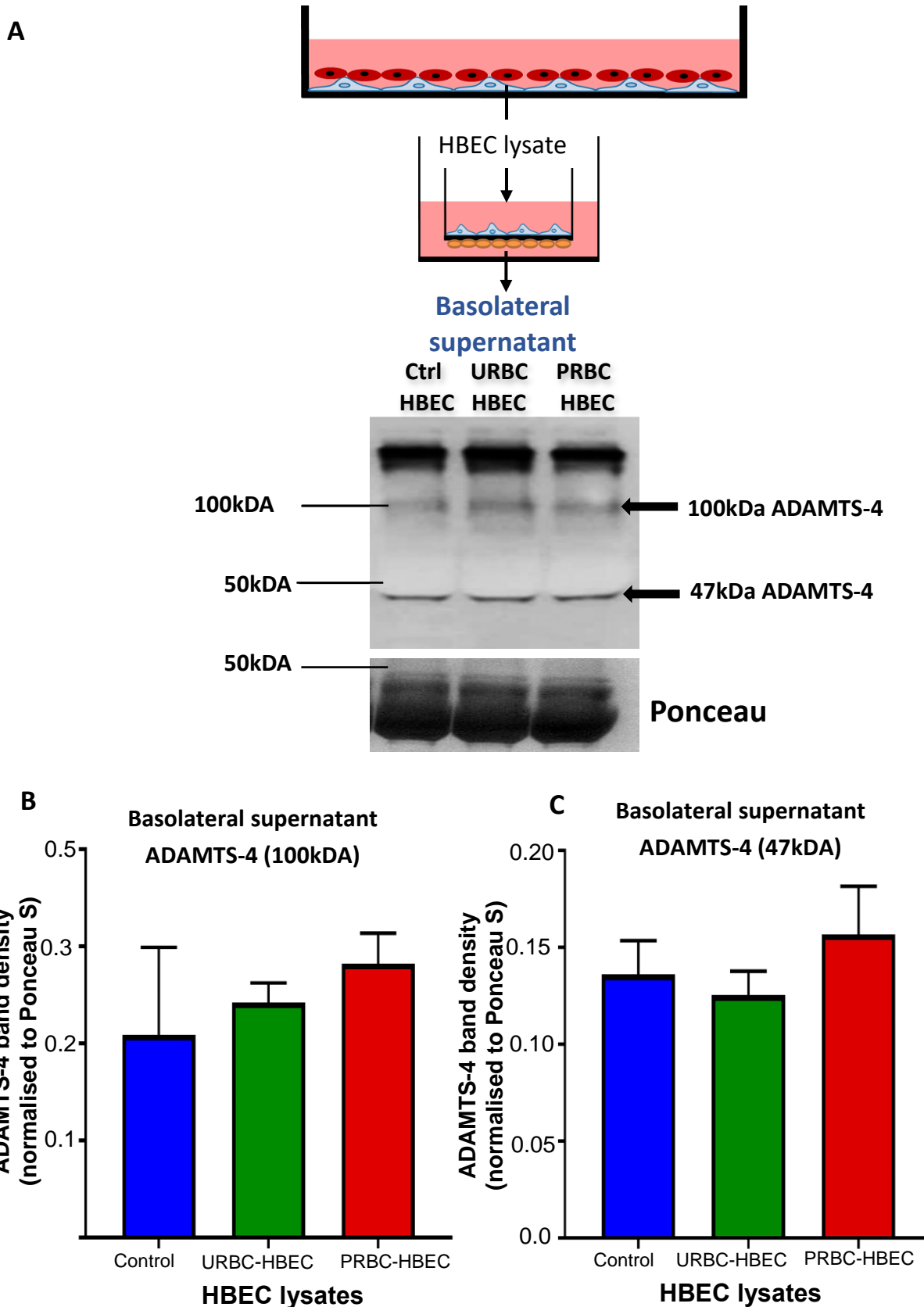


Figure 5.12 ADAMTS-4 expression in basolateral supernatant of astrocytes following treatment of the HBEC-astrocyte BBB with HBEC lysates. (A) In the basolateral side ADAMTS-4 bands at 100kDa and 47kDa were observed. Densitometry analysis on the 100kDa band (B) and 47kDa band (C) showed a higher band density in basolateral supernatants following treatment with PRBC-HBEC lysate (n=2).

5.4 Discussion

In this study we set out to investigate the indirect effect of sequestration of PRBC on astrocytes and HBEC in the HBEC-astrocyte BBB. To do this we studied GFAP, ICAM-1 and ADAMTS-4 expression in astrocytes.

GFAP has been shown to be upregulated during astrocyte activation and damage and is one of the most widely used markers to study astrocyte activation in disease (Sofroniew *et al.*, 2010; Sofroniew, 2015, 2009).

Cell based ELISA showed GFAP expression was unchanged in astrocytes treated with coculture supernatants (Figure 5.3A). Cell based ELISA measured the total amount of GFAP and did not consider the different forms of GFAP produced by astrocytes in response to different inflammatory mediators. Western blot analysis showed the presence of 3 bands of GFAP between 45-60kDA (Figure 5.3B). The band at 60kDA could be the GFAP isoform, GFAP δ produced as a result of alternative splicing of GFAP (Roelofs *et al.*, 2005). Increased GFAP δ isoforms have been observed in a subpopulation of astrocytes present in lesions associated with epilepsy (Martinian *et al.*, 2009). GFAP bands at 45kDA could be proteolytic fragments of GFAP. Proteolytic fragments of GFAP between 38-50kDA can be found in the CSF of traumatic brain injury (TBI) patients (Zhang *et al.*, 2014).

Our results suggest that inflammatory mediators present in the PRBC-HBEC coculture supernatants possibly caused damage to astrocytes resulting in the release of GFAP δ and GFAP breakdown products (GFAP-BDP) into the supernatant (Figure 5.3C).

Although this analysis was not physiological, it represented the scenario where the BBB was compromised and inflammatory mediators in the luminal side of the BBB had leaked to the basolateral side and were in direct contact with astrocytes.

GFAP expression *in vitro* is upregulated even without stimulation of astrocyte cultures and this depicts a state different from that of *in vivo* normal resting astrocytes. A trend towards a decrease in GFAP expression was observed in the astrocyte supernatant after a 5-hour exposure of the HBEC-astrocyte BBB to inflammatory mediators present in the PRBC-HBEC coculture supernatant (Figure 5.4A). This could have been due to a protective response produced by astrocytes to protect the BBB from damage. Astrocytes may release factors like the sonic hedgehog (SHH) that can reduce proinflammatory cytokines and can also reduce BBB permeability (Alvarez *et al.*, 2013).

Interestingly, our results suggest that longer exposure (48 hours) of the HBEC-astrocyte BBB to inflammatory mediators present in the PRBC-HBEC coculture supernatant could have caused damage to astrocytes, resulting in the increased release of cell-associated GFAP from astrocytes into the supernatant (Figure 5.4B and 5.5). Elevated GFAP levels were observed in the serum and CSF of children with severe TBI within 24 hours of admission. It was suggested that increased levels of GFAP in the serum could be due to BBB disruption during TBI resulting in GFAP leakage into the blood (Fraser *et al.*, 2011). Disruption of the BBB during TBI could result in and an increased GFAP expression in astrocytes and this could ultimately get released into the luminal side of the BBB (Fraser *et al.*, 2011).

It is well known that ADAMTS-4 is produced by astrocytes and these proteases can breakdown aggrecan and brevican components of the extracellular matrix of the BBB. In the spinal cord lysates of rats increased degradation of aggrecan by ADAMTS-4 was observed. ADAMTS-4 was shown to degrade recombinant brevican into proteolytic fragments. Thus, in this study we also examined ADAMTS-4 as a marker for astrocyte activation following exposure of the HBEC-astrocyte BBB to endothelial cell derived factors.

An increase in ADAMTS-4 expression in the astrocyte lysate was observed, following exposure of the HBEC-astrocyte BBB to PRBC-HBEC coculture supernatant for 48 hours (Figure 5.7). Increased expression of ADAMTS-4 is thought to be beneficial during CNS injury. Following spinal cord injury increased ADAMTS-4 expression and cleavage by aggrecan were observed (Gottschall *et al.*, 2015; Tauchi *et al.*, 2012). In the same study, administration of ADAMTS-4 after spinal cord injury (SCI) into the rat spinal cord, stimulated motor functional recovery (Gottschall *et al.*, 2015; Tauchi *et al.*, 2012). In our study increased ADAMTS-4 levels observed could have been a neurorepair mechanism.

We also examined ICAM-1 as a marker for astrocyte activation in cerebral malaria. ICAM-1 is constitutively expressed at very low levels in astrocytes and upregulated by astrocytes in response to inflammatory stimuli such as TNF α and IL-1 β *in vitro* (Hurwitz *et al.*, 1992; Lee *et al.*, 2000). A significant increase in sICAM-1 levels was observed in astrocyte supernatant following exposure of the HBEC-astrocyte BBB to inflammatory mediators present in the PRBC-HBEC coculture supernatant for 48 hours (Figure 5.8B). Significantly higher levels of sICAM-1 observed at 48 hours compared to 5 hours (Figure 5.8A and Figure 5.8B) suggest that longer exposure of HBEC-astrocyte BBB to inflammatory mediators present in the PRBC-HBEC coculture supernatant caused activation of astrocytes leading to an increased expression and cleavage of sICAM-1. Studies by Lyons and Benveniste (1998), showed that ICAM-1 was cleaved from astrocyte surface and released into the cell culture supernatant following treatment of astrocytes with TNF α for 21 hours (Lyons and Benveniste, 1998). ICAM-1 expression on astrocytes has been observed in some neurological disorders. High levels of sICAM-1 were observed in the serum of CM patients (Adukpo *et al.*, 2013). In TBI, elevated sICAM-1 levels were observed in the CSF of patients with severe BBB damage whereas there was no increase in sICAM-1 levels in patients with mild BBB damage (Pleines *et al.*, 1998). Reactive astrocytes

were observed at the periphery of neuritic plaques in the brains of AD patients (Akiyama *et al.*, 1993). In MS where BBB disruption occurs, astrocytes present in MS plaques irregularly expressed ICAM-1 (Sobel *et al.*, 1990). *In vitro*, incubation of murine astrocytes with sICAM-1 resulted in the secretion of the proinflammatory chemokine (macrophage inflammatory protein-2) (Otto *et al.*, 2002). The significant increase in sICAM-1 levels in the astrocyte supernatant from 5 to 48 hours ($p < 0.05$) suggests a higher inflammatory response occurs the longer the BBB is exposed to inflammatory mediators and this can eventually be detrimental to neurons. This could explain why survivors of CM are left with long term neurological deficits.

Previously in chapter 4, treatment of the HBEC-alone BBB with PRBC-HBEC lysates caused a trend towards an increase in BBB permeability. In this study we wanted to see if these lysates would cause any changes to astrocytes in the HBEC-astrocyte BBB by examining GFAP and ADAMTS-4 expression.

Western blot analysis showed the presence of 2 bands (between 38-50kDa) in the luminal supernatants whereas only one GFAP band was present in the basolateral supernatant (Figure 5.10A). GFAP bands observed in the luminal supernatants suggest that astrocytes on the basolateral side of the transwell crossed the permeable membrane separating the HBEC and astrocyte on the transwell (Figure 5.10A). These results were consistent with data from Takeshita *et al.* (2014) which showed that human astrocytes *in vitro* crossed the transwell membrane to the luminal side and were in close proximity with BBB-EC (Takeshita *et al.*, 2014). These results indicated that our HBEC-astrocyte BBB model allows endothelial cells and astrocytes to position themselves in close proximity around each other to facilitate communication with each other, as is the case within the NVU *in vivo*.

Endothelial cell-derived proteases such as calpain produced by HBEC in the BBB or HBEC lysates (from coculture experiments) could have caused breakdown of GFAP in astrocytes found on the luminal side of the HBEC-astrocyte BBB into bands between 38-50kDa.

GFAP is susceptible to calpain-mediated induced proteolysis resulting in breakdown products between 38-44kDa (Yang and Wang, 2015). Calpain was shown to be upregulated in endothelial cells of the brain cortex after traumatic brain injury in humans (Alluri *et al.*, 2016; Bralic and Stemberga, 2012). Proteolytic fragments of GFAP between 38-50kDa can be found in the CSF of traumatic brain injury patients (Zhang *et al.*, 2014).

Increased exposure of the HBEC-astrocyte BBB to PRBC HBEC lysate possibly caused damage to astrocytes causing an increased release of GFAP into the basolateral supernatant.

The presence of only one band of GFAP in the basolateral supernatant, suggests that GFAP had not undergone proteolytic cleavage such as the astrocytes in the luminal side of the BBB and were not in contact with calpain produced by HBEC (Figure 5.10A).

Direct exposure of astrocytes to different stimuli may cause damage to astrocytes, resulting in the release of GFAP breakdown products of different sizes. This was observed in this study where direct exposure of astrocytes to inflammatory mediators present in the coculture supernatants and to IL-1 β produced GFAP bands between 45-60kDa and GFAP BDP between 38-50kDa respectively (Figure 3.19 and Figure 5.3).

Western blot analysis showed 2 bands of ADAMTS-4 at 100kDa and 47kDa (Figure 5.11 A, Figure 12A). The 100kDa proform of ADAMTS-4 is converted by a furin-like protease to the inactive form of 75kDa which is associated with the ECM in cells (Gao *et al.*, 2002; Hashimoto *et al.*, 2004). The 75kDa form is further processed in the ECM to produce the 60kDa and 50kDa forms that are released into the culture medium (Gao *et al.*, 2002; Hashimoto *et al.*, 2004). Elevated levels of the 47kDa ADAMTS-4 form was shown to increase following

treatment of cartilage with IL-1 α and it was suggested that this form had strong aggrecanase activity (Kashiwagi *et al.*, 2004). More of the 100kDA proform of ADAMTS-4 was expressed in the luminal supernatant compared to the basolateral supernatant from the HBEC-astrocyte BBB treated with the PRBC-HBEC lysate (Figure 5.11A, Figure 5.12A). This suggested that more of the 47kDA active form of ADAMTS-4 was being produced in the basolateral side.

Increased activation of astrocytes in the HBEC-astrocyte BBB could have resulted in astrogliosis causing astrocytes to produce an increase in the chondroitin sulphate proteoglycans (CSPG) that prevent neurite growth (Cross *et al.*, 2006). An increased production of active ADAMTS-4 by astrocytes would have resulted in the breakdown of CSPG acting as a neurorepair mechanism.

Differential expression of GFAP, ICAM-1 and ADAMTS-4 observed in this study could represent the broad spectrum of changes that occur during astrogliosis in cerebral malaria.

It could be that where moderate astrogliosis occurs, an increase in GFAP or ICAM-1 expression can be observed in the astrocytes. However, in cases where a more severe astrogliosis occurs then increased ICAM-1 or GFAP is released from astrocytes into the culture supernatants. Mild to moderate astrogliosis can result in repair of tissues (Sofroniew, 2015, 2009). Increased levels of ADAMTS-4 can be a neurorepair mechanism and this could be why some survivors of cerebral malaria are not left with long-term neurological sequelae. However, mild to moderate astrogliosis can also result in abnormal astrogliosis and eventually result in neurological dysfunction and this could be responsible for the neurological sequelae observed in some survivors of cerebral malaria (Hunt *et al.*, 2006). Nonetheless, variations between samples were observed in this study. GFAP and ADAMTS-4 levels in the astrocyte supernatant following treatment of the HBEC-astrocyte BBB with PRBC-HBEC coculture supernatants were more variable than ICAM-1. In the case of ICAM-1, 5 out of 8 samples showed an increase in

sICAM-1 levels after treatment of the HBEC-astrocyte BBB with PRBC-HBEC coculture supernatants.

In conclusion, we have demonstrated that inflammatory mediators present in the PRBC-HBEC coculture supernatant can result in an increased release of ICAM-1, suggesting activation of astrocytes in the HBEC-astrocyte BBB. Astrocyte activation during cerebral malaria may be both beneficial and detrimental to the brain depending on the degree of astrogliosis.

This is the first-time astrocyte activation in cerebral malaria has been investigated using an *in vitro* HBEC-astrocyte BBB model.

**Chapter 6 : Effect of serum from malaria patients on
BBB permeability *in vitro***

6.1 Introduction

Clinical *Plasmodium falciparum* malaria presents either as uncomplicated malaria, severe malaria or cerebral malaria (CM). Although the pathogenesis of cerebral malaria has been extensively investigated, the exact cause of this disease is yet to be determined. Sequestration of PRBC to the BBB, secretion of cytokines and chemokines, BBB breakdown have all been suggested to contribute to CM pathogenesis. During CM, sequestration of PRBC to endothelial cells is believed to cause activation of the endothelium.

Proinflammatory cytokines such as TNF- α , IFN- γ , IL-6, IL-1, IL-4 and IL-8 were significantly elevated in the serum of patients with CM compared to patients with severe and uncomplicated malaria, (Mandala *et al.*, 2017). These cytokines were also shown to cause disruption of the endothelial cell (EC)-BBB *in vitro* (de Vries *et al.*, 1996; Yu *et al.*, 2013).

Chemokines such as MCP-1 were found in the serum of malaria patients and were shown to reduce TEER and increase permeability of mouse brain endothelial cells *in vitro* (Stamatovic *et al.*, 2005; Yao and Tsirka, 2014).

Although inflammatory mediators have been shown to be present in the serum of malaria patients in different studies, there is no existing study to date showing the effect of these mediators on BBB integrity during cerebral malaria.

Results from previous studies (Chapter 4) showed that inflammatory mediators produced in response to sequestration of PRBC to endothelial cells caused a statistically significant increase in the HBEC-alone BBB permeability. In this study we set out to investigate the effect of inflammatory mediators present in the serum of malaria patients on the integrity of the HBEC-alone BBB.

6.2 Methods

6.2.1 Serum from malaria patients

Serum samples were obtained from children as part of an ongoing study by Professor Ben Gyan at the Noguchi Memorial Institute for Medical Research (NMIMR), Ghana. Written informed consent was obtained from parents/guardians of the children in Ghana by Professor Gyan. All consent forms are retained by Professor Gyan. Ethical approval for these samples was obtained from the Institute Review Board of the NMIMR and the Ghana Health Service Ethical Committee. The serum samples were provided as anonymised serum samples via a Material Transfer Agreement between NMIMR and Keele University, UK (appendix 7) which was approved by the Keele University Ethical Review Panel on 5th April 2017, for this pilot study. Serum samples used in this study were frozen archived samples and transported from NMIMR to Keele University using approved carrier services. Serum samples were stored at -20°C in the Human Tissue Act (HTA) approved freezer HTA-25 in room156B of the Huxley Building, Keele University. Once thawed for use in an experiment, the samples were aliquoted into eppendorf tubes at smaller volumes of 20µl (to avoid repeated freeze/thaw cycles). These aliquots were also stored at -20°C in the Human Tissue Act (HTA) approved freezer HTA-25 in room156B of the Huxley Building, Keele University.

Patient samples were grouped in the following categories; patients with complicated malaria, severe malaria, cerebral malaria and healthy controls. All malaria patients had asexual blood parasitaemia ranging between 32-212880 parasite density/µl on admission. Body temperature of the patients were taken at time of admission and ranged from 37°C to 40°C. 3 different patient serum samples from the 4 different cohorts were analysed in this pilot study.

6.2.2 FITC dextran permeability assay

The *in vitro* HBEC-alone BBB was used to investigate the effect of malaria serum samples and healthy control serum samples on BBB permeability using the FITC dextran permeability assay, described in Chapter 4, section 4.2.3. The HBEC-alone BBB was set up as in Chapter 3, section 3.2.7.

HBEC was treated with a 1 in 10 dilution of serum samples from healthy control, uncomplicated malaria, severe malaria and cerebral malaria patients (Table 6.1) as described in Chapter 4, section 4.2.3 and a FITC dextran permeability assay was performed as in Chapter 4, section 4.2.3 (Figure 6.1).

Table 6.1 Summary of patient serum used in the treatment of the HBEC-alone BBB model

Treatment	Temperature (°C)	Parasitaemia (density/ μ l)
Healthy Control	36°C-37°C	0
Uncomplicated malaria	40°C	3120-59000
Severe malaria	37°C-40°C	2240-212880
Cerebral malaria	37°C-38°C	32-82000

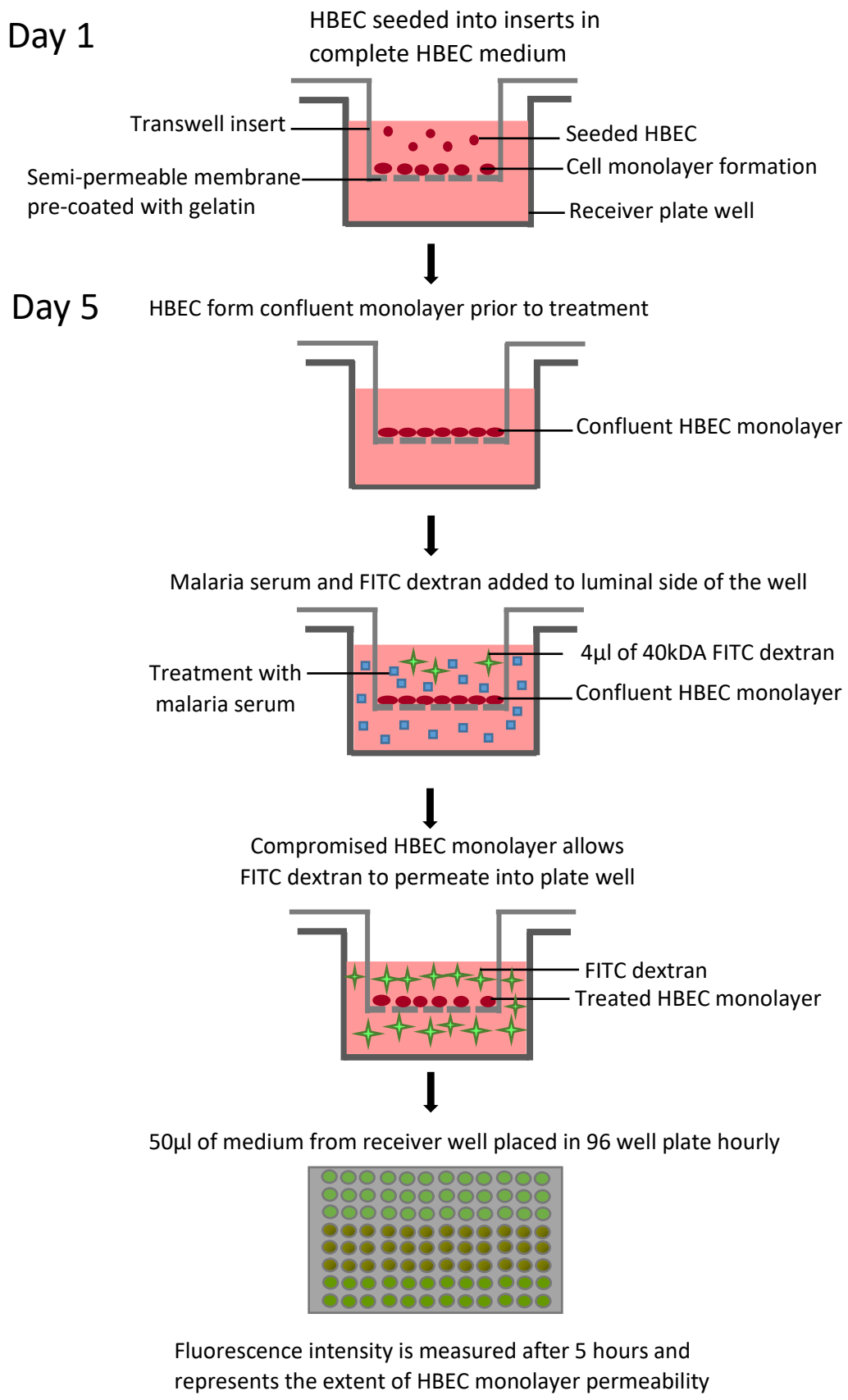


Figure 6.1 Schematic showing FITC dextran permeability assay of HBEC-alone BBB treated with serum from malaria patients.

6.2.3 Statistical analysis

Results from FITC dextran permeability assay were normalised against the healthy controls.

FITC dextran permeability assay was analysed as in Chapter 4, section 4.2.1.1.

A 2-way ANOVA was used to analyse the effect of the different serum samples on HBEC-alone BBB permeability over 5 hours.

6.3 Results

6.3.1 Effect of serum from malaria patients on HBEC-alone BBB permeability

FITC dextran permeability assays were performed to determine the effect of serum from malaria patients on HBEC-alone BBB integrity. 3 different patient serum samples from the 4 different cohorts were analysed in this study. All the serum from malaria samples caused an increase in HBEC-alone BBB permeability from 1 to 3 hours compared to the control serum from healthy patients (Figure 6.2). After 3 hours, variable effects on the HBEC-alone BBB permeability was observed (Figure 6.2). Serum from CM patients caused a further marked increase in HBEC-alone BBB permeability whereas serum from severe malaria and uncomplicated malaria patients produced only small fluctuations with permeability decreasing by 5 hours (Figure 6.2). Overall, serum from CM patients caused a bigger increase in HBEC-alone BBB permeability compared to serum from severe and uncomplicated malaria patients (Figure 6.2).

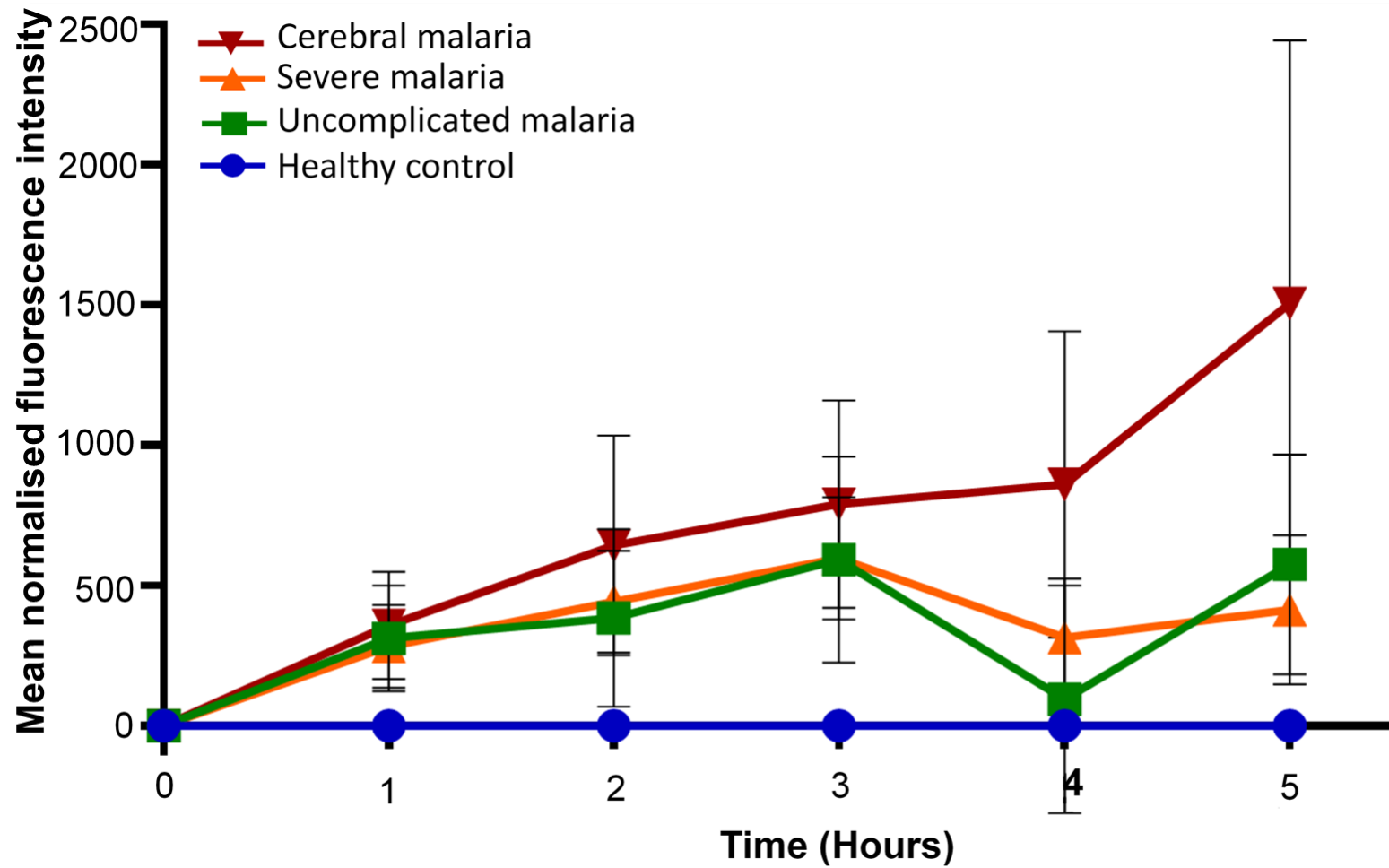


Figure 6.2 Effect of serum from malaria patients on HBEC-alone BBB permeability. A trend towards an increase in BBB permeability was observed in the HBEC monolayer treated with serum from malaria patients as compared to serum from healthy patients. N=3 Error bars \pm 1 SEM.

6.4 Discussion

This the first study in malaria research where the effect of serum from malaria patients on HBEC-alone BBB permeability has been investigated. Results showed that all serum samples from malaria patients caused an increase in HBEC-alone BBB permeability (Figure 6.2). Serum from CM patients produced the biggest increase in HBEC-alone BBB permeability.

Although the serum samples from malaria patients used in this study were diluted, they still had a pronounced effect on HBEC-alone BBB permeability. Thus, if the HBEC-alone BBB was treated with neat serum samples from malaria patients, a bigger increase in BBB permeability may have been observed. Our results suggest that factors present in the serum of malaria patients could be causing the HBEC-alone BBB disruption we observed.

Several factors such as inflammatory mediators, chemokines, angiogenic factors, metalloproteases and parasite derived factors have been found in the serum of malaria patients and can contribute to BBB disruption (Armah *et al.*, 2005).

Proinflammatory mediators such as TNF α , IFN γ , IL-6, IL-1 were significantly higher in the serum of CM patients, moderately elevated in severe malaria and marginally but significantly raised in serum of patients with uncomplicated malaria (Mandala *et al.*, 2017). IL-4 and IL-8 levels were considerably elevated in serum of CM patients compared to serum from severe and uncomplicated malaria patients (Mandala *et al.*, 2017). These inflammatory mediators have previously been shown to cause BBB disruption and an increase in BBB permeability *in vitro*. Indeed, a reduction in EC-BBB *in vitro* was observed following treatment of rat cerebral endothelial cells with IL-6, TNF α and IL-1 (de Vries *et al.*, 1996). Similarly, treatment of HUVEC with IL-8 caused an increase in EC-BBB permeability and a reduction in tight junction proteins occludin, ZO-1 and Claudin-5 (Yu *et al.*, 2013). The chemokine MCP-1 has also been observed in the serum of malaria patients. MCP-1 caused a redistribution of tight junction

proteins ZO-1 and occludin and caused an increase in permeability of mouse brain endothelial cells *in vitro* (Stamatovic *et al.*, 2005; Yao *et al.*, 2014). It is possible that the inflammatory mediators and chemokines discussed above could be present in the serum of malaria patient samples used and could be responsible for the increase in HBEC-alone BBB permeability observed.

Angiogenic factors, Angiopoietin (ANGPT) and Vascular endothelial growth factor (VEGF) that have been found in the serum and plasma of malaria patients could also be present in the serum of malaria patients used in this study. Angiopoietin-1 (ANGPT-1) is found in endothelial cells under basal conditions and preserve vascular quiescence (Lovegrove *et al.*, 2009). This function is interrupted by ANGPT-2 which enhances endothelial cell permeability (Lovegrove *et al.*, 2009). An increase in ANGPT-2 is linked with an increase in vascular permeability (Lovegrove *et al.*, 2009). Serum levels of ANGPT-1 were significantly reduced whereas ANGPT-2 levels were significantly upregulated in CM patients compared to uncomplicated malaria patients (Lovegrove *et al.*, 2009). Vascular endothelial cell growth factor (VEGF) induces proliferation of endothelial cells and microvascular permeability (Furuta *et al.*, 2010). Raised levels of VEGF were observed in the plasma of patients with uncomplicated malaria compared with healthy controls (Furuta *et al.*, 2010). Thus, it is possible that VEGF and increased levels of ANGPT-2 were present in the serum of malaria patients used in this study and may have contributed to the increase in BBB permeability observed.

Matrix metalloproteases (MMPs) are proteolytic enzymes that can degrade tight junction proteins, extracellular matrix (ECM) proteins and cleave proinflammatory cytokines and thus if these proteases were present in the serum of malaria patients used in this study, they could have caused breakdown of the HBEC-alone BBB resulting in an increase BBB permeability.

Indeed, MMP-9, MMP-8 and tissue inhibitors of matrix metalloproteinases (TIMP)-1, have been observed in the serum of malaria patients (Dietmann *et al.*, 2008; Polimeni *et al.*, 2014). MMP-8 and TIMP-1 levels in the serum from severe malaria patients were higher than that of uncomplicated malaria patients (Dietmann *et al.*, 2008).

When testing serum of malaria patients, parasite derived factors need to also be considered. Parasite derived factors such as glycosylphosphatidylinositol (GPI) and histidine-rich protein 2 (HRP2) released through rupture of PRBC during the intraerythrocytic life cycle of malaria, can be found in the serum of malaria patients and have been shown to cause an increase in EC-BBB permeability *in vitro* (Coronado *et al.*, 2014; Pal *et al.*, 2016). *In vitro* studies have implicated a role of HRP2 in BBB disruption during CM. Pal *et al.* (2016) showed a time dependent reduction in TEER occurred following addition of PRBC to HBEC *in vitro* (Pal *et al.*, 2016). Interestingly, only a small change in BBB disruption was observed when a PRBC clone that contained a deletion of the HRP2 was added to HBEC *in vitro* (Pal *et al.*, 2016). Also, immunohistochemical analysis showed HRP2 caused rearrangement of tight junction proteins Claudin-5 and adherens junction proteins VE-cadherin in HBEC *in vitro* (Pal *et al.*, 2016).

Purified *Plasmodium falciparum*-GPI was shown to cause a reduction in TEER of human dermal microvascular endothelial cells *in vitro* (Gillrie *et al.*, 2007). Thus, if the parasite derived factors HRP2 and GPI were present in the serum of malaria patients tested in this study, they could have contributed to the disruption in HBEC-alone BBB integrity observed.

Higher levels of proinflammatory cytokines such as TNF α , IFN γ , IL-6, IL-1 were observed in the serum of CM patients compared to severe and uncomplicated malaria patients. These cytokines were previously shown to cause BBB disruption *in vitro*. It is possible that higher

levels of proinflammatory cytokines in the serum of cerebral malaria patients used in this study may have caused a bigger increase in HBEC-alone BBB permeability than that of serum from severe and uncomplicated malaria patients. Also, factors present in the serum of CM patients but absent in the serum of uncomplicated and severe malaria patients could be the reason HBEC-alone BBB permeability was higher in CM patients than serum from other malaria patients. Although the increase in HBEC-alone BBB permeability caused by serum from malaria samples were consistent in all studies, only 3 malaria serum samples from each cohort that is cerebral, severe and uncomplicated malaria and healthy patients were tested. Thus, we must be cautious in interpreting results observed in this study and a bigger cohort study using more serum samples from malaria patients needs to be performed to verify the results obtained in this study. It will be interesting to investigate what factors are present in the serum of malaria patients used in this study by proteomics. After identification of these proteins, the exact roles of these factors in BBB disruption will be further investigated.

The bigger increase in BBB permeability induced by the serum from malaria patients compared to PRBC-HBEC coculture supernatants was not surprising, considering serum has a larger range of soluble factors such as angiogenic factors, proinflammatory cytokines, proteases, parasite derived factors that have the potential to cause increased permeability of the endothelial cell monolayer. However, the PRBC-HBEC coculture supernatants only represented inflammatory mediators released from endothelial cells in response to direct contact with PRBC.

The next phase in this study will be to investigate the effect of serum from malaria patients on HBEC-astrocyte BBB permeability and components of the HBEC-astrocyte BBB such as endothelial cells and astrocytes. This will provide a better understanding on the effect of

mediators released during cerebral malaria on the different components of the NVU such as astrocytes. Since astrocytes are found on the basolateral side of the BBB, understanding what happens to astrocytes during cerebral malaria could give an improved comprehension on how activation of astrocytes might affect neurons and could contribute to neurological damage observed in CM survivors.

Chapter 7 : Final discussion

7.1 General discussion

In this study we used the HBEC-alone BBB and our newly developed BBB model composed of HBEC and astrocytes grown in tandem to better understand the CM pathogenesis. Previous studies in our laboratory studied the effect of inflammatory mediators released in response to sequestration of PRBC to the BBB during CM using an *in vitro* HBEC-alone BBB model. However, using the HBEC monolayer as a model for CM *in vitro* did not fully depict the effect of sequestration of PRBC on the other components of the BBB such as endothelial cells and astrocytes, that are involved in the development and maintenance of a functional BBB.

The HBEC-astrocyte BBB mimicked the BBB *in vivo* closer than the HBEC-alone BBB. The close proximity of HBEC on the luminal side and astrocytes on the basolateral side of the transwell allowed communication between the two cell types. Detection of GFAP in the luminal side of the transwell suggested that astrocytes end feet had crossed the membrane and was communicating with endothelial cells. The HBEC-astrocyte BBB formed a tighter BBB as indicated by the significantly higher TEER than the HBEC-alone BBB (Chapter 3). Astrocytes secrete soluble factors such as the vascular endothelial growth factor (VEGF), basic fibroblast growth factor (bFGF), transforming growth factor (TGF)- β , glial derived neurotrophic factor (GDNF), ANGPT-1, Sonic Hedgehog (member of the hedgehog family) that are essential for the formation of tight junction proteins and maintenance of the BBB (Alvarez *et al.*, 2013; Cheslow *et al.*, 2016). Endothelial cells also secrete leukemia inhibitor factor, platelet derived growth factor (PDGF) and basic fibroblast growth factor and these have been shown to enhance development of astrocyte processes *in vitro* (Cheslow *et al.*, 2016; Levy *et al.*, 2014). Crosstalk between these two cells allow for the formation of a functional BBB. Release of these factors by the endothelial cells and astrocytes could have caused an increase

in tight junction formation in the HBEC-astrocyte BBB resulting in the higher TEER than the HBEC-alone BBB.

Inflammatory mediators released in response to sequestration of PRBC to BBB were previously shown to cause a significant increase in the HBEC-alone BBB permeability. Treatment of the HBEC-astrocyte BBB with these inflammatory mediators caused no change in BBB permeability (Chapter 4). This suggested that the HBEC-astrocyte BBB was more resilient to inflammatory mediators present in the PRBC-HBEC coculture supernatants than the HBEC-alone BBB.

Astrocytes are known to release factors such as SHH, retinoic acid (RA) and ANGPT-1 in response to BBB injury (Cheslow *et al.*, 2016). Apart from increasing the expression of junctional proteins in endothelial cells, SHH can reduce the secretion of MCP-1 and stop pro-inflammatory immune cells from entering the BBB (Cheslow *et al.*, 2016). RA also increases the expression of junctional proteins VE-cadherin, ZO-1 of endothelial cells and decreases binding of monocytes to endothelial cells (Cheslow *et al.*, 2016). ANGPT-1 enhances tight junction formation (Cheslow *et al.*, 2016). If these factors were released by the astrocytes in the HBEC-astrocyte BBB in response to inflammatory mediators present in the PRBC-HBEC coculture supernatant they could have provided a neuroprotective mechanism protecting BBB breakdown. It is possible exposure of the HBEC-astrocyte BBB to the PRBC-HBEC coculture supernatants for longer than 5 hours may cause an increase in BBB permeability. Prolonged exposure of the HBEC-astrocyte BBB to inflammatory mediators in the PRBC-HBEC coculture supernatant may cause astrocytes to release proinflammatory cytokines such as IL-1 β , VEGF that can cause BBB disruption and an increase in BBB permeability (Cheslow *et al.*, 2016).

We examined the effect of inflammatory mediators released in response to sequestration of PRBC to HBEC, on astrocytes alone and also on the HBEC-astrocyte BBB.

Inflammatory mediators present in the PRBC-HBEC coculture supernatants caused activation of astrocytes resulting in the release of GFAP breakdown products from 38-50kDA (Chapter 5). These results were comparable to traumatic brain injury (TBI) studies where GFAP breakdown products between 38-50kDA were observed in the CSF (Zhang *et al.*, 2014). These results indicated that direct exposure of astrocytes to inflammatory mediators such as TNF α , IL-1 β and MCP-1 could have caused damage to astrocytes.

Short term exposure in the HBEC-astrocyte BBB to inflammatory mediators in the PRBC-HBEC coculture supernatant caused no change in GFAP expression in astrocytes (Chapter 5). This suggested that astrocytes induced neuroprotective response by releasing factors such as SHH, ANGPT-1, RA known to reduce proinflammatory cytokines. Interestingly, longer exposure of the HBEC-astrocyte BBB to inflammatory mediators present in the PRBC-HBEC coculture supernatant for 48 hours caused damage to astrocytes and an increased release of GFAP (Chapter 5). This indicates that GFAP in astrocytes were susceptible to degradation by inflammatory mediators.

Increased exposure of the HBEC-astrocyte BBB to inflammatory mediators present in the PRBC-HBEC coculture supernatant caused overactivation of astrocytes and increased shedding of ICAM-1 from astrocytes (Chapter 5). Activation of ICAM-1 has been found in astrocytes in diseases like AD and MS (Lee *et al.*, 2000). sICAM-1 is produced through proteolytic cleavage of membrane bound ICAM-1. MMP-9 was shown to cleave ICAM-1 from human saphenous vein endothelial cells *in vitro* (Sultan *et al.*, 2004). This protease produced by astrocytes could be responsible for cleaving sICAM-1 into the astrocyte supernatant from the

HBEC-astrocyte BBB. High sICAM-1 levels are associated with CM; thus, our results suggest continuing immunological activation occurs in the brain during CM.

Activation of astrocytes can result in reactive astrogliosis and the formation of glial scar which is composed of chondroitin sulphate proteoglycans (CSPG) (Sofroniew, 2015). Formation of the glial scar can have detrimental consequences, preventing neurite regeneration (Gottschall *et al.*, 2015; Tauchi *et al.*, 2012). ADAMTS-4 was shown to cleave proteins of CSPG known to be elevated following SCI (Gottschall *et al.*, 2015; Tauchi *et al.*, 2012). Addition of ADAMTS-4 after spinal cord injury into the rat spinal cord, reversed neurite outgrowth and stimulated motor functional recovery (Gottschall *et al.*, 2015; Tauchi *et al.*, 2012). Thus, in this study it is possible that increased ADAMTS-4 levels produced by activated astrocytes in the HBEC-astrocyte BBB in response to inflammatory mediators produced in response to sequestration of PRBC (Chapter 5), was causing cleavage of CSPG proteins in the glial scar and enhancing neurorepair.

A broad spectrum of changes occur during astrogliosis in CM. Post-mortem brain tissues of Malawian patients showed mild to moderate astrogliosis (Dorovini-Zis *et al.*, 2011). Our results could represent moderate astrogliosis where the astrocytes are damaged and release GFAP and ICAM-1 into the supernatant after treatment of the HBEC-astrocyte BBB with the PRBC-HBEC coculture supernatant, although there were variations between samples. Moderate astrogliosis can progress to severe astrogliosis which is irreversible and can result in neurological dysfunction observed in some CM survivors (Hunt *et al.*, 2006). Mild to moderate astrogliosis could also be represented by the increase in ADAMTS-4 levels produced as a neurorepair mechanism following astrocyte activation, although there were considerable variations between the samples. This could be the reason some survivors of CM are left with no neurological sequelae. Astrocytes are known to uptake glutamate in the brain and protect

neurons that are vulnerable to glutamate excitotoxicity (Becerra-Calixto and Cardona-Gómez, 2017; Bush *et al.*, 1999). If astrocytes are injured during cerebral malaria, the detrimental accumulation of glutamate can occur in the brain resulting in neuronal damage and may lead to neuronal damage in CM survivors.

Increased levels of proinflammatory mediators in the serum of malaria patients are associated with disease severity during malaria. In this study we showed that serum from malaria patients caused an increase in HBEC-alone BBB permeability as described earlier (Chapter 6). Factors present in the malaria serum such as proinflammatory cytokines, angiogenic factors, matrix metalloproteases (MMP) that were low in the serum from healthy controls could be responsible for this permeability change. TNF- α , IFN- γ , IL-6, IL-1, IL-4, IL-8, MCP-1, ANGPT-1, ANGPT-2, VEGF, MMP-8, MMP-9 have been shown to cause BBB disruption and an increase in BBB permeability *in vitro* (de Vries *et al.*, 1996; Dietmann *et al.*, 2008; Furuta *et al.*, 2010; Lovegrove *et al.*, 2009). Higher levels of inflammatory mediators present in the serum from CM patients could have caused the bigger increase in HBEC-alone BBB permeability observed. This is the first study to investigate the effect of serum from malaria patients on BBB integrity *in vitro*. Thus, it will be interesting to further investigate the effect of serum from malaria patients on the HBEC-astrocyte BBB model.

Conclusion

We have successfully developed *in vitro* HBEC-alone BBB and HBEC-astrocyte BBB models that can be used to investigate mechanisms and processes involved in BBB disruption during cerebral malaria. Our studies suggest inflammatory mediators released in response to sequestration of PRBC to BBB can cause disruption of endothelial cells. Activated and damaged endothelial cells send signals to astrocytes and this can cause astrocyte activation.

Activated astrocytes release GFAP, sICAM-1, ADAMTS-4 in the brain. sICAM-1 can activate microglia the immune cells of the brain. sICAM-1 can also bind to the LFA-1 receptor on microglia activating it. Overactivation of microglia can result in the production of TNF α , reactive oxygen species (ROS) that can cause direct damage to neurons and even loss of neurons. Also, activated astrocyte can release proinflammatory cytokines such as nitric oxide (NO), TNF α , that can directly damage neurons, and this may lead to neurological sequelae in some CM patients. Based on the data in these studies, mechanisms involved in CM pathogenesis can be speculated as shown in Figure 7.1.

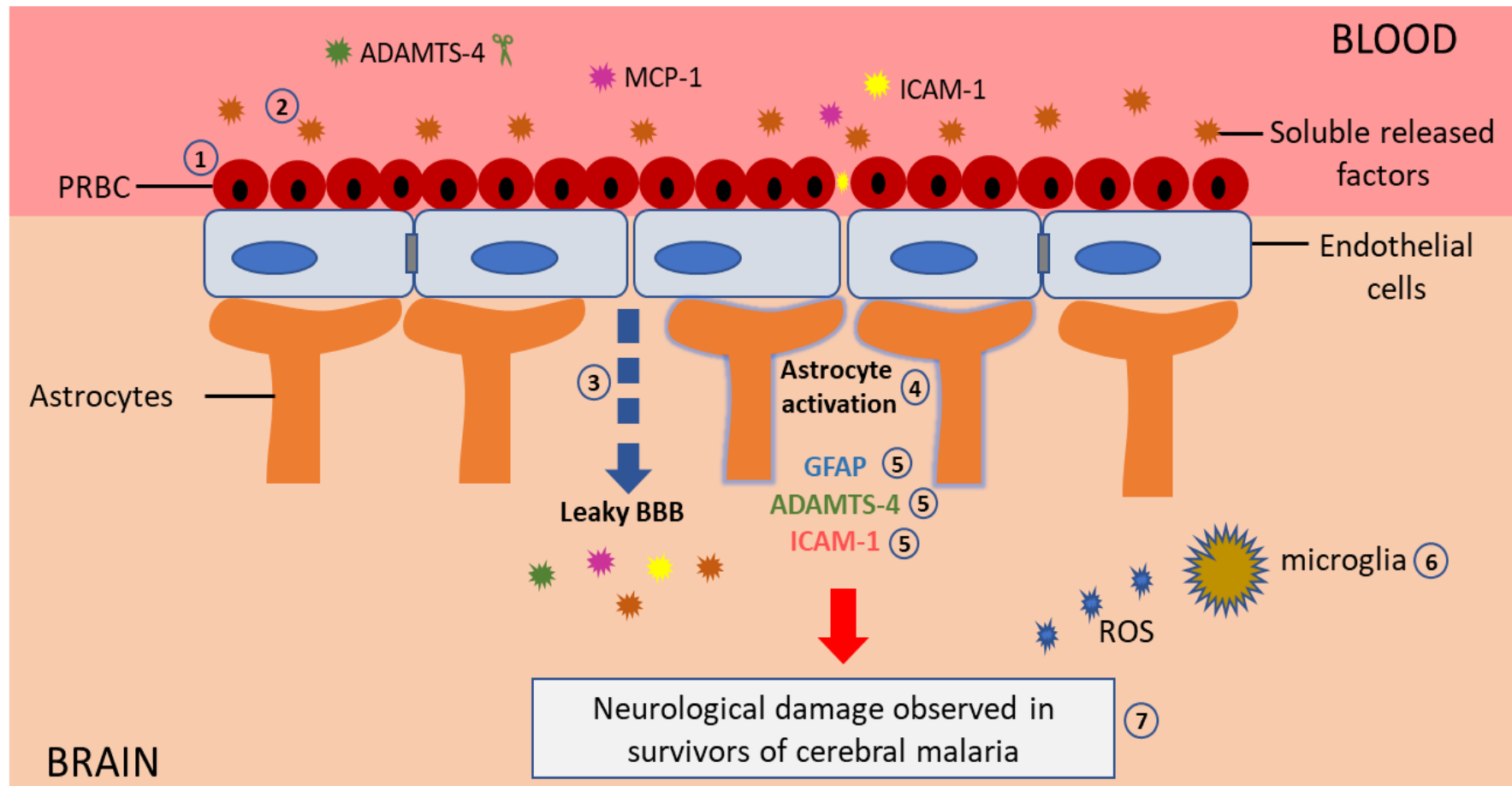


Figure 7.1 The proposed effect of sequestration of PRBC to the BBB during cerebral malaria. During cerebral malaria PRBC sequester to endothelial cells of the BBB (2) resulting in the activation of endothelial and the release of endothelial cell derived factors such as ADAMTS-4, ICAM-1 and MCP-1. (3) These factors may cause activation of endothelial cells. Endothelial cells can send signals to (4) activate astrocytes resulting in the release of (5) GFAP, cleavage of (5) ADAMTS-4 and (5) ICAM-1 from astrocytes. Astrocyte activation and astrocyte damage could eventually lead to (6) activation of microglia. Activated microglia can release reactive oxygen species that can cause damage to neurons and this can lead to (7) neurological damage in some survivors of cerebral malaria.

7.2 Limitations and Future studies

Although this thesis showed the effect of inflammatory mediators released in response to sequestration of PRBC to BBB during CM on the HBEC-alone BBB and the HBEC-astrocyte BBB, there are limitations in this study that need to be addressed in future experiments.

Despite the fact that the HBEC-astrocyte BBB better mirrors the anatomical structure of the BBB *in vivo* than the HBEC-alone BBB, this model lacks physiological shear stress which is vital for differentiation of endothelial cells and maintenance of the BBB. The use of a more dynamic *in vitro* BBB can overcome these limitations. Dynamic BBB models exist for studying interactions between PRBC and endothelial cells. In these models brains endothelial cells are grown under flow-based conditions to mimic blood flow in the microvascular environment *in vivo* (Cooke *et al.*, 2002; Gray *et al.*, 2003; Phiri *et al.*, 2009). The introduction of shear stress to *in vitro* BBB models can increase tight and adherens junctions *in vitro* (Cucullo *et al.*, 2011, 2008) and provides a more accurate picture of what occurs during sequestration in cerebral malaria. To better understand what happens to astrocytes that sit at the basolateral side of the BBB during CM, a more advanced BBB model where HBEC-astrocytes are cocultured on a chip side by side can be used. One of such models is the BBB on a chip model where endothelial cells are grown in a vascular channel, while astrocytes are grown in the tissue compartment (Figure 7.2) (Deosarkar *et al.*, 2015). An interface along the vascular channels allows the tissue compartment and vascular channels to communicate (Deosarkar *et al.*, 2015). The vascular channels are 3 dimensional in geometry and this allows shear force and flow patterns similar to the BBB *in vivo* (Deosarkar *et al.*, 2015) (Figure 7.2). This model will be ideal for studying the effect of sequestration of PRBC on the BBB. Inflammatory mediators released in response to sequestration of PRBC can be injected into the vascular channels on endothelial cells, while astrocytes sit in the tissue compartment. Subsequently, the supernatants and lysates of HBEC

and astrocytes can then be harvested from the chip set up and their response to sequestration of PRBC examined. This will give a better understanding of endothelial and astrocyte activation during cerebral malaria and might shed light on the processes involved in neurological damage observed in CM survivors.

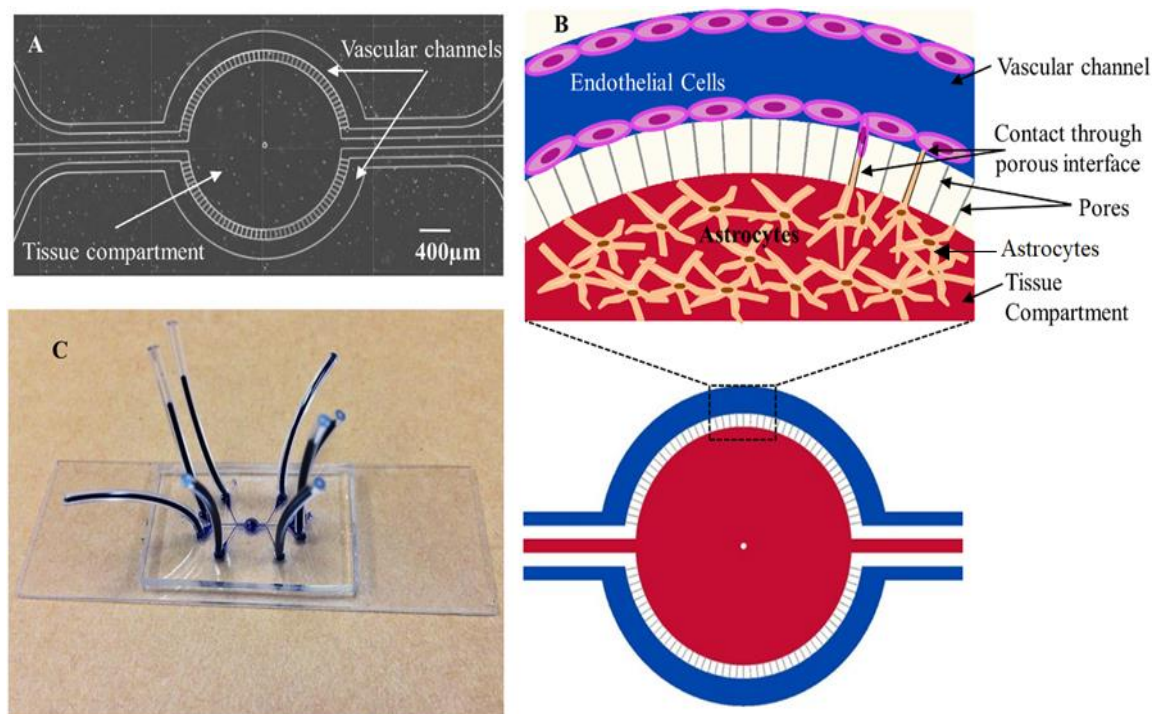


Figure 7.2 BBB on-chip model (A) Illustration of the B³C made up of the tissue compartment in the middle of the device with two vascular channels with flow access openings. (B) Schematic of cell culture of endothelial cells in the vascular channel with astrocytes in the tissue compartment. (C) Device assembled on a microscope glass slide with plastic tubes (dark blue) allowing access to vascular channels and tissue compartment. Image and legend obtained from (Deosarkar *et al.*, 2015).

Future studies will be to identify if specific inflammatory mediators such as IL-8, MCP-1, MMP-8, MMP-9 are present in the serum of malaria patients analysed in this study using an AimPlex multiplex assay (AimPlex Biosciences, 2017). These proteins have been found in the serum of malaria patients and have been shown to cause BBB disruption *in vitro* (de Vries *et al.*, 1996; Dietmann *et al.*, 2008; Mandala *et al.*, 2017; Nagase *et al.*, 1999; Polimeni *et al.*, 2014; Stamatovic *et al.*, 2005; Yao *et al.*, 2014). In this assay, beads coated with specific capture antibodies will be used to trap proteins of interest (such as IL-8, MCP-1, MMP-8, MMP-9). Biotinylated detection antibodies that are specific to the proteins of interest will

subsequently be added to the assay to form an antigen-antibody sandwich to allow detection of specific proteins present in the sample. If IL-8, MCP-1, MMP-8, MMP-9 are identified in the serum of malaria patients tested, inhibitor assays will be performed where specific inhibitors against these proteins will be added to the *in vitro* BBB treated with serum of malaria patients. If addition of these inhibitors results in a decrease in permeability of EC-BBB treated with malaria serum, it suggests these proteins could be involved in BBB breakdown during CM. These proteins can then be further developed into adjunct therapies. Current malaria therapies just target the *Plasmodium falciparum* parasite and thus there is a need to develop adjunct therapies that can be used in combination with antimalarial drugs to prevent BBB disruption, address the inflammatory response produced in CM and reduce the neurological sequelae observed in survivors of CM.

The HBEC-astrocyte BBB used in this study just addressed 2 components of the BBB, astrocytes and endothelial cells but the BBB is part of a neurovascular unit composed of pericytes, endothelial cells, astrocytes and neurons. Thus, it will be ideal to develop a tri cell-culture BBB model made up of neurons, astrocytes and endothelial cells to investigate the effect of sequestration of PRBC on components of the tri cell culture BBB during cerebral malaria. This investigation will shed more light on the effect of astrocyte activation on neuronal dysfunction and how this might be responsible for the neurological sequelae observed in some survivors of CM.

References

- Abbott, Dolman, D.E.M., Yusof, S.R., Begley, D.J., Abbott, N.J., Patabendige, A.A.K., Dolman, D.E.M., Yusof, S.R., Begley, D.J., 2010. Structure and function of the blood–brain barrier. *Neurobiol. Dis.* 37, 13–25.
- Abbott, N.J., 2002. Astrocyte–endothelial interactions and blood–brain barrier permeability. *J. Anat.* 200, 523–534.
- Abbott, N.J., Rönnbäck, L., Hansson, E., 2006. Astrocyte–endothelial interactions at the blood–brain barrier. *Nat. Rev. Neurosci.* 7, 41–53.
- Abbott, N.J., Yusof, S., 2010. Structure and function of the blood-brain barrier. *Front. Pharmacol.* 1.
- Adams, S., Brown, H., Turner, G., 2002. Breaking down the blood-brain barrier: signaling a path to cerebral malaria? *Trends Parasitol.* 18, 360–6.
- Adukpo, S., Kusi, K.A., Ofori, M.F., Tetteh, J.K.A., Amoako-Sakyi, D., Goka, B.Q., Adjei, G.O., Edoh, D.A., Akanmori, B.D., Gyan, B.A., Dodoo, D., 2013. High Plasma Levels of Soluble Intercellular Adhesion Molecule (ICAM)-1 Are Associated with Cerebral Malaria. *PLoS One* 8, e84181.
- Advansta, 2018. Advansta western blot protocol and western blot troubleshooting resources [WWW Document]. URL <https://advansta.com/resources/western-blotting-technical-resources/> (accessed 7.1.18).
- AimPlex Biosciences, 2017. Overview — Aimplex Biosciences, Inc. [WWW Document]. URL <https://www.aimplexbio.com/product-overview/> (accessed 9.24.18).
- Akiyama, H., Kawamata, T., Yamada, T., Tooyama, I., Ishii, T., McGeer, P.L., 1993. Expression of intercellular adhesion molecule (ICAM)-1 by a subset of astrocytes in Alzheimer disease and some other degenerative neurological disorders. *Acta Neuropathol.* 85, 628–34.
- Alluri, H., Grimsley, M., Anasooya Shaji, C., Varghese, K.P., Zhang, S.L., Peddaboina, C., Robinson, B., Beeram, M.R., Huang, J.H., Tharakan, B., 2016. Attenuation of Blood-Brain Barrier Breakdown and Hyperpermeability by Calpain Inhibition. *J. Biol. Chem.* 291, 26958–26969.
- Almelli, T., Ndam, N.T., Ezimegnon, S., Alao, M.J., Ahouansou, C., Sagbo, G., Amoussou, A., Deloron, P., Tahar, R., 2014. Cytoadherence phenotype of *Plasmodium falciparum*-infected erythrocytes is associated with specific pfemp-1 expression in parasites from children with cerebral malaria. *Malar. J.* 13, 333.
- Alvarez, J.I., Dodelet-Devillers, A., Kebir, H., Ifergan, I., Fabre, P.J., Terouz, S., Sabbagh, M., Wosik, K., Bourbonnière, L., Bernard, M., van Horssen, J., de Vries, H.E., Charron, F., Prat, A., 2011. The Hedgehog pathway promotes blood-brain barrier integrity and CNS immune quiescence. *Science* 334, 1727–31.
- Alvarez, J.I., Katayama, T., Prat, A., 2013. Glial Influence on the Blood Brain Barrier. *Glia* 61, 1939–1958.
- Alvarez, J.I., Saint-Laurent, O., Godschalk, A., Terouz, S., Briels, C., Larouche, S., Bourbonnière, L., Larochelle, C., Prat, A., 2015. Focal disturbances in the blood–brain barrier are associated with formation of neuroinflammatory lesions. *Neurobiol. Dis.* 74, 14–24.

- Ampawong, S., Chaisri, U., Viriyavejakul, P., Nontprasert, A., Grau, G.E., Pongponratn, E., 2014. Electron microscopic features of brain edema in rodent cerebral malaria in relation to glial fibrillary acidic protein expression. *Int. J. Clin. Exp. Pathol.* 7, 2056.
- Armah, H., Wiredu, E.K., Dodoo, A.K., Adjei, A.A., Tettey, Y., Gyasi, R., 2005. Cytokines and Adhesion Molecules Expression in the Brain in Human Cerebral Malaria. *Int. J. Environ. Res. Public Heal. Int. J. Environ. Res. Public Heal.* 2, 123–131.
- Armah, H.B., Wilson, N.O., Sarfo, B.Y., Powell, M.D., Bond, V.C., Anderson, W., Adjei, A.A., Gyasi, R.K., Tettey, Y., Wiredu, E.K., Tongren, J.E., Udhayakumar, V., Stiles, J.K., 2007. Cerebrospinal fluid and serum biomarkers of cerebral malaria mortality in Ghanaian children. *Malar. J.* 6.
- Attwell, D., Buchan, A.M., Charpak, S., Lauritzen, M., Macvicar, B.A., Newman, E.A., 2010. Glial and neuronal control of brain blood flow. *Nature* 468, 232–43.
- Baeten, K.M., Akassoglou, K., 2011. Extracellular matrix and matrix receptors in blood-brain barrier formation and stroke. *Dev. Neurobiol.* 71, 1018–39.
- Ballabh, P., Braun, A., Nedergaard, M., 2004. The blood–brain barrier: an overview: Structure, regulation, and clinical implications. *Neurobiol. Dis.* 16, 1–13.
- Baron, S., 1996. *Medical Microbiology*. University of Texas Medical Branch, Department of Microbiology, Galveston (TX).
- Bartoloni, A., Zammarchi, L., 2012. Clinical aspects of uncomplicated and severe malaria. *Mediterr. J. Hematol. Infect. Dis.* 4, e2012026.
- Baruch, D.I., Pasloske, B.L., Singh, H.B., Bi, X., Ma, X.C., Feldman, M., Taraschi, T.F., Howard, R.J., 1995. Cloning the *P. falciparum* gene encoding PfEMP1, a malarial variant antigen and adherence receptor on the surface of parasitized human erythrocytes. *Cell* 82, 77–87.
- Baruch, D.I., Rogerson, S.J., Cooke, B.M., 2002. Asexual blood stages of malaria antigens: cytoadherence. *Chem Immunol* 80, 144–162.
- Bauer, H.-C., Krizbai, I.A., Bauer, H., Traweger, A., 2014. You Shall Not Pass; tight junctions of the blood brain barrier. *Front. Neurosci.* 8, 392.
- Baumann, E., Preston, E., Slinn, J., Stanimirovic, D., 2009. Post-ischemic hypothermia attenuates loss of the vascular basement membrane proteins, agrin and SPARC, and the blood–brain barrier disruption after global cerebral ischemia. *Brain Res.* 1269, 185–197.
- Becerra-Calixto, A., Cardona-Gómez, G.P., 2017. The Role of Astrocytes in Neuroprotection after Brain Stroke: Potential in Cell Therapy. *Front. Mol. Neurosci.* 10, 88.
- Beeson, J.G., Rogerson, S.J., Cooke, B.M., Reeder, J.C., Chai, W., Lawson, A.M., Molyneux, M.E., Brown, G. V., 2000. Adhesion of *Plasmodium falciparum*-infected erythrocytes to hyaluronic acid in placental malaria. *Nat. Med.* 6, 86–90.
- Bengtsson, A., Joergensen, L., Rask, T.S., Olsen, R.W., Andersen, M.A., Turner, L., Theander, T.G., Hviid, L., Higgins, M.K., Craig, A., Brown, A., Jensen, A.T., 2013. A novel domain cassette identifies *Plasmodium falciparum* PfEMP1 proteins binding ICAM-1 and is a target of cross-reactive, adhesion-inhibitory antibodies. *J. Immunol.* 190, 240–249.
- Billig, E.M.W., O'Meara, W.P., Riley, E.M., McKenzie, F.E., 2012. Developmental allometry

- and paediatric malaria. *Malar J.* 11, 64.
- Bio-Rad, 2018. Introduction to Western Blotting Immunoblotting Bio-Rad [WWW Document]. URL <https://www.bio-rad-antibodies.com/western-blotting-immunoblotting-introduction.html> (accessed 7.1.18).
- Birbeck, G.L., Molyneux, M.E., Kaplan, P.W., Seydel, K.B., Chimalizeni, Y.F., Kawaza, K., Taylor, T.E., 2010. Blantyre Malaria Project Epilepsy Study (BMPEs) of neurological outcomes in retinopathy-positive paediatric cerebral malaria survivors: a prospective cohort study. *Lancet Neurol.* 9, 1173–1181.
- Blanchette, M., Daneman, R., 2015. Formation and maintenance of the BBB. *Mech. Dev.* 138, 8–16.
- Brahmachari, S., Fung, Y.K., Pahan, K., 2006. Induction of glial fibrillary acidic protein expression in astrocytes by nitric oxide. *J. Neurosci.* 26, 4930–4939.
- Bralic, M.S. V., Stemberga, V., 2012. Calpain expression in the brain cortex after traumatic brain injury. *Coll. Antropol.* 130, 187–198.
- Brown, H., Hien, T.T., Day, N., Mai, N.T.H., Chuong, L. V., Chau, T.T.H., Loc, P.P., Phu, N.H., Bethell, D., Farrar, J., 1999. Evidence of blood-brain barrier dysfunction in human cerebral malaria. *Neuropathol. Appl. Neurobiol.* 25, 331–340.
- Brown, H., Rogerson, S., Taylor, T., Tembo, M., Mwenechanya, J., Molyneux, M., Turner, G., 2001. Blood-brain barrier function in cerebral malaria in Malawian children. *Am. J. Trop. Med. Hyg.* 64, 207–213.
- Brown, H.C., Chau, T.T., Mai, N.T., Day, N.P., Sinh, D.X., White, N.J., Hien, T.T., Farrar, J., Turner, G.D., 2000. Blood-brain barrier function in cerebral malaria and CNS infections in Vietnam. *Neurology* 55, 104–111.
- Bush, T.G., Puvanachandra, N., Horner, C.H., Polito, A., Ostefeld, T., Svendsen, C.N., Mucke, L., Johnson, M.H., Sofroniew, M. V., 1999. Leukocyte Infiltration, Neuronal Degeneration, and Neurite Outgrowth after Ablation of Scar-Forming, Reactive Astrocytes in Adult Transgenic Mice. *Neuron* 23, 297–308.
- Butt, A.M., Jones, H.C., Abbott, N.J., 1990. Electrical resistance across the blood-brain barrier in anaesthetized rats: a developmental study. *J. Physiol.* 429, 47–62.
- Cabezas, R., Avila, M., Gonzalez, J., El-Bachá, R.S., Báez, E., García-Segura, L.M., Jurado Coronel, J.C., Capani, F., Cardona-Gomez, G.P., Barreto, G.E., 2014. Astrocytic modulation of blood brain barrier: perspectives on Parkinson's disease. *Front. Cell. Neurosci.* 8, 211.
- Cardoso, F.L., Brites, D., Brito, M.A., 2010. Looking at the blood–brain barrier: molecular anatomy and possible investigation approaches. *Brain Res. Rev.* 64, 328–363.
- Chakravorty, S.J., Carret, C., Nash, G.B., Ivens, A., Szeszak, T., Craig, A.G., 2007. Altered phenotype and gene transcription in endothelial cells, induced by *Plasmodium falciparum*-infected red blood cells: pathogenic or protective? *Int. J. Parasitol.* 37, 975–87.
- Chakravorty, S.J., Craig, A., 2005. The role of ICAM-1 in *Plasmodium falciparum* cytoadherence. *Eur. J. Cell Biol.* 84, 15–27.
- Chen, F., Ohashi, N., Li, W., Eckman, C., Nguyen, J.H., 2009. Disruptions of occludin and

- claudin-5 in brain endothelial cells in vitro and in brains of mice with acute liver failure. *Hepatology* 50, 1914–1923.
- Cheslow, L., Alvarez, J.I., 2016. Glial-endothelial crosstalk regulates blood–brain barrier function. *Curr. Opin. Pharmacol.* 26, 39–46.
- Clark, I., Rocket, K., Cowden, W., 1992. Possible Central Role of Nitric Oxide in Conditions Clinically Similar to Cerebral Malaria. *Lancet* 340, 894–896.
- Clark, I.A., Virelizier, J.L., Carswell, E.A., Wood, P.R., 1981. Possible importance of macrophage-derived mediators in acute malaria. *Infect. Immun.* 32, 1058–1066.
- Collins, W.E., Jeffery, G.M., 2007. *Plasmodium malariae*: parasite and disease. *Clin. Microbiol. Rev.* 20, 579–92.
- Combes, V., Guillemin, G.J., Chan-Ling, T., Hunt, N.H., Grau, G.E.R., 2012. The crossroads of neuroinflammation in infectious diseases: endothelial cells and astrocytes. *Trends Parasitol.* 28, 311–319.
- Cooke, B.M., Coppel, R.L., Nash, G.B., 2002. Analysis of the Adhesive Properties of *Plasmodium falciparum*-Infected Red Blood Cells Under Conditions of Flow. In: *Malaria Methods and Protocols*. Humana Press, New Jersey, pp. 561–570.
- Corning Incorporated, 2018. Guidelines for Use: Transwell® Permeable Supports | Life Sciences Corning [WWW Document]. URL <https://www.corning.com/worldwide/en/products/life-sciences/products/permeable-supports/transwell-guidelines.html> (accessed 6.30.18).
- Coronado, L.M., Nadovich, C.T., Spadafora, C., 2014. Malarial hemozoin: from target to tool. *Biochim. Biophys. Acta* 1840, 2032–41.
- Cowman, A.F., Berry, D., Baum, J., 2012. The cellular and molecular basis for malaria parasite invasion of the human red blood cell. *J. Cell Biol.* 198, 961–971.
- Cox, F.E.G., 2010. History of the discovery of the malaria parasites and their vectors. *Parasit Vectors* 3, 5.
- Craig, A.G., Grau, G.E., Janse, C., Kazura, J.W., Milner, D., Barnwell, J.W., Turner, G., Langhorne, J., Malaria”, on behalf of the participants of the H.R. meeting on “Animal M. for R. on S., 2012. The Role of Animal Models for Research on Severe Malaria. *PLoS Pathog.* 8, e1002401.
- Cross, A.K., Haddock, G., Surr, J., Plumb, J., Bunning, R.A.D., Buttle, D.J., Woodroffe, M.N., 2006. Differential expression of ADAMTS-1, -4, -5 and TIMP-3 in rat spinal cord at different stages of acute experimental autoimmune encephalomyelitis. *J. Autoimmun.* 26, 16–23.
- Cucullo, L., Couraud, P.-O., Weksler, B., Romero, I.-A., Hossain, M., Rapp, E., Janigro, D., 2008. Immortalized Human Brain Endothelial Cells and Flow-Based Vascular Modeling: A Marriage of Convenience for Rational Neurovascular Studies. *J. Cereb. Blood Flow Metab.* 28, 312–328.
- Cucullo, L., Hossain, M., Puvenna, V., Marchi, N., Janigro, D., 2011. The role of shear stress in Blood-Brain Barrier endothelial physiology. *BMC Neurosci.* 12, 40.
- D’Alessandro, S., Basilico, N., Prato, M. 2013. pd., 2013. Effects of *Plasmodium falciparum*-

- infected erythrocytes on matrix metalloproteinase-9 regulation in human microvascular endothelial cells. *Asian Pac. J. Trop. Med.* 6, 195–199.
- Daneman, R., Prat, A., 2015. The blood-brain barrier. *Cold Spring Harb. Perspect. Biol.* 7, a020412.
- Daneman, R., Zhou, L., Kebede, A.A., Barres, B.A., 2010. Pericytes are required for blood-brain barrier integrity during embryogenesis. *Nature* 468, 562–6.
- De Boer, A.G., Gaillard, P.J., 2006. Blood–brain barrier dysfunction and recovery. *J. Neural Transm.* 113, 455–462.
- De Souza, J.B., Hafalla, J.C.R., Riley, E.M., Couper, K.N., 2018. Cerebral malaria: why experimental murine models are required to understand the pathogenesis of disease. *Parasitology* 137, 755-772.
- de Vries, H.E., Blom-Roosemalen, M.C.M., Oosten, M. van, de Boer, A.G., van Berkel, T.J.C., Breimer, D.D., Kuiper, J., 1996. The influence of cytokines on the integrity of the blood-brain barrier *in vitro*. *J. Neuroimmunol.* 64, 37–43.
- Deininger, M.H., Winkler, S., Kremsner, P.G., Meyermann, R., Schluesener, H.J., 2003. Angiogenic proteins in brains of patients who died with cerebral malaria. *J. Neuroimmunol.* 142, 101–111.
- Deosarkar, S.P., Prabhakarandian, B., Wang, B., Sheffield, J.B., Krynska, B., Kiani, M.F., 2015. A Novel Dynamic Neonatal Blood-Brain Barrier on a Chip. *PLoS One* 10, e0142725.
- DeStefano, J.G., Williams, A., Wnorowski, A., Yimam, N., Searson, P.C., Wong, A.D., 2017. Real-time quantification of endothelial response to shear stress and vascular modulators. *Integr. Biol. (Camb).* 9, 362–374.
- Dietmann, A., Helbok, R., Lackner, P., Issifou, S., Lell, B., Matsiegui, P.B., Reindl, M., Schmutzhard, E., Kremsner, P.G., 2008. Matrix metalloproteinases and their tissue inhibitors (TIMPs) in *Plasmodium falciparum* malaria: serum levels of TIMP-1 are associated with disease severity. *J. Infect. Dis.* 197, 1614–1620.
- Dohgu, S., Yamauchi, A., Takata, F., Naito, M., Tsuruo, T., Higuchi, S., Sawada, Y., Kataoka, Y., 2004. Transforming Growth Factor- β 1 Upregulates the Tight Junction and P-glycoprotein of Brain Microvascular Endothelial Cells. *Cellular and Molecular Neurobiology* 24, 491-497.
- Dorovini-Zis, K., Schmidt, K., Huynh, H., Fu, W., Whitten, R.O., Milner, D., Kamiza, S., Molyneux, M., Taylor, T.E., 2011. The neuropathology of fatal cerebral malaria in Malawian children. *Am. J. Pathol.* 178, 2146–2158.
- Dossi, E., Vasile, F., Rouach, N., 2018. Human astrocytes in the diseased brain. *Brain Res. Bull.* 136, 139–156.
- Doumbo, O.K., Thera, M.A., Kone, A.K., Raza, A., Tempest, L.J., Lyke, K.E., Plowe, C. V, Rowe, J.A., Koné, A.K., Raza, A., Tempest, L.J., Lyke, K.E., Plowe, C. V, Rowe, J.A., 2009. High levels of *Plasmodium falciparum* rosetting in all clinical forms of severe malaria in African children. *Am. J. Trop. Med. Hyg.* 81, 987–993.
- Dunst, J., Kamena, F., Matuschewski, K., 2017. Cytokines and Chemokines in Cerebral Malaria Pathogenesis. *Front. Cell. Infect. Microbiol.* 7, 324.

- El-Assaad, F., Whewey, J., Mitchell, A.J., Lou, J., Hunt, N.H., Combes, V., Grau, G.E.R., 2013. Cytoadherence of *Plasmodium berghei*-infected red blood cells to murine brain and lung microvascular endothelial cells *in vitro*. *Infect. Immun.* 81, 3984–91.
- Esser, C., Bachmann, A., Kuhn, D., Schuldt, K., Förster, B., Thiel, M., May, J., Koch-Nolte, F., Yáñez-Mó, M., Sánchez-Madrid, F., 2014. Evidence of promiscuous endothelial binding by *Plasmodium falciparum*-infected erythrocytes. *Cell. Microbiol.* 16, 701–708.
- Flannery, C.R., Zeng, W., Corcoran, C., Collins-Racie, L.A., Chockalingam, P.S., Hebert, T., Mackie, S.A., McDonagh, T., Crawford, T.K., Tomkinson, K.N., LaVallie, E.R., Morris, E.A., 2002. Autocatalytic cleavage of ADAMTS-4 (Aggrecanase-1) reveals multiple glycosaminoglycan-binding sites. *J. Biol. Chem.* 277, 42775–80.
- Fontijn, R.D., Volger, O.L., Fledderus, J.O., Reijkerkerk, A., De Vries, H.E., Horrevoets, A.J.G., 2008. SOX-18 controls endothelial-specific claudin-5 gene expression and barrier function. *Am J Physiol Hear. Circ Physiol* 294, 891–900.
- Fraser, D., Ward, R.E., Farrell, C., Sainte-Justine, C., Kesselman, M., 2011. Severe traumatic brain injury in children elevates glial fibrillary acidic protein in cerebrospinal fluid and serum. *Cerebrovascular Proteomics View project DDePICT View project. Pediatr. Crit. Care Med.* 12.
- Furuta, T., Kimura, M., Watanabe, N., 2010. Elevated levels of vascular endothelial growth factor (VEGF) and soluble vascular endothelial growth factor receptor (VEGFR)-2 in human malaria. *Am. J. Trop. Med. Hyg.* 82, 136–9.
- Gao, G., Westling, J., Thompson, V.P., Howell, T.D., Gottschall, P.E., Sandy, J.D., 2002. Activation of the proteolytic activity of ADAMTS4 (aggrecanase-1) by C-terminal truncation. *J. Biol. Chem.* 277, 11034–41.
- Giampietro, C., 2016. VE-cadherin complex plasticity: EPS8 and YAP play relay at adherens junctions. *Tissue Barriers* 4.
- Giebel, S.J., Menicucci, G., McGuire, P.G., Das, A., 2005. Matrix metalloproteinases in early diabetic retinopathy and their role in alteration of the blood–retinal barrier. *Lab. Investig.* 85, 597–607.
- Gillrie, M., Krishnegowda, G., Lee, K., Buret, A., Robbins, S., Looareesuwan, S., Gowda, D., Ho, M., 2007. Src-family kinase–dependent disruption of endothelial barrier function by *Plasmodium falciparum* merozoite proteins. *Blood* 110, 3426–3435.
- Gordon, G.R.J., Howarth, C., MacVicar, B.A., 2011. Bidirectional control of arteriole diameter by astrocytes. *Exp. Physiol.* 96, 393–399.
- Gottschall, P.E., Howell, M.D., 2015. ADAMTS expression and function in central nervous system injury and disorders. *Matrix Biol.* 44–46, 70–76.
- Grau, G.E.R., Craig, A.G., 2012. Cerebral malaria pathogenesis: revisiting parasite and host contributions. *Future Microbiol.* 7, 291–302.
- Gray, C., McCormick, C., Turner, G., Craig, A., 2003. ICAM-1 can play a major role in mediating *P. falciparum* adhesion to endothelium under flow. *Mol. Biochem. Parasitol.* 128, 187–193.
- Griffiths, M.J., Shafi, M.J., Popper, S.J., Hemingway, C.A., Kortok, M.M., Wathen, A., Rockett, K.A., Mott, R., Levin, M., Newton, C.R., Marsh, K., Relman, D.A.,

- Kwiatkowski, D.P., 2005. Genomewide Analysis of the Host Response to Malaria in Kenyan Children. *J. Infect. Dis.* 191, 1599–1611.
- Gromnicova, R., Davies, H.A., Sreekanthreddy, P., Romero, I.A., Lund, T., Roitt, I.M., Phillips, J.B., Male, D.K., 2013. Glucose-Coated Gold Nanoparticles Transfer across Human Brain Endothelium and Enter Astrocytes *in vitro*. *PLoS One* 8, e81043.
- Gruenberg, J., Allred, D.R., Sherman, I.W., 1983. Scanning electron microscope-analysis of the protrusions (knobs) present on the surface of *Plasmodium falciparum*-infected erythrocytes. *J. Cell Biol.* 97, 795–802.
- Guizetti, J., Scherf, A., 2013. Silence, activate, poise and switch! Mechanisms of antigenic variation in *Plasmodium falciparum*. *Cell. Microbiol.* 15, 718–726.
- Gurney, K.J., Estrada, E.Y., Rosenberg, G.A., 2006. Blood–brain barrier disruption by stromelysin-1 facilitates neutrophil infiltration in neuroinflammation. *Neurobiol. Dis.* 23, 87–96.
- Gurses, M.S., Ural, M.N., Gulec, M.A., Akyol, O., Akyol, S., 2016. Pathophysiological Function of ADAMTS Enzymes on Molecular Mechanism of Alzheimer’s Disease. *Aging Dis.* 7, 479–90.
- Haddock, G., Cross, A., Plumb, J., Surr, J., Buttle, D., Bunning, R., Woodroffe, M. 2006. Expression of ADAMTS-1, -4, -5 and TIMP-3 in normal and multiple sclerosis CNS white matter. *Multiple Sclerosis* 12, 386-396.
- Hamel, M.G., Mayer, J., Gottschall, P.E., 2005. Altered production and proteolytic processing of brevican by transforming growth factor b in cultured astrocytes. *J. Neurochem* 93, 1533–1541.
- Hansen, D.S., 2012. Inflammatory responses associated with the induction of cerebral malaria: lessons from experimental murine models. *PLoS Pathog.* 8, e1003045.
- Hashimoto, G., Shimoda, M., Okada, Y., 2004. ADAMTS4 (aggrecanase-1) interaction with the C-terminal domain of fibronectin inhibits proteolysis of aggrecan. *J. Biol. Chem.* 279, 32483–91.
- Hawkes, M., Elphinstone, R.E., Conroy, A.L., Kain, K.C., 2013. Contrasting pediatric and adult cerebral malaria: the role of the endothelial barrier. *Virulence* 4, 543–55.
- Hawkins, B.T., Davis, T.P., 2005. The blood-brain barrier/neurovascular unit in health and disease. *Pharmacol. Rev.* 57, 173–185.
- Hawkins, B.T., Gu, Y.H., Izawa, Y., Del Zoppo, G.J., 2013. Disruption of dystroglycan-laminin interactions modulates water uptake by astrocytes. *Brain Res.* 1503, 89–96.
- He, Y., Yao, Y., Tsirka, S.E., Cao, Y., 2014. Cell-culture models of the blood-brain barrier. *Stroke.* 45, 2514-2526.
- He, Y., Zheng, Q., Jiang, M., Sun, S., Christiansen, T.G., Kassem, M., Karsdal, M.A., Bay-Jensen, A.C., 2015. The Effect of Protease Inhibitors on the Induction of Osteoarthritis-Related Biomarkers in Bovine Full-Depth Cartilage Explants. *PLoS One* 10, e0122700.
- Helms, H.C., Abbott, N.J., Burek, M., Cecchelli, R., Couraud, P.-O., Deli, M.A., Förster, C., Galla, H.J., Romero, I.A., Shusta, E. V, Stebbins, M.J., Vandenhaute, E., Weksler, B., Brodin, B., 2016. *In vitro* models of the blood–brain barrier: An overview of commonly

- used brain endothelial cell culture models and guidelines for their use. *J. Cereb. Blood Flow Metab.* 36, 862–890.
- Ho, M., Hickey, M.J., Murray, A.G., Andonegui, G., Kubes, P., 2000. Visualization of *Plasmodium falciparum*-endothelium interactions in human microvasculature: mimicry of leukocyte recruitment. *J. Exp. Med.* 192, 1205–1211.
- Hunt, N.H., Ball, H.J., Hansen, A.M., Khaw, L.T., Guo, J., Bakmiwewa, S., Mitchell, A.J., Combes, V., Grau, G.E.R., 2014. Cerebral malaria: gamma-interferon redux. *Front. Cell. Infect. Microbiol.* 4.
- Hurwitz, A.A., Lyman, W.D., Guida, M.P., Calderon, T.M., Berman, J.W., 1992. Tumor necrosis factor alpha induces adhesion molecule expression on human fetal astrocytes. *J. Exp. Med.* 176, 1631–6.
- Huveneers, S., Oldenburg, J., Spanjaard, E., van der Krogt, G., Grigoriev, I., Akhmanova, A., Rehmann, H., de Rooij, J., 2012. Vinculin associates with endothelial VE-cadherin junctions to control force-dependent remodeling. *J. Cell Biol.* 196, 641–52.
- Hviid, L., Jensen, A.T.R., 2015. PfEMP1 – A Parasite Protein Family of Key Importance in *Plasmodium falciparum* Malaria Immunity and Pathogenesis. *Adv. Parasitol.* 88, 51–84.
- Idro, R., Jenkins, N.E., Newton, C.R.J.C., 2005. Pathogenesis, clinical features, and neurological outcome of cerebral malaria. *Lancet. Neurol.* 4, 827–40.
- Idro, R., Kakooza-Mwesige, A., Balyejjussa, S., Mirembe, G., Mugasha, C., Tugumisirize, J., Byarugaba, J., 2010. Severe neurological sequelae and behaviour problems after cerebral malaria in Ugandan children. *BMC Res. Notes* 3, 104.
- Jain, K., Sood, S., Gowthamarajan, K., 2013. Modulation of cerebral malaria by curcumin as an adjunctive therapy. *Brazilian J. Infect. Dis.* 17, 579–591.
- Kaisar, M.A., Sajja, R.K., Prasad, S., Abhyankar, V. V, Liles, T., Cucullo, L., 2017. New experimental models of the blood-brain barrier for CNS drug discovery. *Expert Opin. Drug Discov.* 12, 89–103.
- Kantele, A., Jokiranta, T.S., 2011. Review of cases with the emerging fifth human malaria parasite, *Plasmodium knowlesi*. *Clin. Infect. Dis.* 52, 1356–1362.
- Karunaweera, N.D., Grau, G.E., Gamage, P., Carter, R., Mendis, K.N., 1992. Dynamics of fever and serum levels of tumor necrosis factor are closely associated during clinical paroxysms in *Plasmodium vivax* malaria. *Proc. Natl. Acad. Sci. U. S. A.* 89, 3200–3203.
- Kashiwagi, M., Enghild, J.J., Gendron, C., Hughes, C., Caterson, B., Itoh, Y., Nagase, H., 2004. Altered proteolytic activities of ADAMTS-4 expressed by C-terminal processing. *J. Biol. Chem.* 279, 10109–19.
- Keller, A., 2013. Breaking and building the wall: the biology of the blood-brain barrier in health and disease. *Swiss Med Wkly* 143.
- Klein, E.Y., 2013. Antimalarial drug resistance: a review of the biology and strategies to delay emergence and spread. *Int. J. Antimicrob. Agents* 41, 311–7.
- Kulczar, C., Lubin, K.E., Lefebvre, S., Miller, D.W., Knipp, G.T., 2017. Development of a direct contact astrocyte-human cerebral microvessel endothelial cells blood-brain barrier coculture model. *J. Pharm. Pharmacol.* 69, 1684–1696.

- Lee, S.W., Kim, W.J., Choi, Y.K., Song, H.S., Son, M.J., Gelman, I.H., Kim, Y.J., Kim, K.W., 2003. SSeCKS regulates angiogenesis and tight junction formation in blood-brain barrier. *Nat. Med.* 9, 900–906.
- Lee, Y., Du, S., Rhim, H., Lee, E.B., Markelonis, G.J., Oh, T.H., 2000. Rapid increase in immunoreactivity to GFAP in astrocytes *in vitro* induced by acidic pH is mediated by calcium influx and calpain I. *Brain Res.* 864, 220–229.
- Leech, J.H., Barnwell, J.W., Miller, L.H., Howard, R.J., 1984. Identification of a strain-specific malarial antigen exposed on the surface of *Plasmodium falciparum*-infected erythrocytes. *J. Exp. Med.* 159, 1567–1575.
- Lemarchant, S., Pruvost, M., Montaner, J., Emery, E., Vivien, D., Kanninen, K., Koistinaho, J., 2013. ADAMTS proteoglycanases in the physiological and pathological central nervous system. *J. Neuroinflammation* 10, 133.
- Levy, A.F., Zayats, M., Guerrero-Cazares, H., Quiñones-Hinojosa, A., Searson, P.C., 2014. Influence of Basement Membrane Proteins and Endothelial Cell-Derived Factors on the Morphology of Human Fetal-Derived Astrocytes in 2D. *PLoS One* 9, e92165.
- Li, G., Simon, M.J., Cancel, L.M., Shi, Z.-D., Ji, X., Tarbell, J.M., Morrison, B., Fu, B.M., Fu, B.M., 2010. Permeability of endothelial and astrocyte cocultures: *in vitro* blood-brain barrier models for drug delivery studies. *Ann. Biomed. Eng.* 38, 2499–511.
- Lovegrove, F.E., Tangpukdee, N., Opoka, R.O., Lafferty, E.I., Rajwans, N., Hawkes, M., Krudsood, S., Looareesuwan, S., John, C.C., Liles, W.C., Kain, K.C., 2009. Serum angiopoietin-1 and -2 levels discriminate cerebral malaria from uncomplicated malaria and predict clinical outcome in African children. *PLoS One* 4, e4912.
- Lu, P., Takai, K., Weaver, V.M., Werb, Z., 2011. Extracellular matrix degradation and remodeling in development and disease. *Cold Spring Harb. Perspect. Biol.* 3.
- Luissint, A.-C., Artus, C., Glacial, F., Ganeshamoorthy, K., Couraud, P.-O., 2012. Tight junctions at the blood brain barrier: physiological architecture and disease-associated dysregulation. *Fluids Barriers CNS* 9, 23.
- Lyons, P., Benveniste, E., 1998. Cleavage of Membrane-Associated ICAM-1 From Astrocytes: Involvement of a Metalloprotease. *Glia* 22, 103–112.
- MacPherson, G.G., Warrell, M.J., White, N.J., Looareesuwan, S., Warrell, D.A., 1985. Human cerebral malaria. A quantitative ultrastructural analysis of parasitized erythrocyte sequestration. *Am. J. Pathol.* 119, 385–401.
- Magnusson, J.P., Frisé, J., 2016. Stars from the darkest night: unlocking the neurogenic potential of astrocytes in different brain regions. *Development* 143, 1075–86.
- Malaria Vaccine initiative, 2018. Need for a vaccine Malaria Vaccine Initiative [WWW Document]. URL <http://www.malariavaccine.org/malaria-and-vaccines/need-vaccine> (accessed 5.17.18).
- Mandala, W.L., Msefula, C.L., Gondwe, E.N., Drayson, M.T., Molyneux, M.E., MacLennan, C.A., 2017. Cytokine Profiles in Malawian Children Presenting with Uncomplicated Malaria, Severe Malarial Anemia, and Cerebral Malaria. *Clin. Vaccine Immunol.* 24, e00533-16.
- Mark, K.S., Davis, T.P., 2002. Cerebral microvascular changes in permeability and tight

- junctions induced by hypoxia-reoxygenation. *Am. J. Physiol. Circ. Physiol.* 282, H1485-94.
- Martinian, L., Boer, K., Middeldorp, J., Hol, E.M., Sisodiya, S.M., Squier, W., Aronica, E., Thom, M., 2009. Expression patterns of glial fibrillary acidic protein (GFAP)-delta in epilepsy-associated lesional pathologies. *Neuropathol. Appl. Neurobiol.* 35, 394–405.
- Martins, Y.C., Daniel-Ribeiro, C.T., 2013. A new hypothesis on the manifestation of cerebral malaria: the secret is in the liver. *Med. Hypotheses* 81, 777–83.
- McCarthy, K., Skare, I., Stankewich, M., Furuse, M., Tsukita, S., Rogers, R., Lynch, R., Eveline, S., 1996. Occludin is a functional component of the tight junction. *J. Cell Science* 109, 2287–2298.
- Mebius, R.E., Kraal, G., 2005. Structure and function of the spleen. *Nat. Rev. Immunol.* 5, 606–616.
- Medana, I.M., Chan-Ling, T., Hunt, N.H., 1996. Redistribution and degeneration of retinal astrocytes in experimental murine cerebral malaria: relationship to disruption of the blood-retinal barrier. *Glia* 16, 51–64.
- Medana, I.M., Chan-Ling, T., Hunt, N.H., 2000. Reactive changes of retinal microglia during fatal murine cerebral malaria: effects of dexamethasone and experimental permeabilization of the blood-brain barrier. *Am. J. Pathol.* 156, 1055–1065.
- Medana, I.M., Day, N.P., Hien, T.T., Mai, N.T.H., Bethell, D., Phu, N.H., Farrar, J., Esiri, M.M., White, N.J., Turner, G.D., 2002. Axonal injury in cerebral malaria. *Am. J. Pathol.* 160, 655–66.
- Medana, I.M., Idro, R., Newton, C.R.J.C., 2007. Axonal and astrocyte injury markers in the cerebrospinal fluid of Kenyan children with severe malaria. *J. Neurol. Sci.* 258, 93–98.
- Medana, I.M., Turner, G.D.H., 2006. Human cerebral malaria and the blood–brain barrier. *Int. J. Parasitol.* 36, 555–568.
- Mignot, C., Boespflug-Tanguy, O., Gelot, A., Dautigny, A., Pham-Dinh, D., Rodriguez, D., 2004. Human Genome & Diseases: Review Alexander disease: putative mechanisms of an astrocytic encephalopathy. *C. Cell. Mol. Life Sci* 61, 369–385.
- Millington, O.R., Di Lorenzo, C., Phillips, R.S., Garside, P., Brewer, J.M., 2006. Suppression of adaptive immunity to heterologous antigens during *Plasmodium* infection through hemozoin-induced failure of dendritic cell function. *J. Biol.* 5, 5.
- Milner Jr, D.A., Whitten, R.O., Kamiza, S., Carr, R., Liomba, G., Dzamalala, C., Seydel, K.B., Molyneux, M.E., Taylor, T.E., 2014. The systemic pathology of cerebral malaria in African children. *Front. Cell. Infect. Microbiol.* 4.
- Mizee, M.R., Wooldrik, D., Lakeman, K.A.M., Van Het Hof, B., Drexhage, J.A.R., Geerts, D., Bugiani, M., Aronica, E., Mebius, R.E., Prat, A., De Vries, H.E., Reijerkerk, A., 2013. Retinoic Acid Induces Blood-Brain Barrier Development. *J Neurosci* 33, 1660–1671.
- Morita, K., Sasaki, H., Furuse, M., Tsukita, S., 1999. Endothelial claudin: claudin-5/TMVCF constitutes tight junction strands in endothelial cells. *J. Cell Biol.* 147, 185–194.
- Mosnier, L.O., Lavstsen, T., 2016. The role of EPCR in the pathogenesis of severe malaria. *Thromb. Res.* 141 Suppl 2, S46-9.

- Moxon, C.A., Grau, G.E., Craig, A.G., 2011. Malaria: modification of the red blood cell and consequences in the human host. *Br. J. Haematol.* 154, 670–679.
- Moxon, C.A., Wassmer, S.C., Milner, D.A., Chisala, N. V, Taylor, T.E., Seydel, K.B., Molyneux, M.E., Faragher, B., Esmon, C.T., Downey, C., Toh, C.H., Craig, A.G., Heyderman, R.S., 2013. Loss of endothelial protein C receptors links coagulation and inflammation to parasite sequestration in cerebral malaria in African children. *Blood* 122, 842–51.
- Nagase, H., Woessner Jr, J.F., 1999. Matrix metalloproteinases. *J. Biol. Chem.* 274, 21491–21494.
- Nakagawa, S., Má, A., Deli, A., Shinobu, A., Honda, M., Kentaro, A., Nakaoke, R., Yasufumi, A., Niwa, M., Nakagawa, S., Deli, Á.M.A., Nakao, Á.S., Nakaoke, Á.R., Niwa, Á.M., Kataoka, Á.Y., Deli, M.A., Honda, M., Hayashi, Á.K., Kataoka, Y., 2007. Pericytes from Brain Microvessels Strengthen the Barrier Integrity in Primary Cultures of Rat Brain Endothelial Cells. *Cell Mol Neurobiol* 27, 687–694.
- Ndam, T.N., Moussiliou, A., Lavstsen, T., Kamaliddin, C., Jensen, A.T.R., Mama, A., Tahar, R., Wang, C.W., Jespersen, J.S., Alao, J.M., Gamain, B., Theander, T.G., Deloron, P., 2017. Parasites Causing Cerebral Falciparum Malaria Bind Multiple Endothelial Receptors and Express EPCR and ICAM-1-Binding PfEMP1. *J. Infect. Dis.* 215, 1918–1925.
- Nishitsuji, K., Hosono, T., Nakamura, T., Bu, G., Michikawa, M., 2011. Apolipoprotein E regulates the integrity of tight junctions in an isoform-dependent manner in an *in vitro* blood-brain barrier model. *J. Biol. Chem.* 286, 17536–42.
- Nitta, T., Hata, M., Gotoh, S., Seo, Y., Sasaki, H., Hashimoto, N., Furuse, M., Tsukita, S., 2003. Size-selective loosening of the blood-brain barrier in claudin-5-deficient mice. *J. Cell Biol.* 161, 653–660.
- O’Carroll, S.J., Kho, D.T., Wiltshire, R., Nelson, V., Rotimi, O., Johnson, R., Angel, C.E., Graham, E.S., 2015. Pro-inflammatory TNF α and IL-1 β differentially regulate the inflammatory phenotype of brain microvascular endothelial cells. *J. Neuroinflammation* 12, 131.
- Obermeier, B., Daneman, R., Ransohoff, R.M., 2013. Development, maintenance and disruption of the blood-brain barrier. *Nat. Med.* 19, 1584–96.
- Ochola, L.B., Siddondo, B.R., Ocholla, H., Nkya, S., Kimani, E.N., Williams, T.N., Makale, J.O., Liljander, A., Urban, B.C., Bull, P.C., Szeszak, T., Marsh, K., Craig, A.G., 2011. Specific receptor usage in *Plasmodium falciparum* cytoadherence is associated with disease outcome. *PLoS One* 6, e14741.
- Ockenhouse, C.F., Betageri, R., Springer, T.A., Staunton, D.E., 1992. *Plasmodium falciparum*-infected erythrocytes bind ICAM-1 at a site distinct from LFA-1, Mac-1, and human rhinovirus. *Cell* 68, 63–69.
- Okonkwo, D.O., Yue, J.K., Puccio, A.M., Panczykowski, D.M., Inoue, T., McMahon, P.J., Sorani, M.D., Yuh, E.L., Lingsma, H.F., Maas, A.I.R., Valadka, A.B., Manley, G.T., Cheong, M., Cooper, S.R., Dams-O’Connor, K., Gordon, W.A., Hricik, A.J., Hochberger, K., Menon, D.K., Mukherjee, P., Sinha, T.K., Schnyer, D.M., Vassar, M.J., 2013. GFAP-BDP as an acute diagnostic marker in traumatic brain injury: results from the prospective transforming research and clinical knowledge in traumatic brain injury study. *J.*

Neurotrauma 30, 1490–7.

- Olivier, M., Van Den Ham, K., Shio, M.T., Kassa, F.A., Fougeray, S., 2014. Malarial pigment hemozoin and the innate inflammatory response. *Front. Immunol.* 5.
- Otto, V.I., Gloor, S.M., Frenzels, S., Gilli, U., Ammann, E., Hein, A.E., Folkers, G., Trentz, O., Kossmann, T., Morganti-Kossmann, M.C., 2002. The production of macrophage inflammatory protein-2 induced by soluble intercellular adhesion molecule-1 in mouse astrocytes is mediated by src tyrosine kinases and p42/44 mitogen-activated protein kinase. *J. Neurochem.* 80, 824–834.
- Pain, A., Ferguson, D.J., Kai, O., Urban, B.C., Lowe, B., Marsh, K., Roberts, D.J., 2001. Platelet-mediated clumping of *Plasmodium falciparum*-infected erythrocytes is a common adhesive phenotype and is associated with severe malaria. *Proc. Natl. Acad. Sci. U. S. A.* 98, 1805–1810.
- Pal, P., Daniels, B., Oskman, A., Diamond, M., Klein, R., Goldberg, D., 2016. *Plasmodium falciparum* Histidine-Rich Protein II Compromises Brain Endothelial Barriers and May Promote Cerebral Malaria Pathogenesis. *Am. Soc. Microbiol.* 303, 295–303.
- Papa, L., Lewis, L.M., Falk, J.L., Zhang, Z., Silvestri, S., Giordano, P., Brophy, G.M., Demery, J.A., Dixit, N.K., Ferguson, I., Liu, M.C., Mo, J., Akinyi, L., Schmid, K., Mondello, S., Robertson, C.S., Tortella, F.C., Hayes, R.L., Wang, K.K.W., 2012. Elevated levels of serum glial fibrillary acidic protein breakdown products in mild and moderate traumatic brain injury are associated with intracranial lesions and neurosurgical intervention. *Ann. Emerg. Med.* 59, 471–83.
- Pasternak, N.D., Dzikowski, R., 2009. PfEMP1: an antigen that plays a key role in the pathogenicity and immune evasion of the malaria parasite *Plasmodium falciparum*. *Int. J. Biochem. Cell Biol.* 41, 1463–1466.
- Pekny, M., Pekna, M., 2004. Astrocyte intermediate filaments in CNS pathologies and regeneration. *J. Pathol.* 204, 428–437.
- Pekny, M., Wilhelmsson, U., Pekna, M., 2014. The dual role of astrocyte activation and reactive gliosis. *Neurosci. Lett.* 565, 30–38.
- Petty, M.A., Lo, E.H., 2002. Junctional complexes of the blood–brain barrier: permeability changes in neuroinflammation. *Prog. Neurobiol.* 68, 311–323.
- Petzold, A., 2015. Glial fibrillary acidic protein is a body fluid biomarker for glial pathology in human disease. *Brain Res.* 1600, 17–31.
- Phiri, H., Montgomery, J., Molyneux, M., Craig, A., 2009. Competitive endothelial adhesion between *Plasmodium falciparum* isolates under physiological flow conditions. *Malar. J.* 8, 214.
- Pleines, U.E., Stover, J.F., Kossmann, T., Trentz, O., Morganti-Kossmann, M.C., 1998. Soluble ICAM-1 in CSF coincides with the extent of cerebral damage in patients with severe traumatic brain injury. *Journal of Neurotrauma.* 15, 399–409.
- Polimeni, M., Prato, M., 2014. Host matrix metalloproteinases in cerebral malaria: new kids on the block against blood-brain barrier integrity. *Fluids Barriers CNS* 11, 1.
- Ponsford, M.J., Medana, I.M., Prapansilp, P., Hien, T.T., Lee, S.J., Dondorp, A.M., Esiri, M.M., Day, N.P., White, N.J., Turner, G.D., 2012. Sequestration and microvascular congestion

- are associated with coma in human cerebral malaria. *J. Infect. Dis.* 205, 663–671.
- Porter, S., Clark, I.M., Kevorkian, L., Edwards, D.R., 2005. The ADAMTS metalloproteinases. *Biochem. J.* 386, 15–27.
- Pradel, G., Frevert, U., 2001. Malaria Sporozoites Actively Enter and Pass Through Rat Kupffer Cells Prior to Hepatocyte Invasion. *Hepatology* 33, 1154–1165.
- Prudêncio, M., Mota, M.M., Mendes, A.M., 2011. A toolbox to study liver stage malaria. *Trends Parasitol.* 27, 565–574.
- Qiu, L.-B., Zhou, Y., Wang, Q., Yang, L., Liu, H.-Q., Xu, S.-L., Qi, Y.-H., Ding, G.-R., Guo, G.-Z., 2011. Synthetic gelatinases inhibitor attenuates electromagnetic pulse-induced blood–brain barrier disruption by inhibiting gelatinases-mediated ZO-1 degradation in rats. *Toxicology* 285, 31–38.
- Ranford-Cartwright, L.C., Sinha, A., Humphreys, G.S., Mwangi, J.M., 2010. New synchronization method for *Plasmodium falciparum*. *Malar. J.* 9, 170.
- Reichmann, G., Villegas, E.N., Craig, L., Peach, R., Hunter, C.A., Viguier, M., Snounou, G., Rénia, L., 1999. The CD28/B7 interaction is not required for resistance to *Toxoplasma gondii* in the brain but contributes to the development of immunopathology. *J. Immunol.* 163, 3354–62.
- Rénia, L., Wu Howland, S., Claser, C., Charlotte Gruner, A., Suwanarusk, R., Hui Teo, T., Russell, B., Ng, L., 2012. Cerebral malaria: Mysteries at the blood-brain barrier. *Virulence* 3, 183–191.
- Rimm, D.L., Koslov, E.R., Kebriaei, P., Cianci, C.D., Morrow, J.S., 1995. Alpha 1(E)-catenin is an actin-binding and -bundling protein mediating the attachment of F-actin to the membrane adhesion complex. *Proc. Natl. Acad. Sci. U. S. A.* 92, 8813–8817.
- Riss, T.L., Moravec, R.A., Niles, A.L., Duellman, S., Benink, H.A., Worzella, T.J., Minor, L., 2016. Assay Guidance Manual [Internet] [WWW Document]. 2013. URL https://www.ncbi.nlm.nih.gov/books/NBK144065/pdf/Bookshelf_NBK144065.pdf (accessed 7.1.18).
- Roelofs, R.F., Fischer, D.F., Houtman, S.H., Sluijs, J.A., Van Haren, W., Van Leeuwen, F.W., Hol, E.M., 2005. Adult human subventricular, subgranular, and subpial zones contain astrocytes with a specialized intermediate filament cytoskeleton. *Glia* 52, 289–300.
- Rollins, B.J., Yoshimura, T., Leonard, E.J., Pober, J.S., 1990. Cytokine-activated human endothelial cells synthesize and secrete a monocyte chemoattractant, MCP-1/JE. *Am. J. Pathol.* 136, 1229–33.
- Ronaldson, P.T., Davis, T.P., 2011. Targeting blood-brain barrier changes during inflammatory pain: An opportunity for optimizing CNS drug delivery. *Ther. Deliv.* 1015–1041.
- Rowe, J.A., Claessens, A., Corrigan, R.A., Arman, M., 2009. Adhesion of *Plasmodium falciparum*-infected erythrocytes to human cells: molecular mechanisms and therapeutic implications. *Expert Rev. Mol. Med.* 11, e16.
- Saadoun, S., Papadopoulos, M.C., Davies, D.C., Krishna, S., Bell, B.A., 2002. Aquaporin-4 expression is increased in oedematous human brain tumours. *J. Neurol. Neurosurg. Psychiatry* 72, 262–265.

- Saitou, M., Furuse, M., Sasaki, H., Schulzke, J.D., Fromm, M., Takano, H., Noda, T., Tsukita, S., 2000. Complex phenotype of mice lacking occludin, a component of tight junction strands. *Mol. Biol. Cell* 11, 4131–4142.
- Schachtrup, C., Ryu, J.K., Helmrick, M.J., Vagena, E., Galanakis, D.K., Degen, J.L., Margolis, R.U., Akassoglou, K., 2010. Fibrinogen triggers astrocyte scar formation by promoting the availability of active TGF-beta after vascular damage. *J. Neurosci.* 30, 5843–54.
- Scherf, A., Hernandez-Rivas, R., Buffet, P., Bottius, E., Benatar, C., Pouvelle, B., Gysin, J., Lanzer, M., 1998. Antigenic variation in malaria: in situ switching, relaxed and mutually exclusive transcription of var genes during intra-erythrocytic development in *Plasmodium falciparum*. *EMBO J.* 17, 5418–5426.
- Scherf, A., Lopez-Rubio, J.J., Riviere, L., 2008. Antigenic variation in *Plasmodium falciparum*. *Annu.Rev.Microbiol.* 62, 445–470.
- Shabani, E., Hanisch, B., Opoka, R.O., Lavstsen, T., John, C.C., 2017. *Plasmodium falciparum* EPCR-binding PfEMP1 expression increases with malaria disease severity and is elevated in retinopathy negative cerebral malaria. *BMC Med.* 15, 183.
- Smith, J., Craig, A.G., Kriek, N., Hudson-Taylor, D., Kyes, S., Fagan, T., Pinches, R., Baruch, D.I., Newbold, C.I., Miller, L.H., 2000a. Identification of a *Plasmodium falciparum* intercellular adhesion molecule-1 binding domain: a parasite adhesion trait implicated in cerebral malaria. *Proc. Natl. Acad. Sci. U. S. A.* 97, 1766–1771.
- Smith, J., Subramanian, G., Gamain, B., Baruch, D.I., Miller, L.H., 2000b. Classification of adhesive domains in the *Plasmodium falciparum* Erythrocyte Membrane Protein 1 family. *Mol. Biochem. Parasitol.* 110, 293–310.
- Smith, J.D., Chitnis, C.E., Craig, A.G., Roberts, D.J., Hudson-Taylor, D.E., Peterson, D.S., Pinches, R., Newbold, C.I., Miller, L.H., 1995. Switches in expression of *Plasmodium falciparum* var genes correlate with changes in antigenic and cytoadherent phenotypes of infected erythrocytes. *Cell* 82, 101–110.
- Smith, J.D., Craig, A.G., 2005. The Surface of the *Plasmodium falciparum*-infected Erythrocyte. *Curr. Issues Mol. Biol.* 7, 81-93.
- Smith, J.D., Rowe, J.A., Higgins, M.K., Lavstsen, T., 2013. Malaria's deadly grip: cytoadhesion of *Plasmodium falciparum*-infected erythrocytes. *Cell. Microbiol.* 15, 1976–1983.
- Sobel, R.A., Mitchell, M.E., Fondren, G., 1990. Intercellular Adhesion Molecule-1 (ICAM-1) in Cellular Immune Reactions in the Human Central Nervous System. *Am. of Pathology* 136.
- Sofroniew, M. V., Vinters, H. V., 2010. Astrocytes: Biology and pathology. *Acta Neuropathol.* 119, 7–35.
- Sofroniew, M. V., 2009. Molecular dissection of reactive astrogliosis and glial scar formation. *Trends Neurosci.* 32, 638–47.
- Sofroniew, M. V., 2015. Astrogliosis. *Cold Spring Harb. Perspect. Biol.* 7, a020420.
- Sreekanthreddy, P., Gromnicova, R., Davies, H., Phillips, J., Romero, I.A., Male, D., 2015. A three-dimensional model of the human blood-brain barrier to analyse the transport of nanoparticles and astrocyte/endothelial interactions. *F1000Research* 4, 1279.

- Srinivasan, B., Kolli, A.R., Esch, M.B., Abaci, H.E., Shuler, M.L., Hickman, J.J., 2015. TEER measurement techniques for *in vitro* barrier model systems. *J. Lab. Autom.* 20, 107–26.
- Stamatovic, S.M., Shakui, P., Keep, R.F., Moore, B.B., Kunkel, S.L., Rooijen, N. Van, Andjelkovic, A. V, 2005. Monocyte chemoattractant protein-1 regulation of blood–brain barrier permeability. *J. Cereb. Blood Flow Metab.* 25, 593–606.
- Stins, M.F., Gilles, F., Kim, K.S., 1997. Selective expression of adhesion molecules on human brain microvascular endothelial cells. *J. Neuroimmunol.* 76, 81–90.
- Stolp, H.B., Liddelov, S.A., Sá-Pereira, I., Dziegielewska, K.M., Saunders, N.R., Gomez-Gonzalez, B., Meeker, R., 2013. Immune responses at brain barriers and implications for brain development and neurological function in later life. *Frontiers in integrative neuroscience* 7,61.
- Storm, J., Craig, A.G., 2014. Pathogenesis of cerebral malaria--inflammation and cytoadherence. *Front. Cell. Infect. Microbiol.* 4, 100.
- Su, X., Heatwole, V.M., Wertheimer, S.P., Guinet, F., Herrfeldt, J.A., Peterson, D.S., Ravetch, J.A., Wellems, T.E., 1995. The large diverse gene family var encodes proteins involved in cytoadherence and antigenic variation of *Plasmodium falciparum*-infected erythrocytes. *Cell* 82, 89–100.
- Sue Griffin, W.T., Stanley, L.C., Ling, C., White, L., Macleod, V., Perrot, L.J., White, C.L., Araoz, C., 1989. Brain interleukin 1 and S-100 immunoreactivity are elevated in Down syndrome and Alzheimer disease. *Proc. Natl. Acad. Sci. USA* 86, 7611–7615.
- Sultan, S., Gosling, M., Nagase, H., Powell, J.T., 2004. Shear stress-induced shedding of soluble intercellular adhesion molecule-1 from saphenous vein endothelium. *FEBS* 564, 161-165.
- Susomboon, P., Maneerat, Y., Dekumyoy, P., Kalambaheti, T., Iwagami, M., Komaki-Yasuda, K., Kawazu, S., Tangpukdee, N., Looareesuwan, S., Kano, S., 2006. Down-regulation of tight junction mRNAs in human endothelial cells co-cultured with *Plasmodium falciparum*-infected erythrocytes. *Parasitol. Int.* 55, 107–112.
- Takeshita, Y., Obermeier, B., Cotleur, A., Sano, Y., Kanda, T., Ransohoff, R.M., 2014. An *in vitro* blood-brain barrier model combining shear stress and endothelial cell/astrocyte co-culture. *J. Neurosci. Methods* 232, 165–72.
- Tauchi, R., Imagama, S., Natori, T., Ohgomori, T., Muramoto, A., Shinjo, R., Matsuyama, Y., Ishiguro, N., Kadomatsu, K., 2012. The endogenous proteoglycan-degrading enzyme ADAMTS-4 promotes functional recovery after spinal cord injury. *J. Neuroinflammation* 9, 53.
- Tavares, J., Formaglio, P., Thiberge, S., Mordelet, E., Van Rooijen, N., Medvinsky, A., Menard, R., Amino, R., 2013. Role of host cell traversal by the malaria sporozoite during liver infection. *J. Exp. Med.* 210, 905–915.
- Tietz, S., Engelhardt, B., 2015. Brain barriers: Crosstalk between complex tight junctions and adherens junctions. *J. Cell Biol.* 209, 493–506.
- Timothy Jegla, 2015. Neurobiology — Chapter 2.2 Nerve cells, Neural Circuitry, and Behavior [WWW Document]. URL <http://biol469.tumblr.com/post/102308669175/chapter-22-nerve-cells-neural-circuitry-and> (accessed 7.2.18).

- Trager, W., Jensen, J., 1976. Human Malaria. *Science*. 193, 673–675.
- Tripathi, A.K., Sullivan, D.J., Stins, M.F., 2006. *Plasmodium falciparum*-infected erythrocytes increase intercellular adhesion molecule 1 expression on brain endothelium through NF-kappaB. *Infect. Immun.* 74, 3262–3270.
- Tripathi, A.K., Sullivan, D.J., Stins, M.F., 2007. *Plasmodium falciparum*–Infected Erythrocytes Decrease the Integrity of Human Blood-Brain Barrier Endothelial Cell Monolayers. *J. Infect. Dis.* 195, 942–950.
- Tse, M.T., Chakrabarti, K., Gray, C., Chitnis, C.E., Craig, A., 2004. Divergent binding sites on intercellular adhesion molecule-1 (ICAM-1) for variant *Plasmodium falciparum* isolates. *Mol. Microbiol.* 51, 1039–1049.
- Turner, G.D., Morrison, H., Jones, M., Davis, T.M., Looareesuwan, S., Buley, I.D., Gatter, K.C., Newbold, C.I., Pukritayakamee, S., Nagachinta, B., 1994. An immunohistochemical study of the pathology of fatal malaria. Evidence for widespread endothelial activation and a potential role for intercellular adhesion molecule-1 in cerebral sequestration. *Am. J. Pathol.* 145, 1057–1069.
- Turner, L., Lavstsen, T., Berger, S.S., Wang, C.W., Petersen, J.E.V. V, Avril, M., Brazier, A.J., Freeth, J., Jespersen, J.S., Nielsen, M.A., Magistrado, P., Lusingu, J., Smith, J.D., Higgins, M.K., Theander, T.G., 2013. Severe malaria is associated with parasite binding to endothelial protein C receptor. *Nature* 498, 502–505.
- Tykhomyrov, A., Nedzvetsky, V., 2016. Glial Fibrillary Acidic Protein (GFAP): on the 45th Anniversary of its Discovery. *Neurophysiology* 48, 54–71.
- Urban, B.C., Todryk, S., 2006. Malaria pigment paralyzes dendritic cells. *J. Biol.* 5, 4.
- van der Heyde, H.C., Nolan, J., Combes, V., Gramaglia, I., Grau, G.E., 2006. A unified hypothesis for the genesis of cerebral malaria: sequestration, inflammation and hemostasis leading to microcirculatory dysfunction. *Trends Parasitol.* 22, 503–8.
- van Hensbroek, M.B., Palmer, A., Onyiorah, E., Schneider, G., Jaffar, S., Dolan, G., Memming, H., Frenkel, J., Enwere, G., Bennett, S., Kwiatkowski, D., Greenwood, B., 1996. The effect of a monoclonal antibody to tumor necrosis factor on survival from childhood cerebral malaria. *J. Infect. Dis.* 174, 1091–1097.
- van Meer, G., Simons, K., 1986. The function of tight junctions in maintaining differences in lipid composition between the apical and the basolateral cell surface domains of MDCK cells. *EMBO J.* 5, 1455–1464.
- VandenBerg, S., 2010. Astrocytes [WWW Document]. URL http://missinglink.ucsf.edu/lm/introductionneuropathology/response_to_injury/Astrocytes.htm (accessed 5.18.18).
- Viebig, N.K., Levin, E., Dechavanne, S., Rogerson, S.J., Gysin, J., Smith, J.D., Scherf, A., Gamain, B., 2007. Disruption of var2csa gene impairs placental malaria associated adhesion phenotype. *PLoS One* 2, e910.
- Viebig, N.K., Wulbrand, U., Förster, R., Andrews, K.T., Lanzer, M., Knolle, P.A., 2005. Direct activation of human endothelial cells by *Plasmodium falciparum*-infected erythrocytes. *Infect. Immun.* 73, 3271–7.
- Wallez, Y., Huber, P., 2008. Endothelial adherens and tight junctions in vascular homeostasis,

- inflammation and angiogenesis. *Biochim. Biophys. Acta - Biomembr.* 1778, 794–809.
- Wassmer, S.C., Combes, V., Candal, F.J., Juhan-Vague, I., Grau, G.E., 2006. Platelets potentiate brain endothelial alterations induced by *Plasmodium falciparum*. *Infect. Immun.* 74, 645–53.
- Wassmer, S.C., Lepolard, C., Traore, B., Pouvelle, B., Gysin, J., Grau, G.E., 2004. Platelets reorient *Plasmodium falciparum*-infected erythrocyte cytoadhesion to activated endothelial cells. *J. Infect. Dis.* 189, 180–189.
- Weksler, B., Romero, I., Couraud, P.O., 2013. The hCMEC/D3 cell line as a model of the human blood brain barrier. *Fluids and Barriers of the CNS.* 10.
- Wertheimer, S.J., Myers, C.L., Wallace, R.W., Parks, T.P., 1992. Intercellular Adhesion Molecule-1 Gene Expression in Human Endothelial Cells. *The Journal of Biological Chemistry.* 267, 12030-12035.
- White, N.J., 2008. *Plasmodium knowlesi*: the fifth human malaria parasite. *Clin. Infect. Dis.* 46, 172–173.
- White, N.J., Pukrittayakamee, S., Hien, T.T., Faiz, M.A., Mokuolu, O.A., Dondorp, A.M., 2014. Malaria. *Lancet* 383, 723–735.
- WHO, 2014. Severe Malaria Section 1: Epidemiology of severe falciparum malaria. *Trop. Med. Int. Heal.*
- WHO, 2017. World Malaria Report 2017. *World Malar. Rep.* 2017.
- WHO, 2018. Malaria [WWW Document]. World Health Organisation. URL <http://www.who.int/malaria/en/> (accessed 4.25.18).
- William, T., Jelip, J., Menon, J., Anderios, F., Mohammad, R., Awang Mohammad, T.A., Grigg, M.J., Yeo, T.W., Anstey, N.M., Barber, B.E., 2014. Changing epidemiology of malaria in Sabah, Malaysia: increasing incidence of *Plasmodium knowlesi*. *Malar. J.* 13, 390.
- Wong, A.D., Ye, M., Levy, A.F., Rothstein, J.D., Bergles, D.E., Searson, P.C., 2013. The blood-brain barrier: an engineering perspective. *Front. Neuroeng.* 6.
- Wosik, K., Cayrol, R., Dodelet-Devillers, A., Berthelet, F., Bernard, M., Moumdjian, R., Bouthillier, A., Reudelhuber, T.L., Prat, A., 2007. Neurobiology of Disease Angiotensin II Controls Occludin Function and Is Required for Blood-Brain Barrier Maintenance: Relevance to Multiple Sclerosis. *J. Neurosci.* 27, 9032–9042.
- Yamazaki, Y., Kanekiyo, T., 2017. Blood-Brain Barrier Dysfunction and the Pathogenesis of Alzheimer's Disease. *Int. J. Mol. Sci.* 18.
- Yang, Z., Wang, K.K.W., 2015. Glial fibrillary acidic protein: from intermediate filament assembly and gliosis to neurobiomarker. *Trends Neurosci.* 38, 364–74.
- Yao, Y., Tsirka, S.E., 2011. Truncation of monocyte chemoattractant protein 1 by plasmin promotes blood-brain barrier disruption. *J. Cell Sci.* 124, 1486–95.
- Yao, Y., Tsirka, S.E., 2014. Monocyte chemoattractant protein-1 and the blood-brain barrier. *Cell. Mol. Life Sci.* 71, 683–97.
- Yu, H., Huang, X., Ma, Y., Gao, M., Wang, O., Gao, T., Shen, Y., Liu, X., 2013. Interleukin-8

regulates endothelial permeability by down-regulation of tight junction but not dependent on integrins induced focal adhesions. *Int. J. Biol. Sci.* 9, 966–79.

Zhang, Y., Huang, C., Kim, S., Golkaram, M., Dixon, M.W.A., Tilley, L., Li, J., Zhang, S., Suresh, S., 2015. Multiple stiffening effects of nanoscale knobs on human red blood cells infected with *Plasmodium falciparum* malaria parasite. *Proc. Natl. Acad. Sci. U. S. A.* 112, 6068–73.

Zhang, Z., Zoltewicz, J.S., Mondello, S., Newsom, K.J., Yang, Z., Yang, B., Kobeissy, F., Guingab, J., Glushakova, O., Robicsek, S., Heaton, S., Buki, A., Hannay, J., Gold, M.S., Rubenstein, R., Lu, X.M., Dave, J.R., Schmid, K., Tortella, F., Robertson, C.S., Wang, K.K.W., 2014. Human Traumatic Brain Injury Induces Autoantibody Response against Glial Fibrillary Acidic Protein and Its Breakdown Products. *PLoS One* 9, e92698.

Zlokovic, B. V., 2008. The blood-brain barrier in health and chronic neurodegenerative disorders. *Neuron* 57, 178–201.

Appendices

Appendix 1: List of kits

Name	Catalogue number	Manufacturer
Human ADAMTS-4	DY4307-05	R&D systems
Human GFAP	DY2594-05	R&D systems
Human CD54/ICAM-1 ELISA kit	851590005	Diaclone

Appendix 2: List of reagents and chemicals

Reagent and chemical	Catalogue number	Supplier
10% Sodium Dodecyl Sulphate solution (SDS)	10265153	Fisher Scientific
10X Blocking buffer	B6429	Sigma-Aldrich
Ammonium persulfate	10744171	Fisher Scientific
Astrocyte medium	1801	ScienCell
Biorad protein assay Dye reagent concentrate	500-0006	Biorad
Bis-Acrylamide 29:1 (40% solution)	BP1408	Fisher Scientific
Bovine serum albumin solution	A7284	Sigma-Aldrich
Bromophenol blue	114391	Sigma-Aldrich
Cryo-SFM	C-29910	Promocell
Donkey serum	D9663	Sigma-Aldrich
Dulbecco's Phosphate buffered saline	D8537	Sigma-Aldrich
Fluorescein isothiocyanate–dextran (Mw 40,000)	FD40S	Sigma-Aldrich
Foetal Bovine serum	F9665	Sigma-Aldrich
Gelatin solution (Type-B)	G1393	Sigma-Aldrich
Gentamicin	1405410	Sigma
Giemsa stain	295595000	Acros Organics
Glycerol	BPE229	Fisher Scientific
Glycine	BP381	Fisher Scientific
GM6001	364206	Calbiochem

HEPES buffer solution	H0887	Sigma-Aldrich
Histopaque [®] -1077	10771	Sigma-Aldrich
Hydrogen Peroxide solution	H1009	Sigma-Aldrich
IL-1 β (Human, Recombinant)	201-LB	R&D system
L-Glutamine	G7513	Sigma-Aldrich
Methanol	BP110	Sigma-Aldrich
New born-calf serum (Bovine)	N4762	Sigma-Aldrich
Normal goat serum (NGS)	S-1000	Vector laboratories
Paraformaldehyde	P6148	Sigma-Aldrich
Penicillin-Streptomycin	P0781	Sigma-Aldrich
Pierce [™] ECL western blotting substrate	32209	Thermo Scientific
Ponceau S	81462	Fluka
Precision Plus [™] Protein Ladder	161-0375	Bio Rad
Protein assay standard (II) Bovine serum albumin	500-0007	Biorad
RIPA buffer	R0278	Sigma-Aldrich
RPMI-1640	R0833	Sigma-Aldrich
Sodium Chloride	BPE358	Fisher Scientific
Sulphuric acid solution	J/8420/17	Fisher Scientific
TEMED	T9281	Sigma-Aldrich
TMB peroxidase substrate	172-1068	Bio Rad
Tris Base	BP152	Fisher Scientific
Tris Hydrochloric	BP153	Fisher Scientific
Triton X-100	BP151	Fisher Scientific
Trypsin-EDTA solution	T4049	Sigma-Aldrich
Tween 20	BPE337	Fisher Scientific

Appendix 3: List of equipment

Equipment	Manufacturer
Benchtop centrifuge	Sigma
Benchtop centrifuge, Midispin	Eppendorf
Benchtop centrifuge, Minispin	Eppendorf
Biosafety cabinet, Category III	NuAIRE
Biosafety cabinet	SterilGard
CO ₂ incubator	Galaxy R
Compound microscope	CETI
Deionised water	ELGA
Endohm EVOM	Precision instrument
FluorChem M	Protein simple
Fluorescence microscope	Nikon Eclipse 80i microscope Images acquired using a Hamamatsu ORCA camera
Glomax Multi+ Detection System	Promega
Haemocytometer	Hawksley
Heat block	Grant
Inverted microscope	Motic
Magnetic Stirrer	Scientific Laboratories Supplies
pH meter	Denver instrument
Pump	Star lab
Rocking platform	Luckham
Vortex mixer	Stuart Scientific laboratory supplies
Water bath	Stuart Scientific
MiniProtean 3	Bio-Rad Laboartories

Appendix 4: List of antibodies

Antibody	Catalogue number	Supplier
Anti-ADAMTS-4 (K-20)	sc-16533	Santa Cruz Biotechnology
Anti-Claudin-5 (H-52)	sc-28670	Santa Cruz Biotechnology
Anti-ICAM-1 (15.2)	sc-107	Santa Cruz Biotechnology
Anti-Mouse IgG-FITC	F0257	Sigma-Aldrich
Anti-Mouse IgG-R- Phycoerythrin antibody	P9670	Sigma-Aldrich
Anti-Rabbit IgG-FITC	F7512	Sigma-Aldrich
Anti-Vinculin	V9264	Sigma-Aldrich
Cy TM -conjugated AffiniPure Donkey Anti-Rabbit IgG	711-165-152	Jackson Immuno Research Laboratories
Donkey anti-goat IgG	sc-2020	Santa Cruz
Goat anti-mouse HRP conjugate	170-6516	Biorad
Goat anti-rabbit Alex Fluor 488	FP-SA5000	Cheshire Sciences
Goat anti-rabbit HRP conjugate	172-1019	Biorad
Polyclonal Rabbit Anti-GFAP	Z0334	Dako

Appendix 5: Table of Buffers

1x SDS-PAGE running buffer pH 8.3		
Chemical	Final concentration	Weight/Volume
Tris-base	25mM	3.03g
Glycine	192mM	14.4g
SDS	0.1% (w/v)	1g
Makeup to 1L with dH₂O		

1X Transfer buffer		
Chemical	Final concentration	Weight/Volume
Tris-base	25mM	6.06g
Glycine	192mM	28.8
Methanol	10% (v/v)	400
Makeup to 2L with dH₂O		

Tris-base 1.5M	
Chemical	Weight/Volume
Tris-Cl	36.33g
Makeup to 200ml with dH₂O	

Tris-Cl 1M	
Chemical	Weight/Volume
Tris-base	24.22g
Makeup to 200ml with dH₂O	

APS 10% (w/v)	
Chemical	Weight/Volume
Ammonium sulphate	1g
Makeup to 10ml with dH₂O	

1X Blocking solution	
Chemical	Weight/Volume
10X Blocking Buffer	5ml
dH₂O	45ml
Total volume	50ml

1X TBST pH 7.6		
Chemical	Final concentration	Weight/Volume
Tris base	20mM	2.4 g
	150mM	8.0 g
dH₂O	-	800 ml
Total volume		1L

Resolving and stacking gel preparation for SDS PAGE gel

	10% resolving gel	5% stacking gel	
40% Polyacrylamide	5 ml	1.25 ml	Fisher Scientific
1.5 M Tris Cl (pH 8.8)	5 ml	-	Fisher Scientific
1 M Tris Cl (pH 6.8)	-	1.25 ml	Fisher Scientific
dH₂O	9.6 ml	7.3 ml	
10% SDS	0.2 ml	0.1 ml	Fisher Scientific
10% APS	135µl	0.1 ml	Biorad
TEMED	12µl	12 µl	Sigma
Final volume	20 ml	10 ml	

Appendix 6: Media and components used in media

HBEC complete medium

Media components	Quantity
RPMI	500ml
Foetal bovine serum	50ml (10% final)
Newborn calf serum	25ml (5% final)
L-glutamine	5ml (1% final)
P/S	5ml (1% final)

Blank media

Media components	Quantity
RPMI	500ml
L-glutamine	5ml (1% final)
P/S	5ml (1% final)

Quiescent media 5% FBS (Q5% FBS media)

Media components	Quantity
Blank media	50ml
Foetal bovine serum	2.5ml (5% final)

Quiescent media 1% FBS (Q1% FBS media)

Media components	Quantity
Blank media	50ml
Foetal bovine serum	500 μ l (1%)

AM

Media components	Quantity
Astrocyte medium	500ml
Foetal bovine serum	10ml
Penicillin/streptomycin	5ml
5ml	100X astrocyte growth supplement

AM/HBEC media

Media components	Quantity
Astrocyte medium	49.5ml
1% of Q1% FBS media	500µl

Appendix 7: Materials Transfer Agreement

Noguchi Memorial Institute for Medical Research

MATERIALS TRANSFER AGREEMENT

The Noguchi Memorial Institute for medical Research agrees to provide the University of Keele with certain materials solely for the purposes stated herein and subject to the following conditions:

1. The parties to this Agreement are:

The University of Keele, a university established by the University of Keele Act 1962 (10 & 11 Eliz. 2 Ch Xv) and the granting of a Royal Charter in 1962, of Keele, Staffordshire ST5 5BG hereinafter called the "RECIPIENT" and

The Noguchi Memorial Institute for Medical Research, a constituent member of the College of Health Sciences of the University of Ghana Legon, hereinafter known as "NMIMR,"

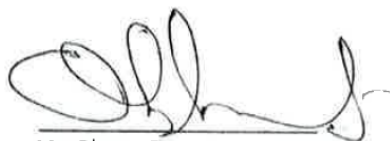
The research (as hereinafter defined) will be conducted by DR. SABRASTI J. CHAKRAVORTY, hereinafter called "SCIENTIST".

2. The Material that is covered by this Agreement includes: plasma samples from malaria-infected humans that will be provided by NMIMR, hereinafter called "Material". The material is considered proprietary to NMIMR. NMIMR shall be free, in its sole discretion, to distribute the Material to others and to use it for its own purposes.
3. The Material shall be used by the SCIENTIST in research to be carried out at Keele's premises to conduct studies to understanding the mechanisms underlying changes in the blood brain barrier in cerebral malaria (the "Research")
4. This Agreement shall take effect immediately upon it being signed by both the parties and shall continue until completion of the Research.
5. The RECIPIENT will fully bear the cost of shipping the Material.
6. Neither SCIENTIST nor RECIPIENT shall distribute, release, or in any way transfer the Material to any person or entity other than the laboratory personnel under the SCIENTIST'S direct supervision, and the SCIENTIST and RECIPIENT shall ensure that no one will be allowed to take or send the Material to any other location, unless written permission is obtained from NMIMR. The RECIPIENT agrees that the Material will only be used for the purposes of the Research and will not be used for any other purpose. Neither the Material nor any biological materials treated therewith will be used in human beings.
7. The RECIPIENT shall have no rights (Including Intellectual Property Rights) on the Material other than as provided in this Agreement. At the written request of NMIMR, the RECIPIENT will return or destroy all unused Material.

8. The Material is experimental in nature and it is provided WITHOUT WARRANTY OF MERCHANTABILITY OR FITNESS FOR A PARTICULAR PURPOSE OR ANY OTHER WARRANTY, EXPRESS OR IMPLIED. NMIMR MAKES NO REPRESENTATION OR WARRANTY THAT THE USE OF THE MATERIAL WILL NOT INFRINGE ANY PATENT OR OTHER PROPRIETARY RIGHT.
9. In no event shall NMIMR be liable for any use by the SCIENTIST or RECIPIENT of the Material for any loss, claim, damage or liability, of whatsoever kind or nature, which may arise from, or in connection with the SCIENTIST's or RECIPIENT's use, handling or storage of the Material.
10. The SCIENTIST and RECIPIENT will use the Material in compliance with all laws, governmental regulations and guidelines applicable to the Material, including any especially applicable to research with human plasma.
11. This Agreement is not assignable, whether by operation of law or otherwise, without the prior written consent of NMIMR.
12. The parties acknowledge that the Research will be carried out at the RECIPIENTS premises in the United Kingdom and agree that this Agreement shall be governed by the laws of England and Wales and shall be subject to the non-exclusive jurisdiction of the English courts.

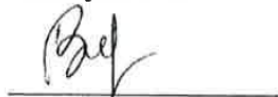
THE NOGUCHI MEMORIAL INSTITUTE
FOR MEDICAL RESEARCH (NMIMR)
P.O. Box LG 581
Legon, Accra, Ghana

KEELE UNIVERSITY
School of Life Sciences, Institute for
Research and Technology, Keele
University, Keele, United Kingdom ST5
5BG



Mr. Okyere Boateng
Institute Administrator, NMIMR

Date: 17th February, 2017
Providing Scientist:



Name: Dr. Ben Adu Gyan
Title: Investigator, Dept of Immunology, NMIMR



Dr Mark Bacon, Director of Engagement
and Partnerships

Date:
Recipient Scientist:



Dr. Sabrasti Chakravorty
ISTM, Keele University